A study of tailoring acoustic porous material properties when designing lightweight multilayered vehicle panels

Eleonora Lind Lind Nordgren

CONSERVATOIRE NATIONAL DES ARTS ET MÉTIERS

–

ROYAL INSTITUTE OF TECHNOLOGY

le cnam

KTH VETENSKAP OCH KONST

KTH Engineering Sciences

École Doctorale du Conservatoire National des Arts et Métiers

Laboratoire de Mécanique des Strucutres et des Systèmes Couplés (LMSSC)

THÈSE DE DOCTORAT

présentée par : **Eleonora LIND NORDGREN**

soutenue le : **7 Septembre 2012**

pour obtenir le grade de : **Docteur du Conservatoire National des Arts et Métiers**

Spécialité : **Mécanique**

A STUDY OF TAILORING ACOUSTIC POROUS MATERIAL PROPERTIES WHEN DESIGNING LIGHTWEIGHT MULTILAYERED VEHICLE PANELS

Jury composé de:

M. OLOFSSON U.	Royal Institute of Technology (KTH), Suède	*Président du jury*
M. GÖRANSSON P.	Royal Institute of Technology (KTH), Suède	*Directeur de thèse*
M. OHAYON R.	Cnam, France	*Directeur de thèse*
M. DEÜ J.-F.	Cnam, France	*Co-directeur de thèse*
M. DAZEL O.	LAUM, France	*Rapporteur*
M. DESMET W.	KU Leuven, Belgique	*Rapporteur*
M. DAVIDSSON P.	Creodynamics AB, Suède	*Examinateur*
M. HÖRLIN N.-E.	Royal Institute of Technology (KTH), Suède	*Examinateur*

Contents

Part I

Résumé des travaux de thèse

Chapter 1

Introduction

L'impact de la plupart des activités humaines sur l'environnement est devenu un problème de plus en plus important à l'échelle globale. La problématique principale concerne aujourd'hui le réchauffement climatique, causé, principalement, par l'émission de dioxyde de carbone et d'autres gaz à effet de serre. En Suède, environ 26% de la consommation en énergie est due à l'industrie du transport et selon Åkerman et Höjer [1] cela est déjà trop. Afin de maintenir un environnement durable, l'énergie utilisée dans l'industrie du transport devrait être réduite de 60% d'ici l'année 2050. Cela peut uniquement être réalisé en effectuant des changements au niveau des modes de transport tout en réduisant de manière significative l'intensité de l'énergie du transport. Plusieurs aspects d'un véhicule doivent être pris en compte afin d'en améliorer l'efficacité énergétique. En dehors de la motorisation elle-même, la résistance au roulement, les propriétés aérodynamiques et la masse du véhicule sont quelques caractéristiques qui influencent grandement l'énergie consommée durant le cycle de vie total du véhicule.

La réduction de la masse du véhicule est, de ce fait, une des nombreuses stratégies permettant de réduire la consommation en carburant ou en énergie, afin d'obtenir des transports plus efficaces et ayant moins d'impact négatif sur l'environnement. En parallèle, les exigences en matière de sécurité et de confort ne peuvent pas être abaissées, les modifications apportées à la structure doivent donc permettre de maintenir voire d'améliorer ces propriétés. Cela peut être réalisé, e.g. en apportant des changements profonds dans les matériaux sélectionnés et dans la conception globale, et la mise en oeuvre de structures multifonctionnelles et multicouches légères et rigides (e.g. panneaux sandwichs et composites) dans la production industrielle a augmenté régulièrement depuis un certain temps. Toutefois, l'introduction de nouvelles conceptions légères induit souvent une augmentation des problèmes de bruit et de vibration, en particulier dans le domaine des basses fréquences. En règle générale, les vibrations de structure indésirables et le bruit se propagent dans la structure et rayonnent, par exemple, à partir des surfaces de finition à l'intérieur de l'habitacle du véhicule. De ce fait, le comportement dynamique de ce panneau intérieur a un impact majeur sur le bruit rayonné, et sur le niveau de bruit à l'intérieur de l'habitacle.

Une méthode souvent utilisée pour améliorer le bruit, les vibrations et la rudesse (NVH) dans un véhicule, est l'ajout de matériaux poro-élastiques et visco-élastiques flexibles, lorsqu'il n'est pas possible de réaliser des modifications majeures des panneaux intérieurs. Toutefois, l'ajout de matériaux est problématique en vis à vis de l'objectif de réduction du poids. Cela augmente également le coût global (matériaux et assemblage) et l'espace alloué autrement aux passagers du véhicule. Il serait, de toute évidence, préférable d'inclure les exigences acoustiques et dynamiques dès la conception du panneau, ou bien, en deuxième option, d'assurer le meilleur ratio possible performance par masse ajoutée, en matière de coût et de volume, pour tout traitement ultérieur effectué.

Une façon courante d'améliorer la performance d'un panneau acoustique est de combiner différents matériaux poro-élastiques et visco-élastiques en plusieurs couches présentant différentes propriétés physiques et mécaniques, telles que l'amortissement, l'élasticité, la viscosité et la densité. Déterminer quels matériaux combiner et quelles propriétés rechercher dans chaque couche afin d'obtenir des résultats satisfaisants, est aujourd'hui une tâche longue et coûteuse qui nécessite la connaissance préalable de combinaisons fonctionnant avec succès, l'expérience d'ingénierie ainsi que des essais poussés. De toute évidence, il existe un besoin d'outils informatiques capables de prévoir et d'optimiser le comportement de ces structures multicouches.

Ce travail constitue une première tentative visant à démontrer les possibilités d'adaptation des matériaux poreux à des fins spécifiques. Fait correctement, il peut potentiellement générer des améliorations notables en matière de confort NVH, avec un minimum de volume et masse ajoutée.

Chapter 2

Description et conception du milieu poreux

Les matériaux d'intérêt dans cette thèse sont les matériaux poreux, qui sont des matériaux hétérogènes formés d'une structure poreuse élastique saturée en fluide. Le fluide est supposé être interconnecté à travers le milieu, formant des pores ouverts ou cellules ouvertes. Le fluide interstitiel, e.g. l'air, peut se déplacer par rapport à la structure. De ce fait, quel que soit le fluide enfermé dans la structure, celui-ci est considéré comme faisant parti de la structure étant donné qu'il ne peut se déplacer de manière relative par rapport à celle-ci. Deux exemples typiques de matériaux poreux sont les mousses constituées de cellules ouvertes et les matières fibreuses, voir fig. 2.1 et 2.2. Dans les mousses poreuses, les fibres minces constituant la structure sont souvent désignés par poutres. Les porosités des matériaux utilisés comme absorbants acoustiques sont typiquement élevées, au dessus de 90%, et l'énergie acoustique est transportée à la fois par le fluide dans les pores et par la structure solide. Les ondes sont fortement couplées et se propagent simultanément dans ces deux milieux mais avec des phases et amplitudes différentes. La propagation des ondes dans les milieux poreux est, en d'autres termes, un phénomène d'interaction fluide-structure, se produisant à travers l'ensemble du volume du matériau.

2.1 Dissipation de l'énergie dans les milieux poreux

Lorsque l'énergie acoustique traverse un milieu poreux, une partie de l'énergie mécanique-acoustique est dissipée, i.e. convertie en chaleur. Il existe plusieurs mécanismes différents qui contribuent au comportement acoustique et vibro-acoustique du milieu poreux, certains de ces mécanismes sont brièvement décris ci-après.

Lorsque la structure et le fluide se déplacent l'un par rapport à l'autre, des interactions visqueuses apparaissent à l'interface, entraînant des pertes dans le fluide et dans la structure. La traînée visqueuse est supposée proportionnelle au déplacement relatif et est

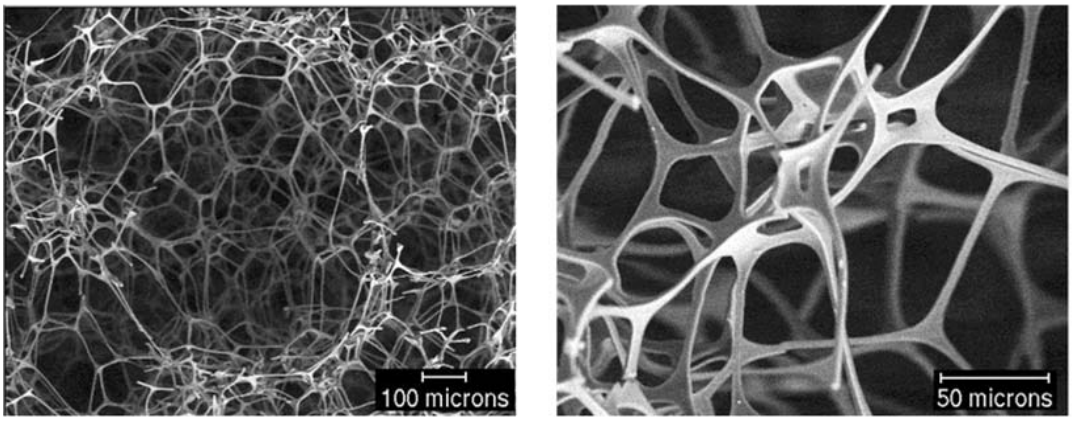

Figure 2.1: Photographie microscopique d'une mousse poreuse avec cellules ouvertes. Avec la permission de Franck Paris (CTTM, France) et de Luc Jaouen (luc.jaouen@matelys.com).

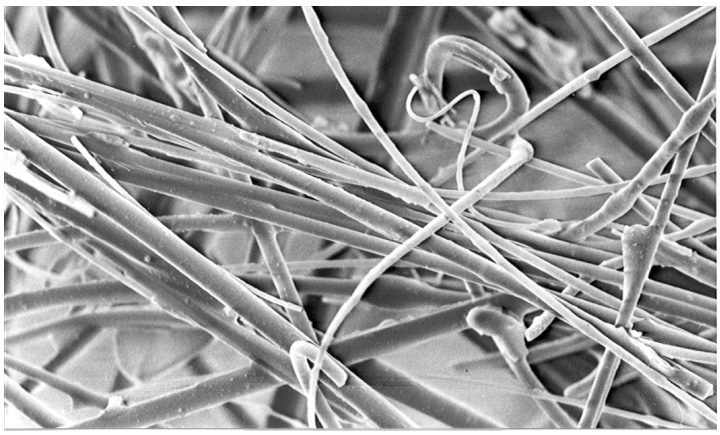

Figure 2.2: Photographie microscopique de matériaux fibreux. Avec la permission de Rémi Guastavino (remi@kth.se).

habituellement décrite en utilisant un facteur proportionnel dépendant de la fréquence. Un tel facteur n'est pas uniquement dépendant de la fréquence, mais aussi, par exemple, dépendant des propriétés géométriques des pores, de la viscosité du fluide interstitiel et de la zone de contact entre la structure et le fluide. A basses fréquences, la couche limite visqueuse à la surface de la poutre est épaisse par rapport au rayon des pores, et la perte de l'énergie acoustique due à la dissipation visqueuse est significative. A des fréquences plus élevées, la couche limite visqueuse entre la structure et le fluide est bien plus petite par rapport au rayon des pores. Pour des oscillations aussi rapides, la dissipation visqueuse est faible par rapport à d'autres phénomènes.

Le mouvement relatif du fluide par rapport à la structure n'entraîne pas uniquement les forces visqueuses mentionnées précédemment. En plus de la traînée visqueuse, il existe d'autres mécanismes qui provoquent des pertes vibro-acoustiques qui sont proportionnelles au déplacement relatif mais indépendantes de la viscosité du fluide. Comme le fluide (ou la structure) est forcée de changer de direction, tout en se déplaçant par rapport à la structure (ou fluide), une force normale à la direction d'accélération d'un élément est appliquée à l'autre. Ces mécanismes, qui seraient présents même sous l'hypothèse d'un fluide non visqueux, créent une augmentation apparente de la masse et sont liés à la géométrie de la structure et au mouvement relatif fluide/structure.

Le déplacement de la structure cause également des pertes internes dépendantes de la fréquence, dues à la relaxation de contrainte-déformation lorsque la structure est déformée. Étant donné que la compressibilité du système entraîne une augmentation de la température due aux cycles de compression et expansion, la dissipation thermoélastique est une autre source de dissipation de l'énergie acoustique. Aux basses fréquences, le processus est isotherme tandis qu'aux hautes fréquences il devient adiabatique. Entre ces deux conditions, la conduction de la chaleur, parmi d'autres phénomènes physiques, provoque des pertes de l'énergie vibro-acoustique.

2.2 La théorie de Biot

Le modèle le plus couramment utilisé pour décrire le comportement acoustique des milieux poreux est attribué à Biot [6] et est souvent désigné par la théorie de Biot, ou parfois comme le modèle de Johnson-Champoux-Allard de la théorie de Biot. Une partie de la théorie de Biot publiée en 1956 est similaire à la théorie contemporaine présentée par Zwikker et Kosten [34] avec pour différence le fait que Biot avait également inclu des effets de contrainte de cisaillement dans la structure élastique du milieu poreux.

Johnson *et al.* [24] ajoutèrent une description améliorée des effets visqueux en introduisant la longueur caractéristique visqueuse, Λ, qui prend en compte les effets visqueux dépendants de la fréquence. Allard et Champoux [3, 10] ajoutèrent la longueur caractéristique thermique, Λ', qui, de manière similaire, inclue les effets des pertes thermiques dépendantes de la fréquence.

Dans le cadre de la théorie de Biot étendue, la structure solide est modélisée comme un milieu continu solide élastique équivalent et le fluide interstitiel comme un milieu de fluide incompressible équivalent, les deux étant décrits par les propriétés mécaniques macroscopiques homogénéisées standards en mécanique des milieux continus. Les deux milieux séparés mais couplés agissent et interagissent donc en occupant le même espace. L'interaction entre la phase solide et fluide est décrite par des paramètres de couplage dérivés de propriétés macroscopiques homogénéisées mesurables. Les propriétés macroscopiques sont utilisées pour calculer des quantités macroscopiques homogénéisées e.g. le déplacement du solide et du fluide, la pression acoustique, la contrainte élastique. Une condition à respecter dans la modélisation des mousses, est que les dimensions microscopiques caractéristiques des mousses, e.g. taille des pores, soient petites par rapport aux dimensions caractéristiques du comportement macroscopique. En acoustique, cette dernière est identifiée comme la longueur d'onde. Pour les modèles et matériaux étudiés ici, cette condition est généralement satisfaite.

Il convient toutefois de noter que la modélisation d'un matériau poro-élastique, en tant que deux milieux distincts et couplés, pose problème aux interfaces du matériau. Des études montrent que les propriétés homogénéisées peuvent différer près de la surface du matériau poro-élastique [18]. Ces types d'effet de frontière pourrait avoir un effet non négligeable, en particulier si la profondeur d'une telle couche limite est grande par rapport à l'épaisseur de la couche de poreux.

Une grande partie des travaux a consisté en l'obtention d'une description des paramètres macroscopiques du matériau ayant un sens physique. De toute importance pour les milieux poreux, les paramètres de couplage peuvent être définis de différentes façons. Selon le modèle de Johnson-Champoux-Allard, ces paramètres sont décrits par:

- *Porosité*, ϕ [1], définie comme la fraction volumique de fluide dans le milieu poreux, $0 < \phi < 1$. Pour des applications en acoustique, la porosité des matériaux est en général supérieure à 0.95.

- *Tortuosité*, α_∞ [1], définie comme le ratio entre le carré de la vitesse moyenne microscopique du fluide et la vitesse moyenne microscopique au carré du fluide, dans un volume supposé de viscosité nulle. De manière pratique, ce paramètre compare la longueur du chemin que le fluide traverse dans un milieu poreux au niveau microscopique à la longueur du chemin traversé au niveau macroscopique, impliquant que $\alpha_\infty \geq 1$. Dans le cas d'un milieu à pores ouverts présentant une porosité élevée, la tortuosité est souvent proche de un, typiquement égale à 1.05.

- *Résistance statique à l'écoulement*, σ^{static} [Nsm^{-4}], définie comme le rapport entre la différence de pression et la vitesse d'écoulement, par unité de longueur. La résistance à l'écoulement est dépendante de plusieurs propriétés physiques dans le milieu poreux, comme la viscosité surfacique entre la structure et la géométrie microscopique du milieu poreux. Ce paramètre peut être mesuré ou

déduit théoriquement à partir e.g. de simulations de Stokes, pour une géométrie microstructurelle donnée.

- *Longueur visqueuse caractéristique*, Λ [m], permettant d'améliorer l'estimation lorsqu'il est nécessaire de tenir compte d'effets dissipatifs causés par des pertes visqueuses au niveau des parois des pores. Lorsque la taille des pores est petite par rapport à l'épaisseur de la couche limite, les effets de dissipation visqueuse ne peuvent pas être négligés. La longueur visqueuse caractéristique offre des possibilités de corrections donnant une meilleur représentation des pertes visqueuses, dépendantes de la fréquence.

- *Longueur thermique caractéristique*, Λ' [m], prenant en compte les échanges thermiques entre la structure et le fluide à la frontière entre les deux, et, par analogie avec la longueur visqueuse caractéristique, offre des possibilités de corrections pour les interactions thermiques fluide-structure dépendantes de la fréquence.

Afin de mieux comprendre les matériaux poreux, il est important d'effectuer des essais expérimentaux afin de caractériser différents matériaux et d'obtenir les paramètres matériaux macroscopiques nécessaires. Il existe plusieurs aspects physiques des matériaux poreux qui ne sont pas encore complètement compris, par exemple, l'influence de la compression statique et de la déformation sur les paramètres matériaux [14] ou les modifications des modules d'élasticité aux éléments frontières d'échantillons de mousses poreuses [18]. Bien-entendu, le travail pour obtenir des données expérimentales est lié de près au développement de modèles mathématiques utilisés afin de décrire ces matériaux complexes et leur comportement.

2.2.1 Principales équations de la théorie de Biot

La théorie de Biot correspond à un modèle lagrangien où les relations de contrainte-déformation sont dérivées de l'énergie potentielle de déformation. Si la théorie de Biot est de manière pratique souvent utilisée sous sa forme isotrope, les principales équations de cette théorie sont données ici sous leur forme anisotrope, de manière similaire aux travaux de Biot [8], Biot et Willis [9] et Allard [2]. Cette présentation des principales équations est en aucune façon complète et doit être considérée comme un court résumé du travail très complet qui a déjà été accompli dans le domaine des matériaux poreux. Pour plus de détails, se référer aux travaux en référence.

Les notations utilisées sont expliquées lorsque introduites et également résumées dans le chapitre 6, à l'exception de la notation tensorielle suivante. Le nombre ordinal du composant dans un système de coordonnées cartésiennes, e.g. $i = 1, 2, 3$ est noté i, j, k. Les dérivées partielles par rapport à x_i s'écrivent $(.)_{,i} = \partial(.)/\partial x_i$. Le delta de Kronecker s'écrit δ_{ij}. La notation tensorielle cartésienne avec la convention

de sommation de Einstein est aussi utilisée, i.e. des indices répétés impliquent une sommation de ces termes.

Équations du moment

En supposant un mouvement harmonique à une fréquence angulaire ω, les équations du moment (dans le domaine fréquentiel) de la structure solide et du fluide peuvent être respectivement écrites comme ci-après:

$$\sigma^{\mathrm{s}}_{ij,j} = -\omega^2 \tilde{\rho}^{11}_{ij} u^{\mathrm{s}}_j - \omega^2 \tilde{\rho}^{12}_{ij} u^{\mathrm{f}}_j \tag{2.1}$$

et

$$\sigma^{\mathrm{f}}_{ij,j} = -\omega^2 \tilde{\rho}^{12}_{ij} u^{\mathrm{s}}_j - \omega^2 \tilde{\rho}^{22}_{ij} u^{\mathrm{f}}_j \tag{2.2}$$

où σ^{s}_{ij} et σ^{f}_{ij} sont les tenseurs de contrainte de Cauchy, respectivement, pour la structure et pour le fluide, et u^{s}_j et u^{f}_j sont les déplacements, respectivement, de la structure et du fluide. Les tenseurs de densité équivalents, $\tilde{\rho}^{11}_{ij}$, $\tilde{\rho}^{12}_{ij}$ et $\tilde{\rho}^{22}_{ij}$ sont les généralisations anisotropes de celles utilisées par Allard [2] et peuvent être définies comme:

$$\tilde{\rho}^{11}_{ij} = \rho_1 \delta_{ij} + \rho^{\mathrm{a}}_{ij} - \frac{\mathrm{i}}{\omega} b_{ij}, \tag{2.3}$$

$$\tilde{\rho}^{12}_{ij} = -\rho^{\mathrm{a}}_{ij} - \frac{\mathrm{i}}{\omega} b_{ij}, \tag{2.4}$$

$$\tilde{\rho}^{22}_{ij} = \phi \rho_0 \delta_{ij} + \rho^{\mathrm{a}}_{ij} - \frac{\mathrm{i}}{\omega} b_{ij}, \tag{2.5}$$

où

$$\rho^{\mathrm{a}}_{ij} = \phi \rho_0 \left(\alpha_{ij} - \delta_{ij} \right) \tag{2.6}$$

avec ρ_0 la masse volumique du fluide ambiant, ρ_1 la masse volumique apparente du matériau poreux et α_{ij} le tenseur de tortuosité. ρ^{a}_{ij} est un coefficient de couplage d'inertie qui représente l'augmentation apparente de la masse due à la tortuosité. Le tenseur de traînée visqueuse b_{ij} prend en compte les forces visqueuses entre la phase solide et le fluide, et est ici défini comme précédemment établi par Johnson *et al.* [24].

$$b_{ij} = \phi^2 \sigma^{\mathrm{static}}_{ij} B_{ij} \left(\omega \right), \tag{2.7}$$

où

$$B_{ij} = \sqrt{1 + i\omega \frac{4\eta\rho_0\alpha_{ij}^2}{\phi^2(\sigma_{ij}^{\text{static}})^2\Lambda_{ij}^2}} \tag{2.8}$$

avec η la viscosité du fluide ambiant.

Équations constitutives

Les deux équations constitutives peuvent être définies par:

$$\sigma_{ij}^{\text{s}} = C_{ijkl}\varepsilon_{kl} + Q_{ij}\theta^{\text{f}} \tag{2.9}$$

et

$$\sigma_{ij}^{\text{f}} = Q_{kl}\varepsilon_{kl}\delta_{ij} + R\theta^{\text{f}}\delta_{ij} \tag{2.10}$$

où C_{ijkl} est le tenseur de Hooke de la structure solide. La dilatation du fluide est donnée par la divergence du déplacement du fluide:

$$\theta^{\text{f}} = u_{k,k}^{\text{f}} \tag{2.11}$$

et la déformation de la structure solide est donnée par le tenseur des déformations de Cauchy

$$\varepsilon_{kl} = \frac{1}{2}\left(u_{k,l}^{\text{s}} + u_{l,k}^{\text{s}}\right). \tag{2.12}$$

Les deux tenseurs des matériaux, R et Q_{ij}, sont définis par

$$R = \frac{\phi^2 K_s}{1 - \phi - K_s C_{ijkl} d_{ij} d_{kl} + \phi K_s/K_f} \tag{2.13}$$

$$Q_{ij} = \left[(1-\phi) - C_{ijkl}d_{kl}\right]\frac{R}{\phi} = \frac{\left[(1-\phi) - C_{ijkl}d_{kl}\right]\phi K_s}{1 - \phi - K_s C_{ijkl} d_{ij} d_{kl} + \phi K_s/K_f} \tag{2.14}$$

où K_s et K_f sont les modules de compressibilité, respectivement, de la structure et du fluide et d_{ij} est le tenseur de souplesse en compressibilité. K_f est obtenu en utilisant le modèle de Lafarge *et al.* [26]. Le fluide étant supposé isotrope, R est une grandeur scalaire. Le couplage de dilatation Q_{ij} est, cependant, un tenseur d'ordre deux en raison de l'anisotropie supposée élastique.

De manière pratique, souvent et dans le cadre de cette thèse, le déplacement du fluide n'est pas utilisé comme une variable dépendante. Le tenseur des contraintes de Cauchy du fluide est alors remplacé par la pression des pores, laquelle est un scalaire, $\sigma_{ij}^{\text{f}} =$

$-\phi p \delta_{ij}$, ce qui permet de réduire le nombre de variables indépendantes de six à quatre.

2.2.2 Représentation matricielle des paramètres matériau

Les propriétés élastiques de la structure solide du matériau poreux peuvent être décrites en utilisant la matrice de Hooke de la structure solide, équivalente au tenseur de Hooke C_{ijkl} utilisé précédemment. La matrice de Hooke est une matrice 6×6 et se compose, dans le cas de matériaux isotropes, de seulement deux paramètres indépendants:

$$\mathbf{C} = \frac{E}{(1+\nu)(1-2\nu)} \begin{bmatrix} 1-\nu & \nu & \nu & 0 & 0 & 0 \\ & 1-\nu & \nu & 0 & 0 & 0 \\ & & 1-\nu & 0 & 0 & 0 \\ & & & \frac{1-2\nu}{2} & 0 & 0 \\ symm. & & & & \frac{1-2\nu}{2} & 0 \\ & & & & & \frac{1-2\nu}{2} \end{bmatrix} \tag{2.15}$$

où E est le module de Young et ν le coefficient de Poisson. Les matériaux anisotropes présentent différents types d'anisotropie, trois desquels sont décrits succinctement ci-après.

1. *Les matériaux isotropes transverses* présentent les même propriétés matériaux dans deux de leur directions principales mais des propriétés différentes dans la troisième direction normale au plan d'isotropie. Un exemple de matériaux isotropes transverses sont les matériaux fibreux. Le nombre de paramètres indépendants permettant de décrire le comportement de ces matériaux est de cinq au maximum.

$$\mathbf{C} = \begin{bmatrix} C_{11} & C_{12} & C_{13} & 0 & 0 & 0 \\ & C_{11} & C_{13} & 0 & 0 & 0 \\ & & C_{33} & 0 & 0 & 0 \\ & & & C_{44} & 0 & 0 \\ symm. & & & & C_{44} & 0 \\ & & & & & \frac{1}{2}(C_{11}-C_{12}) \end{bmatrix} \tag{2.16}$$

2. *Les matériaux orthotropes* présentent trois axes orthogonaux deux à deux et leur propriétés mécaniques sont, en général, différentes dans chaque direction. De plus, il existe des directions principales orthogonales pour lesquelles il n'y a pas de couplage entre la dilatation et le cisaillement. Plusieurs mousses utilisées dans le domaine de l'acoustique présentent un comportement proche de celui des matériaux orthotropes. Le nombre de paramètres indépendants permettant de

décrire le comportement de ces matériaux est de neuf au maximum.

$$\mathbf{C} = \begin{bmatrix} C_{11} & C_{12} & C_{13} & 0 & 0 & 0 \\ & C_{22} & C_{23} & 0 & 0 & 0 \\ & & C_{33} & 0 & 0 & 0 \\ & & & C_{44} & 0 & 0 \\ symm. & & & & C_{55} & 0 \\ & & & & & C_{66} \end{bmatrix} \tag{2.17}$$

3. *Les matériaux complètement anisotropes* présentent des propriétés matériaux différentes dans toutes les directions et les directions principales ne sont pas nécessairement orthogonales. Cela implique que e.g. un mouvement de flexion dans une direction peut induire un mouvement de torsion dans une autre, ou une contrainte en compression peut induire des contraintes en cisaillement. Il s'agit de la description la plus générale possible d'un matériau, elle n'est cependant pas souvent utilisée puisque le nombre de paramètres indépendants permettant de décrire le comportement de ces matériaux peut aller jusqu'à 21.

$$\mathbf{C} = \begin{bmatrix} C_{11} & C_{12} & C_{13} & C_{14} & C_{15} & C_{16} \\ & C_{22} & C_{23} & C_{24} & C_{25} & C_{26} \\ & & C_{33} & C_{34} & C_{35} & C_{36} \\ & & & C_{44} & C_{45} & C_{46} \\ symm. & & & & C_{55} & C_{56} \\ & & & & & C_{66} \end{bmatrix} \tag{2.18}$$

D'autres propriétés matériau telles que la tortuosité, la résistance statique à l'écoulement et la longueur caractéristique visqueuse peuvent quant à elles être décrites par une matrice 3×3 où le nombre de paramètres indépendants nécessaire peut varier entre un, pour un matériau isotrope, et six pour un matériau complètement anisotrope.

1. *Isotrope*

$$\mathbf{S} = \begin{bmatrix} S_1 & 0 & 0 \\ & S_1 & 0 \\ symm. & & S_1 \end{bmatrix} \tag{2.19}$$

2. *Isotrope transversal*

$$\mathbf{S} = \begin{bmatrix} S_1 & 0 & 0 \\ & S_1 & 0 \\ symm. & & S_3 \end{bmatrix} \tag{2.20}$$

3. *Orthotrope*

$$\mathbf{S} = \begin{bmatrix} S_1 & 0 & 0 \\ & S_2 & 0 \\ symm. & & S_3 \end{bmatrix} \tag{2.21}$$

4. *Complètement anisotrope*

$$\mathbf{S} = \begin{bmatrix} S_{11} & S_{12} & S_{13} \\ & S_{22} & S_{23} \\ symm. & & S_{33} \end{bmatrix} \tag{2.22}$$

Pour la plupart des matériaux poreux anisotropes, les matrices de paramètres matériaux sont en grandes parties inconnues et la problématique de mesure/d'obtention de ces paramètres reste toute entière. La majeure partie des techniques utilisées aujourd'hui permettent uniquement de mesurer les équivalents isotropes des propriétés anisotropes. Les travaux en cours sur le développement de techniques de mesure adéquats permettant de caractériser complètement les milieux poreux anisotropes ne sont pas des plus simples. L'anisotropie d'un matériau poreux a cependant un impact sur ses propriétés matériaux macroscopiques homogénéisées et sur son comportement acoustique [25]. Les recherches en cours se concentrent sur le développement de nouvelles techniques de mesure [18] et sur l'étude de géométries de microstructure anisotrope [22, 23, 29]. Il est important de préciser que les principales directions des différentes propriétés matériaux macroscopiques ne s'alignent pas forcément entre elles ou avec les directions principales dans un sens géométrique, nécessitant différents systèmes de coordonnées locaux afin d'être modélisées avec précisions [17, 28, 31].

2.2.3 Modélisation isotrope versus anisotrope

La grande majorité des travaux publiés antérieurement sur la théorie de Biot ne concerne que la modélisation isotrope, les modèles isotropes présentant aujourd'hui des améliorations ne sont donc pas directement transférables à une description anisotrope. Pour exemple, les relations de contrainte-déformation isotropes peuvent être étendues afin d'inclure également les pertes internes dépendantes de la fréquence dues aux mouvements de la structure. Celles-ci peuvent être modélisées en utilisant la loi de Hooke généralisée, proposée par Dovstam [13], laquelle est basée sur le travail de e.g. Biot [7] et Lesieutre [27]. En bref, les pertes internes sont modélisées en ajoutant des termes complexes dépendants de la fréquence à la matrice classique de la loi de Hooke généralisée. Cette loi de Hooke généralisée n'est pas aujourd'hui implémentée dans des modèles de Biot anisotropes étant donné que le comportement de l'amortissement et de ses directions principales comporte encore des inconnues.

De plus, les paramètres matériaux nécessaires à la description des matériaux anisotropes ne sont pas simples à obtenir et de nombreuses questions demeurent quant à leurs directions principales. Ceci souligne la nécessité de développer davantage de techniques de mesure précises afin d'obtenir des informations concernant le comportement physique de matériaux anisotropes. Tous sont des sujets de recherche en cours.

De ce fait, le choix entre l'utilisation de modèles isotropes ou anisotropes lors de la modélisation de matériaux poreux, dépend e.g. de la précision nécessaire, du type de

matériaux poreux à modéliser, de la structure dans lequel il est implémenté, et de la disponibilité éventuelle des paramètres matériaux anisotropes.

2.3 Modélisation aux Éléments Finis (EF)

Les solutions analytiques des équations de Biot existent seulement dans un certain nombre de cas, où les équations peuvent être réduites à un problème 1D, e.g. un plan infini, un problème à symétrie sphérique ou cylindrique infini. Dans la plupart des applications, la complexité du problème nécessite la recherche d'une solution numérique qui permet de prendre en compte des géométries complexes de taille finie, une distribution non-uniforme des conditions aux limites et des chargements, ainsi que le couplage éventuel avec d'autres composants (poreux, solides ou fluides). Ces questions et plusieurs autres ont été abordées dans des travaux antérieurs (cas isotropes et anisotropes) par Hörlin et Göransson [20], Hörlin [19] et Hörlin *et al.* [21], où des solutions tridimensionnelles fondées sur des éléments finis hp [1] ont été développées et évaluées. Afin de déterminer des solutions aux éléments finis pour les équations aux dérivées partielles couplées décrivant le comportement d'un système, il est nécessaire de formuler une forme faible des équations aux dérivées partielles incluant les conditions aux limites. Dans ces travaux, Hörlin évalue différentes formulations faibles, parmi lesquelles une formulation mixte déplacement-pression pour des matériaux poreux isotropes a été proposée par Atalla *et al.* [4, 5]. Cette formulation mixte déplacement-pression a été plus tard étendue par Hörlin et Göransson [20] afin de prendre en compte les matériaux anisotropes. Elle utilise le déplacement de la structure comme variable primale décrivant le mouvement de la structure, et la pression du fluide comme variable primale décrivant le fluide, i.e. formulation (u^s, p), alors que les formulations faibles plus répandues utilisent le déplacement de la structure et du fluide comme variables primales, i.e. formulations (u^s, u^f). Ces dernières requièrent des ressources de calculs importantes lorsqu'appliquées à des systèmes éléments finis de grandes dimensions. La formulation (u^s, p) comme proposée par Atalla *et al.* [5] est considérée aussi précise que la formulation classique (u^s, u^f) avec l'avantage qu'elle demande moins de ressources de calculs pour une même précision de calcul demandée. Elle décrit le matériaux poreux avec un minimum de variables de champ indépendantes, permettant le couplage de deux composants à pores ouverts et celui d'un composant à pores ouverts avec un composant solide, sans introduire d'intégrales de couplage supplémentaires, si les parties solides sont naturellement couplées. Cependant, il s'avère nécessaire d'introduire des intégrales de couplage si il y a couplages entre des composants poreux et des fluides. Cette formulation mixte déplacement-pression proposée vient étayer les travaux actuels d'étude des améliorations possibles d'adaptation des matériaux poreux à des applications spécifiques.

[1] la convergence est obtenue en raffinant le maillage et / ou en augmentant l'ordre d'approximation.

2.4 Corrélations entre les propriétés macroscopiques et microscopiques

Comme mentionné précédemment, les matériaux poreux peuvent être décrits à partir de leurs propriétés macroscopiques homogénéisées, dont plusieurs ont été présentées dans les équations ci-avant. Ces propriétés macroscopiques sont naturellement dépendantes des propriétés géométriques microscopiques et de la nature du matériau de la structure. Ces propriétés géométriques microscopiques sont, par exemple, la taille et la forme des pores, et la section transversale et l'épaisseur des poutres, ou fibres, dans le matériau à pores ouverts. De telles propriétés microscopiques, ainsi que le choix des matériaux, définissent le comportement thermique, élastique, viscoélastique, mécanique et acoustique des matériaux poreux. De ce fait, les propriétés macroscopiques ne peuvent pas être considérées comme indépendantes les unes des autres et ne conviennent donc pas comme variables dans un problème d'optimisation. L'objectif de cette thèse a donc été d'utiliser des lois d'échelle qui relient les propriétés macroscopiques aux propriétés microscopiques sous-jacentes. Ces lois d'échelle devraient de préférence décrire les propriétés macroscopiques des matériaux poreux comme étant continuellement et systématiquement dépendantes des propriétés mécaniques micro-structurelles, permettant de se concentrer directement sur les propriétés microscopiques lors de l'optimisation. Plusieurs chercheurs ont contribué au développement de formulations mathématiques reliant les différentes propriétés matériaux entre elles. Dans le cas d'une structure de mousse à cellules ouvertes avec une porosité élevée, où le matériau des poutres est significativement plus lourd que le fluide interstitiel, l'approche développée par Gibson et Ashby [15] peut fournir des indications importantes pour comprendre le comportement mécanique d'une telle mousse. Gibson et Ashby définisse la structure cellulaire comme une série de sommets reliés par des arêtes. Une configuration très simple consiste en une cellule de forme cubique où les cellules adjacentes sont échelonnées de telle sorte qu'elles se coupent aux points médians, mais le raisonnement est tout aussi valable pour des structures cellulaires plus complexes comme e.g. des dodécaèdres rhombiques ou des tétrakaidécaèdres, fig. 2.3. La structure tétrakaidécaèdre, également appelée cellule de Kelvin, est un choix fréquent parce qu'elle présente un nombre moyen d'arêtes par face, et de faces par cellule, qui semble correspondre de manière satisfaisante à certaines observations, bien que ces travaux nécessitent des compléments [15, 30]. Des études récentes [12] montrent que de telles lois d'échelle fournissent des résultats assez satisfaisants, bien qu'elles se fondent sur des structures de cellules simplifiées et sur d'autres hypothèses implicites qui ne peuvent pas être complètement respectées.

En supposant que la cellule géométrique est isotrope, on montre que, pour toutes les formes de cellules (des mousses) mentionnées ci-avant, la densité relative , ρ^*, pour des mousses cellulaires, est proportionnelle à la longueur et à l'épaisseur des poutres, respectivement, l_s et d_s.

(a) cubique (b) dodécaèdre rhombique (c) tétrakaidécaèdre

Figure 2.3: Exemples de formes de cellule théoriques selon Gibson et Ashby.

$$\frac{\rho^*}{\rho_s} = C^\rho \left(\frac{d_s}{l_s}\right)^2 \tag{2.23}$$

où C^ρ est une constante dépendante de la forme de la cellule et de la forme de la section transversale de la poutre, proche de l'unité pour une mousse à cellule ouverte avec des formes de cellules assez complexes. ρ_s représente la densité du matériau de la structure. Supposant connues les caractéristiques d'une mousse de référence, noté $(.)_{ref}$, mise à l'échelle mais gardant sa structure générale (cellule et forme de poutre), la densité relative peut s'exprimer par:

$$\rho^* = \rho^*_{ref} \left(\frac{d_s}{d_{ref}}\right)^2 \left(\frac{l_{ref}}{l_s}\right)^2. \tag{2.24}$$

L'hypothèse stipulant que le matériau de la poutre est significativement plus lourd que le fluide interstitiel permet d'exprimer la porosité comme suit:

$$\phi = 1 - \frac{\rho^*}{\rho_s}. \tag{2.25}$$

Pour modéliser la variation du module de Young à partir des propriétés microscopiques, les poutres sont supposées se déformer essentiellement en flexion. On suppose de plus que les déformations sont petites et que le comportement du matériau des poutres est élastique linéaire. La déformation au niveau macroscopique peut être couplée à la déformation des poutres dans une cellule cubique en appliquant la théorie des poutres. Si le module de Young de la mousse est calculé comme la déflexion d'une poutre de longueur l_s soumise à mi-longueur à la force F, la déflexion, δ, est proportionnelle à Fl_s^3/E_sI, où E_s est le module de Young du matériau de la structure et I le moment d'inertie de la forme de la poutre, $I \propto d_s^4$. A une échelle macroscopique, la force est fonction de la contrainte de compression macroscopique, σ^*, $F \propto \sigma^* \cdot l_s^2$ et la déformation macroscopique, ε^*, est fonction de la déflexion de la poutre $\varepsilon^* \propto \delta/l_s$. Le module de Young de la mousse peut ainsi être exprimé par:

$$E^* = \frac{\sigma^*}{\varepsilon^*} = \frac{C^{dl} E_s I}{l_s^4} \quad \rightarrow \quad \frac{E^*}{E_s} = C^{dl} \left(\frac{d_s}{l_s}\right)^4 = C^E \left(\frac{\rho^*}{\rho_s}\right)^2 \tag{2.26}$$

ou, lorsque l'on utilise un matériau de référence, par:

$$E^* = E^*_{ref} \left(\frac{\rho^*}{\rho^*_{ref}}\right)^2. \tag{2.27}$$

De vastes travaux par Allard et Champoux [3] et Allard [2] ont également contribué à établir des relations entre les propriétés macroscopiques des mousses et les propriétés structurelles microscopiques. Ces travaux ont été utilisés par Göransson afin de continuer à développer des lois d'échelle qui mettent en relation la longueur visqueuse caractéristique, Λ, et la résistance statique à l'écoulement, σ^{static}, avec la microstructure de la mousse [16]. En supposant un écoulement non visqueux autour d'un cylindre, Allard et Champoux montrent que si la porosité est proche de un, Λ est donnée par:

$$\Lambda = \frac{1}{2\pi L r} \tag{2.28}$$

où L est la longueur totale du cylindre par unité de volume et r est le rayon du cylindre [3]. En retenant la précédente hypothèse de géométrie de cellule, L peut être définie en fonction de la porosité par $\pi r^2 L = \rho^*/\rho^s$, la longueur visqueuse caractéristique s'exprimant alors par [16]

$$\Lambda = \frac{d_s}{4(\rho^*/\rho_s)} = \frac{d_s}{4(1-\phi)}. \tag{2.29}$$

Afin de prendre en compte les effets thermiques, l'hypothèse simplificatrice concernant la longueur caractéristique thermique, Λ', $\Lambda' = 2 \cdot \Lambda$ est retenue. Étant donné que la tortuosité des matériaux hautement poreux est très dépendante de la quantité de pores fermés, et que les matériaux utilisés dans cette thèse sont supposés à pores ouverts, la variation de tortuosité est très faible lorsque les propriétés des matériaux sont modifiées. Toutefois, une loi d'échelle fondée sur le travail de Comiti et Renaud, [11], a été implémentée dans les Articles II et III,

$$\alpha_\infty = 1 - \frac{1-\alpha_{\infty ref}}{\ln(\phi_{ref})} \cdot \ln(\phi). \tag{2.30}$$

De plus, il a été démontré par Allard que Λ peut s'exprimer en fonction des propriétés macroscopiques par:

$$\Lambda = \frac{1}{c_g} \sqrt{\frac{8\alpha_\infty \eta}{\phi \sigma^{static}}} \tag{2.31}$$

où c_g est dépendant de la forme de la coupe transversale des pores. Pour des géométries cylindriques on a $c_g = 1$ [2]. Eq. (2.29) et eq. (2.31) donnent:

$$\sigma^{static} = \frac{8\alpha_\infty \eta}{1-(\rho^*/\rho_s)} \cdot \frac{16(\rho^*/\rho_s)^2}{d_s^2 c_g^2} \tag{2.32}$$

qui, lorsqu'on utilise un matériau de référence, peut s'exprimer par:

$$\sigma^{static} = \sigma_{ref}^{static} \left(\frac{\rho^*}{\rho_{ref}}\right)^2 \cdot \left(\frac{d_{ref}}{d_s}\right)^2 \cdot \frac{\alpha_\infty}{\alpha_{\infty ref}} \cdot \frac{\left(1-\frac{\rho_{ref}}{\rho_s}\right)}{\left(1-\frac{\rho^*}{\rho_s}\right)}. \tag{2.33}$$

2.5 Points notables sur le problème d'optimisation

Pour résoudre un problème d'optimisation, il est nécessaire d'établir une fonction objectif, $f(\mathbf{x})$, qui fournit une valeur numérique représentant les qualités recherchées. La fonction objectif dépend d'une ou plusieurs variables de conception, $\mathbf{x} = [x_1\ x_2 \cdots x_\mathrm{n}]$, avec $\mathbf{x}_\mathrm{min} \leq \mathbf{x} \leq \mathbf{x}_\mathrm{max}$ et peut également être soumise à différentes fonctions de contrainte, $g_\mathrm{i}(\mathbf{x})$. Le problème d'optimisation est souvent présenté sous la forme suivante:

$$\begin{aligned} \min \quad & f(\mathbf{x}) \\ \text{subject to} \quad & g_1(\mathbf{x}) \leq 0 \\ & g_2(\mathbf{x}) \leq 0 \\ & \vdots \\ & g_\mathrm{M}(\mathbf{x}) \leq 0 \\ & \mathbf{x}_\mathrm{min} \leq \mathbf{x} \leq \mathbf{x}_\mathrm{max} \end{aligned} \tag{2.34}$$

Le choix de la fonction objectif et des contraintes est souvent une tâche plus délicate qu'il n'en parait, étant donné qu'il y a souvent plusieurs objectifs à atteindre qui dépendent de différentes variables de conception, communes ou non. Les objectifs définis dans cette thèse, i.e. réduction de l'inconfort acoustique ou réduction de la masse, sont souvent utilisés dans la pratique. D'autres objectifs peuvent impliquer, par exemple, de minimiser le coût des matériaux, l'impact environnemental, le temps d'assemblage ou la consommation de carburant, et le minimum d'un objectif coïncide rarement avec le minimum d'autres. Le problème peut être traité en minimisant un objectif tout en imposant une contrainte aux autres ou en développant une fonction objectif qui intègre plusieurs objectifs dans une seule fonction, par exemple sous forme de somme pondérée. Il existe plusieurs façons d'établir une fonction objectif, tâche non des moindres étant donné que le résultat de l'optimisation dépend inévitablement en grande partie du choix de la fonction objectif et des contraintes.

Dans la pratique, l'optimisation est souvent mise en oeuvre par une forme d'algorithme.

Si les fonctions sont différentiables et dépendantes de variables de conception continues, un algorithme du gradient est souvent approprié. Un tel algorithme requiert des informations sur les valeurs numériques de la fonction objectif, du vecteur gradient et de la matrice Hessienne de la fonction objectif par rapport à $\mathbf{x}$, ainsi que la valeur numérique des fonctions contraintes, des gradients, et les valeurs minimum et maximum des variables de conception. A partir des données d'entrée, l'algorithme fournit des nouveaux paramètres de conception pour lesquels la fonction coût est calculée et ainsi de suite itérativement jusqu'à réalisation d'un critère d'arrêt. Dans des applications pratiques, la fonction objectif et/ou les fonctions contraintes sont souvent très complexes et le résultat d'une simulation par ordinateur. Cela nécessite souvent que les valeurs de gradient et de la matrice Hessienne soient calculées numériquement, en utilisant par exemple les différences finies, entraînant une hausse du coût de calcul pour chaque variable de conception utilisée, et chaque itération pour trouver un minimum.

Une autre difficulté rencontrée lorsqu'une démarche d'optimisation est utilisée est le fait que les fonctions objectifs ne sont pas convexes, c'est à dire, qu'il peut exister un ou plusieurs minima locaux au sein du domaine du paramètre qui ne correspondent pas à la meilleur solution. La meilleure solution est plutôt appelée le minimum global. Ce problème est souvent traité en utilisant plusieurs points d'entrée distincts au sein du domaine du paramètre par comparaison du nombre de minima locaux avec la valeur des fonctions objectifs à ces minima locaux.

Chapter 3

Étude des matériaux poro-élastiques dans des structures multicouches

Ces travaux explorent la possible modification des propriétés microscopiques de matériaux poro-élastiques spécifiques lorsqu'ils sont assemblés dans des panneaux acoustiques multicouches ou multifonctionnels. Bien que la modélisation isotrope constitue la majeure partie de ce travail , l'influence des propriétés matériaux anisotropes et de l'orientation angulaire de ces propriétés est également abordé. Ces études ont consisté en des simulations numériques utilisant la théorie de Biot et l'approche numérique EF décrite dans le chapitre 2. Les modifications des propriétés matériaux ont été choisies en utilisant un optimiseur basé sur un algorithme du gradient [32, 33].

Alors que l'optimisation des propriétés macroscopiques des matériaux poreux utilisée dans le modèle de Johnson-Champoux-Allard permet de fournir certaines informations concernant les possibles combinaisons des propriétés matériaux, elle ne permet pas de déterminer quel type de matériau poreux utiliser ou comment atteindre de telles propriétés dans un matériau poreux. Le matériau résultant serait alors certainement physiquement impossible à réaliser, ce qui rend une telle optimisation peu utile de manière pratique. En décrivant le matériau poro-élastique à partir de ses propriétés microscopiques et en en estimant les paramètres macroscopiques correspondants, le matériau ainsi défini pourra, s'il n'existe pas déjà, être complètement décrit et sera de manière pratique possible à réaliser. D'où la nécessité des lois d'échelle décrites précédemment qui permettent de fournir des corrélations approximatives entre les paramètres microscopiques et macroscopiques.

Afin d'examiner le comportement acoustique et dynamique des matériaux poro-élastiques assemblés dans des panneaux multicouches, un certain nombre de panneaux comprenant des matériaux poreux isotropes ou anisotropes ont été évalués numériquement. Les panneaux ont été excités par différents types de champs de force et les propriétés acoustiques et dynamiques ont été exprimées comme fonction objectif ou fonction contrainte afin de permettre une optimisation. Une telle fonction peut être

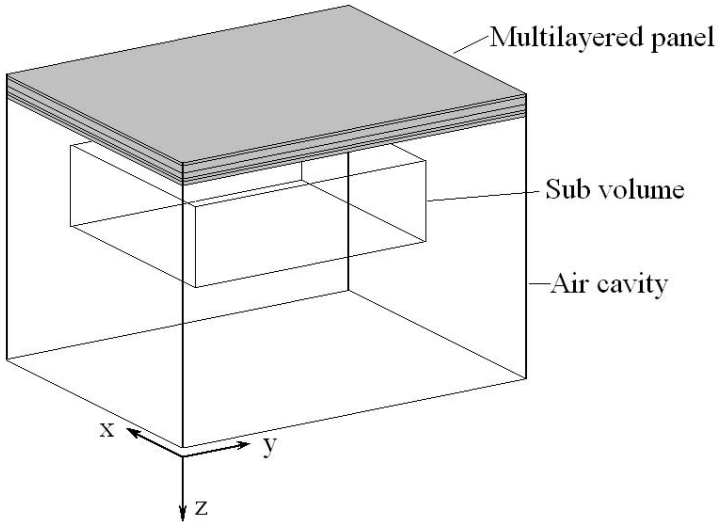

Figure 3.1: Schéma de principe du panneau multicouche connecté à une partition d'une cavité d'air.

choisie d'un certain nombre de façons différentes, mais il n'est pas simple de formuler une description qualitative du son en utilisant une valeur numérique quantitative. Ce dernier aspect représente un champ de recherche à part entière. Dans cette thèse, les mesures acoustiques et dynamiques ont été réalisées sous la forme de réponse acoustique dans une partition d'une cavité d'air connectée au panneau multicouche étudié, fig. 3.1. La réponse acoustique choisie est le niveau de pression acoustique (Sound pressure level - SPL), intrinsèquement dépendant des différents paramètres de conception. La pression acoustique au carré, p_f^2, pour chaque fréquence considérée, f, est calculée comme la moyenne du quarré de la pression acoustique dans un nombre, N, de points dans la partition choisie, eq. (3.2). Cette quantité est par la suite multipliée par la fréquence de résolution, Δf_f, et un facteur de pondération dépendant de la fréquence, C_f, divisée par la pression acoustique de référence au carré, p_0^2, et additionnée sur le domaine de fréquence en entier, eq. (3.1), aboutissant à un niveau de pression acoustique totale, SPL, qui est ensuite minimiser ou maximiser.

$$\langle SPL \rangle_{\Omega_{\text{sub}}}^{C} = 10 \cdot \log \left(\frac{\sum_{f=f_1}^{f_{\max}} \left(p_f^2 \cdot \Delta f_f \cdot C_f \right)}{p_0^2} \right) \tag{3.1}$$

où

$$p_f^2 = \frac{1}{N} \sum_{n=1}^{N} p_{f_n}^2 . \tag{3.2}$$

Comme la pression acoustique totale dans la cavité d'air est calculée pour chaque

fréquence dans le domaine de fréquence choisi, le coût en terme de ressource et temps de calcul pour évaluer eq. 3.1 peut être conséquent. De plus, lorsque les gradients sont calculés en utilisant les différences finies, une autre évaluation de $\langle SPL \rangle^{C}_{\Omega_{\text{sub}}}$ est nécessaire pour chaque variable de conception. Il est de ce fait très important, dans le processus d'optimisation, de trouver le minimum avec un nombre d'itérations aussi faible que possible. L'optimiseur retenu ici est un optimiseur basé sur la méthode des asymptotes mobiles (Method of Moving Asymptotes - MMA), et ultérieurement sa version globalement convergente [32, 33]. Cet optimiseur fournit de bons résultats en utilisant moins d'itérations que les autres testés.

3.1 Adaptation des paramètres des matériaux poreux pour une performance acoustique améliorée

Un modèle 2D isotrope a d'abord été utilisé pour modéliser un panneau à sept couches, parmi lesquelles une couche a été optimisée microstructurellement. Ce modèle admet pour variables de conception la masse volumique apparente, ρ^*, et l'épaisseur de la poutre, d_s. Le facteur de pondération de l'équation 3.1 est fixé afin de correspondre à la pression acoustique totale avec filtre décibel A ou C. Deux types de mousse poro-élastique à cellule ouverte sont utilisées: une mousse à base de polyuréthane, mousse-PU, et une mousse à base de polyimide, mousse-π. Cinq optimisations différentes ont été effectuées: minimisation de la pression acoustique totale avec filtre décibel A et contrainte sur la masse en utilisant la mousse-PU, minimisation de la pression acoustique totale avec filtre décibel C et contrainte sur la masse en utilisant la mousse-PU, minimisation de la pression acoustique totale avec filtre décibel C et contrainte sur la masse en utilisant la mousse-*pi*, et enfin minimisation de la masse en utilisant, respectivement, la mousse-PU et la mousse-*pi*, et des contraintes sur la pression acoustique totale avec filtre décibel C. La pression acoustique totale a été évaluée sur un domaine de fréquence 100 – 900 Hz. Des contraintes ont également été mises sur les variables de conception afin d'exclure tout résultat n'ayant aucun sens physique.

En utilisant différents points de départ, le minimum final reste inchangé, indiquant que les fonctions objectifs utilisées sont relativement convexes pour l'espace des paramètres et le domaine de fréquence choisi pour ces simulations. Les paramètres de conception résultants montrent également que la fonction filtre a un impact majeur sur le résultat de l'optimisation. En utilisant un filtre décibel A pour la pression acoustique totale, le minimum se trouve à ρ^*=32.5 kg m^{-3} et d_s=14.8×10^{-6} m alors que le minimum se trouve à ρ^*=20.1 kg m^{-3} et d_s=15.5×10^{-6} m en utilisant filtre décibel C pour la pression acoustique totale. En comparant les fonctions de réponse en fréquence, FRF, des panneaux optimisés avec les FRF des panneaux comprenant une mousse avec des paramètres de conception qui ne sont pas optimaux, on remarque que les possibilités d'amélioration du comportement acoustique et dynamique sont significatives,

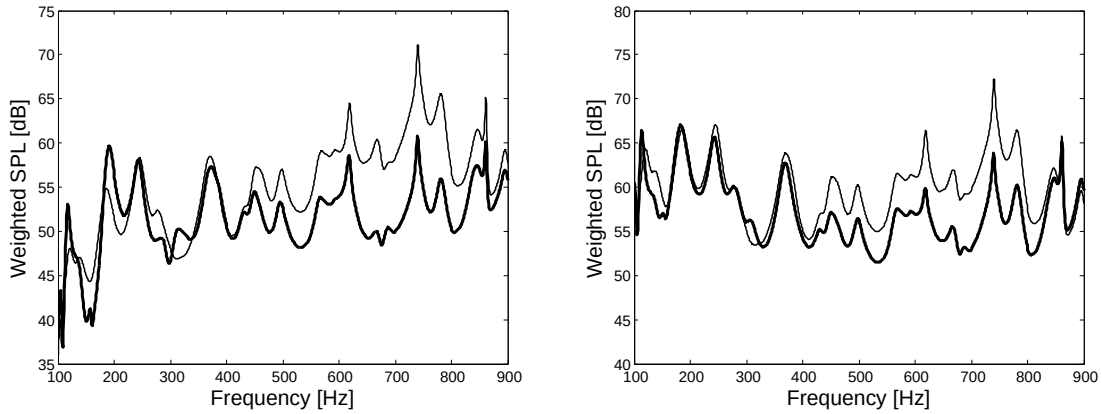

(a) FRF avec filtre décibel A

(b) FRF avec filtre décibel C

Figure 3.2: Fonction de réponse en fréquence pour la solution optimale de mousse (trais épais) et la solution sous-optimale de mousse (trais fin), avec filtre décibel, respectivement, A (à gauche) et C (à droite).

voir fig. 3.2.

En comparant des panneaux comprenant, respectivement, une mousse-PU et une mousse-π, pour ceux avec filtre décibel C pour la pression acoustique, on note que les résultats du panneau comprenant la mousse-PU sont légèrement meilleurs. D'autre part, en minimisant la masse en utilisant des contraintes sur la pression acoustique totale avec filtre décibel C, c'est la mousse-π qui démontre de meilleurs résultats.

L'influence de l'anisotropie a été examinée à l'aide d'un modèle 3D de panneau multicouche quadratique constitué de deux feuilles d'aluminium séparées par deux couches de matériaux poro-élastiques, liées élastiquement à la feuille d'aluminium sur laquelle l'excitation est appliquée, et séparées par une mince couche d'air de l'autre feuille d'aluminium. Deux différents types de panneau ont été utilisés: la configuration A, comprenant une mousse à cellule ouverte orthotrope, et la configuration B, comprenant un matériau fibreux isotrope transverse. Pour chaque configuration, les deux couches sont composées du même type de matériau. Les seules variations introduites sont l'orientation relative des propriétés matériaux dans chaque couche, lesquelles peuvent pivoter indépendamment dans différentes directions et de ce fait induire des propriétés dynamiques globales différentes selon la direction d'excitation, voir fig. 3.3.

La description de l'anisotropie des matériaux poreux se limite à celle de la matrice de Hooke, du tenseur de résistance à l'écoulement et du tenseur de tortuosité. La fonction objectif choisie est la pression acoustique totale sans filtre, éq. 3.1, et les variables de conception sont les angles d'Euler décrivant un axe de rotation fixe Z-Y-X. Les deux couches de poreux pouvant pivoter indépendamment l'une de l'autre et la rotation autour de l'axe z étant redondante pour les matériaux poreux isotropes transverses, le nombre de variables de conception nécessaires est de six pour la configuration A et de quatre pour la configuration B. Les deux minimisations et maximisations ont été effectuées pour un certain nombre de points de départ différents.

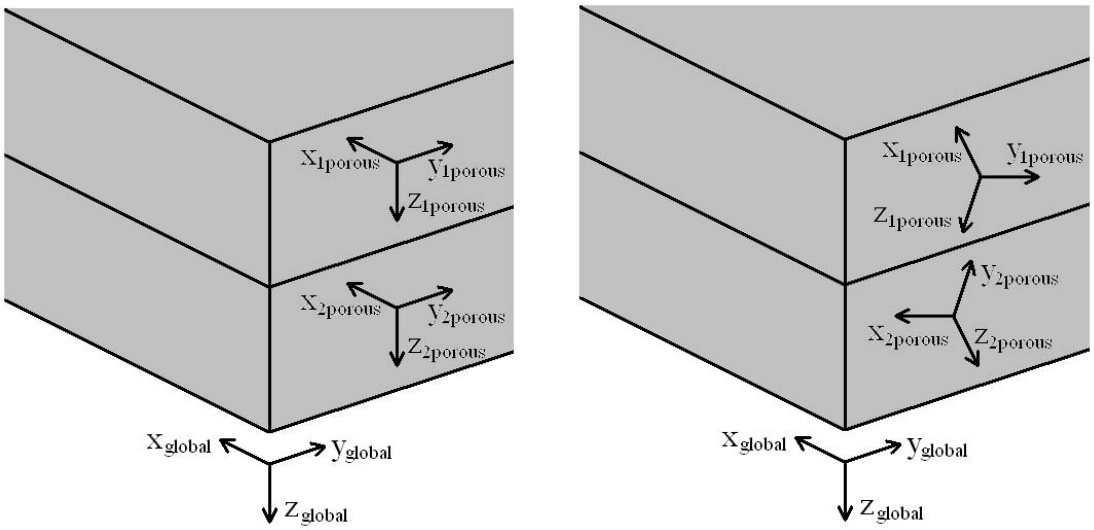

(a) Orientation du matériau poreux avec rotation-[0 0 0] pour chaque couche.

(b) Orientation du matériau poreux avec différentes rotation-[α β γ] pour la couche 1 et la couche 2.

Figure 3.3: Système de coordonnées globaux et locaux et exemple de rotations possibles des couches 1 et 2 dans le panneau utilisé pour la modélisation anisotrope.

Bien que les différents points de départ aient donné plus d'un minimum et maximum, la FRF des différents minima et maxima, correspondant à différentes orientations du matériau, montre de grandes similitudes. Les différences de pression acoustique entre les différents minima sont par ailleurs inférieurs à 0,5 dB. Les résultats globaux montrent que les propriétés acoustiques et dynamiques des panneaux sont sensibles aux variations angulaires des matériaux poreux anisotropes. La différence entre le meilleur des cas et le pire des cas est de 4.6 dB pour la configuration A et de 4.7 dB pour la configuration B.

3.2 Méthode combinée d'optimisation structurelle et acoustique – un outil de conception pluridisciplinaire

Traditionnellement, la problématique des nuisances sonores et vibratoires n'est prise en compte qu'à un stade avancé de la conception, lorsque les principales pièces de la structure sont déjà conçues, et parfois même à un stade encore ultérieur, lorsque le bruit, les vibrations et la rudesse (NVH) sont un fait inévitable. Cette approche implique généralement la nécessité d'un traitement a posteriori de nouvelles conceptions légères, ce qui les rend moins optimisées du point de vue de la masse du véhicule et plus chère qu'initialement prévue. Un outil de conception permettant de prendre en compte les problèmes structurels et acoustiques à un stade précoce de la conception, permettrait de rendre de tels "traitements après coup" redondants. Il serait également avantageux

qu'un tel outil de conception puisse tenir compte des propriétés mécaniques structurelles propre aux matériaux poro-élastiques, bien que limitées. Il en est de même vis à vis des propriétés d'amortissement acoustique naturelles des structures à sandwich légères, tout cela étant idéalement intégré dans un seul processus de conception. Une partie du présent travail a été consacrée à cette problématique complexe de développement d'une méthode combinée d'optimisation structurelle et acoustique de panneaux multicouches, tout en garantissant un temps de calcul raisonnable par rapport aux standards actuels.

Le point de départ de ce concept d'optimisation est de remplacer le toit conventionnel d'une voiture, fig. 3.4, par un panneau multicouche comprenant à la fois des matériaux poreux structurels et acoustiques. Tout en répondant aux exigences structurelles, ce panneau est optimisé en considérant la masse et les propriétés acoustiques et dynamiques du véhicule.

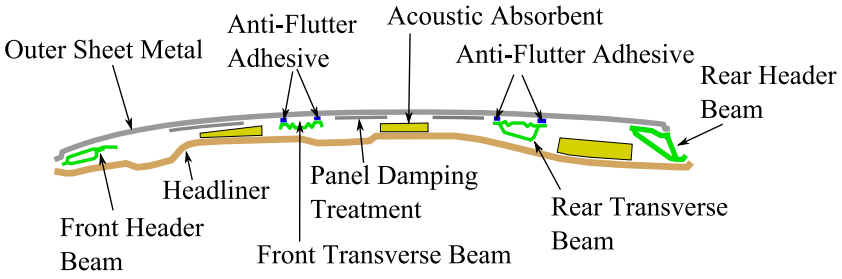

Figure 3.4: Schéma de principe d'un toit conventionnel de voiture.

Le panneau multicouche est représenté par un quart de modèle plan présentant des conditions aux limites de symétrie appliquées dans toutes les couches le long des axes de symétrie. La plaque perforée interne est également fixe dans les directions x, y et z le long de x=0 et y=0. Les forces dynamiques sont appliquées dans les directions x, y et z dans un domaine de fréquence 100 – 500 Hz, voir fig. 3.5. Étant donné que le toit est représenté par un panneau plat dans le modèle numérique, les effets de la surface à double courbure d'un toit classique ont été omis. En outre, il est à noter que les conditions aux limites de symétrie exclues la possibilité de modes de vibration non-symétriques. On ne peut donc pas directement comparer les résultats de la simulation avec ceux d'un toit conventionnel. Cependant, les méthodologies de conception présentées sont valides au sein de leur propre prémisse et pourraient à l'avenir être transférées à des formes plus complexes de panneaux.

La conception générale du panneau léger remplaçant le toit de voiture conventionnel comprend, en externe, une feuille de fibre de carbone (CF) renforcée par un laminé composite à base d'époxy, et, en interne, une feuille de plastique à renfort de fibre de verre. Au milieu des deux feuilles, différentes combinaisons de matériaux poreux structurels et acoustiques ont été utilisées, voire, dans certaines configurations, des couches ou des poches d'air ont été introduites. Pour des raisons pratiques (ressources informatiques), le processus d'optimisation a été divisé en différentes parties lesquelles ont été exécutées dans un ordre séquentiel de manière itérative.

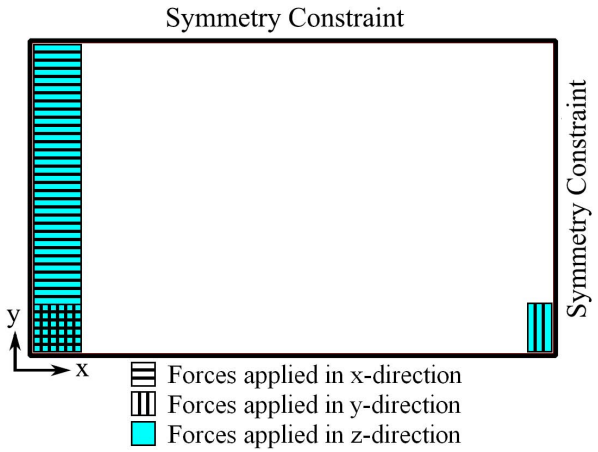

Figure 3.5: Forces dynamiques appliquées au laminé de CF.

Quatre configurations différentes ont été testées initialement, dans lesquelles la mousse structurelle et acoustique a été divisée en plusieurs couches, voir fig. 3.6, sauf autour des arêtes du quart de modèle où la mousse structurelle est directement connectée aux feuilles internes et externes. La mousse A est une mousse-PU et la mousse B une mousse-π.

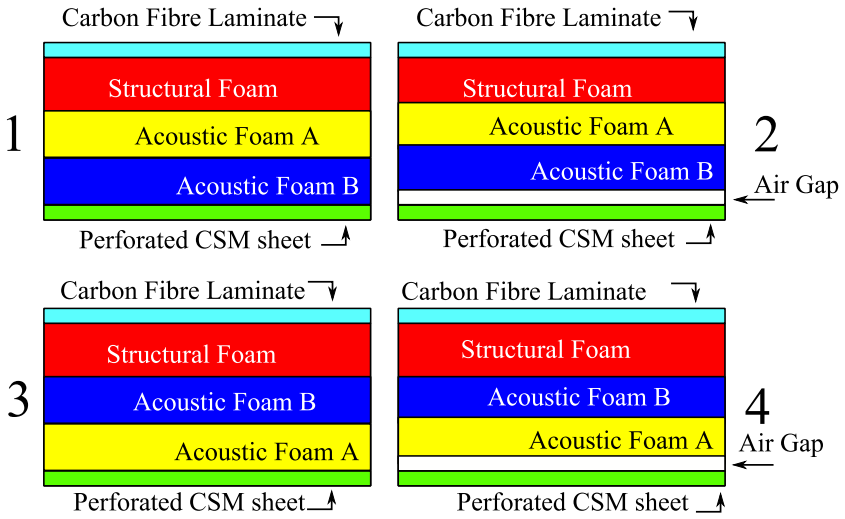

Figure 3.6: Différentes configurations du multicouche.

Le processus itératif commence avec une optimisation de la masse structurelle dans laquelle trois différents cas de chargement sont appliqués (chargement localisé, distribution de pression, analyse modale) et neuf variables de conception et contraintes sont utilisées pour la raideur locale et globale afin que le système n'excède pas un déplacement donné, ni localement ni globalement, et afin que la première fréquence propre du panneau ne dépasse pas un minimum donné. Des contraintes sont également imposées aux neuf variables de conception. Des hypothèses générales ont été émises vis à vis des propriétés des couches acoustiques. Une optimisation acoustique est par la suite effectuée, permettant une optimisation de la longueur relative des poutres et des épaisseurs des couches des deux couches de mousse, en imposant des contraintes sur

l'épaisseur totale. Les résultats de l'optimisation acoustique servent ensuite de données d'entrée pour une deuxième itération commençant par une optimisation structurelle. La convergence est atteinte après deux à trois itérations. Les résultats sont en partie résumés dans la table 3.1.

		Configuration			
		1	2	3	4
Variable		PU-π	PU-π-air	π-PU	π-PU-air
ρ_{poutre}	[kg/m^3]	134	128	143	141
ρ^*_{PU}	[kg/m^3]	38.6	138	138	138
t_{PU}	[mm]	23.0	48.0	47.2	41.5
ρ^*_{pi}	[kg/m^3]	9.31	1.48	2.46	3.86
t_{pi}	[mm]	27.0	1.00	2.46	4.59
Épaisseur totale	[mm]	79.1	78.7	78.7	75.8
Masse totale	[kg]	18.7	27.3	27.8	26.7
Premier mode propre	[Hz]	71.8	46.9	64.7	47.0
SPL	[dB]	60.1	59.3	57.9	58.5

Table 3.1: Résumé des valeurs finales des variables de conception et principaux résultats.

Pendant le processus d'optimisation, on a pu observé que la configuration du multi-couches a une forte influence sur la réponse acoustique du panneau, tout particulièrement pour les configurations sans la couche d'air. Le fait d'introduire une couche d'air résulte en un panneau inévitablement plus mou, présentant un premier mode propre significativement inférieur. Cela est prévisible étant donné que la liaison entre le matériau de la structure et les feuilles est essentielle si l'on souhaite obtenir un panneau sandwich léger et rigide. Malgré sa consistance molle, la présence et le couplage de la mousse acoustique avec les surfaces internes semblent être suffisants pour l'éviter de vibrer et augmenter la raideur de l'ensemble.

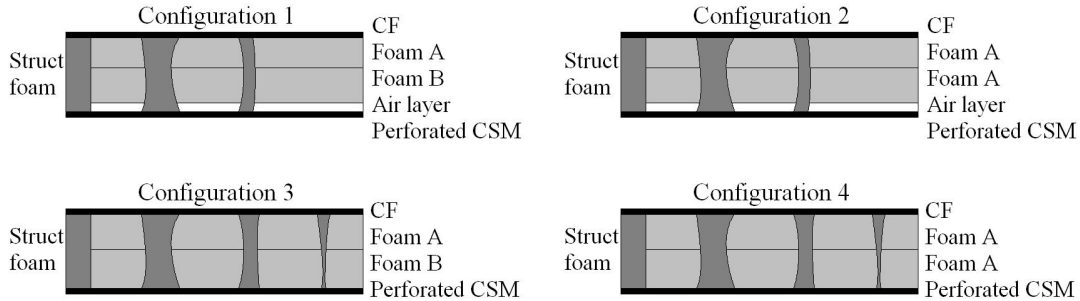

Figure 3.7: Représentation conceptuelle des quatres différentes configurations. Notons que la topologie de la mousse structurelle (gris foncé) diffère entre les configurations comprenant une couche d'air et sans couche d'air.

Pour deuxième étape de cette méthode de conception pluridisciplinaire, la mousse structurelle n'est plus placée dans une couche qui lui est propre mais plutôt distribuée au sein du panneau en utilisant l'optimisation topologique sauf le long des bords du panneau où un cadre de mousse structurelle est utilisé. La partie du volume sans mousse

structurelle est divisée en deux couches de mousse acoustique. Quatre configurations différentes sont mises en place parmi lesquelles une couche d'air a été introduite dans deux d'entre elles, fig. 3.7. La mousse A est une mousse-PU et la mousse B une mousse-π.

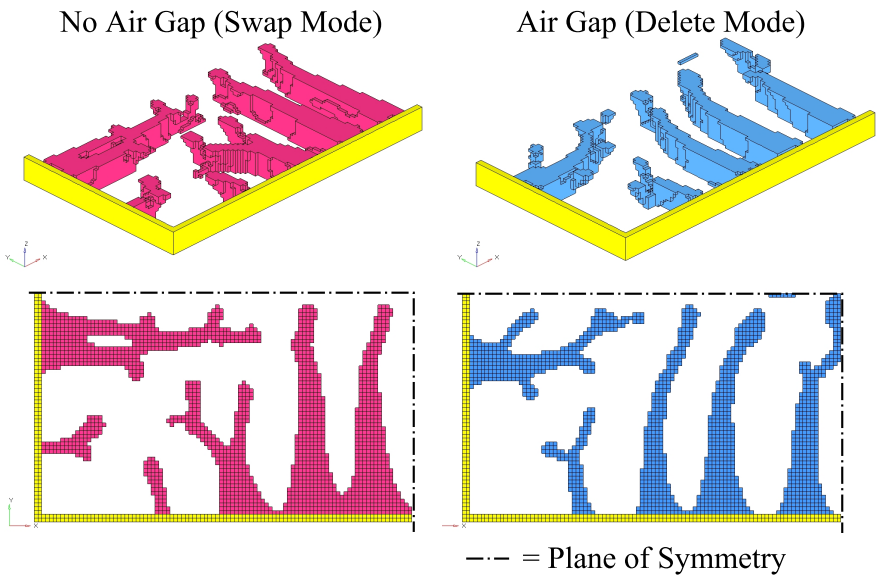

Figure 3.8: Topologie finale de la mousse structurelle dans le modèle 1/4. La partie de gauche est sans couche d'air et celle de droite avec couche d'air. Le cadre d'éléments encastrés est également représenté.

Cette méthodologie débute par une optimisation topologique en utilisant les paramètres généraux de la mousse et quatre cas différents de chargement (chargement localisé, distribution de pression, analyse modale et chargement dans le plan) avec des contraintes sur la raideur locale et globale afin que le système ne dépasse pas un déplacement donné, ni localement ni globalement. Le premier mode propre du panneau doit dépasser une fréquence minimum donnée et une contrainte est mise sur la stabilité dans le plan du panneau (flambage). Il en résulte deux structures de base, une pour les configurations comprenant une couche d'air et une autre pour les configurations sans couche d'air, fig. 3.8. L'étape suivante consiste à obtenir les neuf variables de conception structurelles suivi par l'optimisation des quatre paramètres acoustiques, la longueur relative des poutres et les épaisseurs des deux couches de mousse. Pour des raisons pratiques, le modèle acoustique requiert une augmentation de la taille des éléments par rapport à l'optimisation de structure, voir fig. 3.9. Les résultats sont en partie résumés dans le tableau 3.2.

Les résultats montrent que la mousse acoustique optimisée donne un meilleur niveau de pression acoustique dans la cavité, fig. 3.10. Dans un cas, cependant, cette amélioration est combinée à une pénalité sévère sur la masse. Bien que les configurations un et deux aient les mêmes propriétés de structure, les propriétés acoustiques, influencées uniquement par les couches de mousse acoustiques, sont notablement différentes. La réponse acoustique des configurations trois et quatre montre également que la mousse

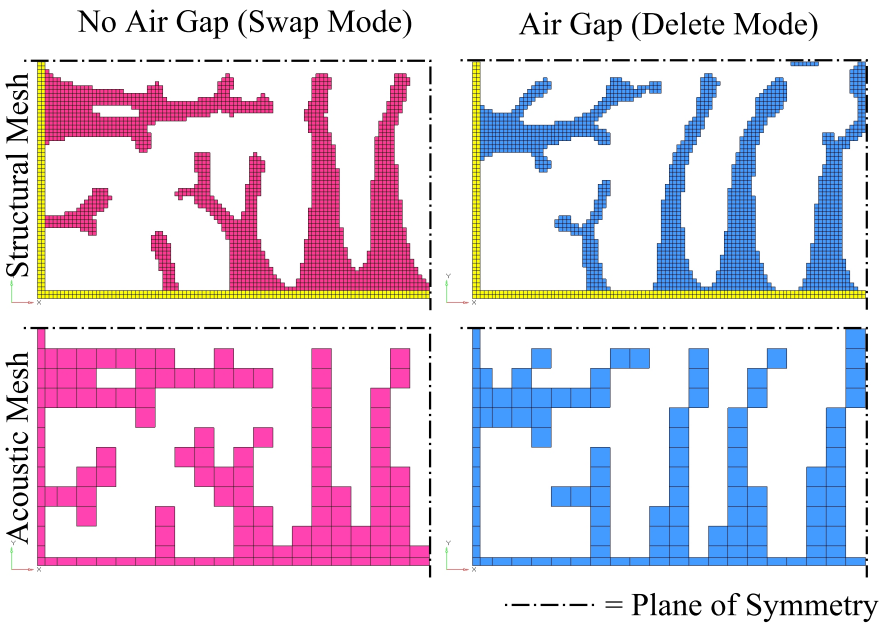

Figure 3.9: Comparaison de mailles EF structurelles (dessus) et acoustiques (dessous) du matériau à coeur de mousse structurelle du modèle 1/4. A gauche sans couche d'air et à droite avec couche d'air. Le cadre d'éléments encastrés est également représenté.

acoustique combinée à différent choix de combinaisons de couche et de propriétés microscopiques, engendre des différences significatives en terme de signature acoustique, fig. 3.11.

		Configuration			
		1	2	3	4
Variable		PU-π-air	PU-PU-air	PU-π	PU-PU
ρ_{poutre}	[kg/m^3]	120	120	105	105
$\rho^*_{couche1}$	[kg/m^3]	36.3	13.5	6.80	5.01
$t_{couche1}$	[mm]	72.9	1.00	1.00	4.08
$\rho^*_{couche2}$	[kg/m^3]	5.29	138	1.96	27.9
$t_{couche2}$	[mm]	1.00	72.9	73.8	70.7
Epaisseur totale	[mm]	77.4	77.4	77.3	77.3
Masse totale	[kg]	18.2	31.6	14.0	17.1
SPL	[dB]	70.5	68.7	74.3	71.6

Table 3.2: Résumé des valeurs finales des variables de conception et résultats principaux.

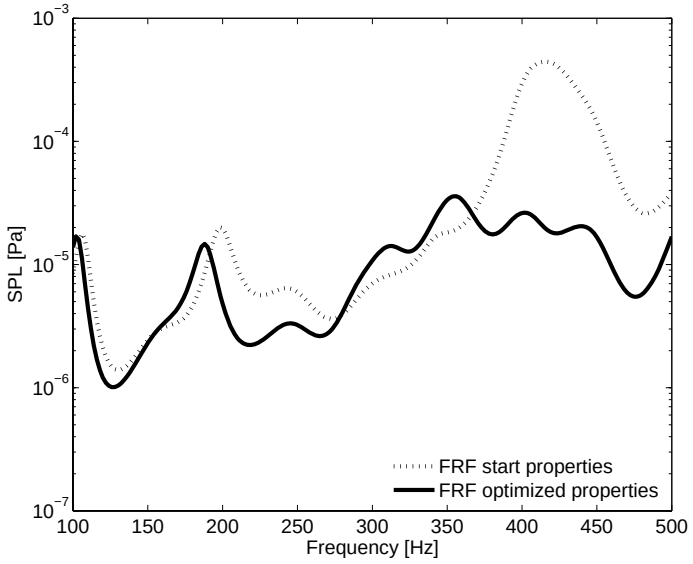

Figure 3.10: Fonction de réponse en fréquence pour les propriétés de départ et les propriétés optimisées de la configuration 1.

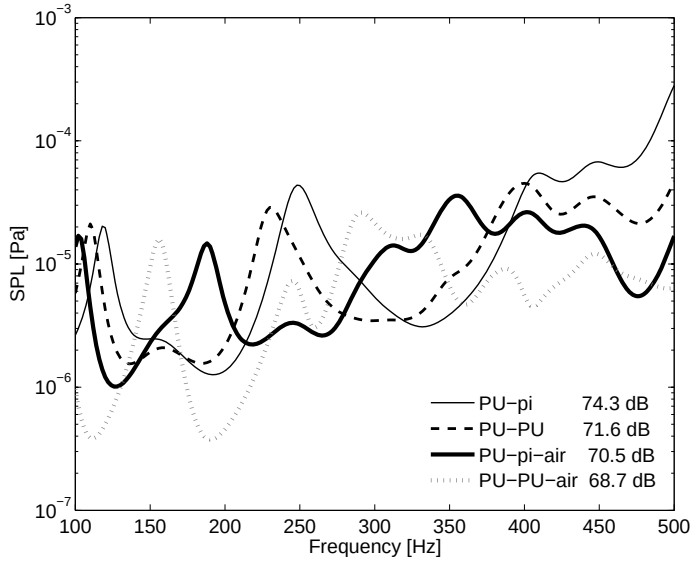

Figure 3.11: Fonctions de réponse en fréquence des propriétés optmisées pour toutes les configurations.

Chapter 4

Conclusions

Le travail présenté dans ce manuscrit montre que de petites modifications des propriétés microscopiques des matériaux poro-élastiques à cellules ouvertes peuvent provoquer des différences dans le comportement macroscopique suffisamment importantes pour impacter la réponse acoustique et dynamique du matériau lorsqu'il est assemblé dans des configurations de panneau multicouches. Dans le cas des matériaux poro-élastiques anisotropes, l'orientation angulaire des propriétés macroscopiques des matériaux dans chaque couche a un impact significatif sur le comportement acoustique et dynamique d'un panneau multicouches. Comme démontré dans des travaux précédents et dans celui-ci, le choix des matériaux poro-élastiques, des combinaisons des couches et des épaisseurs des couches revêt également une grande importance dans la conception des panneaux multicouches. Ces aspects physiques impliquent qu'il existe un fort potentiel pour adapter des structures multicouches à des besoins spécifiques.

Bien que le traitement acoustique ait souvent lieu assez tard dans le processus de conception, il existe potentiellement de grands avantages à combiner les besoins acoustiques et structurels dans des structures de type panneaux multifonctionnels, étant donné que le panneau sandwich présente plusieurs avantages acoustiques déjà intégrés tels qu'un amortissement assez élevé, et le matériau poro-élastique acoustique, en comparaison assez souple, peut contribuer à la performance globale de la structure. Toutefois la combinaison de ces deux disciplines requiert le développement de nouveaux outils de conception, lequel représente un travail considérable. Une petite partie de ce travail a été réalisée dans le cadre de cette thèse.

Afin de déterminer des paramètres matériaux optimaux ou du moins significativement améliorés, une approche d'optimisation a été implémentée dans un outil de modélisation numérique aux EF existant. L'approche d'optimisation se révèle être un moyen assez efficace et utile pour trouver de tels paramètres matériaux. Cependant, l'optimisation d'un panneau dans le but d'obtenir un comportement donné présuppose la définition de ce comportement en termes de valeurs numériques dépendantes des variables de conception. Il convient de souligner que le choix de la fonction objectif est crucial puisque ce choix affecte directement le résultat de l'optimisation. Afin d'obtenir un

résultat satisfaisant, il est également nécessaire de connaitre de manière très détaillée les cas de chargement et les conditions aux limites du système.

Enfin, les approches de modélisation présentées ici pourraient constituer une partie d'un outil de conception assistée par ordinateur, tout particulièrement pour le développement de panneaux légers multicouches. Un tel outil de conception peut être de grande importance dans le développement de futures concepts de véhicules plus légers et de meilleur efficacité énergétique, puisqu'il permettrait de maintenir voire d'améliorer les propriétés NVH lesquelles sont souvent pénalisées lorsqu'on diminue la masse d'une structure.

4.1 Perspectives

Une possible continuation des travaux initiés sur les matériaux poro-élastiques anisotropes serait de développer des lois d'échelles efficaces en terme de calcul, ou d'autres moyens permettant de lier les propriétés microscopiques et macroscopiques de ces matériaux. Il pourrait être également intéressant d'améliorer les lois d'échelles des matériaux isotropes. Il serait aussi nécessaire d'accroitre la compréhension du comportement physique des matériaux poro-élastiques, en particulier lorsqu'ils sont assemblés dans différentes structures (pré-compression des matériaux poreux, difficulté à attribuer des conditions aux limites appropriées, ...). Cela inclut le développement de techniques de mesure des propriétés matériaux macroscopiques, la modélisation de ces propriétés et leur lien avec les propriétés géométriques microscopiques, la compréhension et la modélisation de différents phénomènes d'amortissement, ainsi que la compréhension et la modélisation des variations des propriétés macroscopiques proche des bords d'un domaine matériau poro-élastique. Pour les matériaux poro-élastiques anisotropes, ce besoin est d'autant plus grand que la compréhension des phénomènes dynamiques et acoustiques anisotropes dans de tels matériaux est à ce jour très limitée.

Une meilleur compréhension de la complexité du comportement vibro-acoustique et une étendue des possibilités de conception de panneaux multifonctionnels sont également très recherchées. Cela doit pouvoir être implémenté dans des outils de conception multidisciplinaires et efficaces en terme de ressources de calcul afin de pouvoir être utilisé industriellement.

Une meilleur compréhension des phénomènes et le développement de modèles utilisables industriellement dans ces domaines peuvent permettre de contribuer à accroître la fonctionnalité et à réduire l'impact environnemental des véhicules dans l'avenir.

Bibliography

[1] J. Akerman and M. Höjer. How much transport can the climate stand?-sweden on a sustainable path in 2050. *Energy Policy*, 34(14):1944–1957, 2006.

[2] J.-F. Allard. *Propagation of sound in porous media: modelling sound absorbing materials.* Elsevier Applied Science, 1993.

[3] J.-F. Allard and Y. Champoux. New empirical equations for sound propagation in rigid frame fibrous materials. *J. Acoust. Soc. Am.*, 6(91):3346–3353, 1992.

[4] N. Atalla, M. A. Hamdi, and R. Panneton. Enhanced weak integral formulation for the mixed (u,p) poroelastic equations. *J. Acoust. Soc. Am.*, 109(6):3065–3068, 2001.

[5] N. Atalla, R. Panneton, and P. Debergue. A mixed displacement-pressure formulation for poroelastic materials. *J. Acoust. Soc. Am.*, 104(3):1444–1452, 1998.

[6] M. A. Biot. Theory of propagation of elastic waves in a fluid saturated porous solid. I. Low frequency range. *J. Acoust. Soc. Am.*, 28:168–178, 1956:1.

[7] M. A. Biot. Theory of deformation of a porous viscoelastic anisotropic solid. *J. Appl. Phys.*, 27:459–467, 1956:3.

[8] M. A. Biot. Mechanics of deformation and acoustic propagation in porous media. *J. Appl. Phys.*, 33(4):1482–1498, 1962.

[9] M. A. Biot and D. G. Willis. The elastic coefficients of the theory of consolidation. *J. Appl. Mech.*, 24:594–601, 1957.

[10] Y. Champoux and J.-F. Allard. Dynamic tortuosity and bulk modulus in air-saturated porous media. *J. Appl. Phys.*, 70(4):1975–1979, 1991.

[11] J. Comiti and M. Renaud. New model for determining mean structure parameters of fixed beds from pressure drop measurements. Application to beds packed with parallellepipedal particles. *Chemical Engineering Science*, 44(7):1539–1545, 1989.

[12] O. Doutres, N. Atalla, and K. Dong. Effect of the microstructure closed pore content on the acoustic behavior of polyurethane foams. *J. Appl. Phys.*, 110(6), 2011.

[13] K. Dovstam. Augmented Hooke's law in frequency domain. A three dimensional material damping formulation. *Int. J. Solids Structures*, 32(19):2835–2852, 1995.

[14] A. Geslain, O. Dazel, J.-P. Groby, S. Sahraoui, and W. Lauriks. Influence of static compression on mechanical parameters of acoustic foams. *J. Acoust. Soc. Am.*, 130(2):818–825, 2011.

[15] L. J. Gibson and M. F. Ashby. *Cellular solids — Structure and properties.* Cambridge University Press, second edition, 1997. First published by Pergamont Press Ltd., 1988.

[16] P. Göransson. Acoustic and vibrational damping in porous solids. *Phil. Trans. R. Soc. A*, 364:89–108, 2006.

[17] P. Göransson, R. Guastavino, and N.-E. Hörlin. Measurement and inverse estimation of 3d anisotropic flow resistivity for porous materials. *J. Sound Vib.*, 327(3-5):354–367, 2009.

[18] R. Guastavino and P. Göransson. A 3d displacement measurement methodology for anisotropic porous cellular foam materials. *Polymer Testing*, 26(6):711–719, 2007.

[19] N.-E. Hörlin. 3-D hierarchical hp-FEM applied to elasto-acoustic modelling of layered porous media. *J. Sound Vib.*, 285(4):341–363, 2005.

[20] N.-E. Hörlin and P. Göransson. Weak, anisotropic symmetric formulations of biot's equations for vibro-acoustic modelling of porous elastic materials. *Int. J. Numer. Meth. Engng*, 84(12):1519–1540, 2010.

[21] N.-E. Hörlin, M. Nordström, and P. Göransson. A 3-D hierarchical FE formulation of Biot's eguations for elasto-acoustic modelling of porous media. *J. Sound Vib.*, 254(4):633–652, 2001.

[22] W.-Y. Jang, A. M. Kraynik, and S. Kyriakides. On the microstructure of open-cell foams and its effect on elastic properties. *Int. J. Solids Structures*, 45(7-8):1845–1875, 2008.

[23] W.-Y. Jang, S. Kyriakides, and A. M. Kraynik. On the compressive strength of open-cell metal foams with kelvin and random cell structures. *Int. J. Solids Structures*, 47(21):2872–2883, 2010.

[24] D. L. Johnson, J. Koplik, and R. Dashen. Theory of dynamic permiability and tortuosity in fluid-saturated porous media. *J. Fluid Mech.*, 176:379–402, 1987.

[25] P. Khurana, L. Boeckx, W. Lauriks, P. Leclaire, O. Dazel, and J.-F. Allard. A description of transversely isotropic sound absorbing porous materials by transfer matrices. *J. Acoust. Soc. Am.*, 125(2):915–921, 2009.

[26] D. Lafarge, P. Lemarnier, J.-F. Allard, and V. Tarnow. Dynamic compressibility of air in porous structures at audible frequencies. *J. Acoust. Soc. Am*, 102(4):1995–2006, 1997.

[27] G. A. Lesieutre. Finite elements for dynamic modelling of uniaxial rods with frequency-dependent material properties. *Int. J. Solids Structures*, 28:1567–1579, 1992.

[28] M. Melon, E. Mariez, C. Ayrault, and S. Sahraoui. Acoustical and mechanical characterization of anisotropic open-cell foams. *J. Acoust. Soc. Am.*, 104(5):2622–2627, 1998.

[29] C. Perrot, F. Chevillotte, M. Tan Hoang, G. Bonnet, F.-X. Bécot, L. Gautron, and A. Duval. Microstructure, transport, and acoustic properties of open-cell foam samples: Experiments and three-dimensional numerical simulations. *J. Appl. Phys.*, 111(1), 2012.

[30] C. Perrot, R. Panneton, and X. Olny. From microstructure to acoustic behaviour of porous materials. *Canadian Acoustics - Acoustique Canadienne*, 32(3):18–19, 2004.

[31] S. Sahraoui, E. Mariez, and M. Etchessahar. Linear elastic properties of anisotropic open-cell foams. *J. Acoust. Soc. Am.*, 110(1):635–637, 2001.

[32] K. Svanberg. The method of moving asymptotes — a new method for structural optimization. *Int. J. Numer. Meth. Engng*, 24:359–373, 1987.

[33] K. Svanberg. A class of globally convergent optimization methods based on conservative convex separable approximations. *SIAM Journal on Optimization*, 12(2):555–573, 2002.

[34] C. Zwikker and C. Kosten. *Sound absorbing materials.*, chapter II and III. Elsevier Publishing Company, Amsterdam, 1949.

CONSERVATOIRE NATIONAL
DES ARTS ET MÉTIERS
–
ROYAL INSTITUTE
OF TECHNOLOGY

le cnam

KTH VETENSKAP OCH KONST
KTH Engineering Sciences

Centre for ECO^2 Vehicle Design

A study of tailoring acoustic porous material properties when designing lightweight multilayered vehicle panels

Eleonora Lind Nordgren

Doctoral Thesis

Stockholm, Sweden 2012
The Marcus Wallenberg Laboratory for Sound and Vibration Research
Department of Aeronautical and Vehicle Engineering

Postal address
Royal Institute of Technology
MWL/AVE
SE-100 44 Stockholm
Sweden

Visiting address
Teknikringen 8
Stockholm

Contact
Tel: +46 8 790 79 41
E-mail: eleonora@kth.se

Akademisk avhandling som med tillstånd av Kungliga Tekniska Högskolan i Stockholm framläggs till offentlig granskning för avläggande av teknologie doktorsexamen fredagen den 7:e september 2012, 14:00 i sal F3, Lindstedtsvägen 26, Kungliga Tekniska Högskolan, Stockholm.

TRITA-AVE-2012:52
ISSN-1651-7660
ISBN-978-91-7501-448-7

Abstract

The present work explores the possibilities of adapting poro-elastic lightweight acoustic materials to specific applications. More explicitly, a design approach is presented where finite element based numerical simulations are combined with optimization techniques to improve the dynamic and acoustic properties of lightweight multilayered panels containing poro-elastic acoustic materials.

The numerical models are based on Biot theory which uses equivalent fluid/solid models with macroscopic space averaged material properties to describe the physical behaviour of poro-elastic materials. To systematically identify and compare specific beneficial or unfavourable material properties, the numerical model is connected to a gradient based optimizer. As the macroscopic material parameters used in Biot theory are interrelated, they are not suitable to be used as independent design variables. Instead scaling laws are applied to connect macroscopic material properties to the underlying microscopic geometrical properties that may be altered independently.

The design approach is also combined with a structural sandwich panel mass optimization, to examine possible ways to handle the, sometimes contradicting, structural and acoustic demands. By carefully balancing structural and acoustic components, synergetic rather than contradictive effects could be achieved, resulting in multifunctional panels; hopefully making additional acoustic treatment, which may otherwise undo major parts of the weight reduction, redundant.

The results indicate a significant potential to improve the dynamic and acoustic properties of multilayered panels with a minimum of added weight and volume. The developed modelling techniques could also be implemented in future computer based design tools for lightweight vehicle panels. This would possibly enable efficient mass reduction while limiting or, perhaps, totally avoiding the negative impact on sound and vibration properties that is, otherwise, a common side effect of reducing weight, thus helping to achieve lighter and more energy efficient vehicles in the future.

Résumé

Le présent travail explore la possibilité d'adapter des matériaux poro-élastiques légers pour des applications spécifiques. En particulier, une approche de conception est présentée, combinant simulations par la méthodes des éléments finis et techniques d'optimisation, permettant ainsi d'améliorer les propriétés dynamiques et acoustiques de panneaux multicouches comprenant des matériaux poreux.

Les modèles numériques sont fondés sur la théorie de Biot qui utilise des modèles équivalents fluide/solide avec des propriétés macroscopiques spatialement homogénéisées, décrivant le comportement physique des matériaux poro-élastiques. Afin de systématiquement identifier et comparer certaines propriétés spécifiques, bénéfiques ou défavorables, le modèle numérique est connecté à un optimiseur fondé sur les gradients. Les paramètres macroscopiques utilisés dans la théorie de Biot étant liés, il ne peuvent être utilisés comme variables indépendantes. Par conséquent, des lois d'échelle sont appliquées afin de connecter les propriétés macroscopiques du matériau aux propriétés géométriques microscopiques, qui elles peuvent être modifiées indépendamment.

L'approche de conception est également combinée avec l'optimisation de la masse d'un panneau sandwich structure, afin d'examiner les possibilités de combiner exigences structurelles et acoustiques, qui peuvent être en conflit. En prenant le soin d'établir un équilibre entre composantes acoustiques et structurelles, des effets de synergie plutôt que destructifs peuvent être obtenus, donnant lieu à des panneaux multifonctionnels. Cela pourrait rendre l'ajout de traitements acoustiques redondant, qui par ailleurs annulerait tout ou partie du gain en masse obtenu par optimisation.

Les résultats indiquent un véritable potentiel d'amélioration des propriétés dynamiques et acoustiques de panneaux multi-couches, pour un ajout minimum en termes de masse et volume. La technique de modélisation développée pourrait également être implémentée au sein d'outils numériques futures pour la conception de panneaux légers de véhicules. Cela aurait le potentiel de réduire substantiellement la masse tout en limitant, voire supprimant l'impact négatif sur les propriétés acoustiques et vibratoires, pourtant une conséquence courante de la réduction de la masse, participant ainsi à l'effort de développement de véhicules futures plus légers et efficaces.

Doctoral thesis

This thesis consists of the following papers:

Paper I
E. Lind Nordgren and P. Göransson. Optimising open porous foam for acoustical and vibrational performance. *Journal of Sound and Vibration* 2010; **329**(7): pp. 753-767.

Paper II
C. J. Cameron, E. Lind Nordgren, P. Wennhage and P. Göransson. Material Property Steered Structural and Acoustic Optimization of a Multifunctional Vehicle Body Panel. Submitted and under revision.

Paper III
C. J. Cameron, E. Lind Nordgren, P. Wennhage and P. Göransson. A Design Method using Topology, Property, and Size Optimization to Balance Structural and Acoustic Performance of Sandwich Panels for Vehicle Applications. Submitted and under revision.

Paper IV
E. Lind Nordgren, P. Göransson and J.-F. Deü. Alignment of anisotropic poro-elastic layers - Sensitivity in vibroacoustic response due to angular orientation of anisotropic elastic and acoustic properties. To be submitted.

Division of Work Between the Authors

Paper I. Nordgren derived the formulations, performed the computations and wrote the paper under the supervision of Göransson.

Paper II and Paper III. The work was performed in collaboration with Cameron on combined acoustic and structural optimization, where the acoustic optimization was performed by Nordgren. The papers were written together, where Nordgren wrote the parts regarding the acoustics in the introduction, optimization and results. Cameron did the same for the structural parts. Conclusions were derived by the aforementioned authors together with supervisors Wennhage and Göransson and written by Nordgren and Cameron together.

Paper IV. Nordgren derived the formulations, performed the computations and wrote the paper under the supervision of Göransson and Deü.

Acknowledgments

The work presented in this thesis has been carried out within in the Centre for ECO^2 Vehicle Design at the Marcus Wallenberg Laboratory (MWL) and within the Smart Structures network at Laboratoire de Mécanique des Structures et des Systèmes Couplés (LMSSC) at the Conservatoire National des Arts et Métiers (CNAM). The financial support is gratefully acknowledged.

First I would like to thank my supervisor, Peter Göransson, for giving me the opportunity to take on this inspiring, gratifying and frustrating challenge, and for your support and guidance along the way. Your confidence in me and this project as well as your great knowledge and devotion to the subject has been invaluable.

Further I would like to thank my other supervisor, Roger Ohayon at LMSSC, and my assistant supervisors, Nils-Erik Hörlin at MWL and Jean-François Deü at LMSSC, for taking the time to answer my many questions varying from theoretical aspects of numerical simulations and computational issues to practical matters related to this joint Swedish-French PhD. Also, I would like to thank the administrative staff for their patience when handling all the different issues of administrative matter.

To Christopher J. Cameron, with whom a substantial part of this work was carried out, thank you for the interesting discussions and the insights in a different research area. The collaborative work has definitely helped me become a more versatile researcher.

To my colleges I would like to extend my thanks for creating such a stimulating and open-minded work environment, especially to Eskil Lindberg for being a great office mate and for sharing your honest and down-to-earth views in all sorts of questions.

I am also grateful to all of my friends and family for making my life so much more enjoyable. Special thanks to my beloved Mamma, Pappa, Syster, Bror and Farmor for their encouragement and genuine love and care throughout my life. And yes, I am now just about finished with "school" ...

Finally, MIKAEL, thank you! Completing this thesis would not have been possible without your love and support. You are truly wonderful! ♡

Contents

Part I

Overview and Summary

Chapter 1

Introduction

The environmental impact caused by human activities in general, has become an increasingly important issue on a global scale. Major parts of the discussion today regard global warming, for which emissions of carbon dioxide and other green house gases are considered responsible. In Sweden approximately 26% of the energy consumption is due to the transport industry, and according to Åkerman and Höjer [1] this is already too much. In order to achieve a sustainable environmental impact the energy used for transport would actually need to be decreased by 60% until year 2050. This can only be done by far reaching changes in transport patterns combined with a significant reduction of energy intensity of transport. Many aspects of a vehicle have to be considered in order to improve the energy efficiency. Apart from the drive line itself, rolling resistance, aerodynamic properties and overall vehicle weight are just a few of many characteristics that highly influence the total life cycle energy consumed.

Reducing the weight of a vehicle is therefore one of many strategies to reduce the fuel or energy consumption and hence achieve more effective transportations with less negative environmental impact. Concurrently, the demands on safety and comfort will not be lowered and changes made to the structure must hence strive to sustain or even improve those properties. This may be accomplished by e.g. far-reaching changes in selected materials as well as overall design, and the implementation of light and stiff multilayered and multifunctional structures (e.g. sandwich panels and sandwich composites) in industrial production has steadily increased for some time. Although, along with the introduction of new lightweight designs, increased problems with noise and vibration often follows, in particular at low frequencies. Typically, unwanted structural vibrations and noise are carried through the structure and radiate, for example, from trim surfaces inside the cabin of a vehicle. Consequently, the dynamic behaviour of such interior trim panel has a major impact on the radiated noise and hence the interior noise levels.

Adding flexible poro-elastic and visco-elastic materials is an often used method to improve noise, vibration and harshness (NVH) comfort in vehicles under such circumstances when major modifications of the interior trim panels are not possible. However, adding material is problematic in view of the goal of reducing weight. It also

adds to the overall cost, material and assembly, and may also take up space that might otherwise come to the benefit of the user. It would of course be highly sought after to include acoustic and dynamic requirements in the original design of the panel or, as a second option, to assure that the best possible performance per added weight, cost and volume of any latterly added treatment is achieved.

A common way to enhance the performance of an acoustic trim panel is to combine different poro-elastic and visco-elastic materials into several layers with different physical and mechanical properties, such as damping, elasticity, viscosity and density. Determining which materials to combine and what properties to look for in each individual layer in order to achieve satisfactory result, is today an expensive and time consuming task that requires knowledge of previously successful combinations, engineering experience as well as extensive testing. Clearly there is a need for computational tools that are able to predict and optimize the behaviour of such multilayered structures.

This work is an initial attempt to demonstrate the possibilities of adapting porous materials to specific purposes. Done correctly, it can potentially generate considerable improvements in NVH comfort with a minimum of added volume and weight.

Chapter 2

Describing and designing porous media

The materials treated in this work are porous materials, consisting of heterogeneous materials constituting an elastic porous framework saturated with fluid. The fluid is assumed to be interconnected throughout the media, so called open pores or open cells. The interstitial fluid, e.g. air, can move relative to the frame, thus any fluid that is enclosed in the framework is considered as part of the frame since it cannot execute relative motion. Two typical porous materials are open cell foam and fibrous material, see fig. 2.1 and 2.2. In porous foam the slender beams constituting the frame are often referred to as struts. The porosities of materials used as acoustic absorbents are normally high, above 90%, and the acoustic energy is carried both through the fluid in the pores as well as through the solid frame material. The waves are strongly coupled and propagate simultaneously along the two paths but with different phase and amplitude. The wave propagation in porous media is, in other words, a fluid-structure interaction phenomenon, occurring throughout the whole volume of material.

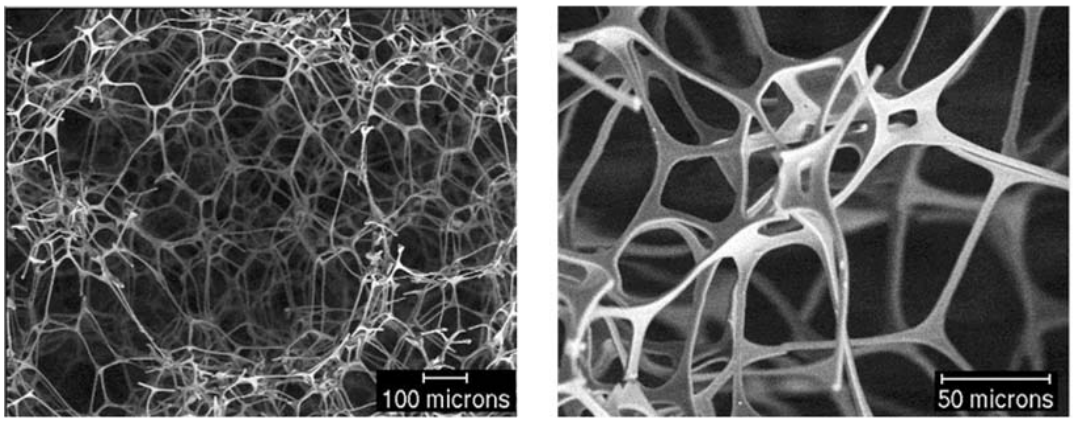

Figure 2.1: Microscopic photography of an open cell porous foam structure. Picture courtesy of Franck Paris (CTTM, France) and Luc Jaouen (luc.jaouen@matelys.com).

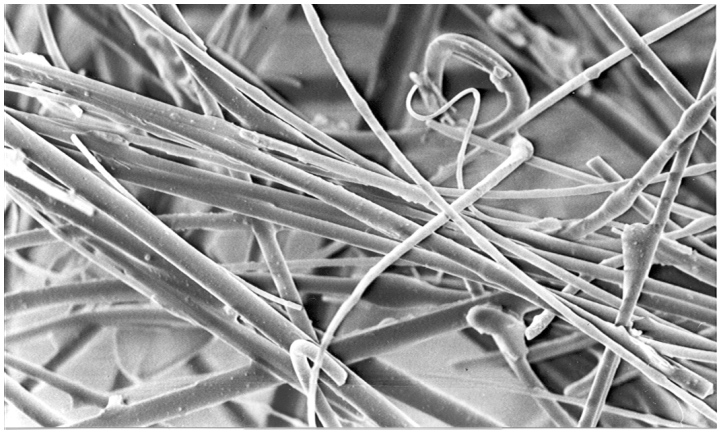

Figure 2.2: Microscopic photography of fibrous material. Picture courtesy of Rémi Guastavino (remi@kth.se).

2.1 Energy dissipation in porous media

When acoustic energy enters a porous media a proportion of the mechanical-acoustical energy will be lost, i.e. converted into heat. There are several different mechanisms that contribute to the advantageous acoustic and vibro-acoustic behaviour of porous media, some of these mechanisms will be briefly described below.

When the frame and the fluid move relative each other, viscous drag will appear at the interface, this will initiate losses in the fluid as well as in the frame. The viscous drag is assumed proportional to the relative displacement and is usually described by using a frequency dependent proportionality factor. Such factor is not only dependent on frequency, but also on, for example, the geometrical properties of the pores, the viscosity of the interstitial fluid and the contact area between the frame and the fluid. At low frequencies the viscous boundary layer at the strut surface is thick relative to the pore radius and the loss of acoustic energy due to viscous dissipation is significant. While at higher frequencies the viscous boundary layer between the frame and the fluid, the viscous skin depth, will be much smaller than the pore radius. At such rapid oscillations the viscous dissipation is small compared to other phenomena.

The movement of fluid relative the frame will not only cause the viscous forces mentioned above. In addition to the viscous drag there are other mechanisms that cause vibro-acoustic energy losses which are proportional to the relative displacement but independent of the viscosity of the fluid. As the fluid (or frame) is forced to change direction, while moving relative to the frame (or fluid), a force normal to the direction of acceleration of one element will be applied to the other. These mechanisms, that would be present even under the assumption of an inviscid fluid, create an apparent increase of mass and are related to the geometry of the frame as well as to the relative motion.

The movement of the frame will also cause frequency dependent internal losses due to the stress-strain relaxation as the frame is deformed. Thermoelastic dissipation

is yet another source of dissipation of acoustic energy as the compressibility of the system yields an increase of temperature due to the compression and expansion cycles. At low frequencies the process is isothermal while as at high frequencies the process becomes adiabatic. In between these conditions, heat conduction among other physical phenomena will cause losses in vibro-acoustic energy.

2.2 Biot theory

The most commonly used model to describe the acoustic behaviour of porous media is attributed to Biot [6] and often referred to as the Biot theory, or sometimes as the Johnson-Champoux-Allard model of the Biot theory. Part of Biot's theory published in 1956 is similar to the contemporary one presented by Zwikker and Kosten [34] with the difference that Biot also included the effects of shear stress in the elastic frame of the porous medium.

Johnson *et al.* [24] added an improved description of the viscous effects by introducing the characteristic viscous length, Λ, which takes frequency dependent viscous effects into account. Allard and Champoux [3, 10] added the characteristic thermal length, Λ', which similarly includes the effects of frequency dependent thermal losses.

Within the extended Biot theory the solid frame is modelled as an equivalent elastic solid continuum and the interstitial fluid as an equivalent compressible fluid continuum, both described by space averaged macroscopic mechanical properties common in continuum mechanics. The two separate but coupled continua are then acting and interacting while occupying the same space. The interaction between the solid and fluid phase is described through coupling parameters derived from measurable macroscopic space averaged properties. The macroscopic properties are used to calculate macroscopic space averaged quantities e.g. solid and fluid displacement, acoustic pressure, and elastic stress. One condition for the above modelling of foams is that the characteristic microscopic dimensions of the foam, e.g. pore size, are small compared to characteristic dimensions of the macroscopic behaviour. In acoustics the latter is identified as the wave length. For the models and materials investigated here, this condition is generally satisfied.

It should however be noted that the modelling of poro-elastic material as two separate, coupled continua is problematic at the boundary of the material. Studies show the homogenized properties may be quite different close to the surface of the poro-elastic material [18]. These types of boundary effect could have a not insignificant impact, especially if the depth of such boundary layer is large compared to the thickness of the porous layer.

A substantial amount of work has been done to obtain physically meaningful descriptions of the macroscopic material parameters. Especially significant for porous media are the

coupling parameters which may be defined in different ways. Within the Johnson-Champoux-Allard model they are mostly described as:

- *Porosity*, ϕ [1], defined as the volume fraction of fluid content in the porous media, $0 < \phi < 1$. For materials used in acoustic applications the porosity is normally larger than 0.95.

- *Tortuosity*, α_∞ [1], defined as the fraction between mean microscopic fluid velocity squared and the mean macroscopic fluid velocity squared averaged over a volume under the assumption of zero viscosity. In practice it compares the length of the path the fluid travels in the porous media on microscopic level with the length of the path on a macroscopic level, implying that $\alpha_\infty \geq 1$. For open porous media with high porosity the tortuosity is often close to one, typically 1.05.

- *Static flow resistivity*, σ^{static} [Nsm^{-4}], defined as the pressure difference over flow velocity per unit length. The flow resistivity is dependent of many different physical properties in the porous media, among them the surface viscosity between the frame and the microscopic geometry of the porous media. This parameter may be measured or theoretically deduced from e.g. Stokes simulations given a certain microstructural geometry.

- *Viscous characteristic length*, Λ [m], helps to improve the estimation when dissipation effects due to viscous losses at the pore walls need to be taken into account. When the pores are small compared to the viscous skin depth the viscous dissipation effects cannot be neglected. The viscous characteristic length provides possibilities for modifications that give better frequency dependent representation of the viscous losses.

- *Thermal characteristic length*, Λ' [m], takes into account the thermal exchange between the frame and the fluid at the boundary, in analogy with the viscous characteristic length, hence similarly provides adjustments for the frequency dependent thermal fluid-structure interactions.

An important part for increased understanding of porous materials is the experimental work carried out to characterize different materials and obtain the macroscopic material parameters needed. There are also still several not fully understood physical aspects of porous materials, for example the influence of static compression, strain or other deformations on the material properties [14] or the changes of elastic moduli at the boundary region of porous foam samples [18]. Naturally the work to obtain experimental data are closely connected to the work of developing mathematical models used to describe these complex materials and their behaviour.

2.2.1 Governing equations

The Biot theory is a Lagrangian model where the stress-strain relations are derived from potential energy deformation. While Biot theory, in practice, often is used in its isotropic form, the anisotropic form of the governing equations, similar to what has been previously stated by Biot [8], Biot and Willis [9] and Allard [2] will be given here. This overview of the governing equations is in no way complete and should be considered as a short summary of the very extensive work that has been previously accomplished in the field of porous materials. The interested reader is referred to the original work for details.

The notations used is explained when introduced and also summarized in Chapter 6, except for the following regarding tensor notation. The component ordinal number in a Cartesian co-ordinate system, e.g. $i = 1, 2, 3$ is noted i, j, k. Partial derivates with respect to x_i is written $(.)_{,i} = \partial(.)/\partial x_i$. Kronecker's delta is δ_{ij}. Also, Cartesian tensor notation with Einstein's summation convention is used, i.e. repeated indices imply a summation of these terms.

Momentum equations

Assuming time harmonic motion at circular frequency ω, the (frequency domain) momentum equations for the solid frame and the fluid respectively may be written as

$$\sigma^{\mathrm{s}}_{ij,j} = -\omega^2 \tilde{\rho}^{11}_{ij} u^{\mathrm{s}}_j - \omega^2 \tilde{\rho}^{12}_{ij} u^{\mathrm{f}}_j \tag{2.1}$$

and

$$\sigma^{\mathrm{f}}_{ij,j} = -\omega^2 \tilde{\rho}^{12}_{ij} u^{\mathrm{s}}_j - \omega^2 \tilde{\rho}^{22}_{ij} u^{\mathrm{f}}_j \tag{2.2}$$

where σ^{s}_{ij} and σ^{f}_{ij} are the Cauchy stress tensors for the frame and the fluid respectively while u^{s}_j and u^{f}_j are the frame and fluid displacements. The equivalent density tensors, $\tilde{\rho}^{11}_{ij}$, $\tilde{\rho}^{12}_{ij}$ and $\tilde{\rho}^{22}_{ij}$ are anisotropic generalizations of those used by Allard [2] and may be defined as

$$\tilde{\rho}^{11}_{ij} = \rho_1 \delta_{ij} + \rho^{\mathrm{a}}_{ij} - \frac{\mathrm{i}}{\omega} b_{ij}, \tag{2.3}$$

$$\tilde{\rho}^{12}_{ij} = -\rho^{\mathrm{a}}_{ij} - \frac{\mathrm{i}}{\omega} b_{ij}, \tag{2.4}$$

$$\tilde{\rho}^{22}_{ij} = \phi \rho_0 \delta_{ij} + \rho^{\mathrm{a}}_{ij} - \frac{\mathrm{i}}{\omega} b_{ij}, \tag{2.5}$$

where

$$\rho_{ij}^{\mathrm{a}} = \phi\rho_0 \left(\alpha_{ij} - \delta_{ij}\right) \tag{2.6}$$

with ρ_0 as the ambient fluid density and ρ_1 as the bulk density of the porous material and α_{ij} is the tortuosity tensor. ρ_{ij}^{a} is an inertial coupling coefficient that represents the apparent increase of mass due to tortuosity. The viscous drag tensor b_{ij} accounts for the viscous body forces between the solid and the fluid phase and is here defined as established by Johnson *et al.* [24].

$$b_{ij} = \phi^2 \sigma_{ij}^{\mathrm{static}} B_{ij}\left(\omega\right), \tag{2.7}$$

where

$$B_{ij} = \sqrt{1 + i\omega \frac{4\eta\rho_0\alpha_{ij}^2}{\phi^2(\sigma_{ij}^{\mathrm{static}})^2\Lambda_{ij}^2}} \tag{2.8}$$

with η being the ambient fluid viscosity.

Constitutive equations

The two constitutive equations may be defined as

$$\sigma_{ij}^{\mathrm{s}} = C_{ijkl}\varepsilon_{kl} + Q_{ij}\theta^{\mathrm{f}} \tag{2.9}$$

and

$$\sigma_{ij}^{\mathrm{f}} = Q_{kl}\varepsilon_{kl}\delta_{ij} + R\theta^{\mathrm{f}}\delta_{ij} \tag{2.10}$$

where C_{ijkl} is the solid frame Hooke's tensor, the fluid dilatation is given by the divergence of the fluid displacement

$$\theta^{\mathrm{f}} = u_{k,k}^{\mathrm{f}} \tag{2.11}$$

and the solid frame strain is given by the Cauchy strain tensor

$$\varepsilon_{kl} = \frac{1}{2}\left(u_{k,l}^{\mathrm{s}} + u_{l,k}^{\mathrm{s}}\right) \tag{2.12}$$

The two material tensors, R and Q_{ij} are defined as

$$R = \frac{\phi^2 K_s}{1 - \phi - K_s C_{ijkl} d_{ij} d_{kl} + \phi K_s / K_f} \tag{2.13}$$

$$Q_{ij} = \left[(1-\phi) - C_{ijkl} d_{kl}\right] \frac{R}{\phi} = \frac{\left[(1-\phi) - C_{ijkl} d_{kl}\right] \phi K_s}{1 - \phi - K_s C_{ijkl} d_{ij} d_{kl} + \phi K_s / K_f} \tag{2.14}$$

where K_s and K_f are the frame and fluid bulk modulus and d_{ij} is the unjacketed compressibility compliance tensor where K_f is obtained using the model by Lafarge *et al.* [26]. As the fluid itself is assumed to be isotropic, R is a scalar quantity. The dilatational coupling Q_{ij} is, however, a second order tensor due to the assumed elastic anisotropy.

Often in practice and also in this work the fluid displacement field is not used as dependent variable. Instead the fluid Cauchy stress tensor is replaced by the pore pressure, which is a scalar unit, $\sigma^{\mathrm{f}}_{ij} = -\phi p \delta_{ij}$, this allows for a reduction of the number of dependent variables from six to four.

2.2.2 Matrix representation of material parameters

The elastic properties of the solid frame of the porous material may be described using the solid frame Hooke's matrix, equivalent to the Hooke's tensor C_{ijkl} used previously. The Hooke's matrix is a 6×6 matrix and for isotropic materials it consists of only two independent parameters:

$$\mathbf{C} = \frac{E}{(1+\nu)(1-2\nu)} \begin{bmatrix} 1-\nu & \nu & \nu & 0 & 0 & 0 \\ & 1-\nu & \nu & 0 & 0 & 0 \\ & & 1-\nu & 0 & 0 & 0 \\ & & & \frac{1-2\nu}{2} & 0 & 0 \\ symm. & & & & \frac{1-2\nu}{2} & 0 \\ & & & & & \frac{1-2\nu}{2} \end{bmatrix} \tag{2.15}$$

where E is the Young's modulus and ν is Poisson's ratio. Anisotropic materials have many different types of anisotropy, three of which will be briefly described here.

1. *Transversely isotropic* materials have equal material properties in two of its principal direction but different ones in the third direction normal to the plane of isotropy. A typical transversely isotropic material is a fibrous material, and describing it

requires up to five independent parameters.

$$\mathbf{C} = \begin{bmatrix} C_{11} & C_{12} & C_{13} & 0 & 0 & 0 \\ & C_{11} & C_{13} & 0 & 0 & 0 \\ & & C_{33} & 0 & 0 & 0 \\ & & & C_{44} & 0 & 0 \\ symm. & & & & C_{44} & 0 \\ & & & & & \frac{1}{2}(C_{11} - C_{12}) \end{bmatrix} \tag{2.16}$$

2. *Orthotropic* materials have three axes which are mutually orthogonal and their mechanical properties are, in general, different in each direction. Further, there exists some orthogonal principal directions where there is no coupling between dilatation and shear. Many acoustic foam materials show tendencies toward orthotropic behaviour and describing them then requires at the most nine different material parameters.

$$\mathbf{C} = \begin{bmatrix} C_{11} & C_{12} & C_{13} & 0 & 0 & 0 \\ & C_{22} & C_{23} & 0 & 0 & 0 \\ & & C_{33} & 0 & 0 & 0 \\ & & & C_{44} & 0 & 0 \\ symm. & & & & C_{55} & 0 \\ & & & & & C_{66} \end{bmatrix} \tag{2.17}$$

3. *Fully anisotropic* materials may have different material properties in every direction and the principal directions are not necessary orthogonal, implying that e.g. bending in one direction may induce twisting in another, or a compressional stress may induce shear stresses. This is the most general material description, however not often used as describing it requires up to 21 independent parameters.

$$\mathbf{C} = \begin{bmatrix} C_{11} & C_{12} & C_{13} & C_{14} & C_{15} & C_{16} \\ & C_{22} & C_{23} & C_{24} & C_{25} & C_{26} \\ & & C_{33} & C_{34} & C_{35} & C_{36} \\ & & & C_{44} & C_{45} & C_{46} \\ symm. & & & & C_{55} & C_{56} \\ & & & & & C_{66} \end{bmatrix} \tag{2.18}$$

Other material properties such as tortuosity, static flow resistivity and viscous characteristic length would instead be described with a 3×3 matrix where the number of independent parameters required would vary between one, for an isotropic material, up to six for a fully anisotropic material.

1. *Isotropic*

$$\mathbf{S} = \begin{bmatrix} S_1 & 0 & 0 \\ & S_1 & 0 \\ symm. & & S_1 \end{bmatrix} \tag{2.19}$$

2. *Transversely isotropic*

$$\mathbf{S} = \begin{bmatrix} S_1 & 0 & 0 \\ & S_1 & 0 \\ symm. & & S_3 \end{bmatrix} \tag{2.20}$$

3. *Orthotropic*

$$\mathbf{S} = \begin{bmatrix} S_1 & 0 & 0 \\ & S_2 & 0 \\ symm. & & S_3 \end{bmatrix} \tag{2.21}$$

4. *Fully anisotropic*

$$\mathbf{S} = \begin{bmatrix} S_{11} & S_{12} & S_{13} \\ & S_{22} & S_{23} \\ symm. & & S_{33} \end{bmatrix} \tag{2.22}$$

For most anisotropic porous materials the material parameter matrices are to a great part unknown and the question of how to effectively measure or otherwise retrieve these parameters is still an open issue. Many of the well established techniques used today measure only the isotropic equivalent of the anisotropic properties. The ongoing work of developing adequate measurement techniques to fully characterize anisotropic porous media is not at all a trivial task. The anisotropy of a porous material does, however, have an impact on the space averaged macroscopic material properties and the acoustic behaviour of the porous material [25]. The ongoing research are focused on new measurement techniques [18] as well as studies of anisotropic microstructural geometries [22, 23, 29]. Further it should be emphasized that the principal directions of the different macroscopic material properties does not necessarily line up with each other or the main directions in a geometrical sense, they may very well require different local coordinate systems to be accurately modelled [17, 28, 31].

2.2.3 Isotropic versus anisotropic modelling

The vast majority of previously published work involving and developing Biot theory concerns only isotropic modelling and therefore the isotropic models today have several improvements that are not readily transferable to an anisotropic description. As an example, the isotropic stress-strain relations may be extended to include also the frequency dependent internal losses due to the movements in the frame. These may be modelled using the augmented Hooke's law (AHL), proposed by Dovstam [13], which is based on work from e.g. Biot [7] and Lesieutre [27]. In brief the internal losses are modelled adding frequency dependent, complex valued terms, to the classic material

modulus matrix of Hooke's generalized law. This augmented Hooke's law is today not implemented in anisotropic Biot models as several unknowns regarding the damping behaviour and its principal directions still remain.

In addition the material parameters needed to describe anisotropic materials are not easy to obtain and many questions remain regarding their principal directions. This emphasizes the need to further develop accurate measurement techniques in order to obtain information regarding the physical behaviour of anisotropic materials. These are all issues for ongoing research.

Therefore, when modelling porous materials, the choice between using isotropic or anisotropic models is dependent on e.g. the accuracy needed, the type of porous material to be modelled, the structure in which it is implemented, and also whether or not the anisotropic material parameters are known or may be obtained.

2.3 FE-modelling

Analytical solutions to Biot's equations exists only for a few special cases where the equation set-ups may be reduced to one dimensional problems, e.g. infinite plane, spherical, and infinite cylinder problems. For most applications of interest the complexity of the problem requires some kind of numerical solution that can handle complex geometries, finite sizes, non-uniform distribution of boundary conditions and loads, as well as the coupling to other porous, solid or fluid components. These issues and several more have been addressed for both the isotropic as well as the anisotropic cases in previous works by Hörlin and Göransson [20], Hörlin [19] and Hörlin *et al.* [21] where three-dimensional hp-based [1] finite element solutions have been developed and evaluated. To formulate finite element solutions to the coupled partial differential equations describing the behaviour of a system, a weak form of the partial differential equations, including boundary conditions, had to be stated. Hörlin evaluated different weak formulations, among them a mixed displacement-pressure formulation for isotropic porous materials as it was proposed by Atalla *et al.* [4, 5]. Later on the mixed displacement-pressure formulation was extended by Hörlin and Göransson [20] to include also anisotropic materials. This formulation uses the frame displacement as the primary variable describing the motion of the frame, and the fluid pressure as the primary variable describing the fluid, i.e. (u^s, p)-formulation, instead of the more common weak formulations which use frame and fluid displacement as primary variables, (u^s, u^f)-formulations. The latter has been shown to require cumbersome calculations when used in large finite element systems. The (u^s, p)-formulation as proposed by Atalla *et al.* [5] is considered as accurate as the classical (u^s, u^f)-formulation with the advantage that it is the better choice with respect to the computational effort required to achieve the wanted accuracy. It describes the porous material with a minimum of dependent

[1] Convergence is achieved by refining the mesh and/or increasing the approximation order.

field variables and it also couples two open pore components, and also an open pore component to a solid one, without any additional coupling integrals, as long as the solid parts are attached to each other. However, couplings between porous components and fluids require coupling integrals to be used. This proposed mixed displacement pressure formulation is underpinning the current work of studying the potential improvements of adapting porous materials to specific applications.

2.4 Correlations between macroscopic and microscopic properties

As stated previously, porous materials are described using the macroscopic space averaged properties, of which several are presented in the equations above. These macroscopic properties are naturally dependent on the microscopic geometrical properties of the frame as well as of the frame material itself. Examples of such geometrical, microscopic properties are the size and shape of the pores, and the cross section and thickness of the struts, or fibres, in the open porous material. Microscopic properties like these will, in combination with material choices, govern the thermal, elastic, viscoelastic, mechanical and acoustic behaviour of the porous material. Hence, the macroscopic properties can not be regarded as independent of one another and are therefore unsuitable as variables in an optimization problem. Instead, the aim in the current work has been to use scaling laws that relate the macroscopic properties to the underlying microscopic properties. Such scaling laws should preferably describe the macroscopic properties of the porous material as being continuously and systematically dependent on the micro-structural mechanical properties, allowing for the optimization to focus directly to the microscopic properties. Several researchers have made contributions in developing mathematical formulations of the relations between different material properties. Assuming an open cell foam structure with high porosity, where the strut material is significantly heavier than the interstitial fluid, the approach taken by Gibson and Ashby [15] may then provide significant guidance in understanding the mechanical behaviour of such a foam. Gibson and Ashby view the cellular structure as vertices joined by edges. A very simple configuration would be a cubic cell shape where adjoining cells are staggered so that their members meet at the mid points, but the reasoning is just as valid for more complex cell structures such as e.g. rhombic dodecahedra or tetrakaidecahedra, fig. 2.3. The last cell structure, tetrakaidecahedra, also referred to as a Kelvin cell, is a common choice because it has an average number of edges per face, and of faces per cell, which seems to correspond well to some observations, but the matter would need further investigation [15, 30]. Recent studies [12] show that such scaling laws, although based on simplified cell structures and possibly different implicit assumptions that may not be completely fulfilled, still give a fairly satisfactory prediction.

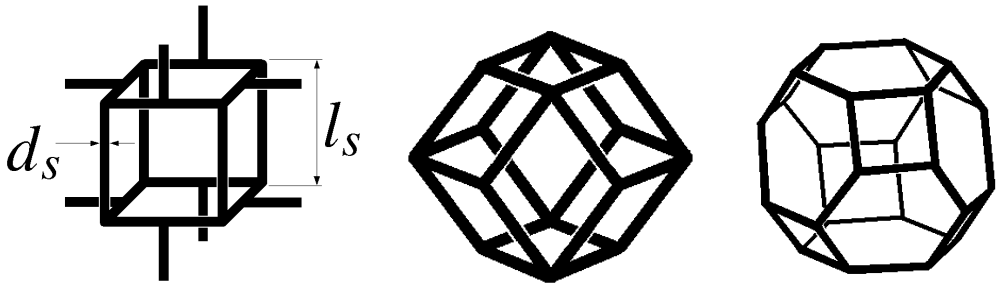

(a) cubic cell (b) rhombic dodecahedra (c) tetrakaidecahedra

Figure 2.3: Examples of theoretical cell shapes according to Gibson and Ashby.

Assuming isotropy in the cell geometry it may be shown, for all of the foam cell shapes mentioned above, that the relative density, ρ^*, for cellular foams is proportional to the length and the thickness of the struts, l_s and d_s respectively.

$$\frac{\rho^*}{\rho_s} = C^\rho \left(\frac{d_s}{l_s}\right)^2 \tag{2.23}$$

where C^ρ is a constant dependent on the cell shape and strut cross section shape, but close to unity for an open cell foam with fairly complex cell shapes. ρ_s is the frame material density. Assuming knowledge of a reference foam, denoted $(.)_{ref}$, which is scaled but still keeping its general cell and strut shape, the relative density may be expressed as

$$\rho^* = \rho^*_{ref} \left(\frac{d_s}{d_{ref}}\right)^2 \left(\frac{l_{ref}}{l_s}\right)^2 \tag{2.24}$$

The assumption that the strut material is significantly heavier than the interstitial fluid allows for the porosity to be expressed as

$$\phi = 1 - \frac{\rho^*}{\rho_s} \tag{2.25}$$

To model the variation of the Young's modulus with the microscopic properties, the struts are assumed to deform primarily in bending. Additionally, small deformations and linearly elastic behaviour of the strut material is also assumed. The deformation on a macroscopic level can be coupled to the deformation of the struts in a cubic cell by applying mechanical laws of deformation of beams. If the Young's modulus of the foam is calculated as the deflection of a beam with length l_s loaded at the midpoint by the force F, the deflection, δ, is proportional to Fl_s^3/E_sI, where E_s is the Young's modulus of the frame material and I is the moment of inertia of the strut shape, $I \propto d_s^4$. On a macroscopic scale the force is related to the macroscopic compressive stress, σ^*, as $F \propto \sigma^* \cdot l_s^2$ and the macroscopic strain, ε^*, is related to the beam deflection as $\varepsilon^* \propto \delta/l_s$. It follows that the Young's modulus for the foam can be expressed as

$$E^* = \frac{\sigma^*}{\varepsilon^*} = \frac{C^{dl} E_s I}{l_s^4} \quad \rightarrow \quad \frac{E^*}{E_s} = C^{dl} \left(\frac{d_s}{l_s}\right)^4 = C^E \left(\frac{\rho^*}{\rho_s}\right)^2 \tag{2.26}$$

or when a reference material is used as

$$E^* = E^*_{ref} \left(\frac{\rho^*}{\rho^*_{ref}}\right)^2 \tag{2.27}$$

Extensive works by Allard and Champoux [3] and Allard [2] have also contributed to establishing relations between the macroscopic foam properties and the microscopic structural properties. Their work have been used by Göransson to further develop scaling laws that relates the viscous characteristic length, Λ, and the static flow resistivity, σ^{static}, to the microstructure of the foam [16]. By assuming inviscid flow around a cylinder Allard and Champoux show that if the porosity is close to one, Λ is given by

$$\Lambda = \frac{1}{2\pi L r} \tag{2.28}$$

where L is the total cylinder length per unit volume and r is the radius of the cylinder [3]. With the former assumption of cellular geometry L can be defined in terms of the porosity as $\pi r^2 L = \rho^*/\rho^s$ which allow for the viscous characteristic length to be expressed as [16]

$$\Lambda = \frac{d_s}{4(\rho^*/\rho_s)} = \frac{d_s}{4(1-\phi)} \tag{2.29}$$

To account for thermal effects the simplified assumption of $\Lambda' = 2 \cdot \Lambda$ has been made for the thermal characteristic length, Λ'. As the tortuosity for highly porous materials is very depend on the closed pore content and the materials used in this work are assumed to be only open pores, the change in tortuosity when the material properties are altered is quite small. However, a scaling law based on work by Comiti and Renaud, [11], have been implemented in Paper II and III,

$$\alpha_\infty = 1 - \frac{1 - \alpha_{\infty ref}}{\ln(\phi_{ref})} \cdot \ln(\phi) \tag{2.30}$$

Further it has been shown by Allard that Λ may be expressed in terms of macroscopic properties as:

$$\Lambda = \frac{1}{c_g} \sqrt{\frac{8\alpha_\infty \eta}{\phi \sigma^{static}}} \tag{2.31}$$

where c_g is dependent on the cross-sectional shape of the pores, for cylindrical geometries $c_g = 1$ [2]. Eq. (2.29) together with eq. (2.31) give

$$\sigma^{static} = \frac{8\alpha_\infty \eta}{1-(\rho^*/\rho_s)} \cdot \frac{16(\rho^*/\rho_s)^2}{d_s^2 c_g^2} \tag{2.32}$$

which when using a reference material may be expressed as

$$\sigma^{static} = \sigma_{ref}^{static} \left(\frac{\rho^*}{\rho_{ref}}\right)^2 \cdot \left(\frac{d_{ref}}{d_s}\right)^2 \cdot \frac{\alpha_\infty}{\alpha_{\infty ref}} \cdot \frac{\left(1-\frac{\rho_{ref}}{\rho_s}\right)}{\left(1-\frac{\rho^*}{\rho_s}\right)} \tag{2.33}$$

2.5 Aspects of optimization

Performing an optimization requires some type of objective function, $f(\mathbf{x})$, that provides a numerical value representing the qualities sought for. This objective function is dependent on one or more design variables, $\mathbf{x} = [x_1\, x_2 \cdots x_\mathrm{n}]$, limited by $\mathbf{x}_\mathrm{min} \leq \mathbf{x} \leq \mathbf{x}_\mathrm{max}$ and may also be subjected to different constraint functions, $g_\mathrm{i}(\mathbf{x})$. The optimization problem is often seen on the form

$$\begin{aligned} \min \quad & f(\mathbf{x}) \\ \text{subject to} \quad & g_1(\mathbf{x}) \leq 0 \\ & g_2(\mathbf{x}) \leq 0 \\ & \vdots \\ & g_\mathrm{M}(\mathbf{x}) \leq 0 \\ & \mathbf{x}_\mathrm{min} \leq \mathbf{x} \leq \mathbf{x}_\mathrm{max} \end{aligned} \tag{2.34}$$

Choosing a proper objective function and constraints is often more difficult than it may seem as in reality there are often many different objectives to meet which are dependent on the same or different design variables. In this work minimizing the acoustic discomfort or minimizing the mass are often the objectives used in practice. Alternative objectives may involve for example minimizing material cost, environmental impact, assembly time or fuel consumption and the minimum of one objective rarely coincide with the minima of the others. The problem may be handled by minimizing one objective while putting constraint on the others or by developing an objective function that incorporates several objectives into one single function, using for example some kind of weighted sum. There are many ways to construct an objective function and the task should not be taken lightly as the outcome of the optimization unavoidably will depend greatly on the choice of objective function and constraints.

In practise the optimization is often performed by some kind of algorithm. If the functions are differentiable and dependent on continuous design variables a gradient based algorithm is often suitable. Such algorithm has to be provided with information of the numerical values of the objective function, the gradient vector and possible parts of the Hessian matrix of that objective function with regard to $\mathbf{x}$, as well as

the numerical value of the constraint functions and possible the gradients and also the minimum and maximum values of the design variables. The algorithm will then, based on the input data, suggest new design parameters for which the cost function is calculated and so on in an iterative fashion until some kind of stop criterion is met. In practical applications are the objective function and/or the constraint functions often very complex and not uncommonly the result of some sort of computer simulation. This often requires the gradient and Hessian values to be calculated numerically, using for example finite differences, which increases the computational cost with every design variable used, and every iteration needed to find a minimum.

Another difficulty when using an optimization approach is that most objective functions are not convex, meaning that it may exist one or more local minima within the parameter range that are not the best solution. The best solution is instead referred to as the global minimum. This issue is most often handled by using several different starting point within the parameter range and then comparing the number of local minima and the value of the objective functions at those local minima.

Chapter 3

Studies of poro-elastic acoustic materials in multilayered structures

This work explores the possible effect of altering the microscopic properties of specific poro-elastic acoustic materials when assembled in multilayered acoustic or multifunctional panels. While the majority of the work concerns isotropic modelling the influence of anisotropic material properties and the angular orientation of those properties is also touched upon. The studies were conducted as numerical simulations using Biot theory and the, for this purpose, suitable FE-based numerical approach described in Chapter 2. The alterations of material properties were chosen by a gradient based optimizer [32, 33].

While optimizing the macroscopic porous material properties used in the Johnson-Champoux-Allard model may render some information concerning sought for combinations of material properties, it does however not provide any knowledge regarding what type of porous material to use or how to achieve such properties in any porous material in reality. Quite possible the resulting material would be physically impossible to realize, thus making such an optimization less useful in practice. By describing the poro-elastic acoustic material with its microscopic properties and thereafter estimate the corresponding macroscopic material parameters the resulting material may be, if not already existing, at least well described and physically possible to create. Hence the need for the previously described scaling laws which provide approximative correlations between microscopic and macroscopic parameters.

To examine the acoustic and dynamic behaviour of poro-elastic materials assembled in multilayered panels a number of different panels, containing either isotropic or anisotropic porous materials, have been numerically evaluated. The panels were exited by different types of force fields and the acoustic and dynamic properties needed to be expressed as an objective function or a constraint function in order to enable an optimization. Such a function may be chosen in a number of different ways and formulating a way to describe good and bad sound quality using a numerical quantitative

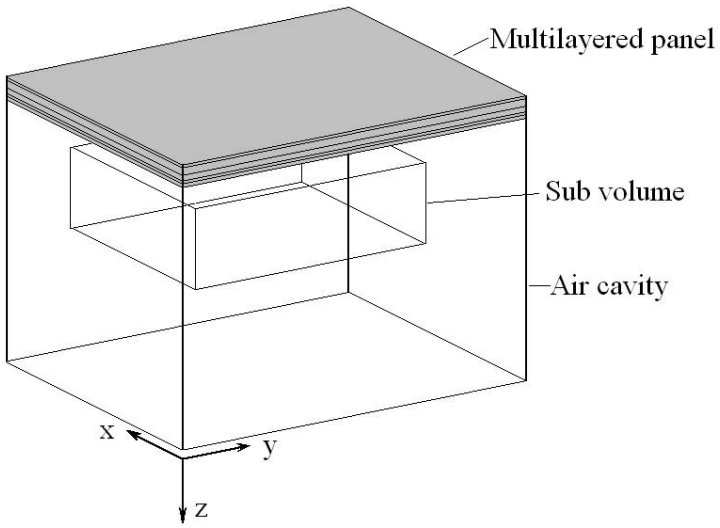

Figure 3.1: Schematic picture of multilayered panel and connected air cavity with subvolume.

value is not an easy task and represents a whole field of research in itself. In this work acoustic and dynamic measure was constructed as the acoustic response in a sub volume of an air cavity connected to the multilayered panel in question, fig. 3.1. The acoustic response was chosen to be the sound pressure level (SPL), inherently dependent on the different design parameters. The sound pressure square, p_f^2, for each evaluated frequency, f, is calculated as the average of the square sound pressure in a number, N, of discrete points in the chosen sub volume, eq. (3.2). This quantity was then multiplied with the frequency resolution, Δf_f, a frequency dependent weighting factor, C_f, divided with the reference sound pressure square, p_0^2, and summed over the entire frequency range, eq. (3.1), resulting in a total sound pressure level, SPL, which is then subject to minimization or maximization

$$\langle SPL \rangle_{\Omega_{\text{sub}}}^{C} = 10 \cdot \log \left(\frac{\sum_{f=f_1}^{f_{\max}} \left(p_f^2 \cdot \Delta f_f \cdot C_f \right)}{p_0^2} \right) \tag{3.1}$$

where

$$p_f^2 = \frac{1}{N} \sum_{n=1}^{N} p_{f_n}^2 \tag{3.2}$$

As the SPL in the air cavity was calculated for each frequency in the chosen frequency range the computational cost to evaluate eq. 3.1 may be quite substantial. In addition when the gradients are calculated using finite differences yet another evaluation of $\langle SPL \rangle_{\Omega_{\text{sub}}}^{C}$ is needed for each design variable. Therefore it is of great importance to,

within the optimization process, find a minimum with as few iterations as possible. The optimizer chosen here was an MMA (Method of Moving Asymptotes) based optimizer, and later on its refined globally convergent version [32, 33], as this optimizer performed well while using less iterations than the tested alternatives.

3.1 Adapting porous material parameters for improved acoustic performance

Initially a 2D-model was used to simulate a panel with seven layers, out of which one was microstructurally optimized, using an isotropic porous material model with the bulk density, ρ^*, and the strut thickness, d_s, as the design variables. The weighting factor in eq. 3.1 was set to correspond to either A-weighted or C-weighted SPL and two different open cell poro-elastic cellular foams were used, a polyurethane based foam, PU-foam, and a polyimide based foam, π-foam. Five different optimizations were executed: minimizing the SPL corresponding to A-weighting with constraint on the mass using PU-foam, minimizing the SPL corresponding to C-weighting with constraint on the mass using PU-foam, minimizing the SPL corresponding to C-weighting with constraint on the mass using *pi*-foam, and finally minimizing the mass using PU-foam and π-foam respectively, with constraints on the SPL corresponding to C-weighting. The SPL was evaluated for a frequency range 100 – 900 Hz. Also, constraints were put on the design variables to exclude results that were physically impossible.

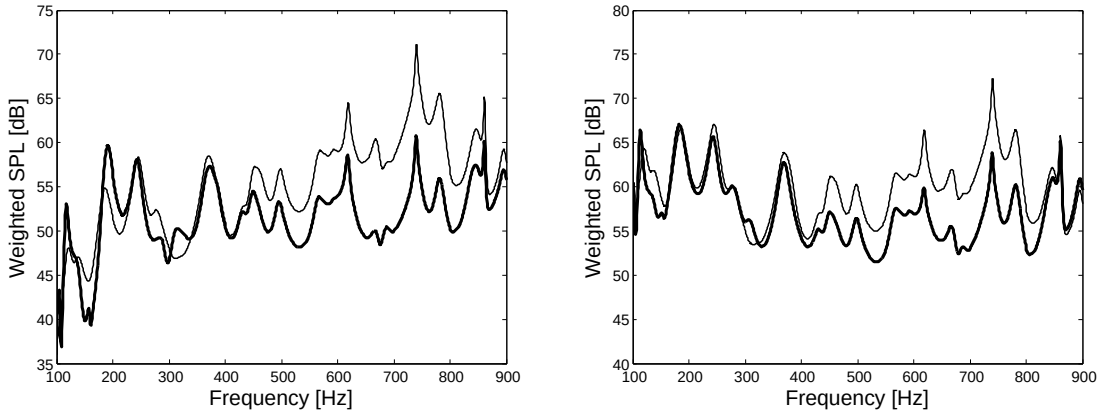

(a) A-weighted FRF

(b) C-weighted FRF

Figure 3.2: Frequency response function for optimal foam solution (thick solid) and suboptimal foam solution (thin solid), weighted with corresponding A-weighting (left figure) and C-weighting (right figure) respectively.

Although different starting points were used the final minimum remained the same, indicating that the objective functions were relatively convex for the parameter space and the frequency range chosen for these simulations. The resulting design parameters also show that the weighting function had a major impact on the outcome of the

optimization, using an A-weighted SPL the minimum was found at ρ^*=32.5 kg m^{-3} and d_s=14.8×10^{-6} m whereas the minimum was found at ρ^*=20.1 kg m^{-3} and d_s=15.5×10^{-6} m when a C-weighted SPL was used. Comparing the frequency response functions, FRFs, of the optimized panels with those of panels containing foam with suboptimal design parameters, also showed that the possibility of improvement in acoustic and dynamic behaviour was significant, see fig. 3.2

When comparing panels containing PU-foam and π-foam respectively, for C-weighted sound pressure optimized panels, the panel containing PU-foam performed slightly better. On the other hand, when minimizing the mass with constraints on C-weighted SPL the result was somewhat in favour of the panel containing π-foam.

The influence of anisotropy was examined using a 3D-model where a quadratic multilayered panel consisting of two aluminium face sheets separated by two layers of poro-elastic material, elastically bonded to the face sheet where the excitation was applied and separated by a thin air gap from the other aluminium face sheet. Two different varieties of the panel were considered: configuration A, containing an open cell orthotropic foam and configuration B, containing a transversely isotropic fibrous material. For both configurations, A and B respectively, both layers consisted of the same material type. The only variations introduced were the relative orientation of the material properties in each layer, which could rotate independently in different directions and thereby possibly achieving different overall dynamic properties considering the direction of excitation, see fig. 3.3.

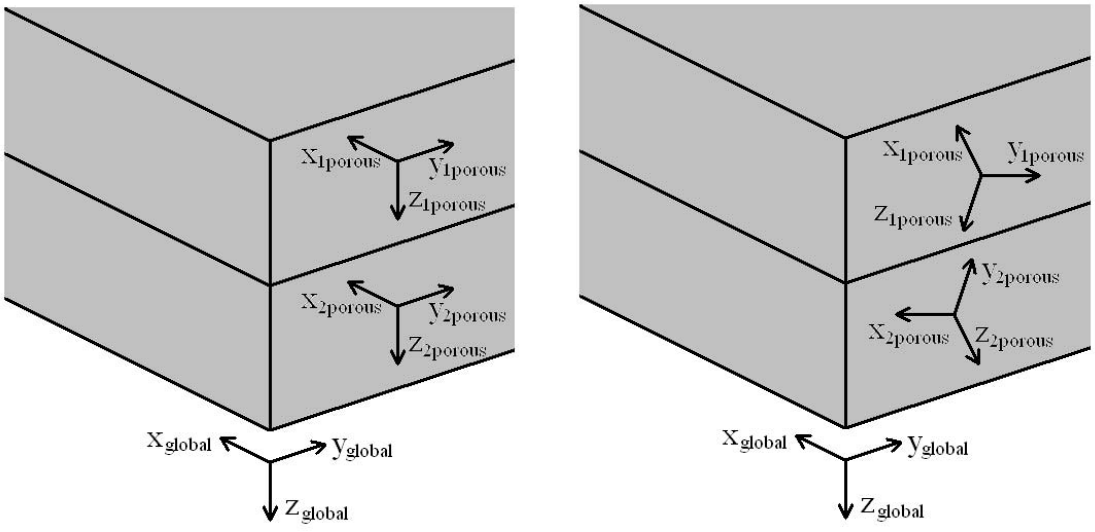

(a) Porous material orientation with [0 0 0]-rotation in both layers.

(b) Porous material orientation with different [α β γ]-rotation in layer 1 and layer 2.

Figure 3.3: Global and local co-ordinate axes and example of possible layer rotations of porous layer 1 and 2 in the panel used in the anisotropic simulation.

The anisotropy of the porous materials were described by and limited to the Hooke's matrix, the flow resistivity tensor and the tortuosity tensor. The objective function

was chosen as the unweighted SPL, eq. 3.1, and the design variables were the Euler angles describing a Z-Y-X fixed axis rotation. As the two porous layers could rotate independently of each other and rotation around the z-axis is redundant for transversely isotropic porous materials the number of design variables needed were six for configuration A and four for configuration B. Both minimizations and maximizations were performed for a number of different starting points.

While the different starting points resulted in more than one minimum and maximum the FRF of the different minima and maxima, although having different material property angles, showed great similarities and the differences in SPL between different minima were also less than 0.5 dB. The overall results show that the acoustic and dynamic properties of the panels were sensitive to angular changes of anisotropic porous materials. The difference between the best case found and the worst case found was 4.6 dB for configuration A and 4.7 dB for configuration B.

3.2 Combined structural and acoustic optimization – a multidisciplinary design tool

Historically, the handling of sound and vibration issues in engineering has taken place in the final stages of the design process when major parts of the structure is already fixed, or sometimes even later, when a noise, vibration and harshness (NVH) problem is already an inevitable fact. This approach may often create the need for after treatment of new lightweight designs, making them less weight optimized and more costly than originally expected. A design tool developed to handle both structural and acoustic issues at an early stage could hopefully make such expensive after treatment redundant. Yet another advantage would be if a design tool could take advantage of the small, but still existing, load bearing capabilities of poro-elastic acoustic materials as well as the naturally occurring acoustic damping properties of lightweight sandwich structures, all within one early design process. Part of the work was dedicated to this complex issue of developing an approach and a method of combining structural and acoustic optimization of multilayered panels within reasonable computational time compared to today's standard.

The starting point for this optimization concept was to replace a conventional car roof, fig. 3.4, with a multilayered panel containing both structural and acoustic porous materials. And while fulfilling the structural requirements, also be optimized considering mass as well as acoustic and dynamic properties.

The multilayered replacement was represented by a flat quarter model with symmetry boundary conditions applied through all layers along the symmetry edges. The inner perforated plate was also fixed in the x-, y- and z-direction along x=0 and y=0. Dynamic forces were applied in x-, y- and z-direction for a frequency range 100 – 500 Hz, fig. 3.5.

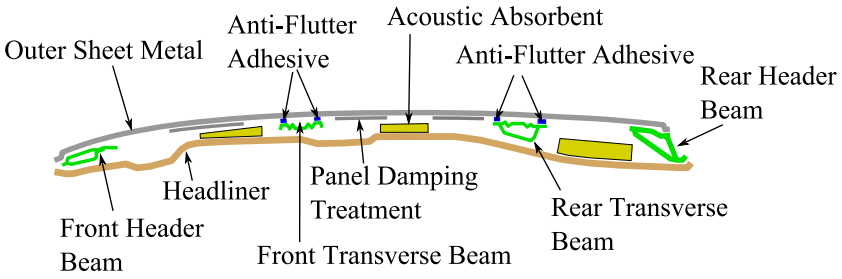

Figure 3.4: Schematic picture of conventional car roof.

As the car roof was represented by a flat panel in the numerical model the effects of the double curved surface of a normal car roof is omitted. Further it should be noted that symmetry boundary conditions preclude non-symmetric modes of vibration. Comparing the results directly with a conventional car roof may therefore be misguiding. However, the conceptual design methodologies presented are valid within their own premiss and may in the future be transferred to more complex panel shapes.

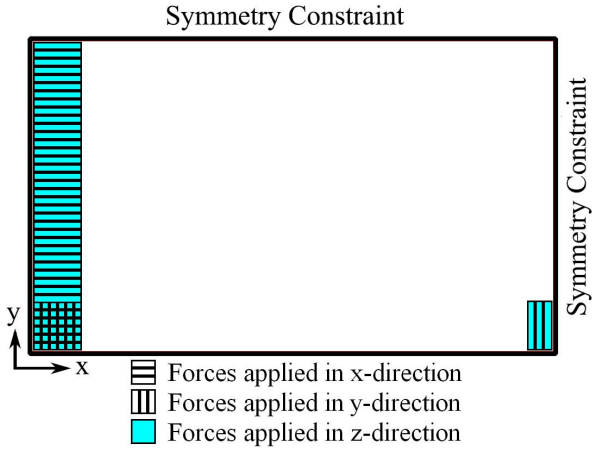

Figure 3.5: Dynamic forces applied to the CF Laminate.

The general design of the lightweight panel replacing the conventional car roof was an outer face sheet of carbon fibre (CF) reinforced epoxy composite laminate and an inner face sheet of perforated CSM (Chopped Strand Mat) GF (Glass Fibre) reinforced plastic. In between the two face sheets different combinations of structural and acoustic porous materials and, in certain configurations, air layers or air pockets were used. For computational reasons the optimization process was divided into different part which were executed in a sequential iterative manner.

Initially four different configurations were tested, where the structural and acoustic foam was divided into different layers, see fig. 3.6, except around the edges of the quarter model where the structural foam directly connected the inner and outer face sheets. Foam A was a PU-foam and foam B a π-foam.

The iterative process started with a structural mass optimization where three different load cases were applied, localised loading, distributed pressure, normal modes analysis,

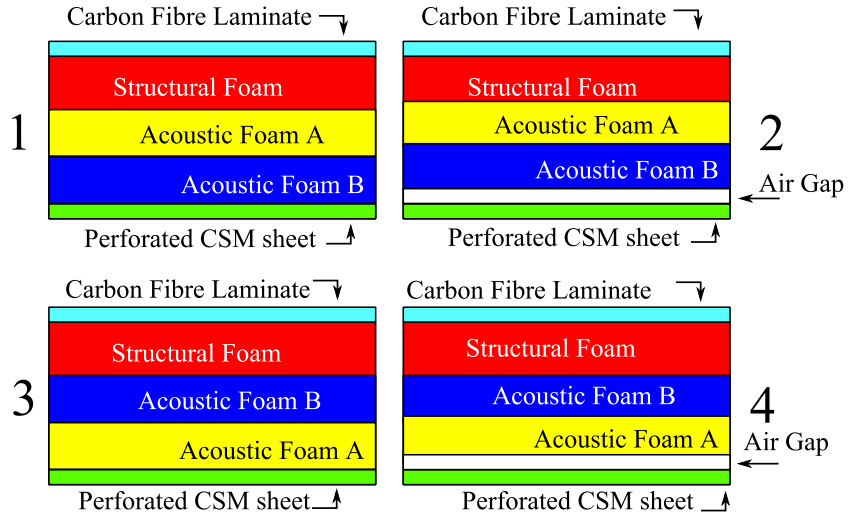

Figure 3.6: Stacking sequence of the different configurations.

using nine design variables and constraints on local and global stiffness so that the system did not exceed a given displacement, neither locally or globally, and so that the frequency of the first eigen mode of the panel would exceed a given minimum. Constraints were also put on the nine design variables. At this point general assumptions were made regarding the properties of the acoustic layers. Thereafter was an acoustic optimization performed, optimizing the relative strut length and the layer thicknesses of the two foam layers, with constraints on the total thickness. The results of the acoustic optimization were then given as input to a second iteration starting with structural optimization. Convergence was achieved after two to three iterations. The results are partly summarized in table 3.1.

		Configuration			
		1	2	3	4
Variable		PU-π	PU-π-air	π-PU	π-PU-air
ρ_{struct}	[kg/m^3]	134	128	143	141
ρ^*_{PU}	[kg/m^3]	38.6	138	138	138
t_{PU}	[mm]	23.0	48.0	47.2	41.5
ρ^*_{pi}	[kg/m^3]	9.31	1.48	2.46	3.86
t_{pi}	[mm]	27.0	1.00	2.46	4.59
Total Thickness	[mm]	79.1	78.7	78.7	75.8
Total Mass	[kg]	18.7	27.3	27.8	26.7
First Eigen Mode	[Hz]	71.8	46.9	64.7	47.0
SPL	[dB]	60.1	59.3	57.9	58.5

Table 3.1: Summary of final values of design variables and main results.

During the optimization process it became clear that the stacking sequence had a great influence on the acoustic response of the panel, especially for the configurations without air gap. Introducing an air gap also resulted in an unavoidably softer panel with a significantly lower first eigen mode. This was expected as the bounding of the core

material to the face sheets is a crucial part of having a structurally stiff low weight sandwich panel. In spite of the softness of acoustic foam its presence and coupling to the inner surface seems to be enough to prevent it from vibrating on its own, and also raising the overall stiffness.

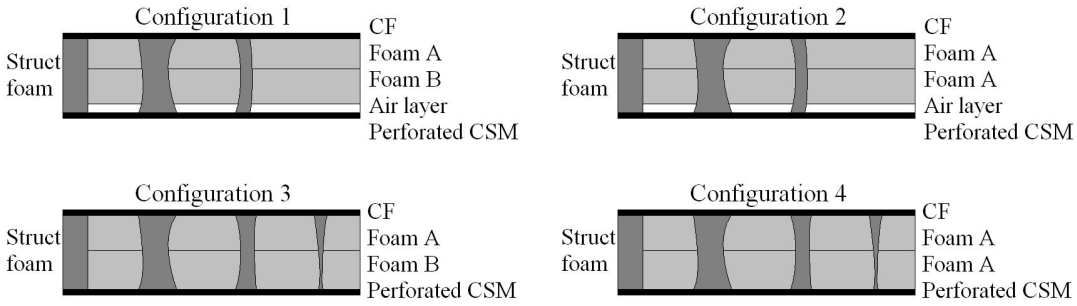

Figure 3.7: Conceptual visualization of the four different configurations. Note that the structural foam topology (dark grey) differs between the air gap and the non air gap configurations.

As a second step of this multidisciplinary design methodology the structural foam was no longer placed in a layer of its own but rather distributed in the core of the panel using topology optimization except along the edges of the panel where a frame of structural foam was used. The part of the core volume without structural foam was divided into two layers of acoustic foam. Four different configurations were set up in which two also an air gap was included, fig. 3.7. Foam A was a PU-foam and foam B a π-foam.

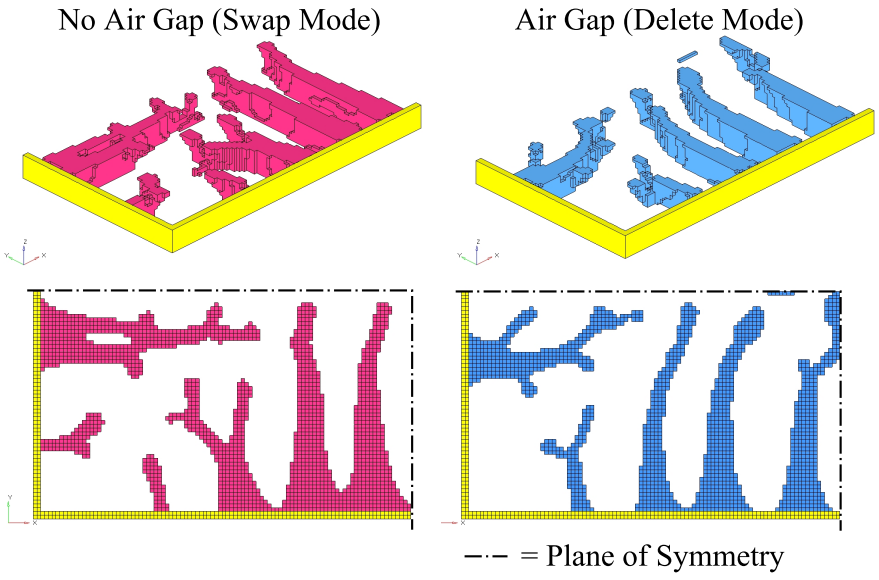

Figure 3.8: Final topology for structural foam in the 1/4 model. Left picture without air gap and right picture with air gap. The frame of fixed elements is also depicted.

This methodology started with a topology optimization using general foam parameters and four different load cases, localized load, distributed pressure, normal modes analysis and in-plane loading, with constraints on local and global stiffness so that the system did not exceed a given displacement, neither locally or globally, also the first eigen mode

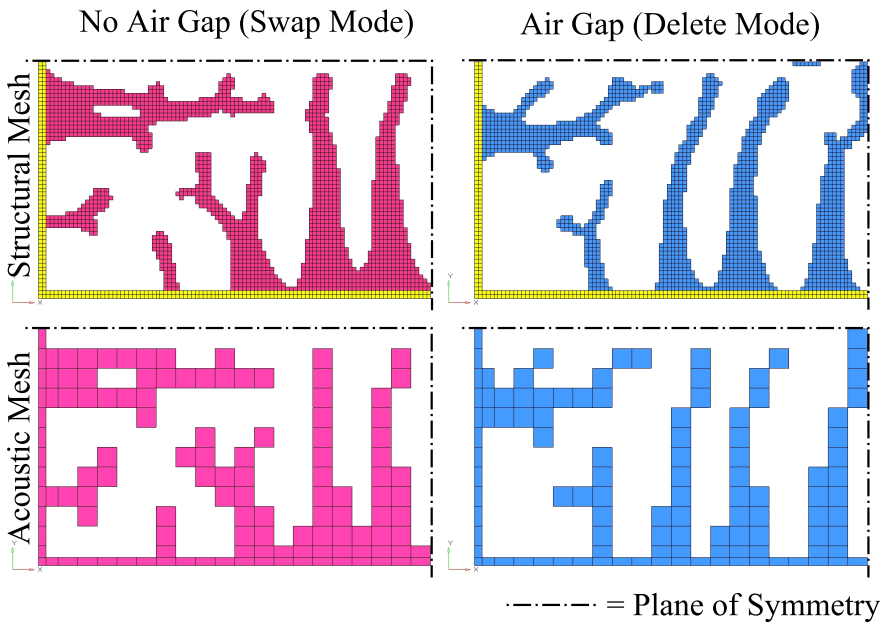

Figure 3.9: Comparison of stuctural (above) and acoustic (below) FE mashes of structural foam core material in the 1/4 model. Left picture without air gap and right picture with air gap. The frame of fixed elements is also depicted.

of the panel should exceed a given minimum frequency and finally a constraint were put on the in plane stability of the panel (buckling). This resulted in two basic structures, one for configurations with air gap and one for configurations without air gap, fig. 3.8. The next step was then the nine structural design variables and finally the four acoustic material parameters were optimized, the relative strut length and the layer thicknesses of the two foam layers. For computational reasons the acoustic model required an increase of element size compared to the structural optimization, see fig. 3.9. The results are partly summarized in table 3.2.

		Configuration			
		1	2	3	4
Variable		PU-π-air	PU-PU-air	PU-π	PU-PU
ρ_{struct}	[kg/m^3]	120	120	105	105
ρ^*_{layer1}	[kg/m^3]	36.3	13.5	6.80	5.01
t_{layer1}	[mm]	72.9	1.00	1.00	4.08
ρ^*_{layer2}	[kg/m^3]	5.29	138	1.96	27.9
t_{layer2}	[mm]	1.00	72.9	73.8	70.7
Total Thickness	[mm]	77.4	77.4	77.3	77.3
Total Mass	[kg]	18.2	31.6	14.0	17.1
SPL	[dB]	70.5	68.7	74.3	71.6

Table 3.2: Summary of final values of design variables and main results.

The results showed that the optimized acoustic foam gave an improved SPL in the air cavity, fig. 3.10. In one case, however, the improvement was combined with a quite severe mass penalty. Although configuration one and two had the same structural

properties the acoustic properties, solely influenced by the acoustic foam layers, were quite different. The acoustic response of configuration three and four also show that the acoustic foam combined with different choice of layer combinations as well as microscopic properties may give significant differences in acoustic signature, fig. 3.11.

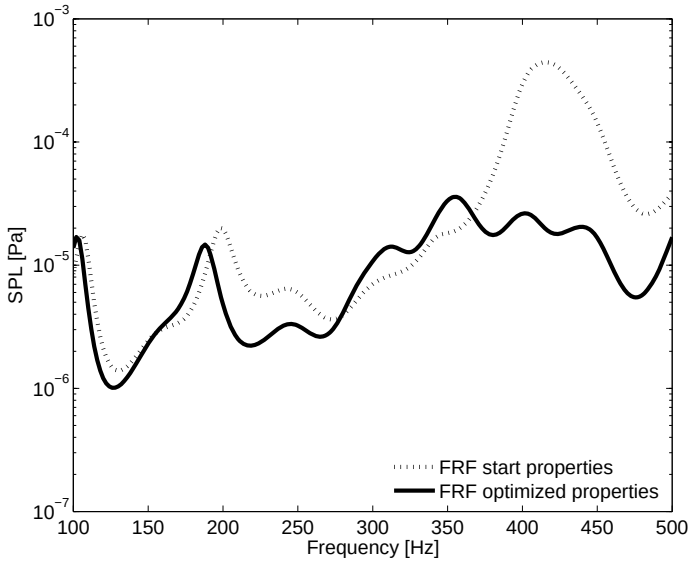

Figure 3.10: Frequency response function for the starting properties and optimized properties of configuration 1.

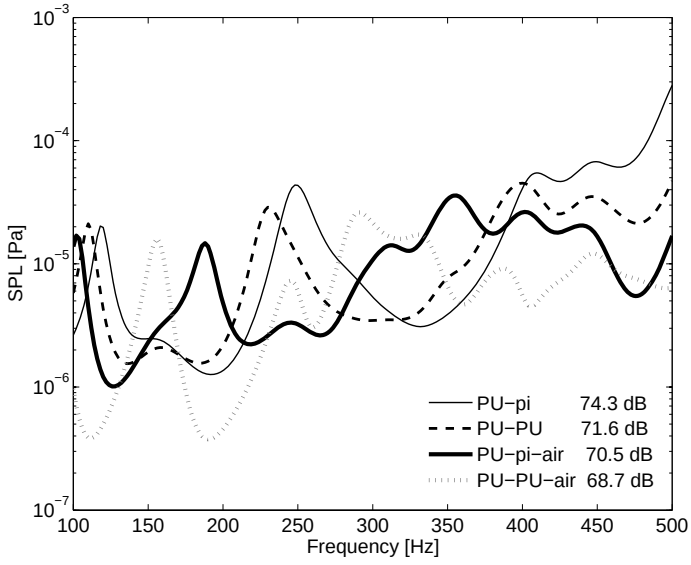

Figure 3.11: Frequency response functions of optimized properties for all configurations.

Chapter 4

Conclusions

The work presented here shows that small alterations of the microscopic geometrical material properties of open cell poro-elastic materials can cause differences of the macroscopic behaviour that is large enough to have a significant impact on the acoustic and dynamic response when assembled in multilayered panel configurations. For anisotropic poro-elastic materials the angular orientation of the macroscopic material properties in individual layers are shown to be important for the overall acoustic and dynamic behaviour of a multilayered panel. As both this and previous work have demonstrated the choice of acoustic poro-elastic materials, layer combinations and layer thicknesses are also of great importance when designing multilayered panels. These physical aspects imply that there are great potential to adapt multilayered structures to specific needs as well as to acoustic and dynamic circumstances.

While previously acoustic treatment has often been added late in the design process there are potentially some great advantages in combining structural and acoustic demands into multifunctional panel structures, as the sandwich panel already have several built-in acoustic benefits, such as fairly high damping, and the acoustic poro-elastic material, however comparably soft, may still contribute to the overall structural performance. However combining these two disciplines requires the development of new design tools, an extensive work of which a small part has been carried out in this thesis.

To efficiently find optimal or at least significantly improved material parameters an optimization approach has been implemented with a previously established finite element numerical modelling tool. The optimization approach is shown to be a fairly efficient and useful way to find such suitable material parameters. However, optimizing a panel for a certain wanted behaviour implicitly demands knowledge of what that behaviour is and how to express it as a numerical value dependent on the design variables. It should be stressed that a properly chosen objective function is crucial as it significantly affects the outcome of the optimization. Achieving a useful result is also dependent of quite detailed knowledge of the load cases and boundary conditions of the system.

Finally, the modelling approaches presented here have the ability of constituting a part of

a useful computer aided design tool, especially when developing lightweight multilayered panels. Such a design tool may be of great importance when striving for lighter and more energy efficient vehicle concepts in the future as it could help maintaining or even improving the NVH properties which are otherwise often penalized when reducing the weight of a structure.

4.1 Future work

A natural continuation of the initialized work on anisotropic poro-elastic material would be to develop computationally efficient scaling laws or other ways to connect microscopic and macroscopic properties for such materials. There is also room for improvement of the suggested scaling laws for isotropic materials. There is a general need for increased understanding of the physical behaviour of poro-elastic materials, especially when assembled in different structures as it may involve several different aspects such as pre-compression of the porous material and difficulties in assigning proper boundary conditions. Achieving such knowledge includes development of measurement techniques of the macroscopic material properties, the physical modelling of those properties and their connection to the geometrical microscopic properties, understanding and modelling of different damping phenomena as well as understanding and modelling of variations of the macroscopic material properties close to the boundaries of a poro-elastic material. For anisotropic poro-elastic materials this need is even greater as the understanding of anisotropic acoustic and dynamic phenomenas in such materials is today quite limited.

To better understand the complex coupled structural acoustic behaviour and to further extend the possibilities of designing mass and space efficient multifunctional panels is also highly sought after. Such knowledge must also be implemented in usable computationally efficient multidisciplinary design tools in order for it to truly make a difference in industrial production techniques.

Increasing the understanding and developing usable models in these areas may be a significant contribution to increase functionality and lower the environmental impact of vehicles and other structures in the future.

Chapter 5

Summary of papers

Paper I

Optimising open porous foam for acoustical and vibrational performance.

E. Lind Nordgren and P. Göransson

A computational method for optimizing microstructural properties of open cell porous foam assembled in multilayered acoustic panels is presented. The method uses previously established scaling techniques to link the microstructural properties to the classical Biot-Johnson-Champoux-Allard macroscopic parameters. This combined with Biot theory allows for calculations of an objective function and also its gradients by using finite differences and thereafter to access a gradient based optimizer. The outer surface of the panel was excited by three separate force fields and the acoustic properties of the panel were evaluated by calculating the sound pressure level for a frequency range 100 – 900 Hz in an air cavity attached to the panel. Different cost functions were tested and the results suggested that if alterations of the microscopic properties of the foam are made, the foam may be adapted to specific environmental conditions and thereby achieve improved acoustic behaviour as well as reduced weight. The choice of cost functions, as well as the chosen frequency range, was however greatly influencing the outcome of the optimization and must be chosen with care.

Paper II

Material Property Based Structural and Acoustic Optimization of a Multifunctional Vehicle Body Panel.

C. J. Cameron, E. Lind Nordgren, P. Wennhage and P. Göransson

A novel design approach involving combined structural and acoustic optimization is proposed that allows for a multilayered load bearing sandwich panel with integrated acoustic capabilities. The method is based on an iterative two-step optimization technique where a mass minimizing structural optimization is followed by an acoustic optimization. The outcome of the acoustic optimization was then used as a starting point for the next iteration beginning with structural optimization. Four different configurations were tested, two of which had an air gap included. Apart from the air gap the panels consisted of a thin carbon fibre laminate face sheet, one layer of structural closed cell polymer foam, two layers of lightweight open cell poro-elastic acoustic foam followed by the optional air gap and finally a thin perforated glass fibre reinforced inner face sheet. The structural as well as the acoustic optimization allowed for variation of the microscopic properties as well as variation of the layer thicknesses within certain boundary conditions. The acoustic response was evaluated for a frequency range 100 – 500 Hz by calculating the sound pressure level in an air cavity connected to the panel. Evaluating the resulting panels it was obvious that the presence or absence of an air gap, as well as the stacking sequence of the acoustic foam layers were of great importance for acoustic and dynamic properties while for the static structural properties the influence of the stacking sequence of the acoustic foam was small or insignificant. The results also indicated that there may be potential advantages of introducing acoustic absorbents in load bearing sandwich panels as the acoustic absorbers, in spite of their low stiffness, still contribute to the overall stiffness of the panel while also being able to improve dynamic and acoustic properties.

Paper III

A Design Method using Topology, Property, and Size Optimization to Balance Structural and Acoustic Performance of Sandwich Panels for Vehicle Applications.

C. J. Cameron, E. Lind Nordgren, P. Wennhage and P. Göransson

A combined structural and acoustic optimization process including topology optimization for load bearing panels is presented. Several different optimization stages were

used starting with a topology optimization to establish the most effective locations for load bearing material within the core of the panel. As a result the inner and outer surface of a panel were connected through a finger like framework of stiff, closed cell, structural foam. Thereafter was a mass optimization process used to tune the exact properties of the outer and inner face sheet as well as the structural foam. The remaining sandwich core volume, not occupied by structural foam was then filled with open cell poro-elastic acoustic materials divided into different layers. Four different configurations were tested, two of which had an air gap next to the inner surface and two had not. The acoustic response was evaluated for a frequency range 100 – 500 Hz by calculating the sound pressure level in an air cavity connected to the panel as the panel was excited by three different dynamic forces. Although the outer and inner surface of the panel were connected by stiff structural foam the results showed that the acoustic properties were still quite affected by small changes in the microstructure of the acoustic porous materials. The design methodology developed also showed a potential to combine and handle not only the intrinsic coupling but also the conflicts between the two physical mechanisms addressed, by offering a new approach to systematically deal with the combined structural and acoustic requirements.

Paper IV

Alignment of anisotropic poro-elastic layers - Sensitivity in vibroacoustic response due to angular orientation of anisotropic elastic and acoustic properties.

E. Lind Nordgren, P. Göransson and J.-F. Deü

A numerical experiment was performed to explore the influence of angular changes of anisotropic poro-elastic layers in multilayered acoustic panels. Two different materials were tested, one orthotropic open cell lightweight acoustic foam and one transversely isotropic fibrous material. The simulation set up consisted of two independent layers of the same porous material connected to an aluminium plate along one surface and separated from an identical aluminium plate through an air gap along the other surface. The sensitivity to angular changes of the porous layers was evaluated as an optimization problem where an objective function was both minimized and maximized in order to compare possible extremal points. The outer surface of each panel was excited by a unit force for a frequency range 100 – 700 Hz and the objective function was defined as the sound pressure level in an air cavity connected to the inner surface. The results showed that anisotropy of poro-elastic acoustic absorbers as well as their angular orientation both had significant influence in terms of acoustic properties of multlayered panels.

Chapter 6

Appendix

6.1 Notations in latin letters

Variable	
$b(\omega)$	viscous drag parameter
$B(\omega)$	frequency dependent function
c_g	pore shape dependent constant
C	solid frame Hooke's tensor
C^{ρ}	material dependent scaling constant for bulk density
C^{dl}	material dependent scaling constant for bulk Young's modulus
C^{E}	material dependent scaling constant for bulk Young's modulus
d	unjacketed compressibility compliance tensor
d_s	average strut thickness of solid frame
E_s	Young's modulus for solid frame material
E^*	Young's modulus for homogenized porous material
K_f	bulk modulus of fluid in the pores
K_s	bulk modulus of the solid frame material
l_s	average strut length of solid frame
p	acoustic pressure
Q	material tensor
R	material scalar
u^f	displacement vector of fluid
u^s	displacement vector of frame

6.2 Notations in greek letters

Greek letter	
α_∞	tortuosity
ε^s	solid frame strain tensor
η	fluid viscosity
θ^f	divergence of fluid displacement
Λ	viscous characteristic length
Λ'	thermal characteristic length
ν	Poisson's ratio
ρ_0	density of fluid
ρ_1	bulk density of solid frame
$\tilde{\rho}^{11}$	complex dynamic mass density for the solid phase
$\tilde{\rho}^{12}$	complex dynamic inertial coupling factor
$\tilde{\rho}^{22}$	complex dynamic mass density for the fluid phase
ρ_a	coupling factor modelled as added density
ρ_s	density of solid frame material
ρ^*	bulk density of solid frame
σ^f	Cauchy stress tensor for fluid
σ^s	Cauchy stress tensor for frame
σ^{static}	static flow resistivity of porous material
ϕ	porosity, volume fraction of open pore fluid content
ω	frequency

6.3 Material properties of reference materials

The Polyurethane foam (PU-foam) and Polyimide foam (π-foam) used as reference foam in this work had the following material properties.

Material property		PU-foam	π-foam
ρ_s	[kg m^{-3}]	1100	1400
E_s	[Pa]	$450 \cdot 10^6$	$1400 \cdot 10^6$
α_∞	[1]	1.17	1.17
ρ_0^*	[kg m^{-3}]	35.4	8
E_0	[Pa]	$164 \cdot 10^3$	$848 \cdot 10^3$
σ_0	[kg m^{-3} s^{-1}]	4500	$1000 \cdot 10^3$
Λ_0	[m]	$96.1 \cdot 10^{-6}$	$39 \cdot 10^{-6}$

Bibliography

[1] J. Akerman and M. Höjer. How much transport can the climate stand?-sweden on a sustainable path in 2050. *Energy Policy*, 34(14):1944–1957, 2006.

[2] J.-F. Allard. *Propagation of sound in porous media: modelling sound absorbing materials.* Elsevier Applied Science, 1993.

[3] J.-F. Allard and Y. Champoux. New empirical equations for sound propagation in rigid frame fibrous materials. *J. Acoust. Soc. Am.*, 6(91):3346–3353, 1992.

[4] N. Atalla, M. A. Hamdi, and R. Panneton. Enhanced weak integral formulation for the mixed (u,p) poroelastic equations. *J. Acoust. Soc. Am.*, 109(6):3065–3068, 2001.

[5] N. Atalla, R. Panneton, and P. Debergue. A mixed displacement-pressure formulation for poroelastic materials. *J. Acoust. Soc. Am.*, 104(3):1444–1452, 1998.

[6] M. A. Biot. Theory of propagation of elastic waves in a fluid saturated porous solid. I. Low frequency range. *J. Acoust. Soc. Am.*, 28:168–178, 1956:1.

[7] M. A. Biot. Theory of deformation of a porous viscoelastic anisotropic solid. *J. Appl. Phys.*, 27:459–467, 1956:3.

[8] M. A. Biot. Mechanics of deformation and acoustic propagation in porous media. *J. Appl. Phys.*, 33(4):1482–1498, 1962.

[9] M. A. Biot and D. G. Willis. The elastic coefficients of the theory of consolidation. *J. Appl. Mech.*, 24:594–601, 1957.

[10] Y. Champoux and J.-F. Allard. Dynamic tortuosity and bulk modulus in air-saturated porous media. *J. Appl. Phys.*, 70(4):1975–1979, 1991.

[11] J. Comiti and M. Renaud. New model for determining mean structure parameters of fixed beds from pressure drop measurements. Application to beds packed with parallellepipedal particles. *Chemical Engineering Science*, 44(7):1539–1545, 1989.

[12] O. Doutres, N. Atalla, and K. Dong. Effect of the microstructure closed pore content on the acoustic behavior of polyurethane foams. *J. Appl. Phys.*, 110(6), 2011.

[13] K. Dovstam. Augmented Hooke's law in frequency domain. A three dimensional material damping formulation. *Int. J. Solids Structures*, 32(19):2835–2852, 1995.

[14] A. Geslain, O. Dazel, J.-P. Groby, S. Sahraoui, and W. Lauriks. Influence of static compression on mechanical parameters of acoustic foams. *J. Acoust. Soc. Am.*, 130(2):818–825, 2011.

[15] L. J. Gibson and M. F. Ashby. *Cellular solids — Structure and properties.* Cambridge University Press, second edition, 1997. First published by Pergamont Press Ltd., 1988.

[16] P. Göransson. Acoustic and vibrational damping in porous solids. *Phil. Trans. R. Soc. A*, 364:89–108, 2006.

[17] P. Göransson, R. Guastavino, and N.-E. Hörlin. Measurement and inverse estimation of 3d anisotropic flow resistivity for porous materials. *J. Sound Vib.*, 327(3-5):354–367, 2009.

[18] R. Guastavino and P. Göransson. A 3d displacement measurement methodology for anisotropic porous cellular foam materials. *Polymer Testing*, 26(6):711–719, 2007.

[19] N.-E. Hörlin. 3-D hierarchical hp-FEM applied to elasto-acoustic modelling of layered porous media. *J. Sound Vib.*, 285(4):341–363, 2005.

[20] N.-E. Hörlin and P. Göransson. Weak, anisotropic symmetric formulations of biot's equations for vibro-acoustic modelling of porous elastic materials. *Int. J. Numer. Meth. Engng*, 84(12):1519–1540, 2010.

[21] N.-E. Hörlin, M. Nordström, and P. Göransson. A 3-D hierarchical FE formulation of Biot's eguations for elasto-acoustic modelling of porous media. *J. Sound Vib.*, 254(4):633–652, 2001.

[22] W.-Y. Jang, A. M. Kraynik, and S. Kyriakides. On the microstructure of open-cell foams and its effect on elastic properties. *Int. J. Solids Structures*, 45(7-8):1845–1875, 2008.

[23] W.-Y. Jang, S. Kyriakides, and A. M. Kraynik. On the compressive strength of open-cell metal foams with kelvin and random cell structures. *Int. J. Solids Structures*, 47(21):2872–2883, 2010.

[24] D. L. Johnson, J. Koplik, and R. Dashen. Theory of dynamic permiability and tortuosity in fluid-saturated porous media. *J. Fluid Mech.*, 176:379–402, 1987.

[25] P. Khurana, L. Boeckx, W. Lauriks, P. Leclaire, O. Dazel, and J.-F. Allard. A description of transversely isotropic sound absorbing porous materials by transfer matrices. *J. Acoust. Soc. Am.*, 125(2):915–921, 2009.

[26] D. Lafarge, P. Lemarnier, J.-F. Allard, and V. Tarnow. Dynamic compressibility of air in porous structures at audible frequencies. *J. Acoust. Soc. Am*, 102(4):1995–2006, 1997.

[27] G. A. Lesieutre. Finite elements for dynamic modelling of uniaxial rods with frequency-dependent material properties. *Int. J. Solids Structures*, 28:1567–1579, 1992.

[28] M. Melon, E. Mariez, C. Ayrault, and S. Sahraoui. Acoustical and mechanical characterization of anisotropic open-cell foams. *J. Acoust. Soc. Am.*, 104(5):2622–2627, 1998.

[29] C. Perrot, F. Chevillotte, M. Tan Hoang, G. Bonnet, F.-X. Bécot, L. Gautron, and A. Duval. Microstructure, transport, and acoustic properties of open-cell foam samples: Experiments and three-dimensional numerical simulations. *J. Appl. Phys.*, 111(1), 2012.

[30] C. Perrot, R. Panneton, and X. Olny. From microstructure to acoustic behaviour of porous materials. *Canadian Acoustics - Acoustique Canadienne*, 32(3):18–19, 2004.

[31] S. Sahraoui, E. Mariez, and M. Etchessahar. Linear elastic properties of anisotropic open-cell foams. *J. Acoust. Soc. Am.*, 110(1):635–637, 2001.

[32] K. Svanberg. The method of moving asymptotes — a new method for structural optimization. *Int. J. Numer. Meth. Engng*, 24:359–373, 1987.

[33] K. Svanberg. A class of globally convergent optimization methods based on conservative convex separable approximations. *SIAM Journal on Optimization*, 12(2):555–573, 2002.

[34] C. Zwikker and C. Kosten. *Sound absorbing materials.*, chapter II and III. Elsevier Publishing Company, Amsterdam, 1949.

Part II

Appended papers

Journal of Sound and Vibration 329 (2010) 753–767

Contents lists available at ScienceDirect

Journal of Sound and Vibration

journal homepage: www.elsevier.com/locate/jsvi

Optimising open porous foam for acoustical and vibrational performance

Eleonora Lind-Nordgren *, Peter Göransson

KTH Aeronautical and Vehicle Engineering, Marcus Wallenberg Laboratory of Sound and Vibration Research, SE-100 44 Stockholm, Sweden

ARTICLE INFO

Article history:
Received 23 February 2009
Received in revised form
26 August 2009
Accepted 8 October 2009
Handling Editor: Y. Auregan
Available online 31 October 2009

ABSTRACT

A computational method for designing optimal arrangements of multilayer noise and vibration treatments in general and porous open cell foam in particular is discussed. The method uses finite element solutions to Biot's equations for poroelastic materials and provides data to evaluate cost functions and gradients. The porous material is parameterised using scaling laws linking the microscopic properties to the classical parameters, i.e. averaged elasticity, flow resistivity and characteristic viscous and thermal lengths. The cost function is either in terms of weight or in terms of the pressure response in a finite cavity, complemented with constraints on the other. However, care must be taken when choosing the cost function, as this will greatly affect the outcome of the optimisation. Observations made during the optimisation process indicate a limited number of minima within the parameter range of interest as well as beneficial continuity around these minima, thus enabling a meaningful optimisation. The results suggest that if alterations of the microscopic properties of the foam are made, the foam may be adapted to specific environmental conditions and thereby achieve improved acoustic behaviour as well as reduced weight.

1. Introduction

Flexible porous foams with open cells are generally considered to be good sound absorbers and vibration isolators, and are therefore often used to improve the noise vibration and harshness (NVH) comfort, commonly in automotive applications. However, adding such materials in vehicles generally has a negative impact on the overall weight and consequently the fuel or energy consumption. Hence, it is necessary to achieve the best possible performance, per added weight and cost, from the added material. In current practice, efficient use of porous foam often involves multiple layers of various open cell foam, i.e. foam with different mechanical and material properties. Designing such complex structures, fulfilling various requirements, is at best a very time consuming task due to the extensive testing needed to achieve good results. Furthermore, there is also the question of defining the acoustic performance of a specific foam or combination of foam layers. At present, lightweight porous acoustic multilayer trim components are traditionally specified in terms of sound absorption and transmission loss. Foam that is developed according to this way of characterising their efficiency may, however, be sub-optimal in specific applications where for example structure borne sound is a major part of a vibration problem. Clearly there is a need for computational tools and procedures that are able to predict and optimise the behaviour of such multilayered structures. The present paper presents such a methodology for optimising porous layers in a multilayered configuration.

* Corresponding author. Tel.: +46 8 7907941; fax: +46 8 7906122.
E-mail address: eleonora@kth.se (E. Lind-Nordgren).

0022-460X/$ - see front matter © 2009 Elsevier Ltd. All rights reserved.
doi:10.1016/j.jsv.2009.10.009

Nomenclature

$b(\omega)$	frequency-dependent viscous drag parameter
c_g	pore shape dependent constant
C^ρ	foam dependent scaling constant for bulk density
C^σ	foam dependent scaling constant for static flow resistivity
C^E	foam dependent scaling constant for bulk E-modulus
d_s	average strut thickness of solid frame
E^s	Young's modulus for solid frame material
E^*	Young's modulus for homogenised foam
l_s	average strut length of solid frame
p	acoustic pressure
Q	dilatational coupling factor between fluid and solid frame
R	bulk modulus of fluid phase at zero solid frame dilatation
$\overline{u}_i^f$	Cartesian component of average fluid displacement
$\overline{u}_i^s$	Cartesian component of average solid displacement
α_∞	tortuosity
η	dynamic viscosity
λ	bulk Lamé's parameter at constant fluid pressure
$\hat{\lambda}$	bulk dynamic Lamé's
Λ	viscous characteristic length
Λ'	characteristic thermal length
μ	bulk Lamé's shear parameter
$\hat{\mu}$	bulk dynamic Lamé's shear parameter
ρ_a	inertial coupling factor, $\rho_a = -\rho_{12}$
ρ_f	density of fluid
ρ_s	density of solid frame material
ρ^*	bulk density of solid frame
σ^{static}	static flow resistivity of foam
ϕ	porosity, volume fraction of open pore fluid content
ω	frequency

In flexible porous foam, the vibroacoustic energy is carried both through the fluid in the pores (e.g. air) and through the solid frame material itself. The waves are strongly coupled and propagate simultaneously along the two phases with different amplitude and relative phase angle. Differences in amplitude and phase will transform some of the mechanical-acoustical energy into heat, mainly due to viscoelastic and viscoacoustic phenomena in the solid frame and at the interface between the solid frame and the fluid in the pores.

When modelling wave propagation through a porous medium, the foam is described as a homogenised continuum with co-existing solid and fluid phases with a coupled frame-fluid wave propagation—an approach commonly known as Biot's theory, see e.g. [1–3]. In Biot's theory the macroscopic space averaged properties of the foam, such as bulk density, porosity, flow resistivity and Young's modulus, are required. The dynamic behaviour is then presented as macroscopic space averaged quantities e.g. solid and fluid displacement, acoustic pressure, and elastic stress.

While known macroscopic properties can be used to derive the necessary macroscopic dynamic quantities appearing in Biot's equations, the former are inherently dependent on microscopic properties of the foam, such as geometry (e.g. pore size, strut length and strut thickness) as well as the actual material used for the solid frame. Thus improving the dynamic behaviour by optimising the macroscopic properties independently of one another is doubtful as it would most likely result in a foam that is impossible to realise physically. An alternative approach would be to use scaling laws that relate the macroscopic properties to the microscopic ones, where the latter may be changed independently. This is the approach taken in the current paper.

The objective of the present work is to establish a methodology to estimate the acoustic behaviour of porous foam as well as to explore the possibilities to optimise this behaviour. This is carried out by minimising a cost function when the foam is affected by an oscillating force or other acoustical phenomena. Another purpose of the paper is to show that alterations in the micromechanical properties of foam may have a significant effect on the acoustical behaviour and that, if these micromechanical properties could be controlled, foams could be tailored for specific needs. This may allow for NVH problems to be treated from another point of view than previously possible, i.e. design for application performance.

This paper will briefly review Biot's theory and a proposed set of parametric relations between microscopic structure and macroscopic homogenised properties that may be used in the formulation of a 3-D finite element model providing the response of a multilayered structure. In the model, a panel is connected to an air filled cavity, in a sub-volume of which the sound pressure level is evaluated for a given load. Results from optimisation of one layer in a multilayered configuration are discussed, in particular in view of the frequency weighting functions applied to evaluate the response and the influence the different weighting functions have on the optimal configuration found.

1.1. Related work

Optimising the performance of porous foams, modifying the microstructure geometry, has recently been discussed in the context of structural acoustic performance as well as acoustic absorption, targeting single and multilayer configurations.

Simon et al. [4] performed calculations of transmission loss resonance frequencies of a number of multilayered panels in order to determine the best layer combination. The material database originally consisted of several Nomex honeycomb, fibre glass, Kevlar, carbon and viscoelastic materials. The calculations suggested that due to the high stiffness of the included materials the resulting panel basically followed the mass law for the frequency band 500–5000 Hz and that the high damping provided by the viscoelastic layer was beneficial only at the coincidence frequency. Instead they proposed a solution using foams that are less stiff than e.g. honeycomb. Based on simulations of the transmission loss, which were partly validated in laboratory testing, the conclusion was that sandwich panels with open cell foam provide an adequate option for efficient noise applications.

Focusing on the actual optimisation routine, Tanneau et al. [5] discussed a method using genetic algorithms to optimise the layer combination, in terms of the number of layers and their respective thicknesses. Their optimisation was performed with materials chosen from a list of possible candidates. The list contains a limited number of solids, fluids and foam, where each foam is described with a set of material properties, among them: porosity, flow resistivity, tortuosity and Young's modulus. Such an optimisation may result in a well performing trim panel by using readily available foam, which is of course very attractive in most practical situations. This approach, however, requires previously known material parameters for each material that may be included in the multilayered configuration, a quite extensive and possibly costly measurement task. It also excludes the possibility of designing a new material for a specific task.

Lee et al. [6] performed a topology optimisation using the transfer matrix derived from Biot's equations to maximise the transmission loss. The authors used an MMA optimiser [7] to find the optimal layer sequence consisting of air layers and layers of a specific poroelastic material with fixed properties. The optimisation was performed at single frequencies as well as for narrow and wide frequency bands. The frequencies or frequency bands studied were all between 1 and 5 kHz. Results from the single frequency optimisation show that as the target frequency increases the number of layers increases. In addition the thickness of each layer decreases, partly due to constraints on the total thickness but mainly due to the shorter wavelengths that correspond to high frequencies. The results for single frequency optimisations were also compared with results of narrow band optimisations. As expected were the foams optimised for narrow band frequencies outperformed by the single frequency optimised foam at each individual frequency. The number of layers, however, increased as the upper and lower frequencies of the frequency band were increased, in agreement with the results from the single frequency optimisation.

Work that to some extent explored the influence of geometrical properties was performed by Franco et al. [8], who examined a sandwich panel with different core and face sheet properties. One configuration was a core made of a lattice of truss elements; this allowed independent control of the core stiffness along different directions. The truss like core was modelled as rod elements with the intent to minimise the mean square average inner surface velocity over a chosen frequency range. Their model, however, only regarded Young's modulus in different directions of a truss like unit cell by altering the cross-sectional area of the rod elements in different directions, whereas neither the coupled wave propagation due to the frame–fluid interaction, any of the well established energy dissipative mechanisms of foam nor the effects of damping levels with respect to different frequency bandwidths were included.

In addition the optimal microstructure properties in the context of sound absorption were discussed by Perrot et al., see [9–13]. Using numerical solutions of e.g. Stokes equations, appropriate parameters were calculated for given microstructures and fed into the proper macroscopic relations. They found interesting effects of throat size on absorption level, cell size in the peak absorption frequencies and fibre cross-section shape in the weight of the porous material.

The approach of the present paper explores the possible effects of altering the microscopic structure of a specific foam and the resulting acoustical properties to achieve optimal structural acoustic performance in a given application. It is apparent that the result very well may be a foam that is not presently available, but perhaps still possible to produce. Thus it is expected that this methodology may present new possibilities to predict the necessary acoustic properties and to guide in the future creation of foams that fulfil specific needs. To enable such an optimisation tool, a direct link between the foams microstructural properties and the acoustic performance is a necessity.

2. Modelling aspects

Modelling and optimising the acoustic behaviour of foams in multilayered structures requires the inclusion of several physical mechanisms representing the dynamic frequency-dependent mechanical and acoustical properties of the complex arrangement of different layers of solids, fluids and foam materials. To efficiently and accurately solve the equations governing such behaviour the finite element method is an adequate numerical solution procedure, in particular for intricate structures. However, to ensure a useful result great care has to be taken in the selection of trial solutions as well as handling the many different boundaries and interfaces within the multilayered structure. The complexity of the problem makes it computationally expensive to solve and as each frequency is solved independently, limiting the frequency range is a necessity. Furthermore, optimising the properties of one or more of the included layers requires several iterations, consequently, the optimiser's ability to find a minimum using as few iterations as possible is crucial for success.

2.1. Biot's equations

To describe the macroscopic mechanical behaviour of porous materials Biot's theory is frequently used, see e.g. [1–3]. The Biot theory describes the solid frame of the porous material and the pore fluid as an equivalent elastic solid continuum and an equivalent compressible fluid continuum, respectively. Part of Biot's theory is similar to the contemporary one presented by Zwikker and Kosten in [14] with the difference that Biot also included the effects of shear stress in the elastic frame of the porous medium. While Biot's theory is formulated for general anisotropic materials, the present work has only considered isotropic poroelastic materials. By extending Biot's theory to include internal losses and by treating the solid phase as separated from the fluid phase, the equations for the solid and fluid displacement, $\overline{u}^s$ and $\overline{u}^f$, respectively, may be written as

$$\hat{\mu}\overline{u}^s_{i,jj} + \left(\hat{\lambda} + \frac{Q^2}{R} + \hat{\mu}\right)\overline{u}^s_{j,ij} + \omega^2\rho^*\overline{u}^s_i + (\omega^2\rho_a - \mathrm{i}\omega b)(\overline{u}^s_i - \overline{u}^f_i) + Q\overline{u}^f_{j,ij} = 0 \tag{1}$$

$$R\overline{u}^f_{j,ij} + \omega^2\phi\rho_f\overline{u}^f_i + (\omega^2\rho_a - \mathrm{i}\omega b)(\overline{u}^f_i - \overline{u}^s_i) + Q\overline{u}^s_{j,ij} = 0 \tag{2}$$

Eqs. (1) and (2) assume material isotropy, small displacements and a time harmonic motion $\mathrm{e}^{\mathrm{i}\omega t}$. The constants $\hat{\mu}$, $\hat{\lambda}$, b, Q and R are complex valued material parameters which are dependent on the angular frequency ω.

The parameters $\hat{\mu}$ and $\hat{\lambda}$ represent the elastic-viscoelastic effects and are frequency-dependent analogies to Lamé's constants μ and λ. In other words, $\hat{\mu}$ and $\hat{\lambda}$ introduce frequency-dependent complex damping in the solid frame. They are thoroughly described in the augmented Hooke's law (AHL) introduced by Dovstam [15]. The acoustic-viscoacoustic effects are described by b, Q and R which are the viscous drag constant, the dilatational coupling and the pore fluid bulk modulus, respectively. Further description of the above material parameters may be found in [14,16–19].

2.2. Mechanical properties and scaling laws

In order to carry out a meaningful optimisation of the material properties of the foam, scaling laws, i.e. relations between the macroscopic properties of the foam to the underlying microscopic properties, would be required. Such scaling laws should preferably describe the macroscopic properties of the porous material as being continuously and systematically dependent on the microstructural mechanical properties. Contributions to developing scaling laws and increasing the understanding of the mechanical properties of foam have been made by several researchers.

In works by e.g. Warren and Kraynik [20,21], some mechanical properties, bulk modulus, two shear moduli and Young's modulus, are derived by analysing the stress–strain relations in repeated geometrical cell-shapes using mechanical laws. This relates the macroscopic mechanical properties to microscopic ones, e.g. Young's modulus of certain foam cell shapes to Young's modulus of the strut material and the relative density with a numerical constant that is dependent on e.g. cell shape, strut shape and joint shape. Although their work does not cover all the scaling laws needed for the current optimisation it offers a valuable insight into the microscopic behaviour of foam materials.

For simplicity the elasticity model used in the current paper is based on the work of Gibson and Ashby [22], where an isotropic open cell foam is modelled as a cubic array, see Fig. 1. The scaling laws, however, can be transferred to an arbitrary cell shape, assuming linear elastic properties in the strut material and that the struts primarily deform in bending. The following scaling laws also assume high porosity and that the strut material is significantly heavier than the interstitial fluid. The second assumption allows for the porosity, ϕ, to be expressed in terms of the bulk density of the foam, ρ^*, and the density of the strut material, ρ_s,

$$\phi = 1 - \frac{\rho^*}{\rho_s} \tag{3}$$

where ρ^*/ρ_s is the relative density. Furthermore it may be shown that the relative density is proportional to the thickness and the length of the struts forming the cells,

$$\frac{\rho^*}{\rho_s} = C^\rho\left(\frac{d_s}{l_s}\right)^2 \tag{4}$$

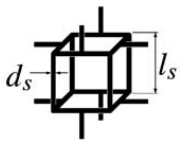

Fig. 1. Cell microstructure as assumed by Gibson and Ashby.

Finally, by simple mechanical reasoning, see [22], Young's modulus, E, can be related to the strut dimensions and consequently to the relative density

$$\frac{E^*}{E_s} = C^E \left(\frac{\rho^*}{\rho_s}\right)^2 = C^E C^\rho \left(\frac{d_s}{l_s}\right)^4 \tag{5}$$

The scaling laws have been further developed by Göransson [23]. Here relations between the microstructure and the viscous characteristic length, Λ, by Allard and Champoux [24], are used to formulate a relation for the characteristic viscous length and the static flow resistivity of the foam, σ^{static}. From Allard and Champoux, it may be deduced that assuming a pore channel with parallel walls:

$$\Lambda = \frac{1}{c_g}\sqrt{\frac{8\alpha_\infty \eta}{\phi \sigma^{\text{static}}}} \tag{6}$$

where c_g is a pore shape dependent constant that for cylindrical geometry is equal to one. η is the viscosity of air and α_∞ is the tortuosity. According to Allard the viscous characteristic length, Λ, may also be derived from the velocity field around a cylinder in an acoustic field [16]. Assuming high porosity and cylindrical struts Λ may be related to the microscopic properties as

$$\Lambda = \frac{d_s}{4(1-\phi)} = \frac{d_s}{4(\rho^*/\rho_s)} \tag{7}$$

The characteristic thermal length, Λ', was approximated as $\Lambda' = 2\Lambda$ [16]. Adopting the common assumption that the parallel duct flow model may be used for an open cell strut like foam, Eqs. (6) and (7) give

$$\sigma^{\text{static}} = \frac{8\alpha_\infty \eta}{1-(\rho^*/\rho_s)} \cdot \frac{16(\rho^*/\rho_s)^2}{c_g^2 d_s^2} \tag{8}$$

where $0 < \rho^*/\rho_s < 1$. Assuming high porosity, $(1-(\rho^*/\rho_s)) \to 1$, constant tortuosity and by using a first-order series expansion, Eq. (8) may be simplified to

$$\sigma^{\text{static}} = \frac{C^\sigma}{d_s^2} \cdot \left(\frac{\rho^*}{\rho_s}\right)^2 \tag{9}$$

Eq. (9) represents the approximate dependence of the flow resistivity on the thickness of the struts as well as the relative density of the porous material. It is an approximation on the same level as Eq. (6) which is commonly used in analysis of open cell foam, having microstructural cell geometries far away from the original cylindrical channel that is the underlying assumption for this relation.

The constants C^ρ, C^E and C^σ are partly dependent on the microscopic mechanical properties of the foam, such as cell shape and to some extent also strut cross section shape and joint region shape. While the scaling laws by Warren and Kraynik [20,21] offers numerical values to some of these constants, they also require knowledge of cell shape, strut cross section shape and to some extent also joint region shape since these constants are dependent on those microscopic mechanical properties of the foam. Such microscopic geometrical properties may vary between different foams and are not always readily specified. The scaling laws presented in the present paper instead require a set of known macroscopic material parameters from an existing foam, as well as knowledge of the strut material properties, in order to acquire the constants C^ρ, C^E and C^σ. Provided that the material properties used to derive these constants are correct the constants will automatically, but maybe not totally, be adapted to cell shape, strut shape and joint shape. Thus, the grossly simplified cubic cell geometry will still capture the most important deformation mechanisms.

The scaling laws in Eqs. (4), (5) and (8) may also be written as

$$\rho^* = \rho_{\text{ref}} \left(\frac{d_s}{d_{\text{ref}}}\right)^2 \left(\frac{l_{\text{ref}}}{l_s}\right)^2 \tag{10}$$

$$E^* = E_{\text{ref}} \left(\frac{\rho^*}{\rho_{\text{ref}}}\right)^2 \tag{11}$$

and

$$\sigma^{\text{static}} = \sigma_{\text{ref}}^{\text{static}} \left(\frac{\rho^*}{\rho_{\text{ref}}}\right)^2 \cdot \left(\frac{d_{\text{ref}}}{d_s}\right)^2 \cdot \frac{\alpha_\infty}{\alpha_{\infty \text{ref}}} \cdot \frac{\left(1-\frac{\rho_{\text{ref}}}{\rho_s}\right)}{\left(1-\frac{\rho^*}{\rho_s}\right)} \tag{12}$$

where Eq. (12) may be simplified into

$$\sigma^{\text{static}} = \sigma_{\text{ref}}^{\text{static}} \left(\frac{\rho^*}{\rho_{\text{ref}}}\right)^2 \cdot \left(\frac{d_{\text{ref}}}{d_s}\right)^2 \tag{13}$$

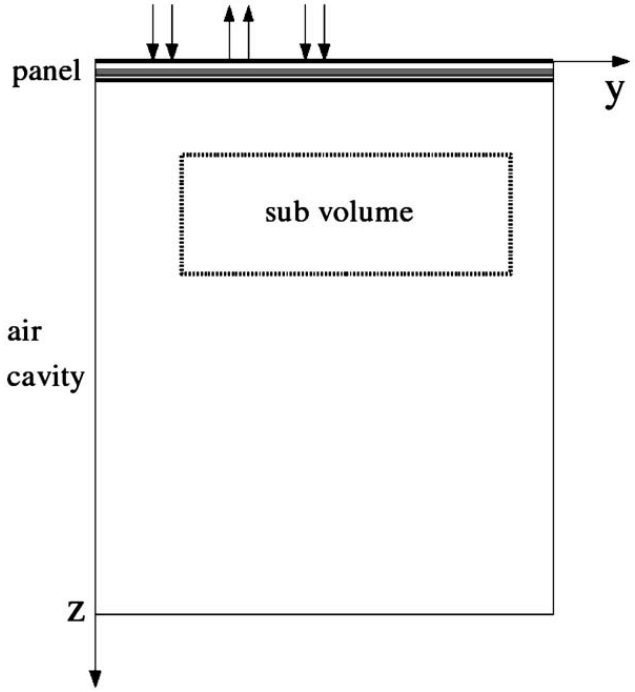

Fig. 2. Schematic picture of FE-model with coordinate system and applied forces.

using the same assumptions as for Eq. (9). The parameters ρ_{ref}, d_{ref}, l_{ref}, E_{ref}, $\sigma_{\mathrm{ref}}^{\mathrm{static}}$ and $\alpha_{\infty\mathrm{ref}}$ corresponds to the density, Young's modulus, strut thickness, strut length, static flow resistivity and tortuosity of the reference foam.

As the properties of the foam used to derive the scaling laws are comparable to the range of foam regarded in the optimisation, the scaling laws presented above, however simplified, may provide a useful tool to estimate the effect of small changes of the microscopic properties of the foam. The material properties for the porous materials used as reference materials in this paper, a polyurethane based and a polyimide based foam (PU-foam and $\pi-$foam, respectively), may be found in Appendix A. The optimisation was then performed for both these types of foam and the results are discussed below.

2.3. FE-modelling

The multilayered structures of interest in vehicle application often involve complex arrangements of different porous materials combined with purely solid or fluid layers, all with their specific boundary conditions and geometries. To calculate the acoustical mechanical response of such an intricate multilayered structure, some kind of numerical solution procedure is required. Such a numerical model must take into account not only the properties of the individual porous layers, e.g. the fluid in the pores, the solid frame structure and the coupling between them. It also has to consider the boundaries to other solid, fluid or porous layers, with appropriate treatment of the kinematic conditions, the mass flow continuity conditions and the relevant stress balances.

Additionally, special care has to be taken in the selection of trial functions to get convergent solutions to Biot's equations, especially for multilayered structures, for which hp-FEM[1] is a convenient finite element base. Here the finite element solutions were obtained using the methods thoroughly discussed and properly addressed in works by Hörlin et al. [25] and by Hörlin [26] and will not be repeated here. For completeness, however, some details of the mesh and the polynomial orders used are given below.

The analysed model is designed to describe the behaviour of an existing system where a multilayered structure acts as a roof panel for a vehicle compartment. The design of the original panel, for which several measures had already been taken to improve the NVH comfort inside the compartment, is used as a starting point and the properties of the individual sub-layers of the panel are given in Appendix B. The original design, as well as the FE-model, consists of a number of different layers intended for load carrying and/or vibration comfort purposes, with the main difference that one of the layers of the original design is a 0.01 m thick layer of air. For identification purposes, the order of the sub-layers were named as: Outer panel sheet—Air gap 1—Foam 1—Solid 1—Solid 2—Air gap 2—Interior panel sheet. The air layer named Air gap 1 is in focus for the present investigation, with the aim to illustrate microstructure optimisation in the present paper. Replacing this air layer with a layer of porous foam of equal thickness will doubtlessly incur a weight penalty. The main question is

[1] Convergence is achieved by refining the mesh and/or increasing the approximation order.

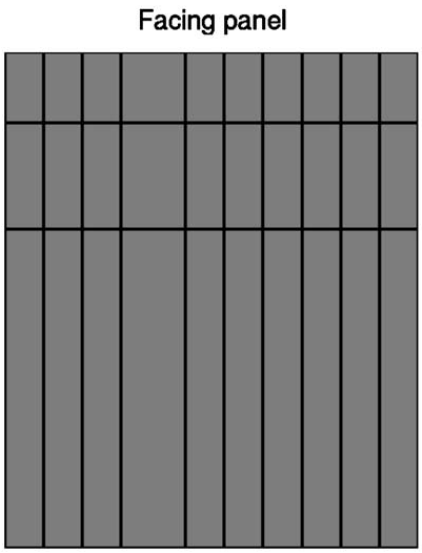

Fig. 3. Mesh of cavity FE-model with surface to panel indicated.

Table 1
Polynomial orders used in z-direction for each individual panel sub-layer, from top to bottom.

Sub-layer	Polynomial order
Outer panel sheet	4
Optimised foam	5
Foam 1	5
Solid 1	4
Solid 2	4
Air gap	2
Interior panel sheet	4

then what improvement in NVH comfort can be expected in exchange for the additional mass and, as a result of the optimisation, what is the best choice of foam to maximise the benefit of the added material?

The modelled panel, with length $L_y = 1.19$ m, consists of seven different layers where the outer and inner surfaces both have solid face sheets. The total thickness of the panel is $L_z^{\text{panel}} = 23.3$ mm and the thickness of the layer of optimised porous foam is 10 mm. The boundaries of each individual porous or solid layer of the panel at $y = 0$ and $y = L_y$ are clamped i.e. zero deflection and zero rotation whereas the boundaries between layers follow kinematic conditions and mass flow continuity requirements as mentioned previously. The outer surface of the panel is driven by three separate force fields, one out of which is 180° out of phase. Thus for $L_z = 0$, positive unit tractions were applied over: $y = 0-0.11$ m and $y = 0.51-0.62$ m; and negative unit traction over $y = 0.33-0.51$ m. The chosen force field is related to the transmission and radiation of structure borne sound, a common source of NVH problems in vehicle acoustics.

In order to enable evaluation of sound pressure levels and sound intensity the panel is connected to an air filled cavity with dimensions $L_y = 1.19$ and $L_z^{\text{cavity}} = 1.4$ m. The total length L_z is consequently $L_z = L_z^{\text{panel}} + L_z^{\text{cavity}}$ m.

For the air filled cavity there is an impedance boundary at $y = L_y$ and $z = L_z$ with a non-frequency-dependent, normal impedance equivalent to $Z = 1180 + 1044$i, which implies an absorption factor of about 50 percent. The last boundary of the air cavity, at $y = 0$, is considered to be acoustically hard (Fig. 2).

A schematic picture of the FE-model for the cavity mesh may be found in Fig. 3. Along the y-direction, a compatible mesh with 10 elements was used for the panel as well as for the cavity. For each of the sub-layers in the panel, one element through the thickness was used. In order to have a reasonably computationally efficient solution, the polynomial orders were adjusted through the different sub-layers as shown in Table 1. The polynomial orders were chosen such that the computed results had a point wise error better than 10 percent, for both displacements and pressures, at the highest frequency studied. In addition the in-plane polynomial orders were adapted to the high and low frequency ranges as discussed below.

2.4. System response

The system response was evaluated for the frequency range 100–900 Hz and the polynomial order of the base functions used to describe the porous layers was varied depending on frequency. At higher frequencies higher-order polynomials, up to 10th order, were needed to dissolve the wave pattern whereas at lower frequencies, below 600 Hz, 6th-order

polynomials were found to be sufficient. Due to the high polynomial order needed at the higher frequencies the calculation becomes very expensive. Despite this, and due to the occurrence of lowly damped acoustic cavity resonances, the frequency resolution was kept at 1 Hz all through the frequency range considered.

The sound pressure square, p_f^2, for each evaluated frequency, f, is calculated as the average of the square sound pressure in a number, N, of discrete points in a sub-volume of the air cavity, Eq. (14). The sub-volume, see Fig. 2, was chosen to represent possible ear positions of hypothetical passengers. It is bound by the following lines; $y = 0.22$ and 1.08 m, $z = 0.2233$ and 0.5233 m. In the results discussed here, N, was chosen to be 16, all points distributed in the y–z plane,

$$p_f^2 = \frac{1}{N}\sum_{n=1}^{N} p_{f_n}^2 \tag{14}$$

2.5. Formulating the optimisation problem

To compare different solutions a cost function was formulated. In the present optimisation problem either mass or sound pressure level were used, implying of course that while trying to minimise one, constraints were put on the other. In order to compare sound pressure levels over the entire frequency range the sound pressure square for each frequency were multiplied with a frequency-dependent weighting factor and a factor for frequency resolution, Δf_f, compensation and then summed over the entire frequency range. The weighting factor was chosen to correspond to either A-weighting, C_f^A, or C-weighting, C_F^C,

$$\langle \mathrm{SPL} \rangle_{\Omega_{\mathrm{sub}}}^{C} = 10 \cdot \log\left(\frac{\sum_{f=f_1}^{f_{\max}} (p_f^2 \cdot \Delta f_f \cdot C_f^C)}{p_0^2}\right) \tag{15}$$

The actual optimisation was performed with an MMA optimiser provided by Svanberg [7]. The input to the MMA optimiser consisted of the numerical values of cost function and its first and second derivate for each variable, the min- and max-values for each variable and also the numerical values of the constraint functions and their first and second derivate. The derivatives and second derivatives were calculated with finite differences and are equivalent to vectors containing the gradient and the diagonal elements of the Hessian matrix, respectively. The variables in the optimiser were chosen to be the bulk density and the strut thickness of the foam. Their respective min- and max-values were set to $8 \le \rho^* \le 70\,\mathrm{kg\,m^{-3}}$ and $10^{-7} \le d_s \le 10^{-4}$ m. These parameter ranges should be feasible and realistic for the problem at hand and furthermore lie in the range of commercially available foams. As a starting value for the strut thickness, $d_s = 10^{-5}$ m was used. For the density $15\,\mathrm{kg\,m^{-3}}$ was used.

2.5.1. Parameter space

Studies of the variation in the frequency response function obtained for varying ρ^* and d_s showed that the bulk density had a clear impact on the frequency response while the strut thickness had a much more modest effect. This was expected from previous experiences; the functional dependence between the bulk density and the flow resistivity for varying strut dimensions, described in Eq. (9) and illustrated by Göransson [23], implied that for very high porosities, above 95 percent, the bulk density indeed is the dominating parameter. For slightly lower porosity, less than 80 percent, the strut thickness becomes increasingly important for the flow resistivity, which characterises the viscous dissipation at low frequencies. The extent to which this applies may of course vary between different foams.

2.5.2. Effects of the weighting function

As described previously, weighted summation over the entire frequency range was performed in order to enable a comparison of the total sound pressure level in the sub-volume. The weighting factor corresponding to C-weighting is almost totally flat in the frequency range 100–900 Hz implying that the summed sound pressure level based on the frequency response shown in Fig. 4 would, for most ρ^*, be dominated by the sound pressure for low frequencies. On the other hand, the weighting factor corresponding to A-weighting would cause the summed SPL to be dominated by the sound pressure in high frequencies, illustrated in Fig. 5. The choice of weighting function will obviously affect the summed SPL and hence the outcome of the optimisation. Assigning a numerical value to an experienced noise, consisting of both tonal and broadband noise is an important but difficult task. The value should represent the total level of annoyance as well as other possible negative effects, a question that is often addressed in psycho-acoustics and cannot be fully investigated here. Historically the A-weighting curve is the most commonly used though it is originally meant as weighting function simulating the experienced noise level at low sound pressure levels. Whereas the B- and C-weighting is more suitable for medium high and high sound pressure levels, respectively. When measuring aircraft noise a special D-weighting is sometimes used. The D-weighting is fairly similar to the B-weighting in the frequency range 100–900 Hz. The A-, B-, C- and D-, weightings are, however, developed only based on the audible sound as it is perceived by the human ear, experienced discomfort due to structural vibrations is not at all accounted for. This raises the question of how to evaluate and compare calculations or measurements of sound pressures and vibrations in regard to acoustic NVH comfort. In short there is no obvious weighting and as in this paper, where the sound pressure is evaluated in an air filled cavity, the total sound pressure level is evaluated using two different weighting functions separately: the A-weighting and the C-weighting. This

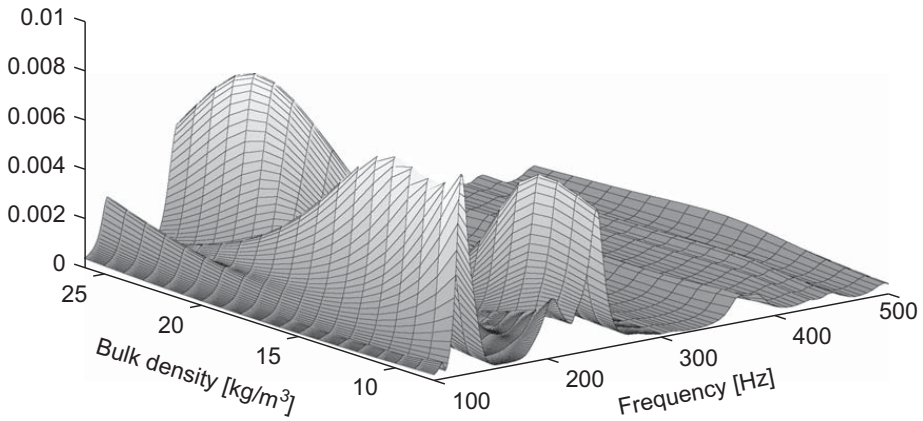

Fig. 4. Frequency response function for different ρ^* at constant $d_s = 10^{-4}$ m.

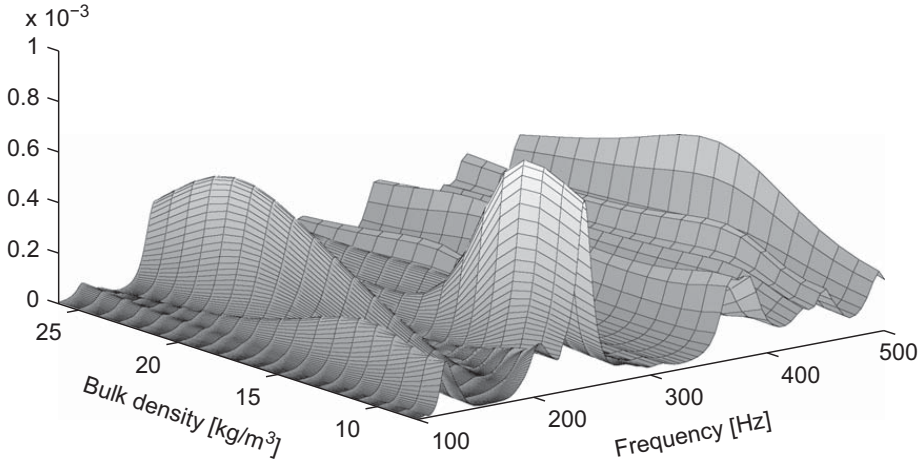

Fig. 5. Frequency response function for different ρ^* at constant $d_s = 10^{-4}$ m, multiplied with weighting factor corresponding to A-weighting.

somewhat arbitrary choice allows for a comparative evaluation of the effects of the weighting itself, not necessarily linked to the real comfort level which still remains an open issue.

2.5.3. Non-convexity

Initially it was assumed that the optimisation problem was non-convex: exhibiting a number of different minima depending on foam material and frequency range evaluated—thus different starting points were tried. However, for the single layer optimisation discussed here it was found that the number of local minima was quite limited within the parameter space and frequency range used. Thus, the choice of starting points for the optimisation turned out to be insignificant.

3. Results

Using the described method the following optimisations were performed for both the PU-foam and the π−foam: minimising the corresponding C-weighted sound pressure level with constraints on the added mass, and minimising the mass with constraints on the corresponding C-weighted sound pressure level inside the sub-volume. For the PU-foam also a minimisation of the corresponding A-weighted sound pressure level was performed in order to compare the result of using different weighting functions.

3.1. Minimising the sound pressure

In the minimisation of the sound pressure, the added mass value of the foam replacing the air gap was constrained to be 0.6 kg. For PU-foam one local minimum was found within the parameter range considered. The optimal parameters ρ^* and d_s did, however, differ depending on whether the corresponding A- or C-weighting were used.

Since adding the extra layer of foam also adds mass to the original configuration it is not sufficient to evaluate the improvement of acoustic behaviour by only comparing the frequency responses with and without foam. The mass alone

would, according to the mass law, lead to at least some transmission loss. The optimised solution with porous foam was therefore also compared with calculations of a plate with only added mass of the same amount as the foam. Finally to consider the effect of potentially sub-optimal foam a comparison was made between the best foam found and the worst foam found. Note that the worst foam found is most likely not the worst possible foam within the parameter range, only the worst that occurred during the optimisation process.

The optimal PU-foam using the corresponding A-weighting, PU^A, was found at $\rho = 32.5\,\mathrm{kg\,m^{-3}}$ and $d_s = 14.8 \times 10^{-6}\,\mathrm{m}$, which corresponds to a porosity $\phi = 0.971$, a Young's modulus $E = 138 \times 10^3\,\mathrm{Pa}$, a static flow resistivity $\sigma^{\mathrm{static}} = 662$ Rayls $\mathrm{m^{-1}}$ ($\mathrm{kg\,m^{-3}\,s^{-1}}$) and a characteristic viscous length $\Lambda = 250 \times 10^{-6}\,\mathrm{m}$. In contrast to the optimal PU-foam using the corresponding C-weighting, PU^C, was found at $\rho = 20.1\,\mathrm{kg\,m^{-3}}$ and $d_s = 15.5 \times 10^{-6}\,\mathrm{m}$, which corresponds to a porosity $\phi = 0.982$ and a Young's modulus $E = 53.0 \times 10^3\,\mathrm{Pa}$, a static flow resistivity $\sigma^{\mathrm{static}} = 233$ Rayls $\mathrm{m^{-1}}$ and a characteristic viscous length $\Lambda = 423 \times 10^{-6}\,\mathrm{m}$. The worst foam found occurred at $\rho = 12.1\,\mathrm{kg\,m^{-3}}$ and $d_s = 16.1 \times 10^{-6}\,\mathrm{m}$ for both weighting functions.

As may be seen in Table 2 the configuration with an optimised foam was significantly better than the original configuration with a layer of air, and the effect was clearly not due to added mass only but is controlled by the dynamic behaviour of the foam. The improvement caused by the added mass was very marginal which is in agreement with estimations made according to the mass law. This effect was expected and clearly visible for both cost functions used during the optimisation. What is more significant is the difference between the optimised foam and the worst foam found. This demonstrates that by adapting the foam to the specific situations, load conditions and surroundings, considerable improvements in acoustic environment may be achieved. The frequency response function for the different panel configurations may be found in Figs. 6–9.

The result and characteristics of the two optimised foams where the two different weighting factors were used showed interesting differences. The A-weighting led to a heavier and much stiffer foam, whereas the C-weighting, where the focus is more on the lower frequencies, lead to a lighter and softer foam. To further look into the possible reasons for this interesting result the displacement of the outer and inner surfaces of the panel was plotted for a number of frequencies for each of the cases. In Fig. 10 the displacements of the outer and inner surfaces at frequency 619 Hz are shown.

It is clear that a soft foam would decouple the two adjacent layer more efficiently than a stiffer one. However, many of the beneficial acoustical properties of foam will be lost when the porosity is increased. High flow resistivity is generally considered beneficial and while the flow resistivity will increase with relative density so will the stiffness and the mechanical coupling between the adjacent layers. This is also the rationale behind the current work, i.e. finding the best

Table 2
Results PU-foam for minimising A-weighted and C-weighted SPL.

Panel description	PU-foam		Configuration with air	
	Best	Worst	Original configuration	With added mass
SPL [dB(A)]	82.2	87.4	89.9	89.4
SPL [dB(C)]	87.8	90.5	94.4	94.1

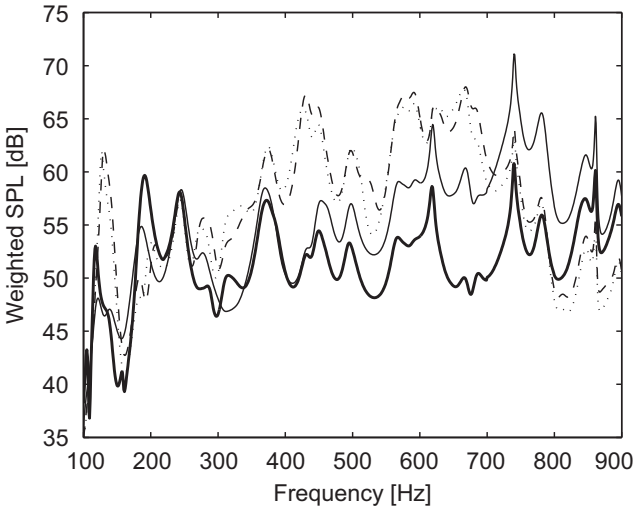

Fig. 6. Frequency response function for: optimal foam solution (thick solid), a sub-optimal foam solution (thin solid), original configuration (dashed) and original configuration with added mass (dotted), weighted with corresponding A-weighting.

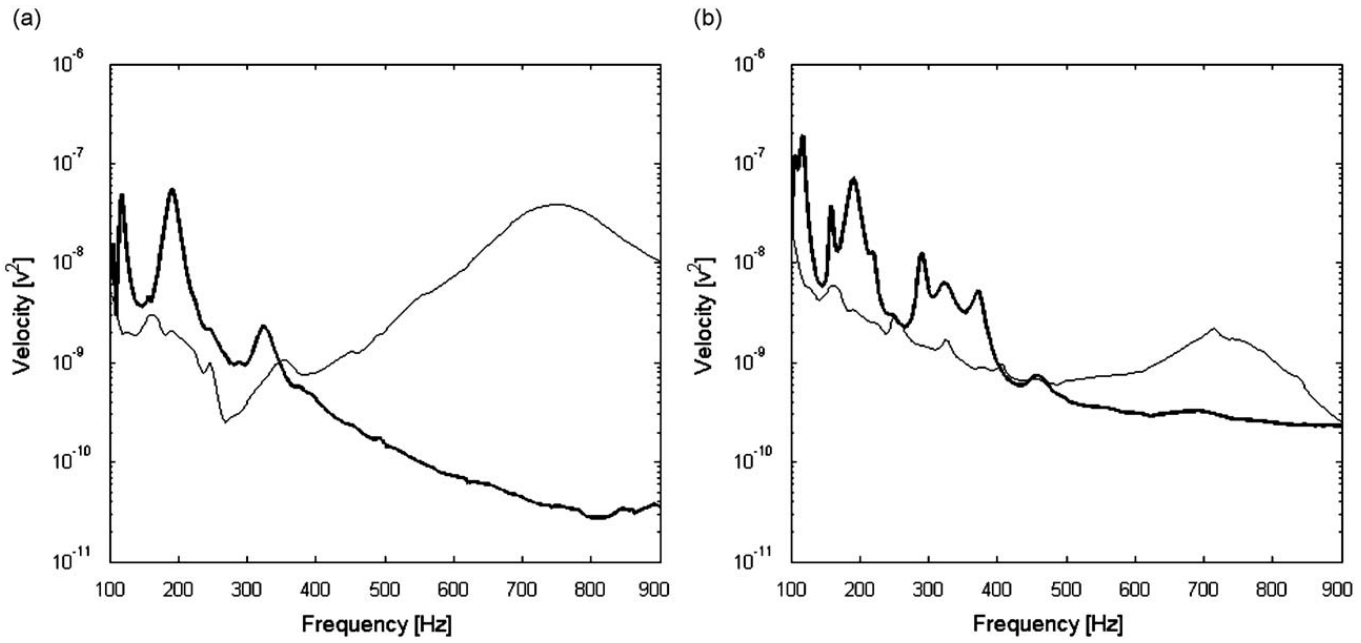

Fig. 7. Surface velocity for outer surface (a) and inner surface (b) for: A-weighted optimal foam solution (thick solid) and sub-optimal foam solution (thin solid).

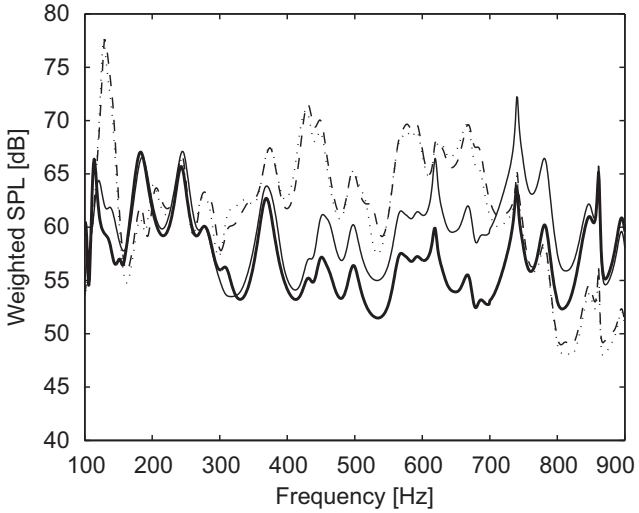

Fig. 8. Frequency response function for: optimal foam solution (thick solid), a sub-optimal foam solution (thin solid), original configuration (dashed) and original configuration with added mass (dotted), weighted with corresponding C-weighting.

balance between variables to maximise the overall benefits. Another way to understand the result from the optimisation using different weighting is in an analogy to a mass-spring system which requires a softer spring to isolate low frequencies as compared to higher frequencies. This might cause the C-weighted optimisation to result in a lower density foam; the increase of flow resistivity is not enough to compensate for the increased transmissibility of low frequency vibrations.

Optimisations were also performed trying to minimise the C-weighted SPL for the $\pi-$foam. The material forming the $\pi-$foam has a Young's modulus more than three times higher than the material forming PU-foam and is slightly heavier, about 30 percent. Such properties generally allow for thinner struts and higher porosities. The results were compared with that of the PU-foam, see Table 3 and Fig. 11. For the $\pi-$foam the minima found had a higher porosity (and lower density) compared to the PU-foam. Despite the lower density the $\pi-$foam was still significantly stiffer than the PU-foam. The frequency responses for the PU-foam and the $\pi-$foam are shown in Fig. 11. Note that the $\pi-$foam tends to be better in the high frequency range and vice versa.

An effect worth noting is that in none of the cases investigated is the optimal strut thickness found close to the minimum strut thickness allowed. Decreasing the strut thickness would increase the flow resistivity without increasing the stiffness, which may at first seem like a rational way to enhance the acoustic performance. But the dissipation of acoustic energy due to flow resistivity is dependent on the relative movement between the frame and the fluid. A great increase in flow resistivity without a corresponding increase in the stiffness may create a system where the possibility of relative

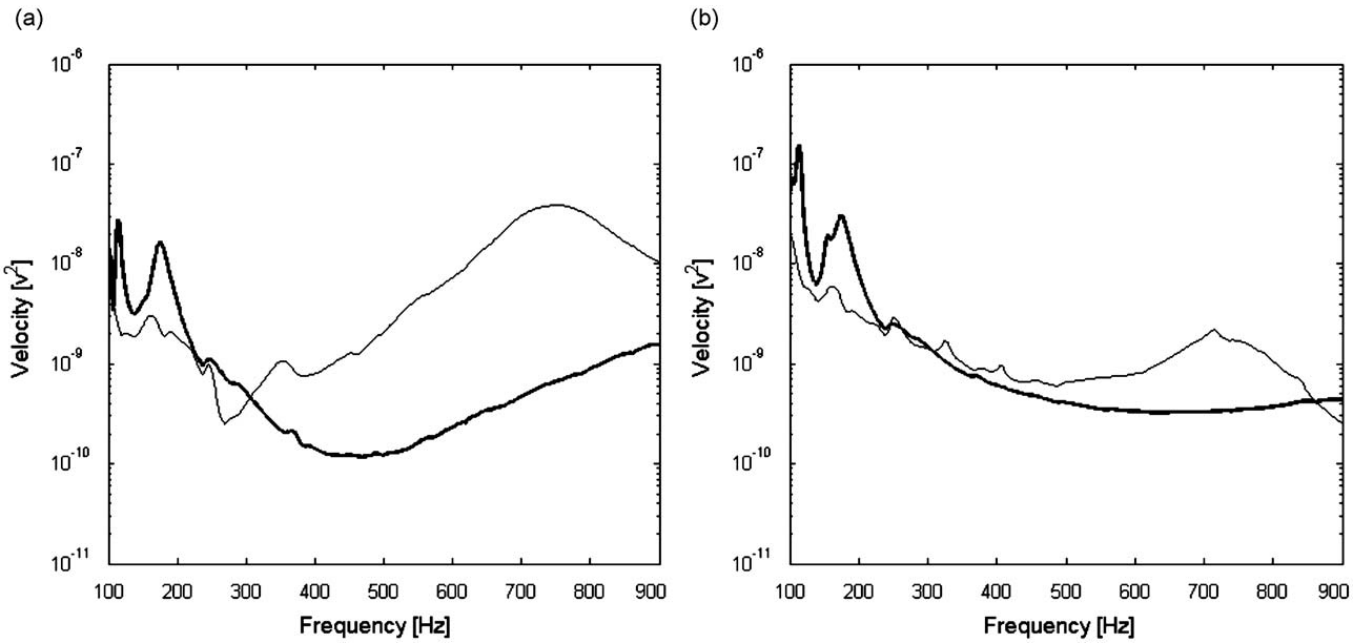

Fig. 9. Surface velocity for outer surface (a) and inner surface (b) for: C-weighted optimal foam solution (thick solid) and sub-optimal foam solution (thin solid).

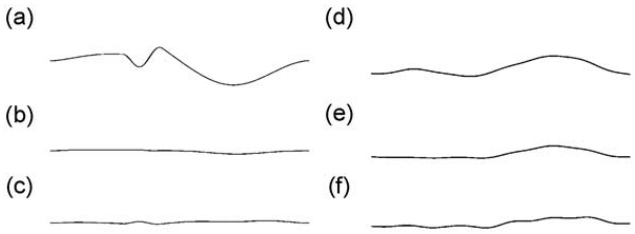

Fig. 10. Displacement of outer and inner surfaces of the multilayered panel at 619 Hz for the worst case foam found and the two optimised foam: (a) outer surface worst case foam, (b) outer surface for C-weighted optimal foam, (c) outer surface for A-weighted optimal foam, (d) inner surface worst case foam, (e) inner surface for C-weighted optimal foam, (f) inner surface for A-weighted optimal foam.

Table 3
Results for PU-foam and $\pi-$foam for minimising C-weighted SPL.

Foam	PU-foam	$\pi-$foam
SPL	87.8	88.7
ρ^*	20.1	15.3
d_s	15.5×10^{-6}	42.9×10^{-6}
ϕ	0.982	0.989
E	53.0×10^3	3121×10^3
σ^{static}	231	398
Λ	424×10^{-6}	1956×10^{-6}

motion between the frame and the fluid is greatly reduced and the waves propagating through the frame and the fluid are therefore forced to move in phase. This would most likely reduce the acoustic performance of the foam. On the contrary, in none of the cases studied is the flow resistivity particularly high. This may at first appear to be suspicious and the reason is not obvious. One possible explanation for this result may be the closed inner and outer surfaces; when air is trapped in a void with very limited possibilities of moving it will appear to be very stiff. The total thickness of the panel is 23.3 mm and some of the constant layers in the panel are either non-porous or have very high flow resistivity. So the fluid movement in z-direction is indeed quite limited. The main movement of fluid within the panel probably occurs in the y-direction, i.e. within the porous layer itself rather than between layers. Enabling good fluid movement within the porous layer may be a reason to keep the flow resistivity fairly low. As mentioned before, the relative frame-fluid motion is an important factor and adds to the dissipation of acoustic energy.

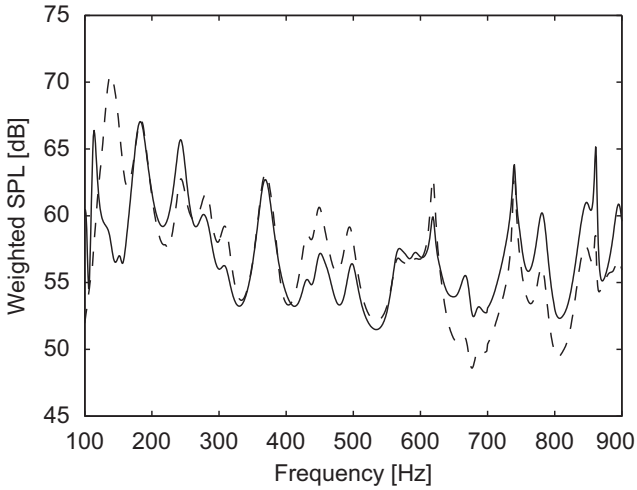

Fig. 11. Frequency response function for SPL optimised PU-foam (solid) and $\pi-$foam (dashed), weighted with corresponding C-weighting.

Table 4
Results minimising mass, constraints on C-weighted SPL.

Foam	PU-foam	$\pi-$foam
SPL	88.8	88.8
ρ^*	14.8	13.4
d_s	5.24×10^{-6}	76.7×10^{-6}
ϕ	0.987	0.990
E	28.6×10^3	2367×10^3
σ^{static}	1094	94.2
Λ	195×10^{-6}	4019×10^{-6}

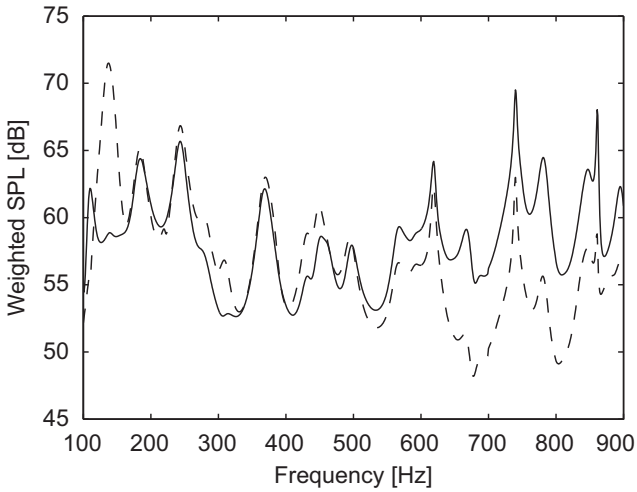

Fig. 12. Frequency response function for mass optimised PU-foam (solid) and $\pi-$foam (dashed). Maximum SPL: 88.8 dB(C), weighted with corresponding C-weighting.

3.2. Minimising the mass

When minimising the mass, constraints were placed on the C-weighted sound pressure level in the air filled cavity; the SPL was not to exceed 88.8 dB(C). Minimisation was performed for the PU foam and the $\pi-$foam using the previously found foam parameters as starting points. The result was as could have been expected: the constraint on the SPL allowed for a slightly lower density for the foam than the one found when minimising the SPL.

The results are presented in Table 4 and Fig. 12 and as can be seen the resulting densities are quite similar, though the effect is not due to the added mass. However, the rest of the foam parameters as well as the frequency responses suggest that the behaviour of the two different panels have significant differences.

4. Conclusions

Despite the limited amount of foam and layer combinations tested, the results presented above suggest realistic changes of the microscopic properties of the foam that may be sufficient to adapt the foam to a specific environmental condition and thereby achieve improved acoustic behaviour as well as reduced weight. The foam studied in this paper shows a non-convex behaviour, however, the number of minima within the parameter range seems to be limited which enables a meaningful optimisation.

These initial attempts to optimise foam on a microscopic level also show the significance of the cost function chosen to evaluate the effectiveness of the foam. By simply using different weighting factors when minimising the sound pressure levels, the optimisation gave very different results. This raises the question of how to formulate a cost function that in the best way describe the characteristics sought for. Such a cost function may include surface velocity, dissipated acoustic energy, sound power or a comparison to a frequency response spectrum chosen in advance. To further elaborate on possible cost functions it is quite possible that an effective cost function may combine one or more of the acoustical estimations above with values referring to weight and cost in some weighted constellation.

Rather than to optimise only one foam layer it would be natural to want to optimise an entire multilayered panel, where the number of layers, the thickness of each layer and the foam properties of each layer are all variables to be considered. The different layers may consist of highly diverse material types, from thin, highly viscoelastic layers to thicker weak layers. The development of new foam material with high stiffness and the ability to form extremely thin struts, 10^{-8} m, may also introduce both new difficulties and new possibilities in the area of multilayered structures.

Acknowledgements

The authors would like to gratefully acknowledge the financial support of the European project Friendcopter, Contract no. AIP3-CT-2003-502773 and the European project Smart Structures, Contract no. MRTN-CT-2006-035559.

Appendix A

The foams used in the presented work were a polyurethane foam (PU-foam), and a polyimide foam ($\pi-$foam), Table A1.

Table A1
Material properties for reference materials.

Material property	PU-foam	$\pi-$foam
ρ_s (kg m^{-3})	1100	1400
E_s (Pa)	450×10^6	1400×10^6
α_∞ [1]	1.17	1.17
ρ_0^* (kg m^{-3})	35.4	8
E_0 (Pa)	164×10^3	848×10^3
σ_0 (kg m^{-3} s^{-1})	4500	1000×10^3
Λ_0 (m)	96.1×10^{-6}	39×10^{-6}

Appendix B

The sub-layers of the panel are given in Tables B1 and B2, one for the solid layers and one for the fixed foam layer.

Table B1
Material properties for solid sub-layers.

Material property	Units	Outer panel sheet	Solid 1	Solid 2	Interior panel sheet
Density	(kg m^{-3})	750	1510	2700	362
Young's modulus	(Pa)	8600×10^9	55×10^4	69×10^9	6.52×10^9
Poisson's ratio	[1]	0.29	0.4	0.31	0.3
Thickness	(m)	0.005	0.001	0.0007	0.0036

Table B2
Material properties for foam sub-layer.

Material property	Units	Foam 1
Bulk density	($kg\,m^{-3}$)	354
Bulk Young's modulus	(Pa)	550×10^3
Poisson's ratio	[1]	0.39
Thickness	(m)	0.005
α_∞	[1]	2.2
σ^{static}	($kg\,m^{-3}\,s^{-1}$)	1×10^6
Λ	(m)	7.7×10^{-6}
Porosity	[1]	0.52

References

[1] M.A. Biot, Theory of propagation of elastic waves in a fluid saturated porous solid. I. Low frequency range, *Journal of the Acoustical Society of America* 28 (1) (1956) 168–178.
[2] M.A. Biot, Theory of propagation of elastic waves in a fluid saturated porous solid. II. Higher frequency range, *Journal of the Acoustical Society of America* 28 (2) (1956) 179–191.
[3] M.A. Biot, Theory of deformation of a porous viscoelastic anisotropic solid, *Journal of Applied Physics* 27 (3) (1956) 459–467.
[4] F. Simon, S. Pauzin, D. Biron, Optimisation of sandwich trim panels for reducing helicopter internal noise, *30th European Rotocraft Forum*, Vol. 2005, 2005, pp. 1025–1033.
[5] O. Tanneau, J.B. Casimir, P. Lamary, Optimization of multilayered panels with poroelastic components for an acoustical transmission objective, *Journal of the Acoustical Society of America* 120 (3) (2006) 1227–1238.
[6] J.S. Lee, E.I. Kim, Y.Y. Kim, J.S. Kim, Y.J. Kang, Optimal poroelastic layer sequencing for sound transmission loss maximization by topology optimization method, *Journal of the Acoustical Society of America* 122 (4) (2007) 2097–2106.
[7] K. Svanberg, The method of moving asymptotes—a new method for structural optimization, *International Journal for Numerical Methods in Engineering* 24 (1987) 359–373.
[8] F. Franco, K.A. Cunefare, M. Ruzzene, Structural-acoustic optimization of sandwich panels, *Journal of Vibration and Acoustics* 129 (3) (2007) 330–340.
[9] C. Perrot, F. Chevillotte, R. Panneton, Bottom-up approach for microstructure optimization of sound absorbing materials, *Journal of the Acoustical Society of America* 124 (2) (2008) 940–948.
[10] C. Perrot, F. Chevillotte, R. Panneton, X. Olny, Bottom-up approach for microstructure optimization of sound absorbing materials, *Invited Paper—Proceedings of the 19th International Congress on Acoustics*, ICA 2007, Madrid, Spain, 2007 (ISBN 84-87985-12-2).
[11] C. Perrot, R. Panneton, X. Olny, From microstructure to acoustic behaviour of porous materials, *Canadian Acoustics—Acoustique Canadienne* 32 (3) (2004) 18–19.
[12] X. Olny, F. Sgard, C. Perrot, R. Panneton, Microscopic and mesoscopic approaches for describing and building sound absorbing porous materials, *Proceedings of the Second TUL-ENTPE Workshop*: 187-206, 2004 (ISBN 2 86834 121 7).
[13] C. Perrot, R. Panneton, X. Olny, R. Bouchard, Mesostructural approach for characterising macroscopic parameters of open cell foams with computed microtomography, *Proceedings of the Institute of Acoustics* 25 (2003) 169–175 (ISBN 1 901656 56 X).
[14] C. Zwikker, C.W. Kosten, *Sound Absorbing Materials*, Elsevier Publishing Company, Amsterdam, 1949 (Chapters II and III).
[15] K. Dovstam, Augmented Hooke's law in frequency domain. A three dimensional material damping formulation, *International Journal of Solids and Structures* 32 (19) (1995) 2835–2852.
[16] J.F. Allard, *Propagation of Sound in Porous Media*: *Modelling Sound Absorbing Materials*, Elsevier Applied Science, 1993.
[17] D. Lafarge, P. Lemarnier, J.F. Allard, V. Tarnow, Dynamic compressibility of air in porous structures at audible frequencies, *Journal of the Acoustical Society of America* 102 (4) (1997) 1995–2006.
[18] S.R. Pride, A.F. Gangi, F.D. Morgan, Deriving the equations of motion for porous isotropic media, *Journal of the Acoustical Society of America* 92 (6) (1992) 3278–3290.
[19] D.L. Johnson, J. Koplik, R. Dashen, Theory of dynamic permeability and tortuosity in fluid-saturated porous media, *The Journal of Fluid Mechanics* 176 (1987) 379–402.
[20] W.E. Warren, A.M. Kraynik, The linear elastic properties of open cell foams, *Journal of Applied Mechanics* 55 (2) (1988) 341–346.
[21] W.E. Warren, A.M. Kraynik, Linear elastic behavior of a low-density Kelvin foam with open cells, *Journal of Applied Mechanics* 64 (4) (1997) 787–794.
[22] L.J. Gibson, M.F. Ashby, *Cellular Solids—Structure and Properties*, second ed., Cambridge University Press, Cambridge, 1997 First published by Pergamont Press Ltd., 1988.
[23] P. Göransson, Acoustic and vibrational damping in porous solids, *Philosophical Transactions of the Royal Society A* 364 (2006) 89–108.
[24] J.F. Allard, Y. Champoux, New empirical equations for sound propagation in rigid frame fibrous materials, *Journal of the Acoustical Society of America* 6 (91) (1992) 3346–3353.
[25] N.E. Hörlin, M. Nordström, P. Göransson, A 3-D hierarchical FE formulation of Biot's equations for elasto-acoustic modelling of porous media, *Journal of Sound and Vibration* 254 (4) (2001) 633–652.
[26] N.E. Hörlin, 3-D hierarchical hp-FEM applied to elasto-acoustic modelling of layered porous media, *Journal of Sound and Vibration* 285 (4) (2005) 341–363.

Material Property Based Structural and Acoustic Optimization of a Multifunctional Vehicle Body Panel

Christopher J. Cameron*
PhD Student
Eleonora Lind Nordgren†
PhD Student
Per Wennhage
Assistant Professor
Peter Göransson
Professor

Centre for ECO^2 Vehicle Design
Department of Aeronautical and Vehicle Engineering
Kunglinga Tekniska Högskolan (KTH)
Teknikringen 8
10044 Stockholm, Sweden

Conventional vehicle passenger compartments often achieve functional requirements using a complex assembly of components. As each component is optimized for a single task, the assembly as a whole is often suboptimal in achieving the system performance requirements. In this paper, a novel iterative design approach based on using a multi-layered load bearing sandwich panel with integrated acoustic capabilities is developed focusing on material properties and their effect on the systems behavior. The proposed panel is meant to fulfil multiple system functionalities simultaneously, thus simplifying the assembly and reducing mass. Open cell acoustic foams are used to achieve acoustic performance, and the effect of altering the stacking sequence as well as introducing an air gap within the acoustic treatment is studied in detail to determine effects on the acoustic and structural performance of the panel as a whole.

Nomenclature

NVH Automotive Noise, Vibration, and Harshness.
CF Carbon Fiber.
GF Glass Fiber.
CSM Chopped Strand Mat.
$V_{f\theta}$ Volume Fraction fiber in lamina with direction θ.
t_θ Thickness of lamina with direction θ.
PET Polyethylene terephthalate.
SPL Sound Pressure Level
d_s average strut thickness of solid frame
E_s Young's modulus for solid frame material
E^* Young's modulus for homogenised foam
l_s average strut length of solid frame
p acoustic pressure
α_∞ tortuosity
Λ viscous characteristic length
Λ' characteristic thermal length
ρ_f density of fluid
ρ_s density of solid frame material
ρ^* bulk density of solid frame
σ^{static} static flow resistivity of foam
ϕ porosity, volume fraction of open pore fluid content
ω frequency

1 Introduction

Functional requirements of a modern automobiles passenger compartment include such things as structural integrity, protection from the elements, aesthetic appearance, and comfort in terms of seating, tactile feedback, and the acoustic environment. In the majority of automobiles, these functional requirements are achieved by assembling a group of components, each optimized to perform a single task. The result of this design ideology is a complex system filled with compromise which is sub-optimal in achieving the global performance requirements.

*Corresponding Author Structural optimization. Email: cjca@kth.se
†Corresponding Author Acoustic optimization. Email: eleonora@kth.se

To achieve structural performance, the vast majority of modern automobiles use pressed metallic components spot welded together in a so called uni-body. In these designs, body panels such as the roof, hood, trunk lid, etc., often have large areas of unsupported sheet metal which vibrates when subjected to external inputs such as aerodynamic loadings, or perturbations from the drivetrain or suspension system. An increased focus on reducing weight in vehicles to reduce emissions and fuel consumption during recent years has often led to increased structural stiffness which corresponds to increased problems with structurally borne sound and vibration within the vehicle. The current state of the art relies to a large degree upon the use of viscoelastic damping treatments to control such vibratory phenomena [1]. These treatments are effective, but they are also heavy and not easily implemented. Experimental methods for locating the optimal placement of such treatments do exist, however they do not guarantee that global optimal solution is reached, rather an optimal solution for the measured configuration [2]. In the end, the effective implementation of such treatment relies heavily on experimentation and the experience of the engineer [3,4].

Further acoustic comfort within the passenger compartment, especially in the higher frequency range, is often achieved by the use of trim panels, absorbent materials behind the trim panels, and the choice of materials used for floor mats and seats. Often, acoustic performance is prioritised lower than aesthetic appeal to the passengers.

An example of what a typical assembly of the above mentioned components looks like in a modern vehicle can bee seen in Fig. 1. Here, it can clearly be seen that a high degree of functional specialization for each component is present.

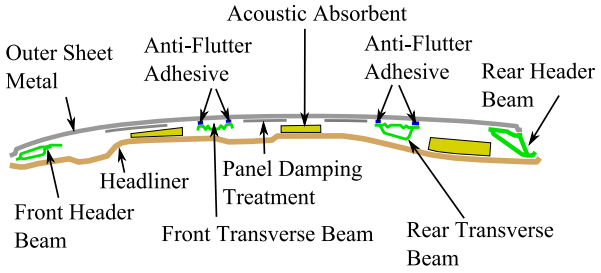

Fig. 1. Cross-section of a traditional vehicle roof system

An alternative method of achieving the necessary structural requirements of such a roof system while reducing mass and eliminating some of the vibrational problems encountered with sheet metal components is through the use of sandwich structures. Increased local bending stiffness as compared to sheet metal components drastically reduces potential vibration problems. The load bearing capacity of sandwich structures also presents the possibility of eliminating additional components necessary with a sheet metal design and thus offering greater weight savings potential. In addition, the use of a sandwich panel allows for an alternative approach to acoustic damping, namely the use of porous elastic media such as light weight, open cell foams. By implementing multiple layers of acoustic foams within the core of a sandwich panel and varying their properties, favourable acoustic behaviour can be achieved at a relatively low weight penalty in contrast to viscoelastic damping treatments. More importantly, the treatments can be accurately tuned for a specific behavioural response using models based on numerical methods for poro-elastic media [5]. The proposed panel should specifically address design challenges in the frequency domain of 100-500 Hz. This frequency range is where a vast majority of structure borne vibration is induced which often corresponds to unwanted and unpleasant acoustic phenomena within the vehicle interior.

Within this paper, a multi-layered, multifunctional sandwich panel concept has been proposed which includes the functionality of the following conventional components present in the roof system of a passenger car: outer sheet metal, panel damping treatments, acoustic absorption treatments, structural reinforcement, and interior trim. The panel consisted of a CF composite external face sheet, a layer of structural polymer foam, a multi-layer acoustic foam treatment, and a perforated inner face sheet of GF CSM. Four configurations of the panel were studied to establish the effect of the acoustic foam stacking sequence, and the effect of an air gap between the inner face sheet and the acoustic foam. This air gap was studied as it may offer potential improvements in the acoustic absorption properties of the panel [6]. These configurations are suggested as a method of meeting the structural and quality needs present in an existing vehicle.

The design methodology developed herein shows the potential for simplifying the complexity of the passenger compartment roof system by examining multiple functional requirements and attempting to achieve them simultaneously in a systematic manor. While the exact panel geometry studied does not match perfectly with that of any given automobile, a potential for mass reduction has been shown as well as the possible effects regarding choice of acoustic foam, stacking sequence, etc. Additionally, a single modular concept with multiple functionalities which replaces a complex collection of parts offers new possibilities in the assembly process which may improve assembly time and ergonomics of installation.

2 Method

The work in this paper was carried out in the following manner.

Firstly, a novel concept was proposed where a system of structural and acoustic components were replaced with a single multi-layered sandwich construction. A flat, 2.0 m x 1.2 m rectangular panel was studied using a quarter model with symmetry conditions to simplify modelling and reduce computational time. Geometric stiffness effects of curved surfaces as found in real vehicles were thus ignored. The design principles presented however are generic and hold true regardless of the geometry studied.

The concept panel was mass optimized using static and normal modes analysis cases and placing constraints on vertical displacements of the centre of the panel for local and global load cases, as well as the frequency of the first normal mode of vibration. Gradient based algorithms implemented in a matlab script and based on the method of moving asymptotes (MMA) [7, 8] were employed in the optimization. In addition to optimizing thickness of the various structural layers, as is often performed in multidisciplinary design work, the material properties themselves have been parameterized such that the mechanical properties and density are altered to achieve the optimal combination of materials for each given layer. This is in contrast to the conventional engineering approach where a given material is chosen "of the shelf" and the thickness is optimized. For the structural step in the optimization, acoustic layers were kept constant and assumed to be linearly elastic. No acoustic effects or structure fluid interactions were accounted for.

The mass optimized panel was then acoustically optimized. A fluid cavity approximately 1.0 m deep was modelled and attached to the panel which was excited dynamically in the frequency range between 100-500Hz. For analysis in this frequency range, finite element analysis was used explicitly. Other acoustic analysis tools such as statistical energy analysis (SEA) were precluded due to the their difficulty in predicting accurately results in the frequency range in question. As with the structural optimization, material properties were parameterized and used to achieve maximum performance from the available space for the acoustic treatment. The upper end of the frequency range studied also represents a performance boundary of current finite element software using modern high performance computational hardware. Model fidelity and accuracy could no doubt be increased, however for the purposes of optimization, long computational time precluded more accurate models being used or higher frequencies from being studied. Sound pressure was minimised for a sub-volume of the cavity, located approximately at the drivers head, and micro-structure of the acoustic foam layers as well as their thicknesses were used as design variables. Structural optimization variables were held constant. The same matlab based MMA tools were used for the acoustic optimization.

Results of the acoustic iteration were used as a starting point for the following iteration of structural optimization. The two step process was repeated until a solution which satisfies both structural and acoustical constraints was achieved with negligible change in parameters between the two optimization steps. This process was repeated for the four proposed panel configurations and the resulting optimal solutions have been compared and discussed.

2.1 Concept Proposal

A conceptual design was proposed based upon geometry of a full size wagon-type passenger car and modelled using a quarter model with symmetry conditions. The panel was multi-layered construction consisting of the following components:

Outer face sheet – CF reinforced epoxy composite laminate

Structural foam layer/frame – Expanded thermoplastic polymer foam (closed cell)

Acoustic foam layer – Multi-layer, low stiffness, open cell elastic foams

Inner face sheet –GF CSM glass fiber reinforced sheet, perforated for acoustic functionality

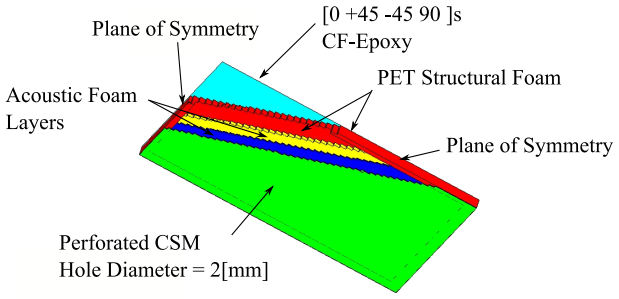

Fig. 2. Cutaway view of panel concept (one fourth of symmetric model)

The exterior face sheet of the panel consisted of an eight layer symmetric quadraxial CF laminate. The core of the panel consisted of a structural foam block with four square pockets removed to allow for the acoustic foam treatment. The "window frame" structure of the structural foam core was necessary to achieve structural integrity of the entire panel. Two different kinds of acoustic foam of strongly differing character were used to allow varying acoustic properties. The innermost face sheet of the panel was a GF CSM reinforced plastic perforated with circular holes in a rectangular pattern to allow fluid interaction between the passenger cavity and the acoustic foam in the sandwich panel. Fig. 2 shows a cutaway view of one quarter of the proposed construction. Fig. 3 shows the configurations used in this work including the presence and absence of the air gap as mentioned in the introduction.

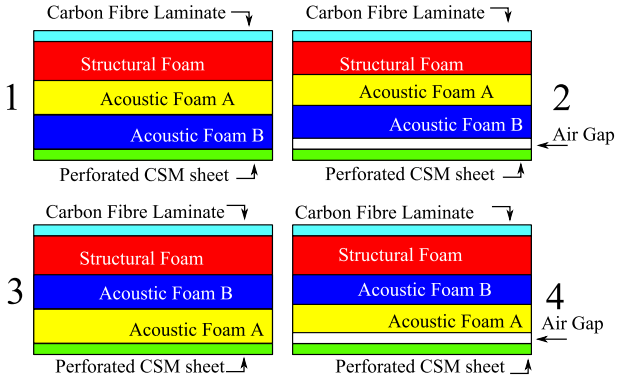

Fig. 3. Stacking sequences of configurations 1-4

2.2 Structural Optimization

2.2.1 Structural modelling

Structural modelling and analysis was performed using the Altair Hyperworks suite. The outer face sheet was modelled using 3-D shell elements and composite laminate properties. Structural and acoustic foam were modelled using multiple layers of brick elements and the perforated inner face sheet was modelled using two layers of brick elements. Linear isotropic material properties were used for all foam components and the inner face sheet. In total the model contained approximately 86000 nodes, 84000 elements, and 270000 degrees of freedom using a nominal mesh size of 10 mm. In the structural optimization step, acoustic interactions were ignored and only mechanical properties were considered.

2.2.2 Design variables and material properties

For the structural optimization, a total of nine design variables were chosen. These variables were as follows:

1. V_{f0} in outer face sheet
2. V_{f45} in outer face sheet
3. V_{f90} in outer face sheet
4. t_0 in outer face sheet
5. t_{45} in outer face sheet
6. t_{90} in outer face sheet
7. Thickness of structural foam layer
8. Density of structural foam layer
9. Thickness of inner face sheet

Fiber volume fraction in each lamina was allowed to vary from 0.01 to 0.6 and mechanical properties were calculated using relationships for basic composite theory taken from the literature [9] and shown in Eqn. (1 - 5). Table 1 shows the material data used. While allowing for a low fiber volume fraction may seem counter intuitive, in cases where demands on mechanical properties are low, mass may be saved by replacing the higher density CF with lower density matrix material.

$$E_{11} = (V_f)E_{f11} + (1.0 - V_f)E_m \tag{1}$$

$$E_{12} = E_{13} = \frac{V_f}{E_f} + \frac{1 - V_f}{E_m} \tag{2}$$

$$G_{12} = G_{13} = \frac{G_m}{1 - \sqrt{V_f}(1 - G_m/G_{f12})} \tag{3}$$

$$G_{23} = \frac{G_m}{1 - V_f(1 - G_m/G_{f12})} \tag{4}$$

$$\nu_{lamina} = V_f \cdot \nu_f + (1 - V_f) \cdot \nu_m \tag{5}$$

Density of the structural foam was chosen as a design variable and used to alter the mechanical properties of the material according to Eqn. (6 - 8), which are taken from the literature [10]. A closed cell, thermoplastic foam was assumed using the mechanical properties of PET.

Table 1. Material properties for matrix, fibers, and CSM sheet (non-perforated)

	Matrix	CF	GF CSM
$E_{11}(tensile)$ $[MPa]$	3200	220600	15000
$G_{12} = G_{23}$ $[MPa]$	1185	30130	5769
ρ $[kg/m^3]$	1125	9000	1700
ν [–]	0.35	0.20	0.3

$$\frac{E_{foam}}{E_{solid}} \approx \phi^2 \left(\frac{\rho_{foam}}{\rho_{solid}}\right)^2 + (1-\phi)\frac{\rho_{foam}}{\rho_{solid}} + \frac{P_0(1-2\nu_{foam})}{E_{solid} - \rho_{foam}/\rho_{solid}} \tag{6}$$

$$\frac{G_{foam}}{E_{solid}} \approx \frac{3}{8}\left(\phi^2(\frac{\rho_{foam}}{\rho_{solid}})^2 + (1-\phi)\frac{\rho_{foam}}{\rho_{solid}}\right) \tag{7}$$

$$\nu_{foam} \approx \frac{1}{3} \tag{8}$$

Manufacturers data for Divinycell P series, and Airex T90 and T92 was obtained from technical data sheets on the respective manufacturers homepage [1] [2] [Retrieved 22/11/2010]. The given properties were correlated with Eqn. (6) and (7), and the assumption that $\phi = 0.8$, as given in the literature [10] was checked for this case.

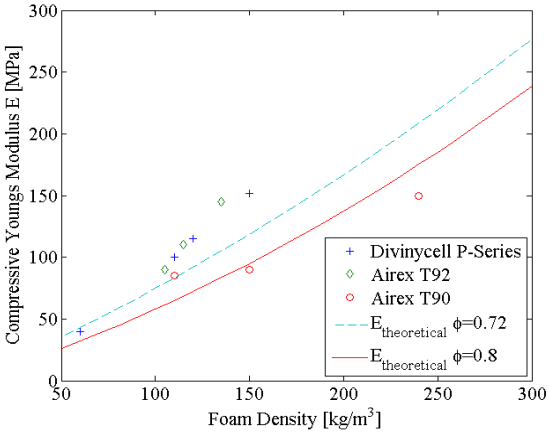

Fig. 4. Compressive modulus as function of density

[1] www.diabgroup.com/europe/products/e_divinycell_p.html

[2] www.corematerials.3acomposites.com/airex-foams.html

Exact agreement between manufacturers data and the above relationships was not obtained. Better agreement in the equation for compressive modulus was obtained using $\phi = 0.72$, which necessitated a scaling factor of 0.8 times the calculated shear modulus to obtain reasonable agreement. Fig.s 4 and 5 show the manufacturers data and theoretical properties as functions of density.

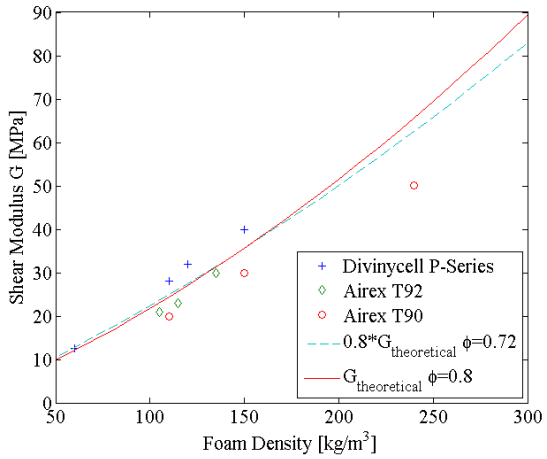

Fig. 5. Shear modulus as function of density

A fixed degree of perforation assuming 2.0 mm holes drilled in a square pattern with 3.5 mm between hole centres was used. This configuration was chosen as it was considered to be the minimum degree of perforation to allow for sufficient acoustic transparency [11]. Tighter hole spacing increases acoustic transparency but reduces bending stiffness and vice versa. Equivalent material properties were used rather than modelling individual holes within the model. The methods used to derive the properties are omitted here for the sake of brevity, and instead the authors would refer to previous work [12] or the original literature for bending stiffness of perforated plates [13–15].

2.2.3 Load cases and boundary conditions

Structural optimization was performed using two static load cases and normal modes analysis. For the first static load case, a pressure equivalent to a hand firmly pressing on the roof was applied on a circular area approximately 100 mm in diameter in the centre of the quarter panel model. For the second static load case a pressure was applied over the entire panel, equivalent to 2000 kg pressing on the entire roof. Boundary conditions applied to the model can be seen in Fig. 6. Symmetry and clamped constraints were applied across the entire thickness (z direction in Fig. 6) of the panel. The boundary conditions used were considered a reasonable representation of how the panel might be fastened to the front and rear headers (large, stiff, crossbeams) and the longitudinal beams in the roof.

For the normal modes analysis case, it should be noted

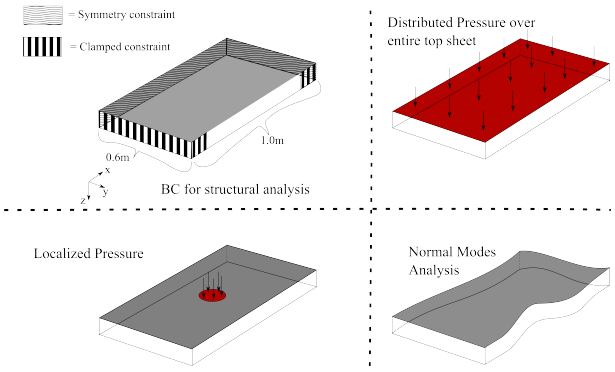

Fig. 6. Top and side view of panel showing boundary conditions

that symmetric boundary conditions preclude non-symmetric modes of vibration. For the given case, this is not a problem as it is primarily the first mode of vibration which is of interest and which generally tends to cause the most acoustic discomfort.

2.3 Acoustic Optimization

2.3.1 Acoustic modeling

To simulate the acoustic behaviour of the panel the panel was connected to an air cavity in which the sound pressure level in typical listener positions could be calculated. The panel was excited using dynamic forces in the x-, y-, and z-direction. The forces were applied over the top surface of the elements along the edge of the CF epoxy top sheet, Fig. 7 and the system response was evaluated for the frequency range 100 – 500 Hz.

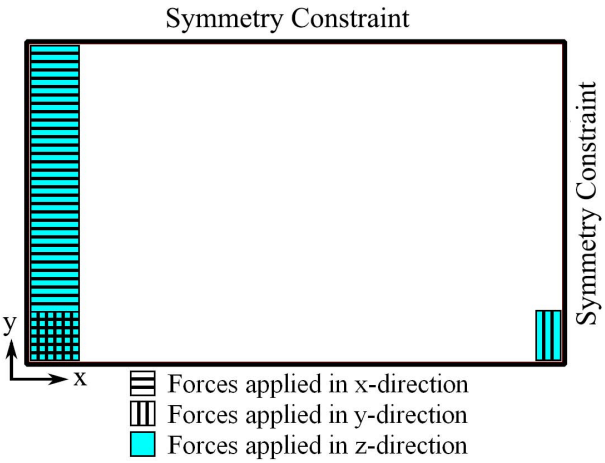

Fig. 7. Dynamic forces applied to the CF Laminate

As the roof was represented by a quarter model, symmetry boundary conditions were applied at the symmetry edges through all layers. The inner perforated plate was also fixed in the x-, y- and z-direction along x = 0 and y = 0 to avoid rigid body motion.

For computational reasons both the excitation and the response of the system was limited to the frequency range 100-500 Hz. The acoustic response of the system was modelled using FE-based numerical methods where the porous foams were modelled using Biot theory [16–18].

The theories used to model the foam assume material isotropy, small displacements and linearly elastic materials. The numerical model must take into account not only the properties of the individual porous layers, e.g. the fluid in the pores, the solid frame structure and the coupling between them. It also has to consider the boundaries to other solid, fluid or porous layers, with appropriate treatment of the kinematic conditions, the mass flow continuity conditions and the relevant stress balances. Also, special care has to be taken in the selection of trial functions to get convergent solutions to Biot's equations, especially for multi-layered structures, for which hp-FEM[3] is a convenient finite element base. Here the finite element solutions were obtained using the methods thoroughly discussed and properly addressed in works by Hörlin et al. [19] and by Hörlin [20] and will not be repeated here. However, the complexity of the problem makes it computationally expensive to solve and as each frequency is solved independently, limiting the frequency range is a necessity.

2.3.2 Design variables and material properties

In order to carry out a meaningful optimization of the acoustic foam it is necessary to use design variables that can be changed independently of one another. In porous foam, several of the parameters used to calculate the response, for example the homogenized Young's modulus, E^*, and the bulk density, ρ^*, are inter related in a quite complex way. An alternative is to use microstructural geometric properties. To relate the macroscopic properties of the foam to the underlying microscopic properties scaling laws are used. Contributions to developing scaling laws and increasing the understanding of the mechanical properties of foam have been made by several researchers, e.g [10, 21–25]. A method for using scaling laws to optimize porous foam in multi-layered structures has been proposed previously [26]. For completeness, however, the more important scaling laws used are summarized below.

$$\rho^* = \rho_{ref}\left(\frac{d_s}{d_{ref}}\right)^2\left(\frac{l_{ref}}{l_s}\right)^2 \tag{9}$$

$$\phi = 1 - \frac{\rho^*}{\rho_s} \tag{10}$$

$$E^* = E_{ref}\left(\frac{\rho^*}{\rho_{ref}}\right)^2 \tag{11}$$

$$\Lambda = \frac{d_s}{4(\rho^*/\rho_s)} \tag{12}$$

$$\Lambda' = 2\cdot\Lambda \tag{13}$$

$$\alpha_\infty = 1 - \frac{1-\alpha_{\infty ref}}{\ln(\phi_{ref})}\cdot\ln(\phi^*) \tag{14}$$

$$\sigma^{static} = \sigma_{ref}^{static}\left(\frac{\rho^*}{\rho_{ref}}\right)^2\cdot\left(\frac{d_{ref}}{d_s}\right)^2\cdot\frac{\alpha_\infty}{\alpha_{\infty ref}}\cdot\frac{\left(1-\frac{\rho_{ref}}{\rho_s}\right)}{\left(1-\frac{\rho^*}{\rho_s}\right)} \tag{15}$$

The acoustic foam A was a Polyurethane foam (PU foam) and the acoustic foam B was a Polyimide foam (pi foam). The reference material properties of the two foams are listed in Table 2.

Material property		PU foam	pi foam
ρ_s	[kg m^{-3}]	1100	1400
E_s	[Pa]	$450\cdot10^6$	$1400\cdot10^6$
$\alpha_{\infty ref}$	[1]	1.17	1.17
ρ^*_{ref}	[kg m^{-3}]	35.4	8
E^*_{ref}	[Pa]	$164\cdot10^3$	$848\cdot10^3$
σ^{static}_{ref}	[kg m^{-3} s^{-1}]	4500	$1000\cdot10^3$
Λ_{ref}	[m]	$96.1\cdot10^{-6}$	$39\cdot10^{-6}$

Table 2. Material properties for reference materials.

The design variable used in the acoustic optimization was the scaled length of the struts l_s/l_{ref} in the two foam layers and the thickness of each foam layer. These design variables will be referred to as l_{PU}, l_{pi}, t_{PU} and t_{pi}. Constraints were put on maximum and minimum relative strut length, which could vary between 0.5 and 5, and maximum and minimum thickness of each layer, which could vary between 1 mm and 50 mm, Constraints were also put on maximum and minimum total thickness.

The aim of the acoustic optimization was to improve the NVH comfort inside the vehicle and the objective function of was chosen to be the unweighted sound pressure level (SPL) in a subvolume of the air cavity, Ω_{sub}, summed over the entire frequency range.

$$\langle SPL\rangle_{\Omega_{sub}} = 10\cdot\log\left(\frac{\sum_{f=f_1}^{f_{max}}\left(p_f^2\cdot\Delta f_f\right)}{p_0^2}\right) \tag{16}$$

The choice of objective function will obviously have a great effect on the outcome of the optimization. Alternative

[3] Convergence is achieved by refining the mesh and/or increasing the approximation order

Table 3. Final values of structural design variables

	Configuration			
Variable	1	2	3	4
V_{f0}	0.60	0.60	0.60	0.60
V_{f45}	0.27	0.26	0.29	0.29
V_{f90}	0.60	0.60	0.60	0.60
t_0[mm]	0.15	0.15	0.15	0.15
t_{45}[mm]	0.15	0.15	0.15	0.15
t_{90}[mm]	0.15	0.15	0.15	0.15
$t_{PETfoam}$[mm]	25.0	25.0	25.0	25.0
$\rho_{PETfoam}[kg/m^3]$	134.2	128.2	142.5	140.5
t_{CSM}[mm]	2.91	3.50	2.86	3.50

objective functions, such as the A-weighted SPL or the radiated sound power, may lead to other results [26]. However, the method presented herein is mainly conceptual and the chosen objective function is one way to compare the performance of the different configurations.

3 Results and Discussion

Two to three iterations per configuration were required to achieve convergence for all configurations. The final values for the structural and acoustic design variables can be seen in Tables 3 and 4.

Table 3 shows the final configuration of the CF laminate for all configurations. Results are quite similar for all configurations. Thickness of each layer was reduced to the minimum allowable value. For the 0°and 90°layers, fiber volume fraction was maximized, however, for the layers of ±45°fiber volume fraction was reduced to approximately half of the maximum allowed value. This may indicate several things, firstly, that the choice of CF may be excessive and that a lower performance fiber may be sufficient. Secondly, the results may indicate that the choice of layup is excessive in this application, fewer layers might be sufficient. Here, special attention must be made to ensure symmetry in the laminate is maintained if layers are removed to avoid coupled bending/twisting problems present in non-symmetric composite laminates. The manufacturability of a laminate with varying degrees of fiber volume fraction in each laminate is also questionable. Ideally, a solution should be sought where all layers maintain the same volume fraction of material, as this can to a certain degree be controlled with conventional composite manufacturing techniques.

Regarding the structural foam density as shown in Table 3, it can be seen that all configurations lie within the region of 128.5 - 142.5 kg/m^3. It would appear that the introduction of an air gap slightly lowers the required density of the structural foam for a given stacking sequence. It would appear then that in order to establish the correct structural foam density, the stacking sequence of acoustic foams, as well as their properties and thickness must be known. This further emphasises the need for an iterative approach. As the purpose of this work is to present a design method rather than a specific solution, the exact value of the foam density is not especially interesting, but rather that the method could be used in selecting which foam material should be used in a final design. While not presented here, it was also found that the resulting density of structural foam was coupled to the type of boundary conditions used, as well as the width of the frame of structural foam around the perimeter of the panel. This is an area where more study is necessary. Thickness of the structural foam reached the maximum value for all four configurations studied which was expected as increasing the thickness of a sandwich panel is the most efficient method of reducing weight and increasing stiffness.

Table 4. Final values of acoustic design variables

	Configuration			
Variable	1	2	3	4
ρ^*_{PU} [kg/m^3]	38.62	137.97	137.74	137.97
E^*_{PU} [MPa]	0.196	2.624	2.615	2.624
ϕ_{PU}	0.966	0.875	0.876	0.876
σ^{static}_{PU} [kg/m^3/s]	5.45e3	1.11e5	1.10e5	1.11e5
t_{PU}	23.04	48.00	47.19	41.49
ρ^*_{pi} [kg/m^3]	9.31	1.48	2.46	3.86
E^*_{pi} [MPa]	1.206	1.357e-3	0.0286	0.129
ϕ_{pi}	0.994	0.999	0.999	0.998
σ^{static}_{pi} [kg/m^3/s]	1.39e6	2.94e4	8.29e4	2.12e5
t_{pi} [mm]	26.96	1.000	2.4617	4.585
SPL [dB]	60.1	59.3	57.9	58.5

Table 5. Results of optimization

	Configuration			
Value	1	2	3	4
Total Thickness [mm]	79.1	78.7	78.7	75.8
Total Mass [kg]	18.7	27.3	27.8	26.7
First Eigen Mode [Hz]	71.8	46.9	64.7	47.0

Table 4 shows the resulting property values and thicknesses for the acoustic foam layers and the resulting sound pressure in the cavity.

Acoustically speaking, the stacking sequence seemed to be more important for the configurations without air gap. Both the foam properties and the resulting SPL differed significantly between configuration 1 and 3 as can be seen in table 4.

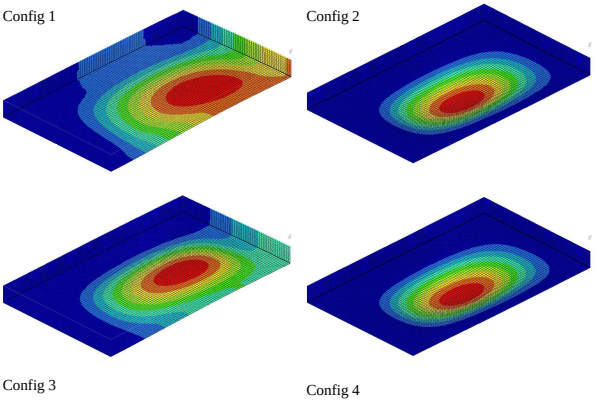

Fig. 8. Eigen mode shapes of the four configurations studied.

The air gap in configuration 2 and 4 seemed to be beneficial for the SPL in the air cavity in the early stages of the optimization. After some iterations, however, the effect of the air gap was no longer as apparent. A direct comparison at the final stages of the optimization is harder to do since the differences in structural and acoustic material properties are so large that the acoustic effects of the gap in itself are not obvious or able to be isolated from other effects.

In the configurations with an air gap the acoustic foam properties as well as the resulting SPL were much more similar, again, see table 4. In the air gap configurations the inner surface is less connected to the rest of the structure and the acoustic foam package seems to act more as a unit. A large difference in impedance between layers is often associated with improved acoustic performance and in the configuration with air gap the major step in impedance is due to the air gap in itself and the need for an impedance step within the acoustic foam treatment is reduced.

In configuration 2, when the pi foam was in contact with the air layer, it was reduced to a very thin and weak foam of high porosity. In contrast, the PU layer was made to be stiff and thick and completely dominated the acoustic foam volume. In configuration 4, on the other hand, the pi foam is no longer in contact with the air layer. Here, it can be seen that the static properties of the pi and PU foam vary a great deal, however due to the flow resistivity, the dynamic properties of the foams are much more similar. In essence, it would appear that rather than have two distinct layers of porous material, the optimization method attempts to create a single acoustically homogeneous layer from two very different foam types. By nature, the acoustic foams used are very different, and regardless of how the design variables used are changed, the resulting foams cannot be exactly the same.

In the configurations without air gap, changes in impedance must be created within the acoustic foam layers. The individual properties of each foam layer may therefore be more important and the two foams are tuned to the specific configuration, where the stacking sequence is the major difference.

Looking at the panels from the top layer down, it can be seen that the stiff structural foam is followed in both configurations 1 and 3 by a fairly soft acoustic foam and thereafter a fairly stiff acoustic foam. Thus, it would appear that the optimal solution is a stiff-soft-stiff foam sequence. PU foam is by nature, rather soft, whereas pi foam is by nature rather stiff. In configuration 1, this allows the foam layers to be tuned within their natural boundaries. In configuration 3 however, the pi foam is made as weak as possible and the PU foam is made as stiff as possible contrary to their reference values. As the optimization attempts to create a stiff foam from a naturally soft foam and vice versa, it makes the PU foam very heavy and the pi foam very porous and light. It is possible that the optimization tries to achieve a similar relative change in impedance in configurations 2 and 4 as in configurations 1 and 3.

Table 5 shows final result of the global properties of the panels. The configurations with an air gap showed significant differences compared to the configurations without air gap. This illustrates that out of both a structural and an acoustic point of view it is important to model air gaps and foam properly. A very lightweight open pore foam can not be approximated with an air gap and modelled as such.

Regarding the thickness of the inner face sheet, a clear trend is discernible; for the configurations where an air gap is present, the thickness is larger. For all configurations, the active constraint was that placed on displacement under the distributed pressure. All configurations fulfilled this constraint equally well, however the two air gap configurations required a thicker inner face sheet to achieve this. This would seem to indicate that despite the relatively low stiffness of the acoustic foams in comparison to other materials in the panel, their contribution to the structural stiffness of the sandwich panel is not negligible.

Regarding the dynamic behavior of the panel, further effects of the air gap can be seen in Table 5 and more graphically in figure 8. The first modes of vibration for configurations 2 and 4 occur at much lower frequencies and are considerably different in character compared with configurations 1 and 3. In the air gap configurations, resonant vibration occurs first in the form of oscillations of the inner face sheet alone within the quarter model, as shown by the rightmost images in figure 8. For configurations 1 and 3, the first mode of vibration resembles more resonant vibration of the entire roof in the whole model as shown by the two leftmost images in figure 8. This can again be explained by the connection to the acoustic foam layers. The coupling to the low stiffness acoustic layers effectively raises the minimum eigen frequency of the panel by preventing the inner face sheet from vibrating on its own. In short, the bond ensures that the panel acts more like a single structure rather than two separate structures attached around the edges.

Regarding the iterative method described in itself, while it has been shown effective, some limitations should be discussed. For the examples presented, convergence was achieved with relatively few iterations. The number of iterations required however may be affected by the suitability of the initial starting point. Should a very poor starting point regarding both structural and acoustic properties be used, more

iterations may be required due to the complex inter-related nature of the structural-acoustic problem.

Certain design variables were quick to converge to a final solution, while others required much more time. In the structural optimization, fiber volume fraction in particular was the design variable requiring the most time to achieve convergence. Why this occurs is not clear. In the acoustic optimization, the thickness of the two acoustic foam layers were the slowest variables to converge. This is perhaps more understandable, as changes in thickness of the acoustic foams effects directly the overall stiffness of the structure which will have a direct impact on the acoustic performance. Thus, any changes in the acoustic foam layer thickness must often be accompanied with changes in the acoustic foam material properties to compensate for the change in overall stiffness.

As the case study provided has used a relatively simple model and geometry, direct comparisons to existing vehicle solutions cannot be made easily, especially in terms of acoustic performance. The outcome of the case study does however suggest that the method could be used on a real vehicle structure and contribute significantly to understanding alternative design options for modern vehicles. In addition it can be stated that the panel does show promise in reducing the mass of the conventional roof system while offering the possibility of tuning the acoustic performance and potentially simplifying the assembly process.

In this paper the optimization process was divided into two steps for several reasons. The optimization algorithm used is gradient based and therefore requires a perturbation iteration for each design variable used in the problem. This can lead to extremely long iteration times for large numbers of design variables. In this case, the acoustic calculations were the most time consuming, requiring approximately 1 min per frequency using 2 Hz intervals on a cluster of 6 multiple processor Linux workstations with 16-32GB of internal memory. Each frequency needs to be calculated separately through the frequency range, and in order to calculate the gradients for each variable, the entire frequency range must be calculated for each perturbation. Understandably, as the number of variables in the problem increase, so does the calculation time. By dividing the problem into two separate optimization loops, variables which primarily affect either structural or acoustic properties can be handled separately and calculation time can be reduced.

For both the structural and acoustic optimization schemes, the concept of material property parametrisation has been thoroughly implemented, and further emphasis is perhaps prudent. The authors propose that the method herein represents a new way of thinking in terms of mechanical design, especially from an industrial perspective. Rather than changing the construction to match the material, both the design and material are altered to achieve the functionality required. While the parametrisation scheme used for the structural optimization variables is based on well established principles, the authors believe this to be the first time such principles have been combined in the form presented and used as a proactive designs tool rather than reactive calculation or estimation tool. In terms of the parametrisation tools and hp-FEM code used for the acoustic analysis, it should be noted that the specific implementation used is unique and represents the forefront of what is possible with current technology and modelling methods. While commercial software capable of calculating acoustics in porous media is beginning to penetrate the market and be used in industrial research and development, none of these implementations allow the flexibility of parameterized acoustic material properties and are most certainly not used in optimization schemes due to the prohibitive length of time required to solve the models.

In the context of the design methodology described herein, the concept of topology optimization might also seem interesting, however within the optimization framework presented, this proves impossible using conventional topology optimization techniques(such as homogenisation/density based methods). This is due partially to the necessity of interpreting resulting topologies between interactions, and due to the inability for such methods to account for the mechanical properties of the acoustic foam in structural analysis when no air gap is presented. The authors hope to present a method to deal with such issues in a separate publication in the near future.

4 Conclusions

An iterative design methodology for a multifunctional body panel which integrates the functionality of the roof system of a passenger car has been proposed and explained. Specifically, system requirements for structural integrity and acoustic performance have been addressed. The method has proven successful at defining material properties and thicknesses for a multifunctional vehicle panel as shown with a case study. The effects of changes to material properties on the behavior of the panel have been studied in detail, and certain key parameters have been identified regarding both the structural and acoustic performance. Light weight, highly porous acoustic foams were used in the core of the panel for acoustic functionality and it was found that despite their relatively low stiffness, they played a critical role in the structural efficiency of the panel. The coupling between inner face sheet and low stiffness foam allowed the inner face sheet to be thinner, and effectively raised the frequency of the first mode of vibration of the panel. Stacking sequence of the acoustic foams had little effect on the structural performance but proved crucial to the acoustic performance and the total panel mass. The effect of introducing an air gap between the face sheet and acoustic foam was difficult to see explicitly in the acoustic performance due to other significant differences in the properties of the panel. Optimization of the acoustic layer thickness proved that a high degree of coupling existed between the acoustic and structural properties of the panel necessitating an iterative approach to the optimization problem. Finally, while direct comparisons to conventional solutions are difficult due to the simplicity of the case study used, the results indicate that the method is promising, and that the proposed panel has potential to provide reduced mass, tuneable acoustic performance, and system simplification which

should reduce time on the assembly line.

Achnowledgements

This work was performed within the Centre for ECO2 Vehicle Design with financial support from the Swedish Agency for Innovation Systems (VINNOVA), KTH, and Saab Automobile AB. The financial support is gratefully acknowledged.

References

[1] Rao, M. D., 2003. "Recent applications of viscoelastic damping for noise control in automobiles and commercial aeroplanes". pp. 457–474.

[2] Reis, D. B., and Nicoletti, R., 2010. "Positioning of deadeners for vibration reduction in vehicle roof using embedded sensitivity". *Journal of Vibration and Acoustics,* **132**(April), pp. 021007–1 – 021007–8.

[3] S.M.Beane, M.M.Marchi, and D.S.Snyder, 1995. "Utilizing optimized panel damping treatments to improve powertrain induced nvh and sound quality". *Applied Acoustics,* **45**(2), pp. 181–187.

[4] J.Bienert, 2002. "Optimisation of damping layers in car bodies". *Proceedings of the 2002 International Conference on Noise and Vibration Engineering, ISMA*, Sept, pp. 2005–2010.

[5] P. Göransson, 2008. "Tailored acoustic and vibrational damping in porous solids – engineering performance in aerospace applications". *Aerospace Science and Technology,* **12**, pp. 26–41.

[6] Cummings, A., Rice, H., and Wilson, R., 1999. "Radiation damping in plates, induced by porous media". pp. 143–167.

[7] Svanberg, K., 1987. "The method of moving asymptotes-a new method for structural optimization". *International Journal for Numerical Methods in Engineering,* **24**(2), Feb, pp. 359–373.

[8] Svanberg, K., 2002. "A class of globally convergent optimization methods based on conservative convex separable approximations". *SIAM J. OPTIM.,* **12**(2), pp. 555–573.

[9] Chamis, C., 1984. "Simplified composite micromechanics equations for strength, fracture toughness and enviromental effects". *SAMPE Quarterly*, July, pp. 41–55.

[10] Gibson, L. J., and Ashby, M. F., 1997. *Cellular Solids: Structure and Properties-Second edition*. Cambridge University Press.

[11] Ihle, A., Ernst, T., Baier, H., Datashvili, L., Hoffmann, J., Göransson, P., Fasold, D., Portela, P., Santos, M., and Santiago-Prowald, J., 2009. "Large porous antenna and spacecraft structures: Thermo-elastic and vibroacoustic modelling and effects and its verification via test.". In 11th European Conference on Spacecraft Structures, Materials and Mechanical testing. Toulouse September 15-17.

[12] Cameron, C. J., Wennhage, P., Göransson, P., and Rhamqvist, S., 2010. "Structural-acoustic design of a multi-functional sandwich panel in an automotive context". *Journal of Sandwich Structures and Materials,* **12**(6), November, pp. 684–708.

[13] A.I.Soler, and W.S.Hill, 1977. "Effective bending properties for stress analysis of rectangular tubesheets". *Transactions of the ASME: Journal of Engineering for Power*, July, pp. 365–370.

[14] K.A.Burgemeister, and C.H.Hansen, 1996. "Calculating resonance frequencies of perforated panels". pp. 387–399.

[15] M.Forskitt, J.R.Moon, and P.A.Brook, 1991. "Elastic properties of plates perforated by elliptical holes". *Applied Mathematical Modelling,* **15**(4), April, pp. 182–190.

[16] M.A.Biot, 1956. "Theory of propagation of elastic waves in a fluid saturated porous solid. i. low frequency range". *J. Acoust. Soc. Am.,* **28**, pp. 168–178.

[17] M.A.Biot, 1956. "Theory of propagation of elastic waves in a fluid saturated porous solid. ii. higher frequency range". *J. Acoust. Soc. Am.,* **28**, pp. 179–191.

[18] M.A.Biot, 1956. "Theory of deformation of a porous viscoelastic anisotropic solid". *J. Appl. Phys,* **27**, pp. 459–467.

[19] Hörlin, N. E., Nordström, M., and Göransson, P., 2001. "A 3-D hierarchical FE formulation of Biot's eguations for elasto-acoustic modelling of porous media.". *J. Sound Vib.,* **254**(4), pp. 633–652.

[20] Hörlin, N. E., 2005. "3-D hierarchical hp-FEM applied to elasto-acoustic modelling of layered porous media.". *J. Sound Vib.,* **285**(4), pp. 341–363.

[21] Warren, W. E., and Kraynik, A. M., 1988. "The linear elastic properties of open cell foams.". *J. Appl. Mech.,* **55**(2), pp. 341–346.

[22] Warren, W. E., and Kraynik, A. M., 1997. "Linear elastic behavior of a low-density Kelvin foam with open cells.". *J. Appl. Mech.,* **64**(4), pp. 787–794.

[23] Allard, J. F., and Champoux, Y., 1992. "New empirical equations for sound propagation in rigid frame fibrous materials.". *J. Acoust. Soc. Am.,* **6**(91), pp. 3346–3353.

[24] Comiti, J., and Renaud, M., 1989. "A new model for determining mean structure parameters of fixed beds from pressure drop measurements: application to beds packed with parallelepipedal particles". *Chemical Engineering Science,* **44**(7), pp. 1539 – 1545.

[25] Göransson, P., 2006. "Acoustic and vibrational damping in porous solids.". *Phil. Trans. R. Soc. A,* **364**, pp. 89–108.

[26] Lind-Nordgren, E., and Göransson, P., 2010. "Optimising open porous foam for acoustical and vibrational performance". *Journal of Sound and Vibration,* **329**(7), pp. 753–767.

A Design Method using Topology, Property, and Size Optimization to Balance Structural and Acoustic Performance of Sandwich Panels for Vehicle Applications

Christopher J. Cameron, Eleonora Lind Nordgren, Per Wennhage, Peter Göransson

Centre for ECO^2 Vehicle Design
Department of Aeronautical and Vehicle Engineering
Kunglinga Tekniska Högskolan (KTH)
Teknikringen 8
10044 Stockholm, Sweden

Abstract

Balancing structural and acoustic performance of a multi-layered sandwich panel is a formidable undertaking. Frequently the gains achieved in terms of reduced weight, still meeting the structural design requirements, are lost by the changes necessary to reach acceptable acoustic performance. Within this paper, a design method for a multifunctional load bearing vehicle body panel is proposed which attempts to achieve a balance between structural and acoustic performance. The approach is based on numerical modelling of the structural and acoustic behaviour in a combined topology, size, and property optimization in order to achieve a three dimensional optimal distribution of structural and acoustic foam materials within the core of a sandwich panel. In particular the effects of the coupling between the face sheets and acoustic foam are examined for its impact on both the structural and acoustic performance of the panel. The results suggest a potential in introducing an air gap between the acoustic foam parts and one of the face sheets, provided that the structural design constraints are met without prejudicing the layout of the different foam types.

Keywords: Vehicle Design, Topology Optimization, NVH, FEM, Sandwich Structures

1. Introduction

Modern vehicle design is the result of a compromise between functional requirements, such as cost, styling, safety, weight, etc.. Often, certain functionalities are achieved with a single component assigned to and optimized for a single task. Assembling a group of such components frequently results in the system requirements being achieved in a suboptimal manner.

In current automotive design, structural functionality is often achieved using a spot welded assembly of stamped steel components known as the body in white (BIW). In such sheet metal structures, achieving acoustic comfort is not a simple process and involves engineering knowledge related to both structural design and noise, vibrations, and harshness (NVH).

An alternative method of addressing the often conflicting structural and NVH requirements on stiffness, weight, and damping is by the use of load bearing sandwich panels with integrated acoustic functionality. By using a sandwich structure, local bending stiffness can be drastically increased, as compared to unsupported sheet metal, and potential vibration problems can be avoided. Proper use of the panel's load bearing capacity may also enable the designer to eliminate redundant sheet metal components and thus achieve greater weight savings. By using lightweight, open cell foams in partitions within the sandwich core an alternative means of acoustic and structural damping can be achieved which can be tuned to acquire a desired behaviour with existing numerical tools [1], at a very low weight penalty compared to conventional solutions.

In such a construction, the structural requirements and NVH requirements are in direct contradiction to one another. The most efficient structure is achieved when structural foam core material is perfectly bonded to the face sheets in order to efficiently transfer shear loads and achieve maximum bending stiffness. High acoustic performance is achieved by using multiple layers of highly compliant visco-elastic foam material which is structurally inefficient. In addition, for acoustic purposes, the inner face sheet of the panel should be perforated to a degree which reduces its structural performance. Further, the presence of an air gap between the acoustic foam treatment and the perforated sheet, which would further decrease structural capacity of such a panel, may provide additional acoustic performance [2].

The objective of this work is to present and explain a method of achieving a balance between the structural and acoustic performance requirements for such a multifunctional panel by the use of topology, size, and property

optimization implemented in a finite element analysis (FEA) framework.

2. Aim and Scope

The method described herein is meant to be a tool for structural acoustic design of a sandwich panel for use in, for example, vehicle applications. It is based upon the assumption that the functional requirements of the panel are known from the outset, and establishing these requirements is not a part of the method in itself. The steps taken to establish the functional requirements used herein can be found in previous work by the authors [3].

To achieve acceptable structural and acoustic requirements, but in a new conceptual design, a multi-layered, multifunctional sandwich panel concept has been proposed. The panel consists of a carbon-fibre composite external face sheet, a core of structural and acoustic polymer foam, and a perforated inner face sheet of chopped strand matt (CSM) glass fibre reinforced plastic. A layered composite material was chosen for the outer face sheet as it offers increased flexibility in terms of tuning mechanical properties, and significant possibilities to mass reduction in relation to sheet metal alternatives. Structural requirements of the panel are achieved by the sandwich created between the composite face sheets and structural foam core material. In comparison to earlier works by the authors, the structural foam core is configured through a topological optimization opening up for three-dimensional material placement. NVH performance is achieved by selecting the correct type, thickness and stacking sequence of porous acoustic foam positioned in partitions of the core where structural foam is not needed.

Assuming that the acoustic foam treatment used is of significantly lower stiffness than the structural foam material, and that the partitions of such material interrupt the continuity of the structure, it can easily be understood that as the relative size of the acoustic treatment increases the structural efficiency of the panel as a whole will be reduced. The overall effect this will have on the acoustic performance is in fact not trivial to predict. A larger volume of acoustic foam may equally well provide higher levels of sound absorption, or it may in fact lead to higher sound levels due to the panels reduced stiffness and altered sensitivity to vibration. Introducing the aforementioned air gap makes the performance even more difficult to predict.

To achieve the necessary structural requirements and maintain a sufficient volume of acoustic foam to be effective, a framework of structural foam ribs could be implemented with acoustic foam pockets between them. A

schematic representation of such a configuration can be seen in figure, 1. While it may be possible to achieve adequate performance in this manner, it is unlikely that an arbitrary configuration, even one based on sound engineering experience and good engineering judgement, will coincide with the minimum weight design.

In addition to the materials described, the idea of using an air gap within the structure in order to increase the acoustic performance is tested. By inserting a thin layer of air into the acoustic treatment of the structure, a change in impedance can be achieved which might offer increased dissipation of acoustic waves within the treatment.

The presence or absence of an air gap is a significant alteration to the sandwich structure, and so two panel configurations are examined. In the first configuration, perfect bonding between all layers is assumed, as in a conventional sandwich structure. In the second configuration, a small air gap is introduced between the inner face sheet and the acoustic foam treatment. An illustration of the proposed panel concept can be seen in figure 1.

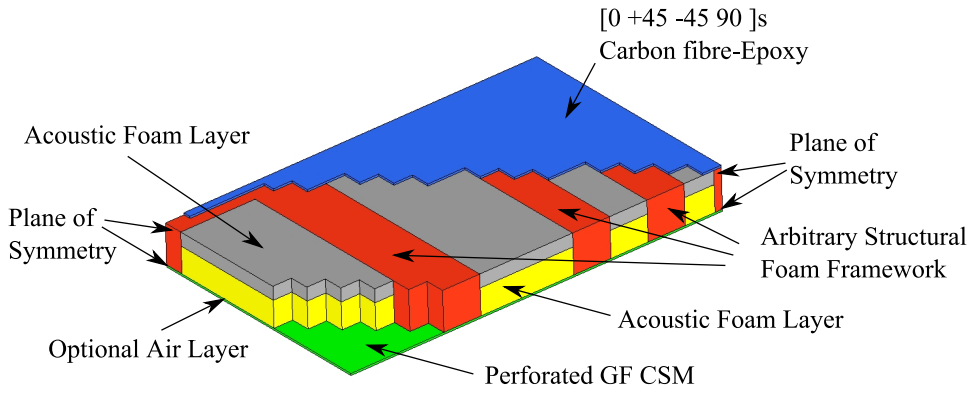

Figure 1: Cutaway view of multifunctional panel concept. 1/4 model size 0.6x1.0 m.

3. The Optimization Design Process

The central idea of this work is that in order to achieve a successful design, functional requirements should be the controlling factor and optimization tools should be used to tailor the desired panel to meet the needs required.

In order to assess certain aspects of structural integrity and NVH performance, computationally expensive forms of FEA are required. These meth-

ods of FEA, coupled with a large number of design variables and gradient based optimization algorithms with their required perturbation iterations, make solving such a complex multi-discpiplinary problem in a single step exceedingly difficult if not impossible using reasonable powerful computational resources. For this reason, it is necessary to analyse the problem and use engineering judgement beforehand to asses which design variables are most likely to exhibit a strong coupling to which functional requirements.

It was decided that a two stage process would be most efficient in terms of computational time. In the first stage of the process, the topology of the foam core would be established. The idea was that regardless of materials and thicknesses, a good approximation of the structure necessary to accommodate the applied loadings could be obtained in this manner. Once a general structure had been obtained, the second stage of structural and acoustic optimization could be applied to optimize the material properties and thicknesses for each of the constituent components. Depending upon the final outcome of the design process, a repetition of the entire loop could be carried out if further confirmation of the design was needed. A flow chart of the process is presented in figure 2 to aid in understanding.

4. Topology Optimization

Assuming that the acoustic foam treatment would be implemented as shown in figure 1, the aforementioned issues regarding the effects of increased or decreased volume of acoustic foam must be properly addressed. In order to achieve the necessary structural requirements while maintaining a sufficient volume of acoustic foam a methodical and repeatable way of distributing structural and acoustic foams within the core was needed. Topology optimization was seen as a good starting point. Within the work presented here, the foundation of the topological optimization component is based upon the method called bi-directional evolutionary structural optimization (BESO). The BESO method is an element based method (rather than density based) which can be applied to an existing FE mesh, and produce a final result which is a complete FE mesh, without the need for interpretation of density results. This was a primary reason for choosing the BESO method over other topology optimization methods. The final result of the topology optimization step could, without alteration, be directly used as input into the next stage of the optimization framework. The BESO method and its mathematical principles have been thoroughly developed and presented within the litera-

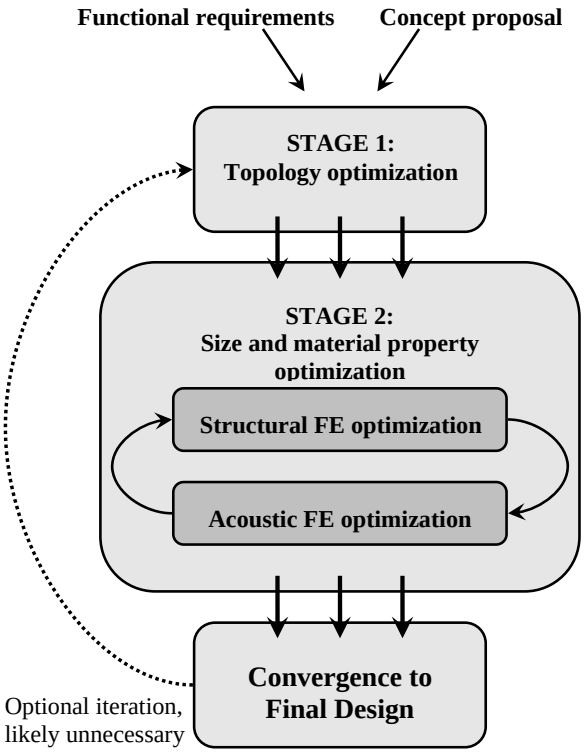

Figure 2: A flow chart of the two stage design process.

ture [4, 5, 6, 7, 8, 9, 10] and are not repeated in depth here. For the sake of clarity however, a few of the basic principles used will be reviewed.

It should be mentioned that the BESO method is by no means related to any kind of genetic algorithm, despite the word "evolutionary" in the name. In brief, the BESO method is an iterative method of creating an effectively stressed structure within a finite element model. For each load case, a sensitivity number is calculated for each element within the allocated design space. The method of calculation of the sensitivity number depends upon the type of analysis being performed. Post-analysis, the elements are sorted according to sensitivity number, and those with the lowest sensitivity number are removed from the design space. For cases where several different analysis are performed, a method of weighting the various sensitivity numbers for a single element is used to achieve a single overall sensitivity number for the element. The process is repeated until the stop constraint for the optimization becomes active.

For static cases, the sensitivity number, α for each element within the design space is calculated according to [6]:

$$\alpha_i = \frac{1}{2}\{u^i\}^T[K^i]\{u^i\} \tag{1}$$

where u^i corresponds to the displacement of the ith element, and K corresponds to the stiffness matrix of the ith element. This static sensitivity number is equivalent to the element strain energy for a given element.

For dynamic analysis such as normal modes analysis, the sensitivity number is described according to [5]:

$$\alpha_i = \frac{1}{m_i}\{u^i\}^T[\omega_i^2[M^i] - K^i]\{u^i\} \tag{2}$$

where in this case u^i corresponds to the eigen vector displacements of the ith element for the eigen frequency α. $[M]$ and $[K]$ correspond to the element mass and element stiffness matrices respectively. m_i corresponds to the mass of element i.

For the case of linear buckling, a sensitivity number for change in buckling load can also be found within the literature [11, 12]:

$$\lambda_i = \{u^i\}^T\left([\Delta K^i] + \lambda_i[K_g^i]\right)\{u^i\} \tag{3}$$

in this case, λ_i represents the change in the load proportionality factor for removal of the element i. $[K_g]$ is the geometric stiffness matrix for the linear buckling eigen value problem.

4.1. Load Cases and Analysis Types of Interest

For the case study presented here, four specific analysis were of interest; linear elastic response to localised loading, linear elastic response to distributed pressure, normal modes analysis, and linear buckling response during in-plane loading. Figure 3 visualises these four analysis types using the 1/4 symmetric model used within the paper. The first load case is static pressure applied to an area approximately 100 mm in diameter at the centre of the panel. The second load case is a static pressure distributed over the entire top surface of the panel. The third load case is a normal modes analysis to determine the natural frequencies of the panel with certain boundary conditions and the final load case is a linear buckling analysis of in-plane loading.

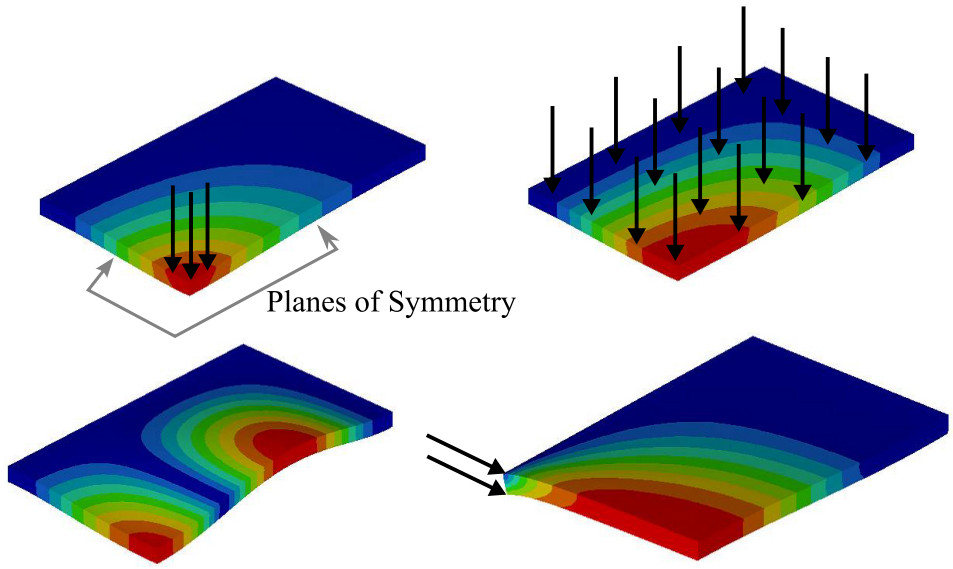

Figure 3: Four load types of interest: Localised loading, distributed pressure, normal modes analysis, and in-plane loading (buckling).

Two configurations of the panel were proposed for study which required two different adaptations to the classical BESO method as developed within the literature. The first adaptations was regarding the calculation of sensitivity number in the linear buckling case, and the second was accommodating for the air gap, or more accurately, lack thereof in the topology optimization.

4.2. Adaptation for buckling load case

The element sensitivity numbers for linear buckling analysis, as shown in equation 3, are developed in the literature [11, 12] using a simple plate. Calculation of the sensitivity number in that case requires direct access to the geometric stiffness matrix for the problem. Gaining access to the geometric stiffness matrix, while perhaps simple in own code or using simple geometry, is difficult if not impossible in commercially available codes. The authors were not able to extract the geometric stiffness matrix accurately from the model, nor find any documentation on how this might be done and so a simple adaptation of the method was proposed for the linear buckling cases.

For the panel in question, solving the linear buckling problem yields eigen values which describe the critical load factor in addition to eigen vectors

which describe the panels out of plane deformation or buckling modes. Using Abaqus, element strain energy, as used in equations 1 and 2, can be calculated for the buckling deformation and easily obtained from the results. The objective in using topology optimization in this case is to place core material most effectively to resist precisely such modes of unstable deformation. Thus, by using this element strain energy and calculating sensitivity numbers for buckling in the same manner as those of the static load case in equation 1, structural foam should be placed to inhibit such modes of deformation.

Once a method of calculating element sensitivity numbers has been established, some method of comparing sensitivity between load cases must be used to establish which elements are of most importance to fulfil which load case. This is achieved within the literature through placing constraints on displacements and eigen frequencies in normal modes analysis [6, 8] and normalising between cases to make sure all constraints are fulfilled [9]. For linear buckling analysis, the critical buckling load was treated as a constraint in precisely the same manor as an eigen value is treated in the literature for normal modes analysis. This allowed the same weighting methods to be used as described above.

The adaptation of the BESO method to the buckling load cases broadens somewhat the methods areas of application. The motivation for the buckling load case adaptation is relatively simple, and as described herein, lacks any thorough mathematical development. Nevertheless, the results appeared to be reasonable and were completely repeatable within the study and thus the authors feel it is justified.

4.3. Adaptation for swap functionality

The second adaptation to the BESO method was necessary for the panel configuration where perfect bonding between all layers is assumed. For the panel configuration with no connection between the inner face sheet and the acoustic foam, i.e. an air gap, adding or removing elements from the sandwich core according to the conventional methods of BESO is sufficient. For the case where a bond was present between the acoustic foam and inner face sheet however, simply removing elements is not acceptable. In previous work [13] the authors have found that the coupling between the inner face sheet and the acoustic foam treatment plays a critical role in not only the acoustic performance, but even in the structural efficiency of the panel. While the acoustic foam is relatively compliant, it does contribute to the transfer of shear loadings in static cases, and provides an elastic support for the inner

face sheet which inhibits resonant vibration. This effect is significant and cannot be ignored during optimization.

To deal with this problem, a swap functionality was implemented wherein elements which should ordinarily be removed from the design space were instead assigned the material properties of the acoustic foam. This swap method is beneficial in multiple ways. Firstly, it obviously retains the acoustic material within the model and accounts for its contribution to the structure. Secondly, it helps to eliminate any potential singularities within the global stiffness matrix which may be caused by elements becoming free-coupled when the design is converging to a final solution and the difference in element sensitivity numbers becomes very small. This swap methodology was only realisable using an element based method such as BESO rather than a density based method.

More formally stated, the topology optimization problem for both configurations proposed was formulated as follows.

$$\begin{aligned} &\text{minimize} && m_{panel} \\ &\text{subject to:} && \\ &\delta Z_{max} \leq a && \{LC1\} \\ &\delta Z_{max} \leq b && \{LC2\} \\ &\omega^{(1)} \geq c && \{LC3\} \\ &\lambda^{(1)} \geq d && \{LC4\} \end{aligned} \tag{4}$$

Where m_{panel} is the panel mass, δZ_{max} the maximum vertical displacement of the panel, $\omega^{(1)}$ the first eigen frequency from normal modes analysis, $\lambda^{(1)}$ the load proportionality factory for the first buckling mode. Constants a–d represent arbitrary values of constraints, and LC1–LC4 are the four load cases described previously.

The BESO parameters and weighting methods, including the novel adaptations described, were implemented in a python script which was run in Abaqus CAE finite element analysis software to solve the optimization problem shown above. The script imported and created Abaqus models, executed the Abaqus FE solver, calculated the element sensitivity numbers, and altered the geometry in the model accordingly. Topology optimization was performed using a one-quarter size model of the entire panel with symmetry

boundary conditions applied through all layers along the symmetry edges to minimize computational time. As a starting point for topology optimization, a core of nearly 100% structural foam was assumed and only a single element was assigned the properties of the acoustic foam. No restrictions were placed on the amount of material to be removed. Optimization was stopped when all constraints were fulfilled and the overall change in mass between iterations was less than a pre-determined small amount.

Convergence of the topology optimization represents completion of the first stage in the overall design process. To maintain emphasis on the design process as a whole rather than a sum of parts, results of the topology optimization stage are presented in the results and discussion section of the paper.

5. Size and Property Optimization

Having established the most effective general shape for structural foam within the core of the panel, the next stage in the proposed design process was to determine the dimensions and mechanical properties of the various layers both in regards to structural and acoustic functionality. As computational resources are a limiting factor, and to gain a more thorough understanding of the overall problem and allow a larger number of design variables, this stage in the design process was split into a two step iterative loop. The fist step addresses structural functionality, and the second step acoustic functionality, both using a number of design variables deemed interesting and relevant for study.

5.1. Structural optimization

To correctly determine the optimal size and material properties from a structural standpoint, a number of parameters were chosen as design variables. While implementing thickness variables is trivial, using material properties as variables required a method of parameterization to some meaningful physical quantity. A list of the variables used is shown below, and following is a brief description of their relevance and parameterization.

1. V_{f0}: Volume fraction fibre in 0°lamina
2. V_{f45}: Volume fraction fibre in $\pm$ 45°lamina
3. V_{f90}: Volume fraction fibre in 90°lamina
4. t_0: Lamina thickness of 0°lamina

5. t_{45}: Lamina thickness of $\pm$ 45°lamina
6. t_{90}: Lamina thickness of 90°lamina
7. t_{ST}: Thickness of structural foam layer
8. ρ_{ST}: Density of structural foam layer
9. t_{CSM}: Thickness of inner face sheet

Volume fraction fibre describes the percentage of fibre reinforcement content in relation to the matrix (i.e. epoxy) content within a layer of composite material. As the amount of fibre increases, so does the stiffness and strength of the composite, however at the expense of added mass as the fibres are of much higher density than the matrix material. This variable was used in each layer of the eight layer laminate to manipulate the mechanical properties according to micro-mechanical relationships well established within in the literature [14]. These relationships can be seen in equations 5 to 9. The subscript numbers in these equations refer to the direction in which the properties are measured, 1 is the axial direction of the fibre, and 2 is the in-plane transverse direction, and 3 is the out of plane direction. Fibre volume fraction was allowed to vary from 0.00 (i.e. 100% matrix) to 0.60 (a typical max value in practice) and layer lamina thickness from 0.010 to 2.875 mm. Table 1 shows the material data used for the outer face sheet. Allowing for such a low fibre volume fraction and thickness in the lamina was seen as a method of checking to see that the selected materials and lay-up were appropriate. Should the fibres prove excessively stiff in a given layer, the matrix material could for example be replaced with lower density matrix material to save mass. Should a certain layer prove unnecessary, it could in practicality be removed from the lay-up.

$$E_{11} = (V_f)E_{f11} + (1.0 - V_f)E_m \tag{5}$$

$$E_{12} = E_{13} = \frac{V_f}{E_f} + \frac{1 - V_f}{E_m} \tag{6}$$

$$G_{12} = G_{13} = \frac{G_m}{1 - \sqrt{V_f}(1 - G_m/G_{f12})} \tag{7}$$

$$G_{23} = \frac{G_m}{1 - V_f(1 - G_m/G_{f12})} \tag{8}$$

$$\nu_{lamina} = V_f \cdot \nu_f + (1 - V_f) \cdot \nu_m \tag{9}$$

	Matrix	CF	GF CSM
$E_{11}(tensile)$ $[MPa]$	3200	220600	15000
$G_{12} = G_{23}$ $[MPa]$	1185	30130	5769
ρ $[kg/m^3]$	1125	9000	1700
ν [–]	0.35	0.20	0.3

Table 1: Material properties for matrix, fibers, and CSM sheet (non-perforated)

The density of the structural foam, ρ_{ST}, was chosen to alter the mechanical properties of the foam according to equations (10) to (12), which are well established in the literature [15]. The foam was assumed to be closed cell, and based on PET. Data for commercially available foams, namely Divinycell P series, and Airex T90 and T92 , was obtained from technical data sheets on the respective manufacturers homepage[1] [Retrieved 22/11/2010]. Properties from the manufacturers were correlated with equation (10) and (11), and the assumption that the porosity, $\phi = 0.8$ from the literature [15] was checked. Exact agreement between manufacturers' data and the theoretical values was not obtained. Better agreement regarding the compressive modulus was obtained using $\phi = 0.7$, which required a scaling factor of 0.8 times the calculated shear modulus to obtain reasonable agreement. Figures 4 and 5 show the manufacturers data and theoretical properties as functions of density. In addition to foam density, thickness of the structural foam core, t_{ST}, was also used as a design variable due to its fundamental importance to sandwich stiffness.

$$\frac{E_{foam}}{E_{solid}} \approx \phi^2 \left(\frac{\rho_{foam}}{\rho_{solid}}\right)^2 + (1-\phi)\frac{\rho_{foam}}{\rho_{solid}} + \frac{P_0(1-2\nu_{foam})}{E_{solid} - \rho_{foam}/\rho_{solid}} \tag{10}$$

$$\frac{G_{foam}}{E_{solid}} \approx \frac{3}{8}\left(\phi^2(\frac{\rho_{foam}}{\rho_{solid}})^2 + (1-\phi)\frac{\rho_{foam}}{\rho_{solid}}\right) \tag{11}$$

$$\nu_{foam} \approx \frac{1}{3} \tag{12}$$

[1] `www.diabgroup.com/europe/products/e_divinycell_p.html`
`www.corematerials.3acomposites.com/airex-foams.html`

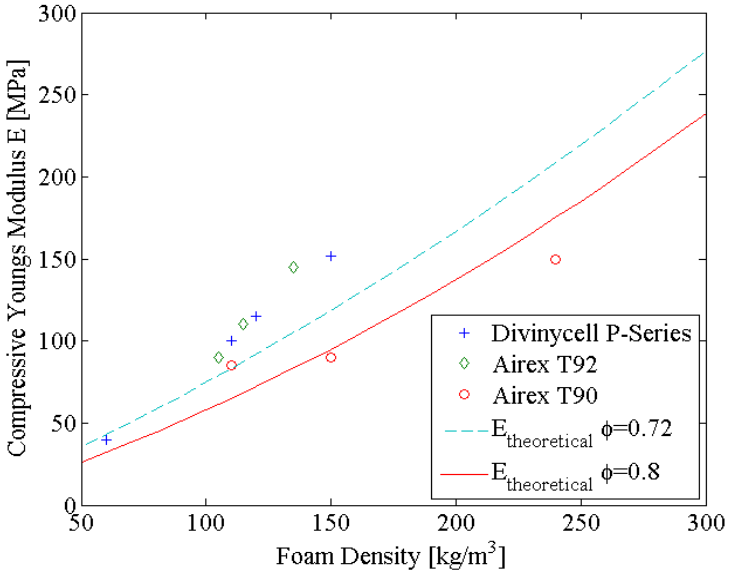

Figure 4: Compressive modulus as function of density.

For the inner face sheet the thickness, t_{CSM}, was the only design variable considered, in order to limit the number of design variables. A fixed degree of perforation assuming 2.0 mm holes drilled in a square pattern with 3.5 mm between hole centres was used. This was considered to be the minimum degree of perforation to allow for sufficient acoustic transparency [16]. Tighter hole spacing increases acoustic transparency but reduces bending stiffness and vice versa. In the model, individual holes were ignored and instead equivalent material properties were used for the perforated sheet and obtained using methods developed in previous work [17].

The exact same optimization problem as described in the previous design stage, i.e. minimize mass subject to functional constraints, was solved using the method of moving asymptotes (MMA) [18, 19]. The output from the final iteration of topology optimization gave the FE model with new topology, and the variables described above for material properties and thickness were implemented in the optimization framework. All material properties relating to the acoustic foam components remained constant. All load cases, boundary conditions and constraints on displacements etc. were the same as in the previous design stage. The optimization was stopped when suffi-

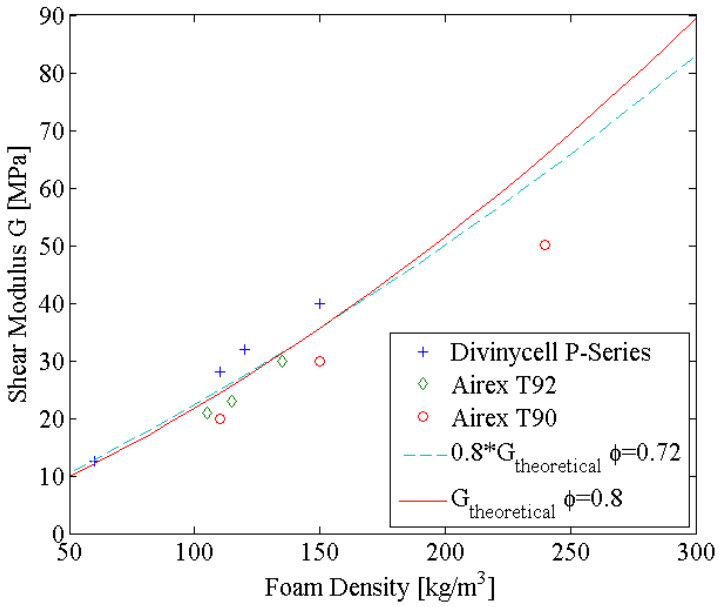

Figure 5: Shear modulus as function of density.

cient convergence in both the objective function and the design variables was achieved. The next step was to optimize the acoustic behaviour and relevant material properties.

5.2. Acoustic Optimization

For this conceptual optimization of acoustic performance the acoustic treatment was placed in layers in the volume not occupied by structural foam elements from the topology optimization. Two different foam layer combinations were used and they were tried both with and without an air gap between the inner face sheet and the acoustic foam combination, a total of four different configurations, figure 6. The acoustic foam A was a comparably soft Polyurethane foam (PU foam) and the acoustic foam B was a relatively stiff Polyimide foam (pi foam).

As can be seen in figure 6, the foams were stacked in an A-B-(air) or A-A-(air) sequence, i.e. in two configurations a single foam was split into two distinct layers. The reason for using two separate layers of the same foam type was to explore the possibility that the foam layers would be perceived as one homogeneous layer by ascribing them the same material properties,

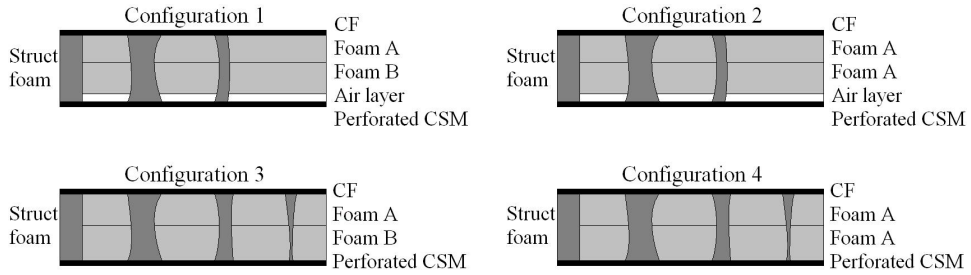

Figure 6: Conceptual visualization of the four different configurations in the acoustic optimization. Note that structural foam topology (dark grey) differs between the air gap and non air gap configurations.

or whether there existed possible benefits in having two separate layers with different material properties as suggested in results previously obtained by the authors. The task of determining the acoustically better choice between a single or multiple layer configuration could then be left to the optimization algorithm.

The acoustic behaviour of the panel was studied using in house FE code. An air cavity of the length and breadth of the panel and 1.5 m in depth (i.e. of comparable size to a vehicle passenger compartment) was attached to the perforated side of the panel and the sound pressure level (SPL) in a sub volume of the cavity generated by dynamically exciting the panel was calculated. The sub volume within the cavity was located approximately where listeners would be positioned, and was considered a good metric for quantifying the acoustic comfort in the vehicle.

Excitation of the panel was in the form of dynamic forces in the x-, y-, and z-direction applied over the top surface of the elements along the edge of the CF epoxy top sheet as seen in figure 7.

As in the structural problem, the roof was represented by a quarter model and symmetry boundary conditions were applied at the symmetry edges through all layers. The inner perforated plate was fixed in the x-, y- and z-direction along $x = 0$ and $y = 0$.

For the dynamic and acoustic analysis, FE-based numerical methods were used where the porous foams were modelled using Biot theory [20, 21, 22]. The theories used to model the acoustic foam assume material isotropy, small displacements and linearly elastic materials. Here the finite element solutions were obtained using the methods thoroughly discussed and properly addressed in works by Hörlin *et al.* [23] and by Hörlin [24] and will not be

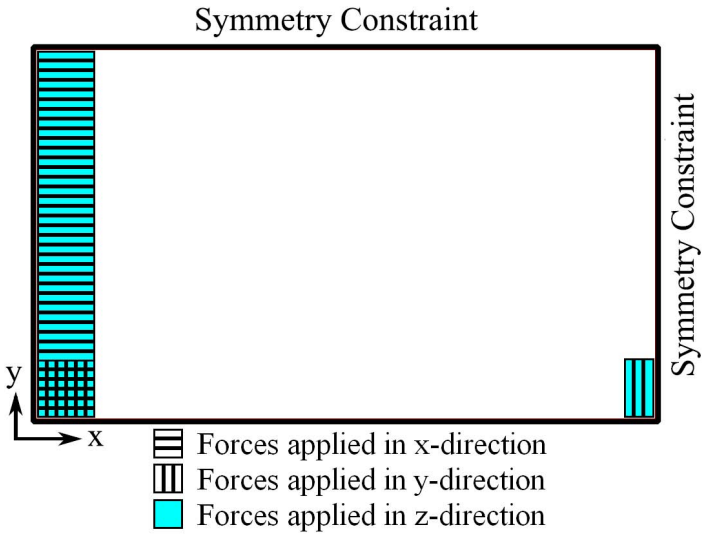

Figure 7: Dynamic forces applied to the CF Laminate.

repeated here. In short, the numerical tools used, account for the properties of the individual porous layers, e.g. the fluid in the pores, the solid frame structure of the cellular foam and the coupling between them. They also addresses the kinematic conditions, the mass flow continuity conditions and the relevant stress balances present at the boundaries between solid, fluid or porous layers. In using such numerical tools, special care must be taken in selecting trial functions to obtain convergent solutions to Biot's equations. This is especially important for multi-layered structures, for which hp-FEM[2] has proven to be a convenient finite element base.

In addition, the nature of the acoustic hp-FEM tool dictated that the final geometry, as obtained from the previous step of the process, had to be simplified somewhat. This simplification was predominantly in terms of the topology geometry refinement of the foam core as it was necessary to increase element size from the 10 mm used in the structural problem to approximately 50 mm for the acoustic problem. The actual geometry used in the problem is shown in the results section of this paper.

To optimize the acoustic foam in a meaningful way, design variables which

[2] Convergence is achieved by refining the mesh and/or increasing the approximation order.

can be changed independently of one another are required. In porous foam the inter-relationship between several of the parameters used to calculate the response, for example the homogenised Young's modulus, E^*, and the bulk density, ρ^*, is quite complex. One approach to address this problem is to relate the macroscopic properties of the foam to the underlying microscopic properties by the use of scaling laws. Contributions to the development of such scaling laws and understanding of the mechanical properties of foam are well documented in the literature by many authors of whom a few are cited here [15, 25, 26, 27, 28, 29]. More specifically, a method of implementing these scaling laws for the express purpose of optimization of porous foam in multi-layered structures has been proposed previously by some of the authors [30]. For the purpose of clarity, a summary of the more important scaling laws used within this work are given below.

$$\rho^* = \rho^*_{ref} \left(\frac{d_s}{d_{ref}}\right)^2 \left(\frac{l_{ref}}{l_s}\right)^2 \tag{13}$$

$$\phi = 1 - \frac{\rho^*}{\rho_s} \tag{14}$$

$$E^* = E^*_{ref} \left(\frac{\rho^*}{\rho_{ref}}\right)^2 \tag{15}$$

$$\Lambda = \frac{d_s}{4(\rho^*/\rho_s)} \tag{16}$$

$$\Lambda' = 2 \cdot \Lambda \tag{17}$$

$$\alpha_\infty = 1 - \frac{1 - \alpha_{\infty ref}}{\ln(\phi_{ref})} \cdot \ln(\phi^*) \tag{18}$$

$$\sigma^{static} = \sigma^{static}_{ref} \left(\frac{\rho^*}{\rho_{ref}}\right)^2 \cdot \left(\frac{d_{ref}}{d_s}\right)^2 \cdot \frac{\alpha_\infty}{\alpha_{\infty ref}} \cdot \frac{\left(1 - \frac{\rho_{ref}}{\rho_s}\right)}{\left(1 - \frac{\rho^*}{\rho_s}\right)} \tag{19}$$

where d_s and l_s are the strut thickness and strut length respectively, ρ_s is the density of the frame material, Λ is the viscous characteristic length, Λ' is the thermal characteristic length, α_∞ is the tortuosity, and σ^{static} is the static flow resistivity. To use these scaling laws in a meaningful way in optimization,

a reference foam is necessary, denoted $(.)_{ref}$. For the acoustic foam A (the Polyurethane foam, PU foam) and for the acoustic foam B (the Polyimide foam, pi foam), the reference material properties are listed in table 2.

Material property		PU foam	pi foam
ρ_s	[kg m^{-3}]	1100	1400
E_s	[Pa]	$450 \cdot 10^6$	$1400 \cdot 10^6$
$\alpha_{\infty ref}$	[1]	1.17	1.17
ρ^*_{ref}	[kg m^{-3}]	35.4	8
E^*_{ref}	[Pa]	$164 \cdot 10^3$	$848 \cdot 10^3$
σ^{static}_{ref}	[kg m^{-3} s^{-1}]	4500	$1000 \cdot 10^3$
Λ_{ref}	[m]	$96.1 \cdot 10^{-6}$	$39 \cdot 10^{-6}$

Table 2: Material properties for reference materials.

More formally stated, the objective function chosen for optimization was the unweighted sound pressure level (SPL) in a sub volume of the air cavity, Ω_{sub}, summed over the entire frequency range.

$$\langle SPL \rangle_{\Omega_{sub}} = 10 \cdot \log \left(\frac{\sum_{f=f_1}^{f_{max}} \left(p_f^2 \cdot \Delta f_f \right)}{p_0^2} \right) \tag{20}$$

The complexity of the numerical problem makes it computationally expensive to solve and as each frequency is solved independently, the frequency range was limited to 100–500 Hz. This was deemed an interesting and relevant frequency area for study with respect to NVH comfort.

The choice of objective function will obviously have a great effect on the outcome of the optimization. Alternative objective functions, such as the A-weighted SPL or the radiated sound power, may lead to other results [30]. However, the method presented herein is mainly conceptual and the chosen objective function is one way to compare the acoustic and dynamic performance of the different configurations.

The design variables used in the acoustic optimization were the scaled length of the struts l_s/l_{ref} in the two foam layers and the thickness of each foam layer. These design variables will be referred to as l_{PU}, l_{pi}, t_{PU} and t_{pi}

respectively. Constraints were put on maximum and minimum relative strut length, which could vary between 0.5 and 3, and maximum and minimum thickness of each layer, which could vary between 1 mm and 50 mm. Constraints were also put on maximum and minimum total thickness. The same optimization framework based on MMA was used for the acoustic problem [18, 19]. The optimization problem was run until convergence of the objective function and design variables were achieved.

5.3. Further Iterations

Once a convergent solution to the acoustic optimization has been achieved, the first iteration of the second stage of the design process is complete. To make certain that changes of the acoustic foam properties have not affected the structural performance significantly, it may be necessary to repeat the second stage of the optimization.

For the case of the model without air gap, this would involve merely assigning the correct material properties to the elements in question. For the case of the air gap, as the acoustic foam is not accounted for, this might best be achieved by the use of a non-structural mass applied to the structure.

Should the final properties of the acoustic treatment differ significantly from those assumed at the outset of the design process, it might require another full iteration of the process. Assuming that the stiffness and density of the acoustic treatment is still of a different order of magnitude compared to the structural foam, this should not be necessary.

6. Results and Discussion

Results from the first stage in the optimization process can be seen in figure 8. The figure shows the resulting topology in the one quarter symmetric model used in optimization. The outer frame of structural foam which was excluded from the design space can also be seen. The images on the left side of the figure show an isometric and top view of the no-air gap topology. Images on the right show the same views for the air gap configuration. For the sake of clarity, it should be emphasised that only one fourth of the entire geometry is shown, and the full panel should be symmetric along the two symmetry planes shown in the figure.

The two resulting structures have both significant similarities and significant differences. Both configurations developed a number of finger-like structural foam beams extending from edges towards the centre of the panel.

The size and geometry of these fingers differs between the two configurations. In the configuration with the air gap, a continuous finger of structural foam developed across the entire width of the panel. No such panel wide structure formed in the non-air gap configuration.

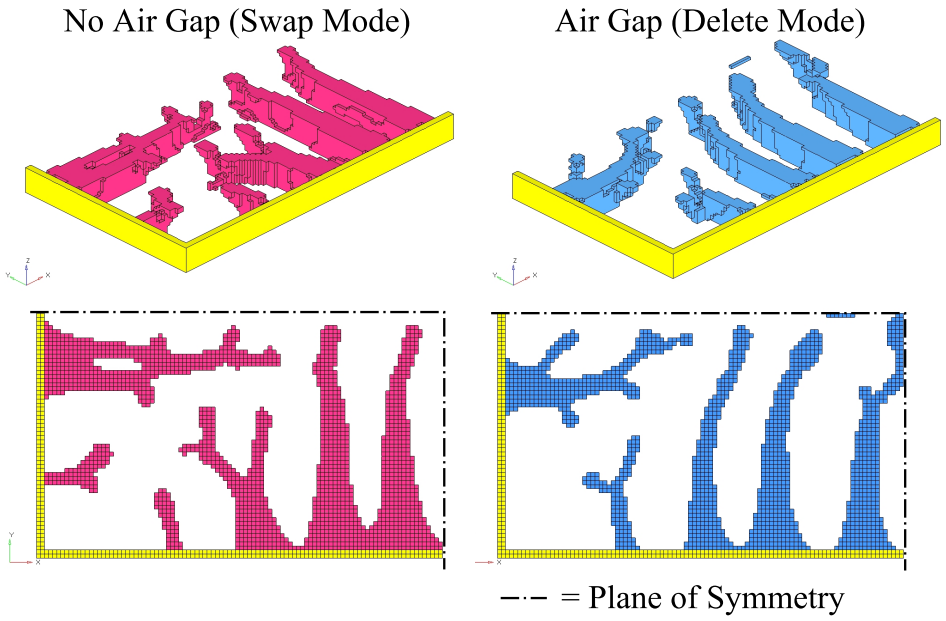

Figure 8: Final topology for structural foam in the 1/4 model. Left - without air gap(swap mode), Right- with air gap(delete mode). Frame of fixed elements is also depicted.

This is perhaps to achieve the necessary minimum frequency for the first eigen mode. It is difficult to draw detailed conclusions regarding the significance of the geometry, however what should be understood is the significance of the fact that there is an obvious difference. The geometry of the final configurations would be difficult if not impossible for a design engineer to predict.

During topology optimization, it also became apparent that the constraining requirement on the design was in fact the displacement restriction on the distributed load case. Constraints on localised loads, normal modes, and critical buckling loads were easily fulfilled using this construction.

As mentioned in the method description, in transition from the structural FE model to the acoustic FE model, a simplification of model geometry, i.e. te aforementioned increase of element size, was required. Figure 9 shows a

comparison between the final topology of the structural foam cores of both panel configurations for the structural and acoustic optimization. In addition, it should be understood that the layout of structural foam in the acoustic model is the same through the entire thickness of the panel core. In the structural model, there was a slight tendency towards three dimensional formations, however the loss in accuracy in modelling these shapes as square blocks is considered low.

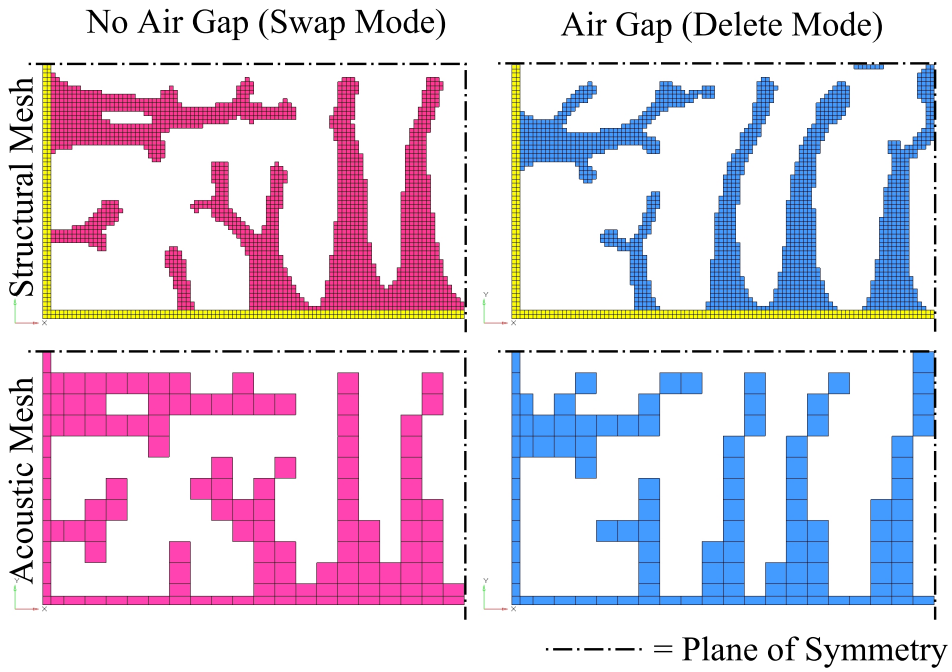

Figure 9: A comparison of structural (above) and acoustic (below) FE meshes of the structural foam core material.

Results for design variables of the structural optimization, as well as the permitted range during optimization, can be seen in table 6. The equivalent mechanical properties calculated from the carbon fibre laminate and used in the acoustic optimization can be seen in table 4.

As the case study has been presented for the purpose of explaining the proposed design method, results here should be seen from that standpoint without placing too much emphasis on the exact values. Within the results, it is clearly obvious that there do exist differences between the air gap and non air gap configuration despite the fact that they are both exposed to

identical load cases and constraints. This is of course directly coupled to the geometry of the foam cores, which is in turn steered by the presence or absence of the air gap.

Regarding the composite laminate face sheet, it is interesting to note that two different configurations with significantly different mechanical properties and lay-ups were achieved during optimization, however their total thickness is nearly identical. The air gap configuration required a face sheet of much higher stiffness than that of the non-gap configuration. While it may not prove possible or desirable to produce such a lay-up, the results of this optimization at least give the designer an indication of which layers are of primary importance, and which layers might be removed and the optimization repeated. Alternatively, it may be a good method to help the engineer choose more conventional material for use in the face sheet. For example, observing the thickness of 1.8 mm and a required equivalent stiffness in the region of 50 MPa, perhaps magnesium would be a better choice in regards to manufacturing despite the weight penalty.

The thickness of the foam core in both examples reached the maximum allowable value. This is not surprising as it is well known that increasing a sandwich structures thickness is the most mass-efficient way of increasing stiffness. In this case, a structural foam density somewhere in the middle of the allowable span was achieved for both configurations. These two variables, thickness and density, are inherently entwined. As long as the load case is such that a foam of more than the minimum density is required, the thickness will be increased as much as possible. Not until the foam reaches minimum density will the optimization begin to reduce the sandwich thickness to shed mass. Further evidence of the importance of the coupling between inner face sheet and acoustic foam can be seen in the higher density, and thus stiffer, structural foam in the air gap configuration.

The degree of perforation, and thus the mechanical properties, of the inner face sheet were identical, and from a practical standpoint, so were the final thicknesses.

The results from the acoustic foam optimization are shown in table 5. The resulting microscopic foam properties as well as foam layer thicknesses differ considerably between configurations. This would seem to imply that the acoustic response of the panel is quite sensitive to changes in acoustic treatment despite the effectiveness of the structural foam sandwich framework. Comparison of the changes in objective function values during the optimization process imply that a significant improvement of the SPL may

Variable	Range	Configuration	
		Air Gap	No Air Gap
V_{f0}	0.000-0.600	0.598	0.596
V_{f45}	0.000-0.600	0.361	0.597
V_{f90}	0.000-0.600	0.388	0.071
t_0[mm]	0.010-2.875	0.320	0.129
t_{45}[mm]	0.010-2.875	0.016	0.222
t_{90}[mm]	0.010-2.875	0.563	0.350
$t_{PETfoam}$[mm]	5.000-75.000	74.9	74.8
$\rho_{PETfoam}[kg/m^3]$	50.000-300.000	120.4	105.3
t_{CSM}[mm]	0.500-5.000	0.654	0.675

Table 3: Final values of structural design variables

Table 4: Equivalent Properties of Outer Face Sheet

	Configuration	
	Air Gap	No Air Gap
$E_{1topsheet}$ [MPa]	50340	29160
$E_{2topsheet}$ [MPa]	57045	20233
$E_{3topsheet}$ [MPa]	4953	4605
$t_{topsheet}$[mm]	1.829	1.846
$\rho_{topsheet}[kg/m^3]$	1423	1382

be achieved by adapting the thickness as well as the microscopic properties of the foam layers to the specific application. The difference in SPL between the starting properties and the optimized properties is naturally very dependent on how well the starting point is chosen in terms of acoustic properties. In this specific case study, the improvement of SPL varied between 2 and 6 dB. Figure 10 shows the initial and final frequency response function (FRF) for configuration 1 which showed the largest improvement. As can be seen, the improvement is mainly in the higher frequency domain, which was the case for all four configurations. Some improvement may however be achieved also at lower frequencies. Generally speaking, it appears that low frequency acoustic performance seems to be ensured by fulfilment of the applied structural constraints, effectively limiting the low frequency panel displacement

amplitude as well as controlling the fundamental eigenmode of the whole panel. For some configurations, the resulting acoustic foam parameters seem to tend toward very low stiffness, low resistivity and low density, similar to the properties that may be found for fibrous wools, possibly having large diameter fibres or perforations. This is an interesting result pointing to the need for a generalization of the acoustic scaling laws applied in the present work, allowing for a wider design space to be introduced.

	Configuration			
	1	2	3	4
	PU-pi-air	PU-PU-air	PU-pi	PU-PU
Acoustic Layer 1				
ρ_1^* [kg/m^3]	36.34	13.51	6.801	5.009
E_1^* [MPa]	0.173	21.2e-3	4.38e-3	2.02e-3
ϕ_1	0.968	0.989	0.995	0.997
σ_1^{static} [kg/m^3/s]	4.766e3	582.4	142.0	76.26
t_1 [mm]	72.9	1.00	1.00	4.08
Acoustic Layer 2				
ρ_2^* [kg/m^3]	5.286	138.0	1.964	27.90
E_2^* [MPa]	0.306	2.62	10.47e-3	99.91e-3
ϕ_2	0.997	0.876	0.999	0.976
σ_2^{static} [kg/m^3/s]	4.103e5	1.109e5	5.228e4	2.685e3
t_2	1.00	72.9	73.8	70.7

Table 5: Final values of acoustic design variables.

Studying the two configurations containing only PU foam, it is apparent that different foam properties in the first and second foam layer is advantageous compared to a thicker homogeneous layer, this was expected as changes in impedance generally are considered beneficial from an acoustic point of view. In general the acoustic layer next to the CF top sheet became softer than the second layer for all configurations. Note however that, according to the optimized configurations, to merely maximize the apparent impedance step is not the best solution. Instead there would appear to be a kind of optimal balance between different material properties, such as Young's modulus, density, flow resistivity, thickness and also impedance.

Observing configuration 3 and configuration 4, it can be seen that even though the structural properties are identical, the final acoustic foam prop-

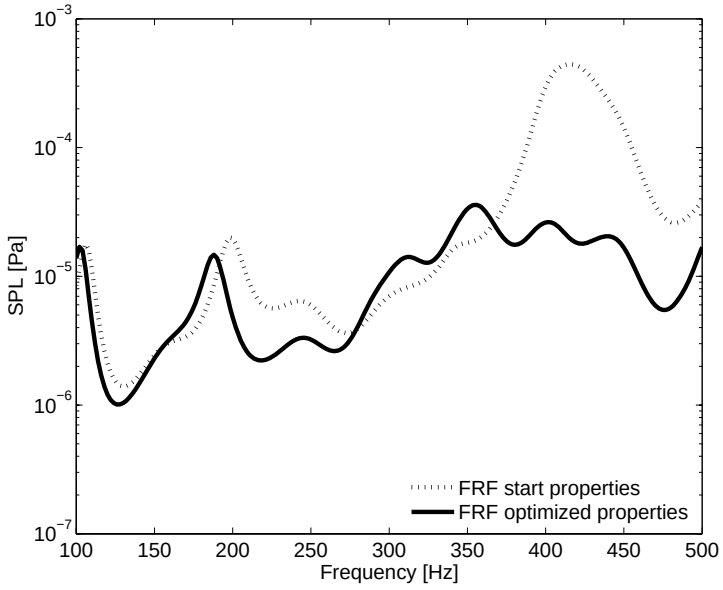

Figure 10: Frequency response function for the starting properties and optimized properties of configuration 1.

erties as well as the FRF, as shown in figure 11, and the total SPL, as shown in table 6, differs significantly. Therefore adjusting the microscopic foam properties, layer properties and stacking sequence to the specific application may give a significant improvement in acoustic performance. Another clear characteristic of the frequency response functions in figure 11 is that all systems appear to be quite damped, especially at the higher frequencies. This is a good result as a primary objective of the multifunctional concept is to make further damping materials redundant.

	Configuration			
Value	1	2	3	4
Total Thickness [mm]	77.4	77.4	77.3	77.3
Total Mass [kg]	18.2	31.6	14.0	17.1
SPL [dB]	70.5	68.7	74.3	71.6

Table 6: Results of optimization

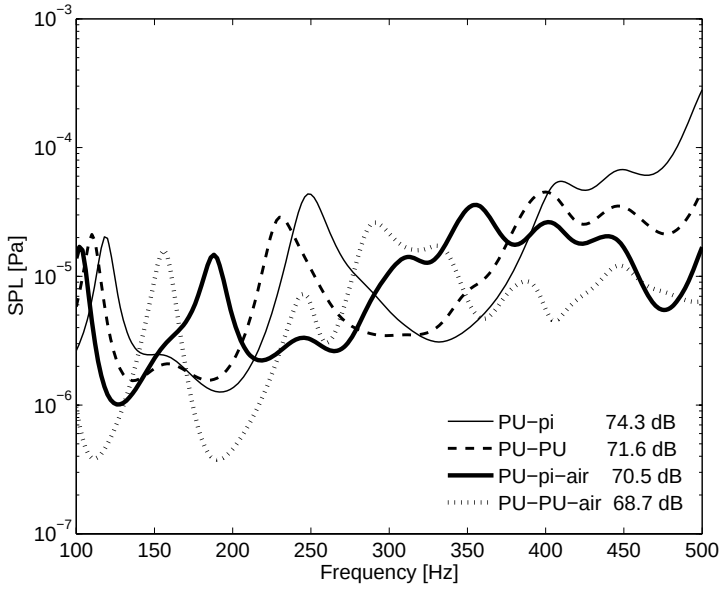

Figure 11: Frequency response function of acoustically optimized configurations.

Studying the frequency response functions of the optimal solution of the four different configurations shows the need to study the entire frequency spectra in question. Despite the fact that all four panels are designed to fulfil identical structural constraints, their dynamic response differs considerably. Should the optimization focus on an extremely limited frequency range, the algorithm may try to improve the objective function by merely pushing a peak response outside of the frequency band of choice. This peak however, can still give a significant contribution to the total SPL. This same reasoning also applies to the frequency resolution of the problem being studied. If steps between excitation frequencies are too large, the algorithm may make changes to move high magnitude responses into to the gaps in excitation, and thus removing the problem from the objective function and the numerical calculations, but not from reality.

Within the results, it is obvious that there do exist general differences between the air gap and non air gap configurations, despite the fact that they are both developed to withstand identical load cases and fulfil the same constraints. This is of course directly coupled to the geometry of the foam cores, which the authors assert is dictated by the presence or absence of the

air gap. For the configurations studied, the results would suggest that the air gap does have a positive influence on sound pressure level in general, however this comes at the cost of a mass penalty, as shown in table 6. Here it can be further emphasised that the often used practice of introducing an air gap into an acoustic treatment, especially an acoustically treated structure, and comparing the result with the original configuration is somewhat misguided. The air gap not only introduces changes in impedance and discontinuities in vibration transfer paths, it also fundamentally changes the nature of the structure in question. Should two layered structures be compared, they should be equivalent. Optimizing a structure for a certain set of loading conditions, and then changing the structure to function with another, effectively renders the optimization process void. One could argue that to achieve an optimal non-gap configuration the topology achieved using the conventional BESO scheme would be sufficient (i.e. removing elements only), and that the second part of the optimization could be carried out with a new mesh accounting for the coupling. Certainly this could be done, however the authors firmly assert that this configuration is not the most optimal for such a panel. While no topology optimization scheme can guarantee that the most optimal solution for the system has been achieved, the authors nevertheless feel that the methods presented here provide a sufficiently robust solution worthy of further study.

As the objective of this work is to present a possible method for combined structural acoustic optimization, parts of the model, load cases and boundary conditions have obviously been idealised. To apply this method in an actual design scenario, a better understanding of the specifics of the problem would be necessary and a certain degree of model refinement required. To do otherwise would be to optimize a solution for a different problem than it was meant to solve.

Regarding the aspects of acoustic comfort, the objective function should reflect the properties sought after. Here, only unweighted SPL has been calculated. There exist a multitude of other metrics which might be appropriate to study. In the field of acoustics this represents an entire sub-topic of research in itself as not only SPL but also attributes like harshness and tonality affect the perception of sound. These phenomena are often addressed in psycho-acoustics and are beyond the scope of the present work. It is however obvious that the choice of objective function will greatly influence the result of the optimization and the properties thus achieved.

7. Conclusions

The design methodology developed herein shows the potential for simplifying the passenger compartment system complexity by examining multiple functional requirements and attempting to achieve them simultaneously in a systematic manner. The proposed multifunctional panel, while not directly comparable to any given automobile car body due to simplifications in geometry, shows a clear potential for mass reduction. A sandwich panel with a core topology tailored to fulfil a multitude of functional load cases can replace numerous conventional components. Combining this topology with an acoustic treatment and optimizing the structural and acoustic performance simultaneously makes certain that the intrinsic coupling and conflicts between the two physical mechanisms are addressed.

Standard topology optimization tools have been adapted to deal with the load cases and materials in question, and with particular focus placed on an air gap in the acoustic treatment for increased acoustic functionality. The effect of such a gap, on both the structure and its acoustic response, was examined and discussed at length. Material properties and layer thicknesses in both the structural and acoustic layers were implemented in the iterative optimization process to achieve maximum possible structural weight savings and acoustic performance simultaneously. The proposed method offers a new approach to systematically deal with the combined structural and acoustic problems encountered in modern vehicle design.

References

[1] P. Göransson, Aerospace Science and Technology 12 (2008) 26–41.

[2] A. Cummings, H. Rice, R. Wilson, J. Sound Vib. 1 (1999) 143–167.

[3] C. J. Cameron, E. Lind, P. Wennhage, P. Göransson, Int. J. Vehicle Structures & Systems (2009) 1–13.

[4] Y. Xie, G. Steven, Computers and Structures 49 (1993) 885–896.

[5] Y. Xie, G. Steven, Computers and Structures 58 (1996) 1067–1073.

[6] D. N. Chu, Y. Xie, A. Hira, G.P.Steven, Finite Elements in Analysis and Design 21 (1996) 239–251.

[7] O. Querin, G. Steven, Y. Xie, Engineering Computations (Swansea, Wales) 15 (1998) 1031–1048.

[8] J. Rong, Y. Xie, X. Yang, Q. Liang, J. Sound Vib. 234 (2000) 177–189.

[9] K. Proos, G. Steven, O. Querin, Y. Xie, AIAA Journal 39 (2001) 2006–2012.

[10] X. Huang, Y. Xie, Structural and Multidisciplinary Optimization 35 (2008) 89–92.

[11] D.Manickarajah, Y. Xie, G. Steven, Finite Elements in Analysis and Design 29 (1998) 205–230.

[12] D.Manickarajah, Y. Xie, G. Steven, Computers and Structures 75 (2000) 45–54.

[13] C. J. Cameron, E. Lind, P. Wennhage, P. Göransson, in: Proceedings of ICCM-17, 17th International Conference on Composite Materials, Edinburgh, Scotland,July 2009.

[14] C. Chamis, SAMPE Quarterly (1984) 41–55.

[15] L. J. Gibson, M. F. Ashby, Cellular Solids: Structure and Properties-Second edition, Cambridge University Press, 1997.

[16] A. Ihle, T. Ernst, H. Baier, L. Datashvili, J. Hoffmann, P. Göransson, D. Fasold, P. Portela, M. Santos, J. Santiago-Prowald, in: 11th European Conference on Spacecraft Structures, Materials and Mechanical testing. Toulouse September 15-17.

[17] C. J. Cameron, P. Wennhage, P. Göransson, S. Rhamqvist, Journal of Sandwich Structures and Materials 12 (2010) 684–708.

[18] K. Svanberg, International Journal for Numerical Methods in Engineering 24 (1987) 359–373.

[19] K. Svanberg, SIAM J. OPTIM. 12 (2002) 555–573.

[20] M.A.Biot, J. Acoust. Soc. Am. 28 (1956) 168–178.

[21] M.A.Biot, J. Acoust. Soc. Am. 28 (1956) 179–191.

[22] M.A.Biot, J. Appl. Phys 27 (1956) 459–467.

[23] N. E. Hörlin, M. Nordström, P. Göransson, J. Sound Vib. 254 (2001) 633–652.

[24] N. E. Hörlin, J. Sound Vib. 285 (2005) 341–363.

[25] W. E. Warren, A. M. Kraynik, J. Appl. Mech. 55 (1988) 341–346.

[26] W. E. Warren, A. M. Kraynik, J. Appl. Mech. 64 (1997) 787–794.

[27] J. F. Allard, Y. Champoux, J. Acoust. Soc. Am. 6 (1992) 3346–3353.

[28] J. Comiti, M. Renaud, Chemical Engineering Science 44 (1989) 1539 – 1545.

[29] P. Göransson, Phil. Trans. R. Soc. A 364 (2006) 89–108.

[30] E. Lind-Nordgren, P. Göransson, J. Sound Vib. 329 (2010) 753–767.

Alignment of anisotropic poro-elastic layers – Sensitivity in vibroacoustic response due to angular orientation of anisotropic elastic and acoustic properties

Eleonora Lind Nordgren[a] and Peter Göransson[b]
Centre for ECO²VehicleDesign, MWL, KTH, 10044Stockholm

Jean-François Deü[c]
Laboratoire de Mécanique des Structures et des Systèmes Couplés (LMSSC), CNAM, Paris

(Dated: August 6, 2012)

Modeling of acoustic porous materials has traditionally assumed open cell structures with isotropic elastic and acoustic properties although all cellular materials are to some extent anisotropic. This has been viewed as an acceptable level of simplification, as in some cases isotropic models give a quite satisfactory correlation between experimental and computed results. However, in other situations the differences are significant, raising questions related to the influence of anisotropy on the acoustic behavior of porous materials, as these are not yet fully understood. In an effort to investigate the effects of anisotropy in the material properties, this paper explores the influence of angular changes of two anisotropic open cell porous materials on their acoustic responses when assembled in multilayered panels. Numerical simulations of two hypothetical multilayered acoustic panels are performed and their acoustic response, as a function of angular changes of anisotropic material properties, is evaluated using gradient based optimization techniques to find and compare possible extremes in acoustic behavior. The results show that anisotropy of the porous material properties as well as their angular orientations both have significant influence on the acoustic response of the panels. This discloses new possibilities to improve already existing acoustic panel without adding extra weight or volume. The results also highlight the importance of further advancing the knowledge of anisotropic porous material behavior.

PACS numbers:

I. INTRODUCTION

Introducing porous materials as elasto-acoustic dissipative components in multilayered structures is a well established way of handling noise and vibration problems. Their low weight combined with their multi-functional character make them quite attractive in a wide range of demanding applications, such as automotive, aerospace, railway, etc. With the increasing interest in reducing the vehicle body weight in order to lower the environmental impact of transportation there is a growing need to model such materials with a high degree of fidelity. In many applications of porous materials, the assumption of isotropic properties yields satisfactory correlations between experimental and computed results. This is particularly true in cases where airborne sound absorption is of interest. However, in situations where the structure-borne properties are important, the sources of differences between predicted and measured results are not fully understood. Biot generalized the theory of porous material to anisotropic modeling[8], opening up for a new research front in the acoustics of poro-elastic materials. Apart from being an interesting subject in itself, this has recently raised questions related to the possible influence of the potentially anisotropic character of poro-elastic materials, including the potential for tailoring of such properties, should they be known in sufficient detail. Both these are within the scope of the present work, aiming at exploring whether the possible anisotropy of the constitutive properties may be important enough to influence the performance, thus possibly explaining the above mentioned discrepancies, to a significant extent. To provide necessary and meaningful data, as well as application cases appropriate for simulations, for such an investigation, material models of anisotropic poro-elastic materials together with proper simulation tools are required. Both these topics are at the front of the research for the acoustics of poro-elastic materials, as an example is the characterization of the acoustic parameters still an issue where more research is needed[16] as complete determination of the acoustic parameters of anisotropic foam requires both time, experience and development of new advanced measurement and estimation techniques[24,13,11,9]. In addition, simulation models allowing for parametric studies are necessary in order to assess the influence of anisotropy on the vibro-acoustic behavior of structures comprising porous materials[18,15,12].

The objective of the present work is to study the performance sensitivity of two different materials, having two different types of material symmetries as well as differing in elastic and acoustic properties, in a numerical experiment. The focus is on the influence of anisotropicity in general, and on the effects of aligning two layers of the same material relative to each other in particu-

[a] E-mail: eleonora@kth.se
[b] E-mail: pege@kth.se
[c] E-mail: jean-francois.deu@cnam.fr

lar. The simulation set up is composed of two layers of porous material in contact with an aluminum plate along one surface and separated from an identical plate through an air gap along the opposite. This particular set up has been chosen in order to stress the influence of both elastic and acoustic properties on the response behavior[10,12]. The sensitivity is analyzed through the solution of an optimization problem using previously published techniques[20]. Clearly there is a need to set an appropriate level of complexity of the anisotropic material models used in this preliminary investigation. While a completely general material model would imply that the elastic, the acoustic, the anelastic and the visco-acoustic material tensors all have their own material coordinate system, it is here assumed for simplicity and transparency that all properties are given in the same reference coordinate system. The relative alignment of the materials is then constructed as rotations of the reference systems, with respect to the body coordinate axes of the two layers.

II. GOVERNING EQUATIONS

A poro-elastic medium consists of an elastic solid containing an interconnected network of pores filled with a viscous fluid. Both the solid and the fluid in the pores are usually considered to be continuous. The porous material is modeled as a homogeneous equivalent solid and a homogeneous equivalent fluid acting and interacting in the same space.

Starting from the early models by Biot[4,5,6] and Biot and Willis[7] the method of modeling foam materials have been developed by e.g. Johnson *et al.*[17], Allard[1], Allard and Champoux[2] and Pride *et al.*[22]

Biot extended the isotropic theory of porous material to allow for anisotropic modeling[8] and there is a general awareness that anisotropy may have a significant influence on the acoustic behavior of porous materials[18]. It is also well established that the many parameters used to characterized materials in the Biot-Johnsson-Champoux-Allard model differ in different direction in anisotropic materials[24,13,11]. However, the acoustic parameters, such as static viscous permeability and viscous characteristic length, in different directions of an almost transversely isotropic foam does not necessarily line up with the main directions visible in the geometrical sense[21].

The mixed anisotropic displacement pressure formulation underpinning the current work, has recently been proposed by Horlin and Goransson[15] and is a generalization of the weak statement derived by Atalla *et al.*[3]. It assumes that the material of the solid frame is linearly elastic and isotropic and that the anisotropy of the material is entirely related to the microstructural geometry. A complete description of the model used here is beyond the scope of the present paper, and the interested reader is referred to the work mentioned above. For completeness, a summary of the most important parts will be given.

A. Anisotropic displacement pressure formulation

When summarizing the mixed anisotropic displacement pressure formulation, the notations used is explained throughout the paper except for the following, regarding tensor notation. The component ordinal number in a Cartesian co-ordinate system, e.g. $i = 1, 2, 3$ is noted i, j, k. Partial derivates with respect to x_i is written $(.)_{,i} = \partial(.)/\partial x_i$. Kronecker's delta is δ_{ij}. Also, Cartesian tensor notation with Einstein's summation convention is used, i.e. repeated indices imply a summation of these terms. Based on this, the strong form of the solid frame equation is given as:

$$\begin{aligned} -C_{ijkl}u^s_{k,l} - \phi\left(\delta_{ij} + \frac{Q_{ij}}{R}\right)p \\ -\omega^2\left(\tilde{\rho}^{11}_{ij} - \tilde{\rho}^{12}_{ik}\hat{\rho}^{22}_{kl}\tilde{\rho}^{12}_{lj}\right)u^s_j \\ -\phi\left(\delta_{ij} + \tilde{\rho}^{12}_{ik}\hat{\rho}^{22}_{kj}\right)p_{,j} = 0, \end{aligned} \tag{1}$$

and the strong form of the fluid equation is:

$$\begin{aligned} -\frac{\phi^2}{R}p - \phi\left(\delta_{kl} + \frac{Q_{kl}}{R}\right)u^s_{k,l} - \frac{\phi^2}{\omega^2}\hat{\rho}^{22}_{kj}p_{,kj} \\ +\phi\left(\delta_{jl} + \hat{\rho}^{22}_{kj}\tilde{\rho}^{12}_{kl}\right)u^s_{l,j} = 0 \end{aligned} \tag{2}$$

where C_{ijkl} is the solid frame Hooke's matrix, u^s_i is the solid frame displacement, ω is the angular frequency [rad/s], ϕ is the porosity, i.e. the volume fraction of open pore fluid content and p is the acoustic pore pressure and

$$R = \frac{\phi^2 K_s}{1 - \phi - K_s C_{ijkl} d_{ij} d_{kl} + \phi K_s / K_f} \tag{3}$$

$$Q_{ij} = \frac{\left[(1-\phi) - C_{ijkl}d_{kl}\right]\phi K_s}{1 - \phi - K_s C_{ijkl} d_{ij} d_{kl} + \phi K_s / K_f} \tag{4}$$

where K_s is the unjacketed frame bulk modulus, d_{ij} is the unjacketed compressibility compliance tensor.

As the fluid itself is assumed to be isotropic, R is a scalar quantity, K_f is obtained using the model by Lafarge *et al.*[19]. The dilatational coupling Q_{ij} is however a second order tensor due to the assumed elastic anisotropy.

The equivalent density tensors, $\tilde{\rho}^{11}_{ij}$, $\tilde{\rho}^{12}_{ij}$ and $\tilde{\rho}^{22}_{ij}$, as well as the tortuosity tensor, α_{ij}, are anisotropic generalizations of those used by Allard[1] and may be defined as

$$\tilde{\rho}^{11}_{ij} = \rho_1\delta_{ij} + \rho^a_{ij} - \frac{\mathrm{i}}{\omega}b_{ij} \tag{5}$$

$$\tilde{\rho}^{12}_{ij} = -\rho^a_{ij} - \frac{\mathrm{i}}{\omega}b_{ij} \tag{6}$$

$$\tilde{\rho}_{ij}^{22} = \phi\rho_0\delta_{ij} + \rho_{ij}^a - \frac{\mathrm{i}}{\omega}b_{ij} \tag{7}$$

$$\rho_{ij}^a = (\alpha_{ij} - \delta_{ij})\,\phi\rho_0 \tag{8}$$

with ρ_0 as the ambient fluid density, ρ_1 as the bulk density of the porous material and α as the tortuosity tensor.

$$\hat{\rho}_{ik}^{22}\tilde{\rho}_{kj}^{22} = \delta_{ij} \tag{9}$$

i.e. $\hat{\rho}_{ik}^{22}$ is the inverse of $\tilde{\rho}_{kj}^{22}$, assuming that the viscous drag tensor, b_{ij}, is invertible[27,11].

III. ANISOTROPIC FOAM MODELS USED

For the sensitivity study discussed here two different porous materials, one fibrous and one cellular, were chosen. These two types of materials are built differently and thus in general could be assumed to have different material symmetries for the three directionally dependent tensors studied here, b_{ij}, α_{ij} and C_{ijkl}. It is primarily for this reason that two materials are investigated, but they also differ in the sense that the properties of fibrous materials are available in the literature while material data for porous foams are as yet subject to intensive research in terms of their anisotropic properties. Thus for the fibrous material the material parameters are taken from previously characterized materials[23], while for the foam the material parameters are hypothetical, although according to the authors' previous experience, reasonable compared to known isotropic and partially known orthotropic and transversely isotropic materials.

In addition, the structural damping related to the solid frame of the porous material is here assumed to be zero for both types of porous materials. The reason for this choice is that the modeling of the damping of anisotropic materials is still an open issue, especially when it comes to the directivity of the dissipation mechanisms[12]. Therefore, to avoid confusion due to an assumed damping model the damping was omitted. Another simplification introduced, without diminishing the value of these preliminary results, is that the viscous characteristic length is assumed to be isotropic although it is, in reality, an anisotropic property. As mentioned before, the knowledge and understanding of anisotropic porous material properties are still limited and often incomplete; therefore simplifications of the description of the materials were felt to be necessary and justified at this stage. On the other hand, should the sensitivities identified with the present model assumptions turn out to be high, this would certainly then add to the future interest for complete and accurate porous material modeling research.

The direction independent material parameters used are presented in Table I.

The assumption made that some of the possibly directionally dependent parameters are taken to be isotropic

Material parameter	Orthotropic foam	Fibrous material
Frame bulk density [kg/m^3]	22.1	14.45
Frame loss factor	0.0	0.0
Porosity	0.980	0.994
Fluid density [kg/m^3]	1.204	1.204
Fluid dynamic visc. [Ns/m^2]	$1.84{\cdot}10^{-5}$	$1.84{\cdot}10^{-5}$
Fluid ratio spec. heats	1.4	1.4
Prandtl number	0.71	0.71
Visc. char. length [m]	$1.1{\cdot}10^{-4}$	$6.25{\cdot}10^{-5}$
Therm. char. length [m]	$7.4{\cdot}10^{-4}$	$12.5{\cdot}10^{-5}$
Therm. form factor	0.25	0.25
Gas constant (air) [m^2/s^{2}K]	286.7	286.7
Absolute temperature [K]	293.15	293.15

Table I. Parameters used in the foam models.

gives the following expression for the viscous drag tensor b_{ij}

$$b_{ij} = \phi^2\sigma_{ij}B_{ij}\,(\omega) \tag{10}$$

where

$$B_{ij} = \sqrt{1 - i\omega\frac{4\eta\rho_0^2\alpha_{ij}^2}{\phi^2\sigma_{ij}^2\Lambda^2}} \tag{11}$$

with σ_{ij} as the static flow resistivity, η as the ambient fluid viscosity, Λ as the viscous characteristic length and no summation over ij in the right hand side is intended.

A. Elastic moduli

In the following tensor and matrix notations will be used interchangeably for presentation of the different directional dependent properties, in particular when numerical values are given the matrix notation is preferred over the tensor notation.

For the elastic properties, both in terms of the magnitude of the elastic moduli as well as the material symmetry itself, fibrous wool and cellular solid materials are quite different. While the fibrous wool is well represented by a transversely isotropic model, having five independent elastic moduli, the hypothetical foam model used here is orthotropic, i.e. it has nine independent elastic moduli. They are here given in the body coordinate (reference system) as Eqs. (12) for the orthotropic foam and (13) for the fibrous material.

$$\mathbf{C}^{\mathrm{foam}} = \begin{bmatrix} 40 & 33 & 37 & 0 & 0 & 0 \\ & 89 & 131 & 0 & 0 & 0 \\ & & 300 & 0 & 0 & 0 \\ & \mathit{symm.} & & 26 & 0 & 0 \\ & & & & 21 & 0 \\ & & & & & 26 \end{bmatrix} \cdot 10^3\ [\mathrm{Pa}] \tag{12}$$

$$\mathbf{C}^{\text{fibrous}} = \begin{bmatrix} 17.2 & 0 & 0 & 0 & 0 & 0 \\ & 17.2 & 0 & 0 & 0 & 0 \\ & & 1.025 & 0 & 0 & 0 \\ & \textit{symm.} & & 1.6 & 0 & 0 \\ & & & & 1.6 & 0 \\ & & & & & 13.7 \end{bmatrix} \cdot 10^3 \text{ [Pa]} \tag{13}$$

B. Flow resistivity and tortuosity

For the flow resistivity tensor, both types of materials are taken as transversely isotropic and are given by Eqs. (14) for the orthotropic foam and (15) for the fibrous material.

$$\sigma^{\text{foam}} = \begin{bmatrix} 37500 & 0 & 0 \\ 0 & 37500 & 0 \\ 0 & 0 & 55000 \end{bmatrix} \text{ [Pa s/m}^2\text{]} \tag{14}$$

$$\sigma^{\text{fibrous}} = \begin{bmatrix} 21000 & 0 & 0 \\ 0 & 21000 & 0 \\ 0 & 0 & 41000 \end{bmatrix} \text{ [Pa s/m}^2\text{]} \tag{15}$$

From these tensors another reason for choosing to include two materials is evident, as for the fibrous material the ratio between visco-acoustic and elastic properties is quite different compared to the more rigid foam giving rise to quite different interactions between the elastic and the acoustic fields in the materials.

Concluding the listing of the directional dependent material properties, for the foam, the tortuosity was assumed to be orthotropic, Eq. (16), while for the fibrous wool it was assumed to be isotropic, Eq. (17).

$$\alpha^{\text{foam}} = \begin{bmatrix} 1.5 & 0 & 0 \\ 0 & 1.0 & 0 \\ 0 & 0 & 2.0 \end{bmatrix} \tag{16}$$

$$\alpha^{\text{fibrous}} = \begin{bmatrix} 1.12 & 0 & 0 \\ 0 & 1.12 & 0 \\ 0 & 0 & 1.12 \end{bmatrix} \tag{17}$$

Note that the principal directions of the static flow resistivity tensors, σ, and the tortuosity, α, are assumed to line up with the principal directions of the solid frame Hooke's matrix, $\mathbf{C}$. This is, however, not necessarily the case for all porous materials[21], the consequences of which would be a natural next step to investigate in the current work.

C. Tensor transformation matrices

In this paper the anisotropic flow resistivity, the anisotropic tortuosity and the anisotropic elastic properties are the three parameters used to describe the anisotropy of the two porous materials, and therefore the only ones that may influence the acoustic properties with angular changes. It is assumed that the material properties may be transformed through a pure rotation around a fixed coordinate system. For the rotation of the second order tensors, i.e. flow resistivity and tortuosity, the following symmetric transformation is used,

$$\mathbf{A} = \begin{bmatrix} a_{11} & a_{12} & a_{13} \\ a_{21} & a_{22} & a_{23} \\ a_{31} & a_{32} & a_{33} \end{bmatrix} \tag{18}$$

with transformations of the type

$$\langle . \rangle^{\text{rot}} = \mathbf{A}^T \langle . \rangle \mathbf{A} \tag{19}$$

applied for $\tilde{\rho}_{ij}^{11}, \tilde{\rho}_{ij}^{22}, \tilde{\rho}_{ij}^{12}$ in Eqs. (5) to (8). In Eq. (18), the two first columns are given through two orthonormal vectors, defining the x^{rot}-y^{rot} plane of the new coordinate system, and the third column is computed as the cross product of these to form the new x^{rot}-y^{rot}-z^{rot} 's coordinate system in which the material properties are computed for a given rotation of the material. Please note that the new x^{rot}-y^{rot}-z^{rot}-coordinate system may be different for the two porous layers in each configuration, as schematically shown in Fig. 3.

Similarly for the fourth order elasticity tensor the following transformation is used

$$\mathbf{T} = \begin{bmatrix} \mathbf{T_{11}} & \mathbf{T_{12}} \\ \mathbf{T_{21}} & \mathbf{T_{22}} \end{bmatrix} \tag{20}$$

where

$$\mathbf{T_{11}} = \begin{bmatrix} a_{11}^2 & a_{12}^2 & a_{13}^2 \\ a_{21}^2 & a_{22}^2 & a_{23}^2 \\ a_{31}^2 & a_{32}^2 & a_{33}^2 \end{bmatrix} \tag{21}$$

$$\mathbf{T_{21}} = \begin{bmatrix} a_{21}a_{31} & a_{22}a_{32} & a_{23}a_{33} \\ a_{11}a_{31} & a_{12}a_{32} & a_{13}a_{33} \\ a_{11}a_{21} & a_{12}a_{22} & a_{13}a_{23} \end{bmatrix} \tag{22}$$

$$\mathbf{T_{12}} = \begin{bmatrix} 2a_{12}a_{13} & 2a_{11}a_{13} & 2a_{11}a_{12} \\ 2a_{22}a_{23} & 2a_{21}a_{23} & 2a_{21}a_{22} \\ 2a_{32}a_{33} & 2a_{31}a_{33} & 2a_{31}a_{32} \end{bmatrix} \tag{23}$$

$$\mathbf{T_{22}} = \begin{bmatrix} a_{22}a_{33} + a_{23}a_{32} & a_{21}a_{33} + a_{23}a_{31} & a_{21}a_{32} + a_{22}a_{31} \\ a_{12}a_{33} + a_{13}a_{32} & a_{11}a_{33} + a_{13}a_{31} & a_{11}a_{32} + a_{12}a_{31} \\ a_{12}a_{23} + a_{13}a_{22} & a_{11}a_{23} + a_{13}a_{21} & a_{11}a_{22} + a_{12}a_{21} \end{bmatrix} \tag{24}$$

where the a_{ij} are given by Eq. (18) and the corresponding transformations being of the type

$$\mathbf{C}^{\text{rot}} = \mathbf{T}^T \mathbf{C} \mathbf{T} \tag{25}$$

IV. OPTIMIZATION PROBLEM TO SOLVE

The basis for the proposed sensitivity analysis approach is to compute maxima and minima of a cost function representing the acoustic response. The acoustic response is calculated using an appropriate simulation model, discussed below, in which the unknown rotations of the constitutive parameters may be varied such that a minimum or a maximum of the acoustic response is found. In the following, the objective function and the constraint functions of the optimization problem are defined.

The cost function was constructed as the acoustic response in a cavity, inherently a function of the different material angles, given by the sound pressure level evaluated in a sub volume of the air cavity connected to the panel. The sound pressure square, p_f^2, for each evaluated frequency, f, is calculated as the average of the square sound pressure in a number, N, of discrete points in the chosen sub volume, Eq. (27). This quantity was then multiplied with the frequency resolution, Δf_f, and summed over the entire frequency range, Eq. (26), resulting in a total sound pressure level, SPL, which is then subject to minimization or maximization.

$$\begin{aligned}\langle SPL(\alpha_1, \beta_1, \gamma_1, \alpha_2, \beta_2, \gamma_2)\rangle_{\Omega_{\text{sub}}} = \\ = 10\log\left(\sum_{f=f_1}^{f_{\max}} \left(p_f^2 \Delta f_f\right)/p_0^2\right)\end{aligned} \tag{26}$$

where

$$p_f^2 = \frac{1}{N}\sum_{n=1}^{N} p_{f_n}^2 \tag{27}$$

and in order to limit the amount of different possible angle combination, without actually limit the possible angular adaptation of the porous layers, the following constraints were used for the design variables

$$\begin{bmatrix} -\pi/2 - 0.01 \\ -\pi/2 - 0.01 \\ -\pi/2 - 0.01 \end{bmatrix} \leq \begin{bmatrix} \alpha_i \\ \beta_i \\ \gamma_i \end{bmatrix} \leq \begin{bmatrix} \pi/2 + 0.01 \\ \pi/2 + 0.01 \\ \pi/2 + 0.01 \end{bmatrix} \tag{28}$$

where α_i, β_i and γ_i, $i = 1, 2$ are the right hand rotations around the z- y- and x-axis respectively. Note that for algorithmically related reasons, i.e. the asymptotic behavior of the optimizer close to the constraint boundaries, the angle limits are slightly increased by a suitable offset. The optimization problem was solved using the GCMMA optimizer by Svanberg[25,26]. As this is a gradient based algorithm, the required gradients were calculated using finite differencing.

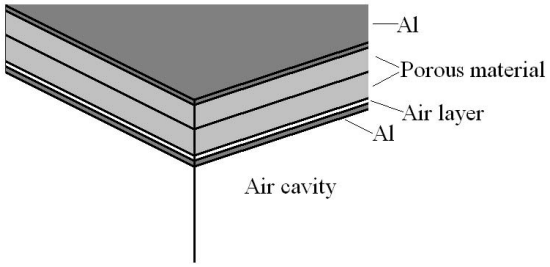

Figure 1. Layer configuration of the tested panels.

V. SIMULATION MODEL FOR ANISOTROPIC POROUS MATERIALS IN A MULTILAYERED CONFIGURATION

To give a first answer to the question whether the acoustic response of multilayered panels containing anisotropic porous materials may be sensitive to angular changes of material properties or relative angular changes between the two dissipative layers, a numerical model was used to examine the acoustic response of a quadratic panel with aluminum face sheets and two layers of poro-elastic material, elastically bonded to the face sheet where the excitation was applied and separated by a thin air gap from the other aluminum face sheet, see Fig. 1.

The panel was 0.5 x 0.5 m and excited by a unit force in the z-direction over one element, see Fig. 2. The model had homogeneous natural boundary conditions along $x = 0$, $x = L_x$, $y = 0$ and $y = L_y$. The air cavity, in which the acoustic response in Eq. (26) was calculated, was 1.4 m in the z-direction and the subvolume had the dimensions 0.3 x 0.3 x 0.3 m and placed in the middle of the air cavity in the x- and y-direction and 0.2 m from the inner surface of the multilayered panel. To reduce the influence of standing waves phenomena, the inner walls of the air cavity at $x = 0$, $y = 0$ and $z = L_z$ were assigned a non-frequency-dependent normal surface impedance of 257+563i which implies an absorption factor of about 55 percent. The boundaries of the air cavity at $x = L_x$ and $y = L_y$ were considered to be acoustically hard.

It should be noted that the simulation model and the exciting force are academic examples, chosen quite arbitrarily, thus rendering the absolute sound pressure in the air cavity of no particular significance. For this reason, in the discussion of the results from the optimization, merely the differences in sound pressure level between different angular changes of the sound absorbing material will be of interest.

Two different configurations were considered: one using an orthotropic foam, configuration A, and one containing a fibrous material, configuration B, which was transversely isotropic, see Table II. As mentioned previously, there were two layers of porous material in each

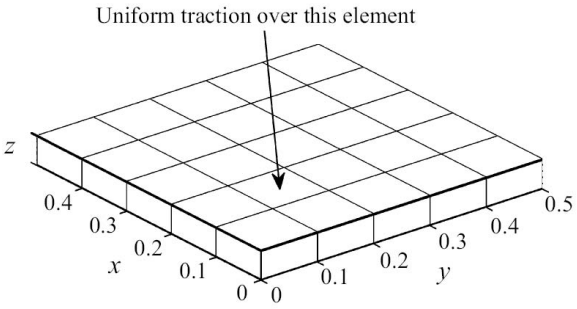

Figure 2. Schematic view of the model used.

Config.	Material	Thickness
A	Aluminum face sheet	0.001 m
	Orthotropic foam	0.042 m
	Orthotropic foam	0.042 m
	Air layer	0.001 m
	Aluminum face sheet	0.001 m
B	Aluminum face sheet	0.001 m
	Fibrous material	0.042 m
	Fibrous material	0.042 m
	Air layer	0.001 m
	Aluminum face sheet	0.001 m

Table II. Configurations studied.

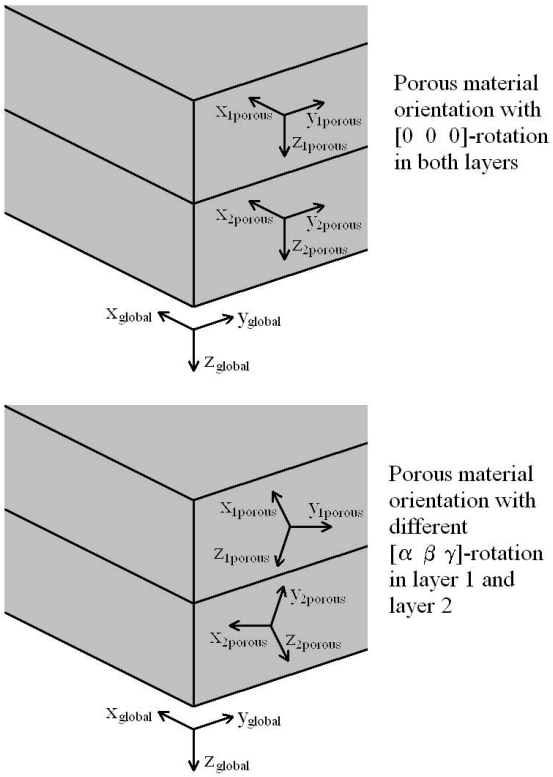

Figure 3. Global and local co-ordinate axes and example of possible layer rotations of porous layer 1 and 2.

panel. For each configuration A and B respectively, though, both layers are of the same material type. The only variations introduced were, the relative orientation of the material properties, which could rotate independently in different directions and thereby possibly achieving different overall dynamic properties considering the direction of excitation, see Fig. 3.

The system was solved using a finite element numerical model with hierarchical polynomials of order ranging from 2 to 5[14]. This was performed for frequency spectra between 100 – 700 Hz with a frequency resolution of 5 Hz.

A. Optimizing the Euler angles

To evaluate the influence of angular changes in anisotropic porous layers the formulated optimization problem were able to rotate the anisotropic material properties of the porous layers by using Euler angles with Z-Y-X fixed axis rotation. Rotating the unit vectors $\mathbf{e}_z$, $\mathbf{e}_y$ and $\mathbf{e}_x$ as

$$\mathbf{e}^{\mathrm{rot}} = \mathbf{R}\mathbf{e} \tag{29}$$

where

$$\mathbf{R} = \mathbf{R}_x(\gamma)\mathbf{R}_y(\beta)\mathbf{R}_z(\alpha) \tag{30}$$

and

$$\mathbf{R}_z = \begin{bmatrix} \cos\alpha & -\sin\alpha & 0 \\ \sin\alpha & \cos\alpha & 0 \\ 0 & 0 & 1 \end{bmatrix} \tag{31}$$

$$\mathbf{R}_y = \begin{bmatrix} \cos\beta & 0 & \sin\beta \\ 0 & 1 & 0 \\ -\sin\beta & 0 & \cos\beta \end{bmatrix} \tag{32}$$

$$\mathbf{R}_x = \begin{bmatrix} 1 & 0 & 0 \\ 0 & \cos\gamma & -\sin\gamma \\ 0 & \sin\gamma & \cos\gamma \end{bmatrix} \tag{33}$$

For the transversely isotropic materials rotation around the z-axis is redundant and therefore α is kept to zero for that configuration. As the two porous layers could rotate independently of each other six Euler angles for configuration A and four Euler angles for configuration B were needed as design variables and the summed SPL, Eq. (26) was used as the objective function. This objective function was both minimized and maximized in order to estimate the possible difference between a worst case and a best case scenario.

For each material five different starting points for the minimization process were used, see Table III and, based

on the result in those starting points, two different starting points were selected for the maximization. It should, however, be pointed out that this analysis cannot be expected to guarantee that the global minimum or maximum has been found. As the objective of the current work was to investigate the sensitivity associated with the orientation of anisotropic porous materials, it does nevertheless indicate to what degree the problem is convex and in addition provide some useful information about the differences between different minima or maxima both in terms of the chosen objective function but also in the resulting Euler angles. And most importantly, it does provide a first estimation of possible differences in acoustic response that may be caused by angular changes of anisotropic acoustic porous materials.

Starting point	Euler angles starting values Layer 1	Layer 2
1	[0 0 0]	[0 0 0]
2	[0.5 0.5 0.5]	[0.5 0.5 0.5]
3	[-0.5 -0.5 -0.5]	[-0.5 -0.5 -0.5]
4	[0.5 0.5 0.5]	[-0.5 -0.5 -0.5]
5	[-0.5 -0.5 -0.5]	[0.5 0.5 0.5]

Table III. Starting points used in minimizations.

The objective of the present paper is not to find the global minimum or maximum of the stated cost function, but to evaluate the sensitivity to the orientation of anisotropic materials in a general sense. To illustrate the behavior of the cost function, Eq. (26), the value at starting point 1, Table III, was used as a reference against which the minima and maxima found were evaluated. As this cost function result involved no angular changes it was considered to be adequate as a reference case, representing for configuration B, with the fibrous material, the actual way most fibrous materials are manufactured, and in fact used in applications. For the configuration with orthotropic foam, configuration A, the choice of reference case is admittedly of a somewhat more arbitrary nature. Fortunately it does not affect the outcome of the present analysis as the most interesting evaluations are made mainly between the maximization and minimization.

VI. RESULTS AND DISCUSSION

As the present study of the acoustic behavior of anisotropic porous materials is based on a forced response simulation model, there are two aspects of the results that should be pointed out before going through the outcome of the optimizations performed. First, as a non-symmetric, localized excitation was used, see Fig. 2, both the global and the relative orientation of the two layers could be expected to be biased by this and in some sense removing a certain level of generality in the results. However, despite this the relative orientation of the material properties of the two layers should on the other hand provide a more general picture of the sensitivity of response as a function of the orientation. For these reasons the results from the optimization analysis are presented in terms of the actual rotations pertaining to minima and maxima found as well as to the corresponding FRFs. Due to the difficulties of showing 3D rotations in a comprehensible way in printable graphs, several different ways of illustrating the results are given below. However, to get a full insight into the actual alignment between the two reference systems it is necessary to view the results dynamically, something which is beyond the format available for a paper. Thus, the interested reader is encouraged to plot and examine the material property rotations using the results in Table IV and VI together with Eqs. (29) to (33), in order to fully explore the outcome of the present work.

A. Orthotropic foam

An overview of the results for the orthotropic foam, using the five starting points in Table III, are found in Table IV.

Start point	Min/ Max	Euler angles end values Layer 1	Layer 2	Diff. SPL [dB]
		Minimizations		
1	A1	[0.45 0.41 -0.25]	[0.38 0.75 -0.25]	-1.2
2	A2	[0.38 0.40 -0.25]	[0.66 0.81 -0.20]	-1.2
3	A3	[-1.46 0.39 -0.20]	[-0.43 0.49 -0.78]	-1.1
4	A4	[1.40 0.36 -0.21]	[-0.12 0.33 -0.80]	-1.1
5	A5	[0.24 0.38 -0.32]	[0.77 0.72 -0.29]	-1.2
		Maximizations		
5	A6	[-0.45 -1.28 -0.65]	[0.58 1.51 0.56]	+3.4
4	A7	[1.28 1.06 1.58]	[-0.89 -1.56 0.36]	+3.2

Table IV. Results overview for orthotropic foam, configuration A. The table show the difference between the resulting SPL and the SPL for rotation [0 0 0].

1. Comparing different extremal points

From Table IV, it may be seen that a comparison of the minima and the maxima gives a level difference, between the best case and the worst case found, of 4.6 dB. The rotation of material properties compared to the global coordinate system may be found in Fig. 4 through 9, where the x- and y-axes are plotted in both positive and negative direction, as a 180° rotation around the material z-axis would have no influence of the physical material behavior. Looking at the results, it may be seen that minima A1, A2 and A5 all had similar material property rotations in layer 1, Fig. 4, and similar in z-direction but with a small deviation of the rotation of the x-y-plane in layer 2, Fig. 5. Minimum A3 and A4 both had very similar property rotations in layer 1, Fig. 6, and similar although not exactly the same in layer 2, Fig. 7. Comparing the two maxima the rotations were the same in layer 2, with the only difference being that the z-axes were

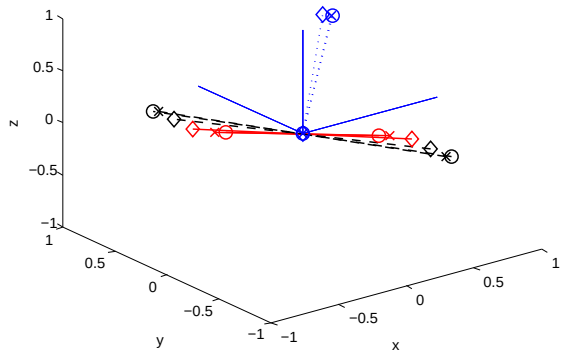

Figure 4. Rotation of material property axes of orthotropic foam in layer 1 for the different minima compared to [0 0 0]-rotation, z-axis=blue dotted, ±y-axis=black dashed, ±x-axis=red solid. A1=◯ A2=× A5=◇.

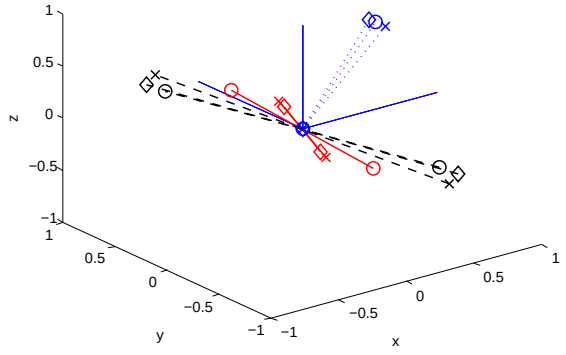

Figure 5. Rotation of material property axes of orthotropic foam in layer 2 for the different minima compared to [0 0 0]-rotation, z-axis=blue dotted, ±y-axis=black dashed, ±x-axis=red solid. A1=◯ A2=× A5=◇.

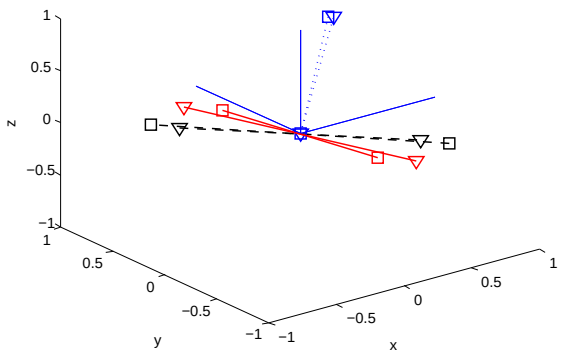

Figure 6. Rotation of material property axes of orthotropic foam in layer 1 for the different minima compared to [0 0 0]-rotation, z-axis=blue dotted, ±y-axis=black dashed, ±x-axis=red solid. A3=▽ A4=□.

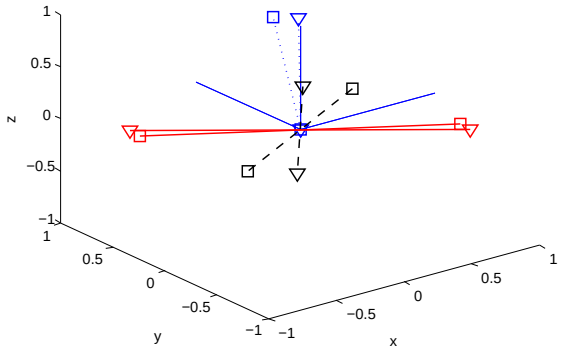

Figure 7. Rotation of material property axes of orthotropic foam in layer 2 for the different minima compared to [0 0 0]-rotation, z-axis=blue dotted, ±y-axis=black dashed, ±x-axis=red solid. A3=▽ A4=□.

pointing in opposite directions, Fig. 9, which does not influence the physical behavior of the orthotropic porous material. This shows that even though there were some constraints put on the design variables the same material angles can be described with different Euler angles and therefore some minima or maxima may actually be closer than they appear when comparing the numerical values of the resulting optimal angles. In addition, the material rotations of layer 1 for the two maxima showed some similarities but were not exactly the same, Fig. 8. An interesting observation is also that for the minima found the z-axis of layer 1 is rotated slightly off the body coordinate z-axis, while for the two maxima the z-axis is rotated almost 90 degrees.

Studying the resulting frequency response functions, FRFs, of the different minima and maxima, Fig. 10, it is quite clear that, although appearing at different material property angles, all minima share important similarities, regarding the frequency response. This observation also holds for the two maxima. Another interesting observation that may be made from the FRFs is that the main improvement in total SPL of the minima compared to the maxima is due to the lower part of the studied frequency range. The two maximization solutions found are clearly above the minimization solutions for frequencies below 250 Hz and at the same time well below for higher frequencies. At the same time all minima found are below the [0 0 0]-rotation response curve, except for frequencies below 150 Hz.

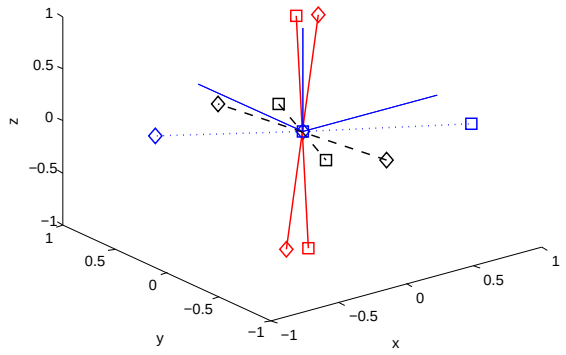

Figure 8. Rotation of material property axes of orthotropic foam in layer 1 for the different maxima compared to [0 0 0]-rotation, z-axis=blue dotted, ±y-axis=black dashed, ±x-axis=red solid. A6=◇ A7=□.

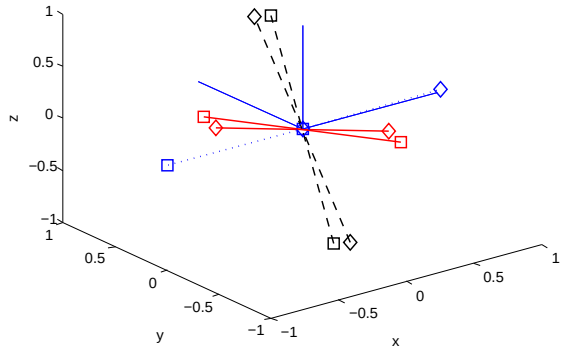

Figure 9. Rotation of material property axes of orthotropic foam in layer 2 for the different maxima compared to [0 0 0]-rotation, z-axis=blue dotted, ±y-axis=black dashed, ±x-axis=red solid. A6=◇ A7=□.

2. *Layer orientation within the different extremal points*

To further illustrate the nature of the different optima found, the relative rotations between layer 1 and 2 for each extremal point, represented in terms of the computed direction cosines between the x-, y-, and z-axes for layer 1 and layer 2 material orientations respectively, are given in Table V.

Relative	Extremal point						
rotation	A1	A2	A3	A4	A5	A6	A7
x-axis	18°	26°	48°	96°	35°	103°	86°
y-axis	9°	22°	49°	100°	33°	78°	90°
z-axis	19°	24°	31°	32°	20°	162°	151°

Table V. Relative rotation between the axes of layer 1 and 2 for each extremal point.

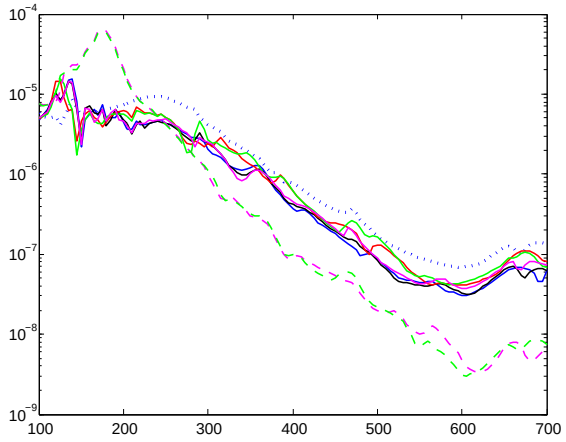

Figure 10. FRF of the different maxima and minima found for the orthotropic foam compared to [0 0 0]-rotation, blue dotted. A1=blue solid, A2=black solid, A3=red solid, A4=green solid, A5=magenta solid, A6=magenta dashed, A7=green dashed.

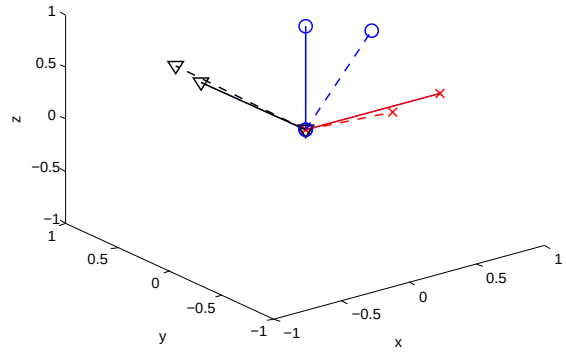

Figure 11. Relative rotation of material property axes of orthotropic material for layer 1 (solid) and layer 2 (dashed) minimum A2. x-axis=× y-axis=▽ z-axis=◯.

Looking at the relative orientation between the first and second layer of the panel there seems to occur some similarities between the different minima and maxima, especially for the relative angle between the z-axes. Especially minima A1, A2 and A5 were quite similar, see Fig. 11 and 12, while for minima A3 and A4 the similarities were not as obvious, mainly due to the deviation of the rotation of the x-y-plane in layer 2 as shown in Fig. 7.

B. Fibrous material

For the transversely isotropic fibrous material, using the five starting points in Table III, an overview of the optima found are shown in Table VI.

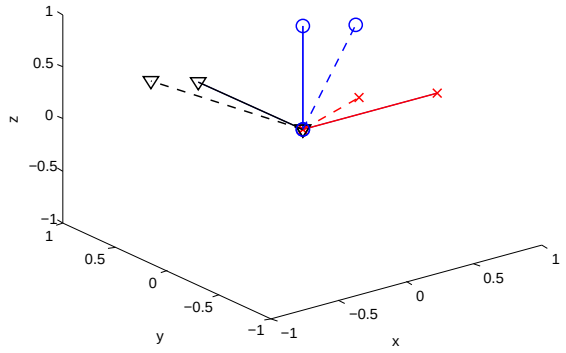

Figure 12. Relative rotation of material property axes of orthotropic material for layer 1 (solid) and layer 2 (dashed) minimum A5. x-axis=× y-axis=▽ z-axis=◯.

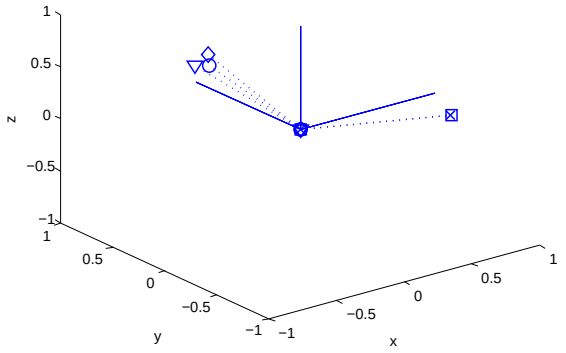

Figure 13. Rotation of material property y-axis for fibrous wool in layer 1 for the different minima compared to [0 0 0]-rotation. B1=◯ B2=× B3=▽ B4=□ B5=◇.

Start point	Min/ Max	Euler angles end values Layer 1	Layer 2	Diff. SPL [dB]
		Minimizations		
1	B1	[0 -0.65 -0.11]	[0 0.42 0.11]	-3.6
2	B2	[0 0.52 1.18]	[0 0.13 -0.85]	-3.3
3	B3	[0 -0.68 -0.25]	[0 0.26 -0.75]	-3.5
4	B4	[0 0.53 1.18]	[0 0.13 -0.86]	-3.3
5	B5	[0 -0.56 -0.22]	[0 0.42 0.46]	-3.7
		Maximizations		
2	B6	[0 0.56 0.55]	[0 0.45 1.00]	+0.6
1	B7	[0 0.93 0.50]	[0 0.92 -1.48]	+1.0

Table VI. Results overview for transversely isotropic fibrous material, configuration B. The table show the difference between the resulting SPL and the SPL for rotation [0 0 0].

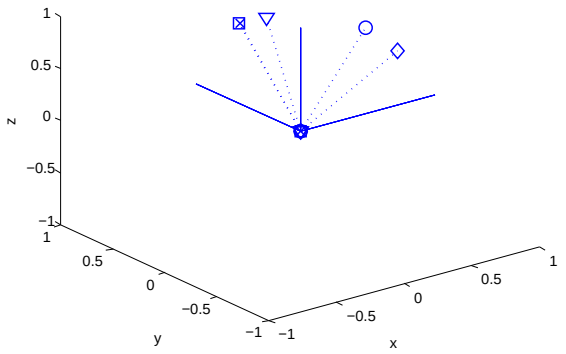

Figure 14. Rotation of material property y-axis for fibrous wool in layer 2 for the different minima compared to [0 0 0]-rotation. B1=◯ B2=× B3=▽ B4=□ B5=◇.

1. Comparing different extremal points

For this material, a comparison between the minima and the maxima found showed a level difference of 4.7 dB. Minima B1, B3 and B5 are close to each other for layer 1 and the same holds for minima B2 and B4. For layer 2 the picture is less clear, although minima B2 and B4 seems close to each other, the pattern is broken by the anomalous behavior of minima B3 which is closer to these two rather than the grouping identified for layer 1. This is clear from Fig. 13 and 14 where the angle of the z-axis of the fibrous material (compared to the no rotation case with Euler angles [0 0 0]) of the different minima for layer 1 and 2 are shown. Similarly the results of the maximizations are shown in Fig. 15 and 16 where the z-axis direction of the material properties in layer 1 are similar for maxima B6 and B7 while the optimal angles are quite different in layer 2 for these two extrema.

For the rather limp fibrous wool, the FRFs computed with the rotation angles pertaining to the different minima and maxima, Fig. 17, show that the variations in the cost function seems to be solely due to changes in the lower part of the frequency range 100 – 200 Hz. In

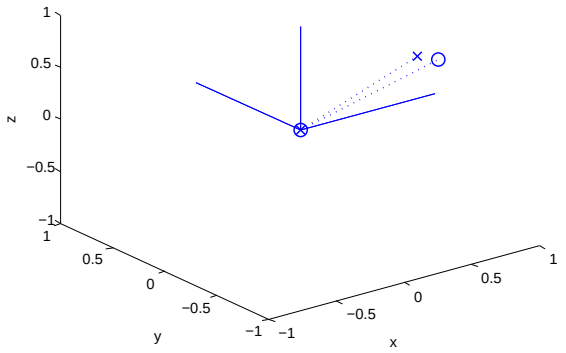

Figure 15. Rotation of material property y-axis for fibrous wool in layer 1 for the different maxima compared to [0 0 0]-rotation. B6=× B7=◯.

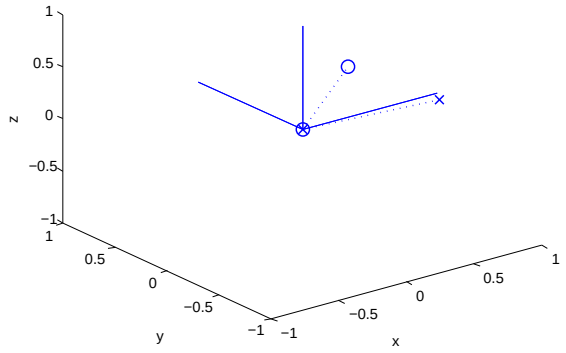

Figure 16. Rotation of material property y-axis for fibrous wool in layer 2 for the different maxima compared to [0 0 0]-rotation. B6=× B7=◯.

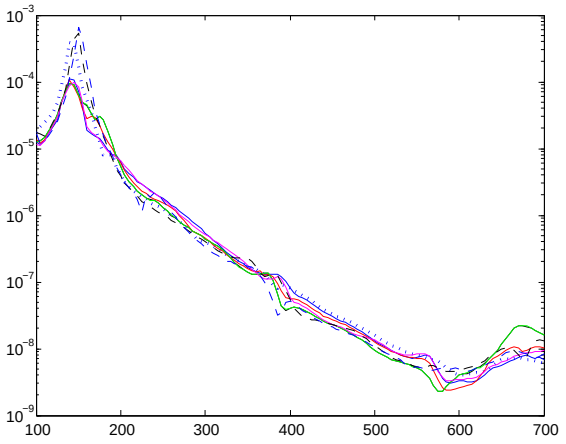

Figure 17. FRF of the different maxima and minima found for the fibrous wool compared to [0 0 0]-rotation, blue dotted. B1=blue solid, B2=black solid, B3=red solid, B4=green solid, B5=magenta solid, B6=black dashed, B7=blue dashed.

addition, the [0 0 0]-rotation response appears to be as high as the computed maxima.

2. Layer orientation within the different extremal points

The relative rotation of the z-axis between layer 1 and 2 for each extremal point is found in Table VII

Relative	Extremal point						
rotation	B1	B2	B3	B4	B5	B6	B7
z-axis	62°	108°	60°	109°	67°	23°	60°

Table VII. Relative rotation between the z-axis of layer 1 and 2 for each extremal point.

Looking at the relative orientation between the first

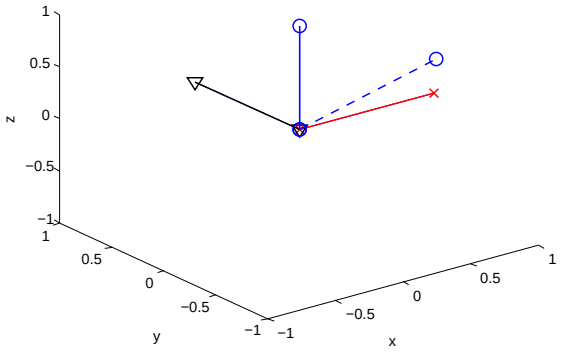

Figure 18. Relative rotation of the z-axis for material properties of transversely isotropic material for layer 1 (solid) and layer 2 (dashed) minimum B1. x-axis=× y-axis=▽ z-axis=◯.

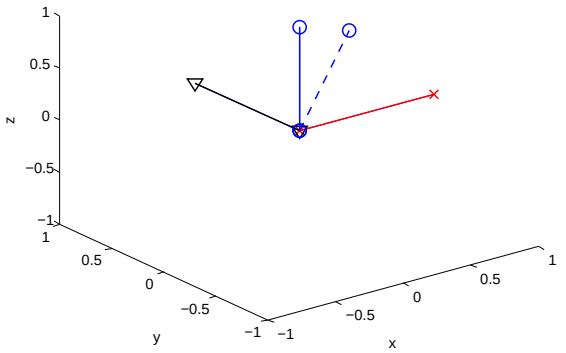

Figure 19. Relative rotation of the z-axis for material properties of transversely isotropic material for layer 1 (solid) and layer 2 (dashed) minimum B3. x-axis=× y-axis=▽ z-axis=◯.

and second layer of the panel a pattern similar to that for the panel with orthotropic foam is not visible. The relative z-axis rotations for extremal point B2 and B4 are naturally more or less identical as they are basically the same minimum. The relative rotations for point B3 and B7 are quite similar, see Fig. 19 and 21 whereas point B1 and B5 have the same relative rotation between the z-axes but with differences when comparing rotation around the z-axis, see Fig. 18 and 20. An explanation of this seemingly different outcome could be that the complete panel behavior is more dependent on the global layer orientations, i.e. compared to the global body coordinate axes of the system, rather than the relative rotations of the different layers.

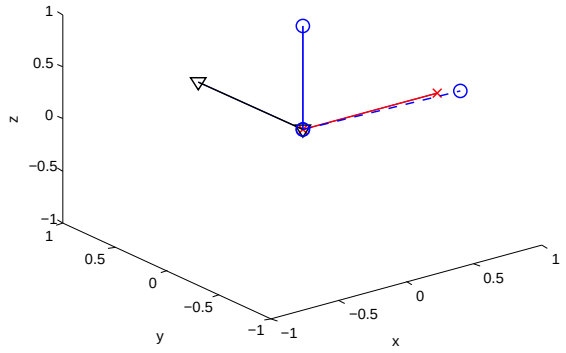

Figure 20. Relative rotation of the z-axis for material properties of transversely isotropic material for layer 1 (solid) and layer 2 (dashed) minimum B5. x-axis=× y-axis=▽ z-axis=◯.

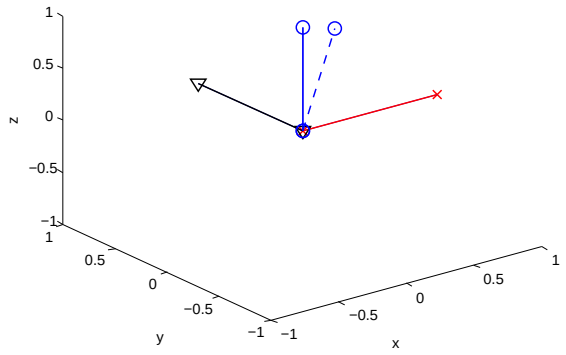

Figure 21. Relative rotation of the z-axis for material properties of transversely isotropic material for layer 1 (solid) and layer 2 (dashed) maximum B7. x-axis=× y-axis=▽ z-axis=◯.

C. Discussion

As a general observation, the min-max searches for both materials verified the importance of the anisotropy as well as the influence of material alignment for such materials. This was manifested through a clear change in acoustic response due to angular changes of the investigated anisotropic materials. Some seemingly different minima found turned out to be rather close to other minima. In general the different minima and maxima did not appear to be scattered all over the design space, on the contrary; there seemed to be different regions within the range of angles permitted in which several minima could be found and other distinctly separated regions containing maxima. This may indicate that there are regions of local minima or maxima in the vicinity of some specific Euler angles.

When looking at the frequency response functions pertaining to the different minima and maxima of configuration A, Fig. 10, it is apparent that the improvement of total SPL is due to improvements in the low frequency region, whereas for frequencies above 250 Hz there is no improvement, in fact, quite the opposite; the maximizations A6 and A7 show lower SPL for frequencies above 250 Hz. This type of trade off between different frequency regions is not uncommon when optimizing acoustic properties[20]. However comparing the FRFs of the minima with that of the [0 0 0]-rotation an improvement, though small, is visible over almost the entire frequency range. This shows that an optimization of acoustic properties does not always need to be a trade off between different frequency ranges.

Focusing on the sensitivity related to the orientation of the material properties, it was observed during the optimization process that, when approaching a minimum the changes in objective function were very small compared to the changes in design variables i.e. the objective function converged significantly faster than the design variables. This suggests that the solutions found, i.e. the resulting SPL, around the minima were quite unaffected by small angular changes. This also had the effect that the optimization was sometimes terminated before the Euler angles were quite converged and the resulting optimized angles may be considered to have an accuracy of about ± 0.005 rad. This accuracy should however be regarded with some caution. As the design variables were not totally converged in some cases and the fact that changing one of them may induce the others to change too there is always a risk, however small, that the optimized design variables would chance dramatically if yet more iterations were allowed.

Regarding the relative orientation of the material properties axes of porous layer 1 and 2 the results are however inconclusive. Intuitively the relative layer orientation should represent one of many important factors in multilayered configurations, this also seems to be the case for the panel containing orthotropic material. For the panel containing transversely isotropic material though a distinct pattern is not visible.

VII. CONCLUDING REMARKS

For both materials tested the changes in cost function were very small towards the end of the optimization process while the angular changes where still visible, thus rendering the extremal points rather insensitive to small angular changes close to the extremal points. A consequence of this is that it opens up for the possibility that the optimal angles for each local minima have not quite reached their final value and could differ slightly if the optimization process was allowed to continue for additional iterations.

Whereas the difference between the maximum SPL and the minimum SPL was significant the difference in SPL between individual minima was quite small. All minima found had a resulting SPL, within 0.2 dB in configuration A and within 0.5 dB in configuration B, even if they

were found at quite different Euler angles. In addition the small difference in FRF between different minima and the apparent tendency to appear in a limited number of minima regions may indicate that once the regions of local minima and maxima have been found, the exact Euler angles are less important, as long as the material angles stay within a minima region and thus avoid maxima regions. For practical applications this would probably be a quite compelling physical feature.

Studying the frequency response functions of configuration A, Fig. 10, it is quite obvious that the improvement in SPL is restricted to frequencies around 200 Hz, substantially improving the SPL at those frequencies at the expense of the SPL at higher frequencies. If the frequency range of interest was altered and thus excluding frequencies below for example 250 Hz the outcome of the optimization would doubtlessly be totally different. A weighting function applied to the FRF or other extensions or limitations of the frequency range would also influence the result. Obviously, a proper choice of objective function and frequency range of interest is therefore of outmost importance to achieve a useful result in practical applications.

Finally one can conclude that there are significant possibilities of improvement in practical applications connected with angular modification of anisotropic material properties of acoustic absorbents. Such improvement can according to the numerical simulations be achieved within an existing acoustic panel using readily available porous material without adding extra weight or volume. However, the knowledge of anisotropic material properties, including their principal directions as well as their structural losses and other damping behavior is today very limited, making anisotropic porous acoustic materials an important area well deserving further research.

VIII. ACKNOWLEDGMENT

This work was performed within the Centre for ECO^2 Vehicle Design. The financial support is gratefully acknowledged.

IX. REFERENCES

[1] J-F. Allard. *Propagation of sound in porous media: modelling sound absorbing materials*. Elsevier Applied Science, 1993.

[2] J.-F. Allard and Y. Champoux. New empirical equations for sound propagation in rigid frame fibrous materials. *J. Acoust. Soc. Am.*, 6(91):3346–3353, 1992.

[3] N. Atalla, M. A. Hamdi, and R. Panneton. Enhanced weak integral formulation for the mixed (u,p) poroelastic equations. *J. Acoust. Soc. Am.*, 109(6):3065–3068, 2001.

[4] M. A. Biot. Theory of propagation of elastic waves in a fluid saturated porous solid. I. Low frequency range. *J. Acoust. Soc. Am.*, 28:168–178, 1956:1.

[5] M. A. Biot. Theory of propagation of elastic waves in a fluid saturated porous solid. II. Higher frequency range. *J. Acoust. Soc. Am.*, 28:179–191, 1956:2.

[6] M. A. Biot. Theory of deformation of a porous viscoelastic anisotropic solid. *J. Appl. Phys.*, 27:459–467, 1956:3.

[7] M. A. Biot and D. G. Willis. The elastic coefficients of the theory of consolidation. *J. Appl. Mech.*, 24:594–601, 1957.

[8] M. A. Biot. Mechanics of deformation and acoustic propagation in porous media. *J. Appl. Phys.*, 33(4):1482–1498, 1962.

[9] J. Cuenca and P. Goransson. An inverse method for the estimation of elastic and anelastic properties of the porous frame of anisotropic open-cell foams. *J. Acoust. Soc. Am.* Accepted for publication June 2012.

[10] P. Göransson. Tailored acoustic and vibrational damping in porous solids – Engineering performance in aerospace applications. *Aerospace Science and Technology*, 12:26–41, 2008.

[11] P. Göransson, R. Guastavino, and N.-E. Hörlin. Measurement and inverse estimation of 3d anisotropic flow resistivity for porous materials. *J. Sound Vib.*, 327(3-5):354–367, 2009.

[12] P. Göransson and N.-E. Hörlin. Vibro-acoustic modelling of anisotropic porous elastic materials: A preliminary study of the in.uence of anisotropy on the predicted performance in a multi-layer arrangement. *Acta Acustica united with Acustica*, 96(2):258–265, 2010.

[13] R. Guastavino and P. Göransson. A 3d displacement measurement methodology for anisotropic porous cellular foam materials. *Polymer Testing*, 26(6):711–719, 2007.

[14] N.-E. Hörlin. 3-D hierarchical hp-FEM applied to elasto-acoustic modelling of layered porous media. *J. Sound Vib.*, 285(4):341–363, 2005.

[15] N.-E. Hörlin and P. Göransson. Weak, anisotropic symmetric formulations of biot's equations for vibro-acoustic modelling of porous elastic materials. *Int. J. Numer. Meth. Engng*, 84(12):1519–1540, 2010.

[16] L. Jaouen, A. Renault, and M. Deverge. Elastic and damping characterizations of acoustical porous materials: Available experimental methods and applications to a melamine foam. *Applied Acoustics*, 69(12):1129–1140, 2008.

[17] D. L. Johnson, J. Koplik, and R. Dashen. Theory of dynamic permiability and tortuosity in fluid-saturated porous media. *J. Fluid Mech.*, 176:379–402, 1987.

[18] P. Khurana, L. Boeckx, W. Lauriks, P. Leclaire, O. Dazel, and J.-F. Allard. A description of transversely isotropic sound absorbing porous materials by transfer matrices. *J. Acoust. Soc. Am.*, 125(2):915–921, 2009.

[19] D. Lafarge, P. Lemarnier, J.-F. Allard, and V. Tarnow. Dynamic compressibility of air in porous structures at audible frequencies. *J. Acoust. Soc. Am*, 102(4):1995–2006, 1997.

[20] E. Lind-Nordgren and P. Göransson. Optimising open porous foam for acoustical and vibrational performance. *J. Sound Vib.*, 329(7):753–767, 2010.

[21] M. Melon, E. Mariez, C. Ayrault, and S. Sahraoui. Acoustical and mechanical characterization of anisotropic open-cell foams. *J. Acoust. Soc. Am.*, 104(5):2622–2627, 1998.

[22] S. R. Pride, A. F. Gangi, and F. D. Morgan. Deriving the equations of motion for porous isotropic media. *J. Acoust. Soc. Am*, 92(6):3278–3290, 1992.

[23] H. J. Rice and P. Göransson. A dynamical model of light fibrous materials. *International Journal of Mechanical Sciences*, 41(4-5):561–579, 1999.

[24] S. Sahraoui, E. Mariez, and M. Etchessahar. Linear elastic properties of anisotropic open-cell foams. *J. Acoust. Soc. Am.*, 110(1):635–637, 2001.

[25] K. Svanberg. The method of moving asymptotes — a new method for structural optimization. *Int. J. Numer. Meth.*

Engng, 24:359–373, 1987.

[26] K. Svanberg. A class of globally convergent optimization methods based on conservative convex separable approximations. *SIAM Journal on Optimization*, 12(2):555–573, 2002.

[27] L. Wang. Flows through porous media: A theoretical development at macroscale. *Transport in Porous Media*, 39(1):1–24, 2000.

le cnam

Eleonora LIND NORDGREN

A study of tailoring acoustic porous material properties when designing lightweight multilayered vehicle panels

KTH VETENSKAP OCH KONST

KTH Engineering Sciences

Résumé :
Le présent travail explore la possibilité d'adapter des matériaux poro-élastiques légers pour des applications spécifiques. En particulier, une approche de conception est présentée, combinant simulations par la méthodes des éléments finis et techniques d'optimisation, permettant ainsi d'améliorer les propriétés dynamiques et acoustiques de panneaux multicouches comprenant des matériaux poreux. Les modèles numériques sont fondés sur la théorie de Biot qui utilise des modèles équivalents fluide/solide avec des propriétés macroscopiques spatialement homogénéisées, décrivant le comportement physique des matériaux poro-élastiques. Afin de systématiquement identifier et comparer certaines propriétés spécifiques, bénéfiques ou défavorables, le modèle numérique est connecté à un optimiseur fondé sur les gradients. Les paramètres macroscopiques utilisés dans la théorie de Biot étant liés, il ne peuvent être utilisés comme variables indépendantes. Par conséquent, des lois d'échelle sont appliquées afin de connecter les propriétés macroscopiques du matériau aux propriétés géométriques microscopiques, qui elles peuvent être modifiées indépendamment.
L'approche de conception est également combinée avec l'optimisation de la masse d'un panneau sandwich structure, afin d'examiner les possibilités de combiner exigences structurelles et acoustiques, qui peuvent être en conflit. En prenant le soin d'établir un équilibre entre composantes acoustiques et structurelles, des effets de synergie plutôt que destructifs peuvent être obtenus, donnant lieu à des panneaux multifonctionnels. Cela pourrait rendre l'ajout de traitements acoustiques redondant, qui par ailleurs annulerait tout ou partie du gain en masse obtenu par optimisation.
Les résultats indiquent un véritable potentiel d'amélioration des propriétés dynamiques et acoustiques de panneaux multi-couches, pour un ajout minimum en termes de masse et volume. La technique de modélisation développée pourrait également être implémentée au sein d'outils numériques futures pour la conception de panneaux légers de véhicules. Cela aurait le potentiel de réduire substantiellement la masse tout en limitant, voire supprimant l'impact négatif sur les propriétés acoustiques et vibratoires, pourtant une conséquence courante de la réduction de la masse, participant ainsi à l'effort de développement de véhicules futures plus légers et efficaces.

Mots clés :
matériaux poroélastiques, matériaux poreux, optimisation, la théorie de Biot, propagation d'onde.

Abstract :
The present work explores the possibilities of adapting poro-elastic lightweight acoustic materials to specific applications. More explicitly, a design approach is presented where finite element based numerical simulations are combined with optimization techniques to improve the dynamic and acoustic properties of lightweight multilayered panels containing poro-elastic acoustic materials.
The numerical models are based on Biot theory which uses equivalent fluid/solid models with macroscopic space averaged material properties to describe the physical behaviour of poro-elastic materials. To systematically identify and compare specific beneficial or unfavourable material properties, the numerical model is connected to a gradient based optimizer. As the macroscopic material parameters used in Biot theory are interrelated, they are not suitable to be used as independent design variables. Instead scaling laws are applied to connect macroscopic material properties to the underlying microscopic geometrical properties that may be altered independently.
The design approach is also combined with a structural sandwich panel mass optimization, to examine possible ways to handle the, sometimes contradicting, structural and acoustic demands. By carefully balancing structural and acoustic components, synergetic rather than contradictive effects could be achieved, resulting in multifunctional panels; hopefully making additional acoustic treatment, which may otherwise undo major parts of the weight reduction, redundant.
The results indicate a significant potential to improve the dynamic and acoustic properties of multilayered panels with a minimum of added weight and volume. The developed modelling techniques could also be implemented in future computer based design tools for lightweight vehicle panels. This would possibly enable efficient mass reduction while limiting or, perhaps, totally avoiding the negative impact on sound and vibration properties that is, otherwise, a common side effect of reducing weight, thus helping to achieve lighter and more energy efficient vehicles in the future.

Keywords :
porous material, poroelastic material, optimization, Biot theory, acoustic wave propagation.